AD_____

AWARD NUMBER: W81XWH-07-1-0057

TITLE: TGF-β Induction of PMEPA1: Role in Bone Metastasis Due to Prostate Cancer

PRINCIPAL INVESTIGATOR: Pierrick G. Fournier, Ph.D.

CONTRACTING ORGANIZATION: University of Virginia
                               Charlottesville, VA   22908

REPORT DATE: January 2009

TYPE OF REPORT: Annual Summary

PREPARED FOR: U.S. Army Medical Research and Materiel Command
                Fort Detrick, Maryland 21702-5012

REPORT DOCUMENTATION PAGE

Form Approved
OMB No. 0704-0188

Public reporting burden for this collection of information is estimated to average 1 hour per response, including the time for reviewing instructions, searching existing data sources, gathering and maintaining the data needed, and completing and reviewing this collection of information. Send comments regarding this burden estimate or any other aspect of this collection of information, including suggestions for reducing this burden to Department of Defense, Washington Headquarters Services, Directorate for Information Operations and Reports (0704-0188), 1215 Jefferson Davis Highway, Suite 1204, Arlington, VA 22202-4302. Respondents should be aware that notwithstanding any other provision of law, no person shall be subject to any penalty for failing to comply with a collection of information if it does not display a currently valid OMB control number. **PLEASE DO NOT RETURN YOUR FORM TO THE ABOVE ADDRESS.**

1. REPORT DATE	2. REPORT TYPE	3. DATES COVERED
1 January 2009	Annual Summary	15 Dec 2006 – 14 Dec 2008

4. TITLE AND SUBTITLE

TGF-β Induction of PMEPA1: Role in Bone Metastasis Due to Prostate Cancer

5a. CONTRACT NUMBER

5b. GRANT NUMBER
W81XWH-07-1-0057

5c. PROGRAM ELEMENT NUMBER

6. AUTHOR(S)

Pierrick G. Fournier, Ph.D.

E-Mail: pf9u@virginia.edu

5d. PROJECT NUMBER

5e. TASK NUMBER

5f. WORK UNIT NUMBER

7. PERFORMING ORGANIZATION NAME(S) AND ADDRESS(ES)

University of Virginia
Charlottesville, VA 22908

8. PERFORMING ORGANIZATION REPORT NUMBER

9. SPONSORING / MONITORING AGENCY NAME(S) AND ADDRESS(ES)
U.S. Army Medical Research and Materiel Command
Fort Detrick, Maryland 21702-5012

10. SPONSOR/MONITOR'S ACRONYM(S)

11. SPONSOR/MONITOR'S REPORT NUMBER(S)

12. DISTRIBUTION / AVAILABILITY STATEMENT
Approved for Public Release; Distribution Unlimited

13. SUPPLEMENTARY NOTES

14. ABSTRACT
TGF-β provided by the bone microenvironment is a key factor in the development of bone metastases. Previous experiments have demonstrated that interference with TGF-β signaling in cancer cells decreases the development of bone metastases. TGF-β stimulates prostate cancer cell signaling and alters their phenotype. TGF-β signaling in cancer is however complex and can lead to the activation of numerous genes. We identified PMEPA1 as the most highly upregulated gene by TGF-β in PC-3 cells and little is known about its function in cells. We have shown that the absence of PMEPA1 in prostate cancer cells increases bone metastases from prostate cancer in a mouse model. This result is consistent with in vitro experiments showing that the membrane-bound isoform PMEPA1a decreases TGF-β signaling via its interaction with E3 ubiquitin ligase and Smad protein, which suggest that membrane-bound PMEPA1 target Smad protein for proteosomal degradation. Interestingly the cytosolic isoform of PMEPA1, which is also induced by TGF-β, prevented PMEPA1a to inhibit TGF-β signaling. It is possible that PMEPA1c compete with PMEPA1a to bind Smads. Their different localization in cells could then explain their different properties. These results suggest that depending on which isoform is the most abundant in cells, PMEPA1 can provide a positive or negative feedback loop for TGF-β signaling.

15. SUBJECT TERMS
No Subject Terms provided.

16. SECURITY CLASSIFICATION OF:

a. REPORT	b. ABSTRACT	c. THIS PAGE	17. LIMITATION OF ABSTRACT	18. NUMBER OF PAGES	19a. NAME OF RESPONSIBLE PERSON USAMRMC
U	U	U	UU		19b. TELEPHONE NUMBER *(include area code)*

Standard Form 298 (Rev. 8-98)
Prescribed by ANSI Std. Z39.18

TABLE OF CONTENTS

Metastasis, the ultimate step of malignancy, is not a randomized process and some sites, such as bone, are preferential targets [1]. At least 65% of patients with advanced breast or prostate cancer will develop bone metastases [2]. Tumor cells in bone disrupt normal bone remodeling to cause an excess in bone destruction and/or bone formation which fuel a vicious cycle [3]. Bone metastases are associated with severe consequences: pain, hypercalcemia, fractures, or nerve compression syndromes and paralysis that drastically reduce quality of life. Moreover, once metastatic cells colonized bone, there is no cure, only palliation. Bone metastases are a major public health problem. Thus, a detailed understanding of the bone metastases process is needed to define targets and design new treatments to cure cancer.

Several studies showed that transforming growth factor-β (TGF-β) is a major mediator of metastasis: it activates epithelial-mesenchymal transition (EMT) [4] and tumor cell invasion [5], increases angiogenesis [6] and induces immunosuppression [7]. TGF-β is also crucial in the bone metastases process [8-10]. Bone is a major source of TGF-β since it is synthesized and trapped in the mineralized matrix by the osteoblasts. It is released and activated during osteoclastic bone resorption [11]. TGF-β acts then on cancer cells to induce the secretion of prometastatic factors such as interleukin (IL)-11 [12], endothelin-1 (ET-1) [13] or parathyroid hormone-related protein (PTHrP) [10]. These proteins in turn induce either an osteoblastic response (ET-1) or osteolysis (PTHrP) [14;15].

We recently identified a new downstream target of TGF-β in the prostate cancer cells PC-3, using micro-array technology. This gene, PMEPA1, was the most highly upregulated by TGF-β (23-fold increase, $P<0.03$). It codes for proteins overexpressed in breast, ovarian and colorectal cancers [16;17]. Although the function of PMEPA1 is unknown, it has been shown to interacts with Nedd4 [18;19], a member of the Nedd4 family of HECT domain E3 ubiquitin ligases (which also includes Smurf1 2, and Tiul1) [20]. HECT E3 ubiquitine ligases are implicated in the degradation of Smad proteins and the regulation of the TGF-β signaling pathway [21;22].

Bone is the most common site for prostate and breast cancer metastasis. Bone-derived TGF-β contributes to this process in many ways: (1) as a prometastatic factor (i.e., EMT, invasion, angiogenesis) and (2) as an inducer of bone active factors (i.e., PTHrP, IL-11 and ET-1) (**Figure 1**). We propose here a new mechanism by which TGF-β promotes bone metastases with the induction of PMEPA1 at the bone metastatic site. *In this proposal, we will test the **hypothesis** that TGF-β released from bone at the site of bone metastases induces the production of PMEPA1. PMEPA1 expression is important for bone metastases development, by interacting with HECT E3 ubiquitin ligases to prevent the degradation of Smad proteins. This results in a continuous activation of the TGF-β pathway in cancer cells housed in bone and perpetuates the vicious cycle to result in the production of more osteolytic and osteoblastic factors.*

Three specific aims will be addressed. **Aim 1**: to characterize the TGF-β induced transcription of PMEPA1 *in vitro*. **Aim 2**: to assess the TGF-β induced upregulation of PMEPA1 and its role in bone metastases formation *in vivo*. **Aim 3**: to characterize the interaction of PMEPA1 with E3 ubiquitin ligases and its involvement in TGF-β signaling regulation.

4

Specific Aim 1: To determine the TGF-β induced transcription of PMEPA1 in vitro
Task 1: Analysis of PMEPA1 variants expression after TGF-β treatments in vitro

The PMEPA1 gene covers 63kb. Alternative splicing and multiple transcription starts give rise to 4 different mRNA variants (Genbank accession numbers: NM_020182, NM_199169, NM_199170 and NM_199171 for variants 1, 2, 3 and 4 respectively). These mRNA are highly similar except in the 5' extremity and code for 3 different protein isoforms that differ at their N-terminus. Isoform a and b both contain a transmembrane domain, while isoform c, the shortest, is cytosolic.

To determine which mRNA variant is the most abundant in PC-3 cells treated or not treated with TGF-β, we used absolute quantitative real-time RT-PCR.

Primers specific for each variants of PMEPA1 have been designed and their amplification product was cloned in a pSC-A linearized according to the manufacturer's instruction (StrataClone™ PCR Cloning Kit, Stratagene) and used to establish standard curves for real-time PCR. Similarly we cloned the amplification products of the primers for the endogenous ribosomal protein L32 to normalize our RT-PCR. PC-3 cells were grown until they reach near confluency and starved in basal media overnight before being treated or not-treated with TGF-β (5ng/mL) for 24 hours. Total RNA was extracted from cell (RNeasy mini-kit, Qiagen) and treated with DNase I to avoid DNA contamination (RNase free DNase set, Qiagen). cDNA were obtained using the SuperScript ™ II reverse transciptase (Invitrogen) and used as template in an absolute quantitative real-time PCR (QuantiTect SYBR green PCR kit, Qiagen) using a BioRad MyiQ thermocycler.

TGF-β significantly increased the expression of all PMEPA1 messenger RNA variants, and variant 2 has the highest induction (≈20-fold) (**Figure 2**). Variant 1 coding for isoform a of the protein has the lowest expression in the presence or absence of TGF-β. Variant 3 and 4 code for the same protein, isoform c but remain less abundant then variant 2 which the most abundant mRNA, in the presence of TGF-β, suggesting that PMEPA1 isoform b is the most abundant in TGF-β-stimulated PC-3 cells. However when we quantified the number of copy of PMEPA1 mRNA using a pair of primer designed in the 3' extremity of the mRNA, we calculated a total amount of mRNA ≈11-times superior to the addition of all the mRNA variants we measured (**Figure 2**). Due to the low nucleotide variation between each variant, we could not change their specific primers to determine whether it would affect the quantification, so we designed a new pair of primers targeting a region closer to the 5' extremity identical to all variants. However both pair of primers for total PMEPA1 detected similar quantities of mRNA (data not shown).

Since we could not solve the problems linked to mRNA quantification, we used an alternative approach with a new antibody against PMEPA1. This antibody was not available when we initiated the project and wrote the proposal. The lack of antibody as that time was considered as a weakness by the Reviewer A during the reviewing process. Before trying to develop our own antibody, we kept on searching manufacturer's catalogs and found a mouse monoclonal antibody directed against an epitope in the C-terminus of PMEPA1 protein (Abnova) which had been recently released. The C-terminus of PMEPA1 is identical to all isoforms and this antibody should detect all of them. To test the antibody, the coding sequence of each PMEPA1 isoform was amplified by PCR using a *Pfu* proof-reading DNA polymerase (Stratagene) and the IMAGE clone 4559576 as a template and the following oligonucleotide primers: forward primer for isoform a 5'-CTAGCTAGCTAGACCATGCACCGCTTGATGGGGGGTCAACAGCACCGCCGCCGCCG-3', forward primer for isoform b 5'-CTAGCTAGCTAGACCATGGCGGAGCTGGAGTTTGTTCAG-3', forward primer for isoform c 5'-CTAGCTAGCTAGACCATGATGGTGATGGTGGTGGT-3', and the reverse primer 5'-CCCAAGCTTGGG GAGAGGGTGTCCTTTCTGTT-3' for all the isoforms. The amplification products were cloned in a pcDNA3.1-Zeo+ plasmid (Invitrogen) between the Nhe I and Hind III restriction sites. We also inserted at the 3' end a V5 epitope tag and a stop codon between the KpnI and EcoRI restriction sites of the plasmid using the following oligonucleotide 5'-CGGGGTACCCCGGGTAAGCCTATCCCTAACCCTCTCCTCGGTCTCGATTCTACGTAGCCG GAATTCCGG-3' and its complementary strand. pcDNA3.1 plasmids expressing LacZ or the different

5

isoforms of PMEPA1-V5 protein were transfected in COS-1 cells. Protein lysates were prepared 24 hours later and analyzed by Western-blotting to detect first PMEPA1 and then V5 (anti-V5 antibody, Sigma) after stripping the membrane. Immunodetection of α-tubuline (anti-α-tubulin antibody, Sigma) was used to confirm the loading of equal amount of proteins.

A signal was detected at the expected molecular weights with the antibody against PMEPA1 only in the wells containing PMEPA1-V5 proteins, not LacZ (**Figure 3**). This signal was similar to the one obtained with the anti-V5 antibody (**Figure 3**). Multiple bands are detected in the protein lysate of the COS cells transfected to express PMEPA1a-V5, by the antibodies against PMEPA1 and V5. It suggests that these bands are due to multiple proteins expressed by the plasmid transfected, while restriction maps and sequencing confirmed the purity and the identity of the plasmid. This result has not been explained yet but does not prevent the use of this new antibody to detect PMEPA1 using Western-Blot.

To characterize the effect of TGF-β on PMEPA1 endogenous protein expression, PC-3 cells were treated with increasing concentration of TGF-β (from 0.1 to 5ng/mL) for 24 hours. Using western-blotting, PMEPA1 was not detected in untreated PC-3 cells (**Figure 4A**). A concentration of TGF-β as little as 0.1ng/mL allowed the detection of PMEPA1 signal and TGF-β-induction appeared maximal at 0.25ng/mL (**Figure 4A**). When PC-3 cells were treated or not treated with 5ng/mL of TGF-β up to 48 hours before preparing protein lysates, western-blotting showed that PMEPA1 protein was detected after 4 hours of TGF-β treatment and PMEPA1 level increased until 24 hours when it reached a plateau (**Figure 4B**). Expression of PMEPA1 induced by TGF-β in PC-3 cells was prevented by using SD-208, a small molecule inhibitor of the kinase activity of the TGF-β type I receptor (Tgfbr1) (**Figure 4C**).

We demonstrated that PMEPA1 protein expression is quickly and stably induced by TGF-β in PC-3 human prostate cancer cells. Expression of PMEPA1 is also very sensitive to TGF-β. Although the expression of all mRNA variants was detected and increased by TGF-β in PC-3 cells, it is the isoforms a and c of PMEPA1 which are the most abundant in PC-3 cells treated with TGF-β as well as in DU145 (prostate), MDA-MB-231 (breast) and A549 (lung).

Task 2: Characterization of TGF-β induction of PMEPA1 and of PMEPA1 promoter

To further understand the mechanism of TGF-β-induced expression of PMEPA1, PC-3 cells were treated up to 48 hours with TGF-β (5ng/mL) in the presence or absence of the specific Tgfbr1 inhibitor, SD-208. Total mRNA were prepared and the expression of all PMEPA1 mRNA variants was measured by real-time semi-quantitative RT-PCR. PMEPA1 mRNA is quickly increased by TGF-β and reaches a pick after 4 hours (**Figure 6**). PMEPA1 upregulation by TGF-β was totally inhibited by SD-208 (**Figure 6**). We also used the classical cycloheximide and actinomycin-D, at concentrations inhibiting PC-3 cell growth. The translation inhibitor cycloheximide did not reverse TGF-β effect showing that PMEPA1 is a direct target gene of the TGF-β pathway (**Figure 6**). The transcription inhibitor, actinomycin D prevented the increase of PMEPA1 mRNA suggesting that TGF-β does not increase the mRNA stability (**Figure 6**).

These results show that TGF-β regulates PMEPA1 expression through transcriptional control.

The analysis of PMEPA1 promoter (up to 3.7 kb upstream of the transcription start of mRNA variant 1 of PMEPA1) showed the presence of 5 consensus Smad binding elements (SBE), 5'-CAGACA-3' (**Figure 7**). This fragment of the PMEPA1 promoter was cloned from a cosmid (BACPAC resources, CHORI) into the pGL3 plasmid, a *firefly* luciferase reporter vector (Promega). The pGL3-PMEPA1 plasmid was co-transfected with the ph*r*Luc-CMV plasmid (Promega), which constitutively expresses *renilla* luciferase, in PC-3 (prostate cancer cells), and HepG2 (hepatocarcinoma) and A459 (lung cancer cells) known for their sensitivity to TGF-β. These cells were treated or not treated with TGF-β (5ng/mL, 24 hours) before measuring dual-luciferase activity with a FB15 Sirius luminometer (Zylux corporation). TGF-β significantly increased PMEPA1 promoter activity in the 3 cell lines tested which was reversed by the Tgfbr1 inhibitor, SD-208 (**Figure 8**). Moreover when A549 cells were transfected to overexpress Smad2, 3 and 4, the TGF-β pathway effectors, PMEPA1 promoter was increased independently of TGF-β (**Figure 8**). Conversely TGF-β-induced activity of PMEPA1 promoter was significantly inhibited by the overexpression of the Smad

inhibitor, Smad7 (**Figure 8**). These results concur to show that TGF-β-induction of PMEPA1 involves Smad proteins.

TGF-β regulates the expression of PMEPA1 through transcriptional control via a molecular mechanism involving Smad proteins.

Task 3: Identify the SBEs and DNA motifs involved in TGF-β regulation of PMEPA1 promoter
Therefore we performed site-directed mutation of the SBEs using the QuickChange Site-Directed Mutagenesis Kit (Stratagene) following the manufacturer's instructions. The five 5'-CAGACA-3' SBEs identified in the 3.7kb fragment were respectively mutated to 5'-tAcAtA-3', 5'-CctgCA-3', 5'-tAGAtA-3', 5'-CAtgtA-3' and 5'-tActCA-3', each creating a new restriction site, which was used to confirm the introduction of each mutation. These constructs with phRL-CMV were transfected in A549 cells and the cells were treated or not treated with TGF-β (24h, 5ng/mL) before measuring the dual-luciferase activity. Mutation of one or all of the SBE did not significantly decrease the promoter activity induced by TGF-β as we would have expected (**Figure 9A**). This lack of effect could be due to additional DNA motifs in the promoter binding Smad proteins or non-Smad protein activated by the non-Smad TGF-β signaling. Thus we tested the effect of the overexpression of the effectors Smad2/3/4 or the inhibitor Smad7 on the activity of the PMEPA1 promoter where the 5 SBEs have been mutated. Mutation of the 5 SBEs decreased the promoter activity induced by Smad2/3/4 when compared to the wild-type promoter, which confirm that these elements are involved but not necessary to the TGF-β induction (**Figure 9B**). However overexpression of Smad7 still decreased the promoter activity induced by TGF-β in presence of the mutated SBEs (**Figure 9B**), demonstrating that TGF-β induction of PMEPA1 promoter is independent of the predicted SBEs.

To determine which region of the promoter is responsible for the TGF-β inducibility, we tested the TGF-β responsiveness of a series of promoter deletion constructs in A549 cells using dual-luciferase assay. Deletion of the first 2.5kb of the promoter, nucleotides -3691 to -1440, did not significantly affect the increased promoter activity induced by TGF-β when compared to the 3.7kb promoter (**Figure 10**). In the remaining 1.5kb fragment, deletion of the first 900bp or last 600bp resulted in a 50% decrease of the PMEPA1 promoter activity induced by TGF-β (constructs -530/+54 and -3691/-484, respectively), and the full activity of the promoter was not restored when the distal 2.5kb of the promoter were added (construct -3691/-484, **Figure 10**). A distal fragment of the promoter containing 4 of the 5 SBE cloned in front of a minimal promoter was not activated when the cells were treated with TGF-β (construct -3691/-1856, **Figure 10**). These results suggest that the TGF-β responsive elements in the PMEPA1 promoter are located within a 1.5kb fragment localized between nucleotides -1440 and +54.

All the fragments of the PMEPA1 promoter containing SBE, showed an increase of luciferase activity in the presence of TGF-β as well as the -530/+54 fragment, which does not contain any SBE, 5'-CAGACA-3' (**Figure 10**). So we co-transfected A549 cells with Smad2, 3 and 4 expression vectors and with the promoter fragments carrying or not carrying SBE. Smad protein overexpression increased the basal promoter activity of the 3.7kb (-3691/+54) and 1.5kb (-1440/+54) fragments (**Figure 11**). However the basal promoter activity of the proximal 0.6kb (construct -530/+54) which does not contain SBE was not affected by Smad2/3/4 overexpression (**Figure 11**). Althoug the promoter activity remained increased when cells were treated with TGF-β (**Figure 11**). This result suggests that TGF-β responsiveness of this fragment is mediated through non-Smad mechanisms.

TGF-β receptors can activate non-Smad signaling via MAP kinase pathway components such as MEK1/2, and JNKs[23;24]. TGF-β-activated kinase 1 (TAK1) and its upstream activator TAK1-binding protein mediate some responses to TGF-β family members. Activation by TGF-β of p38 MAP kinase, which is downstream of TAK1, has also been reported. To examine the non-Smad signaling pathways by which TGF-β increases PMEPA1 expression, the promoter activity of the 3.7kb (-3691/+54) and 0.6kb (-530/+54) fragments was measured in A549 cells treated or not treated with TGF-β, in the presence or absence of specific protein kinase inhibitors: SD-282 (p38 inhibitor), SP600125 (JNK inhibitor) and PD98059 (MEK inhibitor). However none of these inhibitors, alone or combined, had any effect on PMEPA1 promoter activity induced by TGF-β (**Figure 12A**). We confirmed by sqRT-PCR that the same inhibitors had no effect on the levels of PMEPA1 mRNA induced by TGF-β in PC-3 prostate cancer cells (**Figure 12B**).

These results show that TGF-β regulates PMEPA1 expression through transcriptional control. PMEPA1 expression induced by TGF-β is independent of the predicted SBEs. TGF-β induction of the PMEPA1 promoter is controlled by a 1.5kb proximal fragment via both Smad mechanisms as well as non-Smad mechanisms independent of p38, JNK or MEK. As of now, the elements responsible for TGF-β induction of the PMEPA1 promoter remain to be identified. Analysis of the sequence of this 1.5kb fragment using Genomatix-Matinspector to identify other binding sites for transcription factors related to TGF-β signaling showed the presence of 11 putative SP1 sites, as well as GC rich motifs (not shown). Kang et al. found similar elements in the human IL-11 gene (lack of SBE, SP1 motifs, GC rich sequences) that are explaining the TGF-β inducibility of IL-11 promoter(25).

In absence of DNA motifs clearly identified within the 1.5kb fragment, it is not possible to use EMSA and ChIP method to confirm the binding of transcription factors. DNAse 1 footprinting could be used to identify the elements responsible for TGF-β induction in PMEPA1 promoter.

Specific Aim 2: Assess the TGF-β-induced expression of PMEPA1 in vivo
Task 4: In vivo quantification of PMEPA1 expression at sites of bone metastases in a prostate cancer bone metastases model
We have chosen to use species specific sqRT-PCR to measure PMEPA1 expression in bone marrow samples of mice with PC-3 bone metastases treated or not treated with SD-208, an inhibitor of the TGF-β type I receptor (tgfbr1).

The primers used to measure human PMEPA1 and RPL32 (housekeeping gene) mRNA by sqRT-PCR were designed to be specific of the human mRNA and ignore mouse mRNA. RT-PCR with RNA from PC-3 human prostate cancer cells or from mouse bone marrow cells were performed and amplification product were run on agarose gel to control that the primers do not amplify any product from mouse templates (data not shown). We also validated that the RT-PCR efficiency for the human PMEPA1 and RPL32 remained unchanged in the presence or absence of mouse template. The efficiency of the PCR was measured by use of a dilution series of PC-3 cDNA in water or in mouse cDNA to generate amplification curves at different concentration of template. Primers specific for human RPL32 and human PMEPA1 with efficiency of $100 \pm 5\%$ were selected (data not shown).

SD-208 is a pteridine derivative that specifically inhibit the serine kinase activity of the tgfbr1 (IC_{50} = 70nM). We confirmed that SD-208 decreased TGF-β signaling in PC-3 cells using western blotting to detect the phosphorylation of Smad2 and dual-luciferase experiment (**Figure 13**).

To induce osteolytic bone metastases, athymic male mice were inoculated in the left cardiac ventricle wit PC-3 prostate cancer cells. Osteolysis development was surveilled by serial radiography and mice (n=14/group) received SD-208 (50mg/kg/day, po) or the vehicle throughout the whole protocol. SD-208 significantly decreased the osteolysis area induced by PC-3 cells (vehicle $15.3 \pm 2.8mm^2$, SD-208 $6.7 \pm 3.3mm^2$, 56% inhibition, *P*<0.05) (**Figure 14**). However SD-208 did not have any effect on the human PMEPA1 mRNA expression measured by sqRT-PCR in the bone marrow of metastastic tibia and femur collected 54 days after tumor inoculation (**Figure 15**). As a control we measured the expression of the human PTHrP since it has been well established that bone-derived TGF-β induces PTHrP expression at sites of bone metastases, and similarly to PMEPA1 PTHrP expression was not affect by SD-208 (**Figure 15**). Although SD-208 significantly decreased tumor-induced osteolysis, there is still bone destruction and therefore release of TGF-β from the bone matrix. Considering that concentrations of TGF-β has low as 250pg/ml induced PMEPA1 expression *in vitro* (**Figure 4**), it is likely that local concentrations of TGF-β at sites of bone metastases treated with SD-208 were high enough to induce PMEPA1 expression. It is also possible that other factors present at sites of bone metastases induced PMEPA1 expression independently of TGF-β.

Task 5: Effect of PMEPA1 knockdown on the development of bone metastases from prostate cancer cells in mice
To knockdown PMEPA1 expression in PC-3 cells, we used a pLKO.1 vector expressing predesigned shRNA (Sigma) and selected one that efficiently targets PMEPA1. COS7 monkey kidney cells were

transfected with a vector expressing one of the PMEPA1 isoform and an empty pLKO.1 vector or a pLKO.1 vector expressing a shRNA Control (shCtrl) or directed against PMEPA1 (shPMEPA1). PMEPA1 expression was assessed 48 hours later. Using real-time RT-PCR, we measured a 90% decrease of expression of any PMEPA1 mRNA variant induced by shPMEPA1 (**Figure 16A**). The empty pLKO.1 vector or a vector expressing shCtrl had no effect on the expression of PMEPA1 mRNA. By western blot, we confirmed that shPMEPA1 prevented PMEPA1 expression regardless of the isoform (**Figure 16B**). We also transfected decreasing quantities of pLKO.1 shPMEPA1 vector to determine the lowest quantity of vector required to knockdown PMEPA1 and decrease the possibility of non-specific effects of the shRNA (**Figure 16C**).

PC-3 cells were then transfected with a pLKO.1 vector expressing shControl or shPMEPA1. Selection of the clones was obtained after growing the cells for 2 weeks in the presence of puromycin (250ng/ml) and using cloning cylinders. Selection of clones was based on the absence of PMEPA1 protein expression when the cells were treated with TGF-β, using western-blotting (**Figure 17**). Eight clones where PMEPA1 expression was knocked-down were selected for further analysis. Stability of the knockdown was tested by growing the cells in absence of antibiotic during 75 days before testing PMEPA1 knockdown by sqRT-PCR and Western-Blot. We also compared proliferation rate of transfected PC-3 clones against parental PC-3 cells using an MTT assay. We selected PC-3 clones expressing shPMEPA1 (PC-3 shPMEPA1 #5C3 and #1A1) with a proliferation rate similar to parental PC-3 and with a >95% decrease of the expression PMEPA1 mRNA and protein,compared to parental PC-3, in the presence or absence of TGF-β (**Figure 18**). We also selected 2 PC-3 clones transfected to express shCtrl with proliferation rate and PMEPA1 expression similar to PC-3 parental as control (**Figure 18**).

Selected PC-3 shCtrl and shPMEPA1 clones were inoculated in the left cardiac ventricle of 4 week-old, male athymic mice to cause bone metastases (10^5 cells/100µL PBS/mouse, n=12 to 16 per group). The development of malignant osteolysis was surveyed weekly by radiographies of the mice, over 9 weeks (63 days), before euthanizing the mice. The PMEPA1 knockdown in PC-3 cells did not have any significant effect on the occurrence of osteolysis in the mice although there is a trend toward an earlier appearance of osteolysis when compared to PC-3 shCtrl clones (**Figure 19B**). Quantification of the osteolysis by computerized imaging (Metamorph software) showed that PMEPA1 knockdown in PC-3 cells significantly increased osteolytic lesion area on x-ray compared to mice that received PC-3 shCtrl cells (8.8±2.8 and 3.9±1.6mm² for shPMEPA1 clones vs 0.3±0.1 and 0.4±0.2mm² for shCtrl clones, *P*<0.001, at 9 weeks, **Figure 19A-C**).

Knockdown of PMEPA1 expression in PC-3 human prostate cancer cells increased the development of bone metastases in mice, which is opposite to the hypothesis formulated in this project. Processing of bone sample and histomorphometric analysis of skeletal tumor burden and bone destruction are ongoing and should confirm the results from the radiographies.

Task 6: Effect of PMEPA1 expression overexpression on the development of bone metastases from prostate cancer in mice.

As a counter-experiment to PMEPA1 knockdown in PC-3 cells and its effect on bone metastases, we had proposed to overexpress PMEPA1 and test the effect on bone metastases. We had initially planned to test PMEPA1 overexpression in C4-2B prostate cancer cells. However we hypothesized that PMEPA1 can act as a regulator of TGF-β signaling pathway and we observed that C4-2B cells are TGF-β insensitive. Dual-luciferase experiments with a TGF-β reporter promoter, (CAGA)₉, showed no increase of luciferase activity in C4-2Bcells or its precursor LnCap in the presence of TGF-β, while luciferase activity was increased for PC-3, DU-145 or MDA-MB-231 in the same conditions (**Figure 20A**). Moreover TGF-β did not induce PMEPA1 expression in C4-2B cells (**Figure 20B**). Previous studies have reported that LnCap cells, of which C4-2B cells were derived, are insensitive to TGF-β, explaining this by the lack of expression of the TGF-β type 1[26;27] or type 2 receptor[28;29]. Using sqRT-PCR in multiple prostate cancer cells lines, we measured a 150-fold decrease of Tgfbr2 expression in C4-2B cells while Tgfbr1 expression was similar in PC-3 and C4-2B (**Figure 21**). TGF-β insensitivity in C4-2B cells seems then to be due to lack of Tgfbr2 as described by other studies[28;29].

Therefore we decided to overexpress specific isoforms of PMEPA1 in PC-3 cells where the

endogenous expression of PMEPA1 was knocked-down using shPMEPA1 (see Task 5). For that purpose, 4 silent mutations were inserted in the nucleotide sequence recognized by the shPMEPA1 localized in PMEPA1 CDS, coded by a pcDNA3.1 vectors. Mutation of 4 nucleotides was sufficient to decrease the efficiency of shPMEPA1 and allow the re-expression of PMEPA1 protein (**Figure 22**). Plasmids expressing PMEPA1 resistant to shPMEPA1 have been prepared for all 3 isoforms and stable transfection in PC-3 should be performed. However since 2 isoforms of PMEPA1 are expressed in PC-3 cells in the presence of TGF-β (isoforms a and c; see Task 1), we studied first the biological properties of both isoforms on TGF-β signaling in PC-3 cells before testing these cells in mice.

Specific Aim 3: Characterize the interaction of PMEPA1 with Smurf proteins and its involvement in TGF-β signaling regulation

Task 7: Characterize the interaction of PMEPA1 with Smurf proteins

Results from the laboratory of Dr. Mitsuyasu Kato (University of Tsukuba, Japan) presented at the FASEB Summer Research Conference on *The TGF-β Superfamily: Signaling and Development* (Tucson, AZ, 2007) showed in a similar study that PMEPA1 can interact with the E3 ubiquitin ligase Smurf and regulate TGF-β signaling but in a Smurf independent manner. To avoid, duplicating experiments, we focused our work on the effect of PMEPA1 on TGF-β signaling (Task 8).

However, as it will be explained in Task 8, we demonstrated that membrane-bound isoforms of PMEPA1 can decrease TGF-β signaling in a mechanism dependent on the 2 PPxY domains localized in the C-terminus of PMEPA1. The PPxY domains allow PMEPA1 to interact with Nedd4(30) and potentially other HECT E3 ubiquitin ligases. These results suggest that PMEPA1 actually regulates TGF-β signaling in an E3 ubiquitin ligase dependent manner that may not involve Smurf1 and 2 but other protein from this family such as Nedd4, Nedd4-2, Tiul1 or Arkadia. To elucidate the involvement of these proteins, we are in the process of collecting expression vectors from other researchers or IMAGE constructs to clone their cDNA. We will be able to express these proteins and test their effect on PMEPA1 biological properties.

Task 8: Determine the effect of PMEPA1 overexpression or knockdown on TGF-β signaling.

Although the different PMEPA1 isoforms have different N-termini, with a transmembrane-domain for PMEPA1a and b, without for PMEPA1c, the C-termini are identical for all isoforms. They contain 2 PPxY domains that have been reported to interact with the HECT E3 ubiquitin ligase Nedd4 (**Figure 23**)(30). Nedd4 belong to the same family as Smurf1, Smurf2 and Tiul1 that regulates TGF-β signaling via proteosomal degradation. Analysis of the C-terminus sequence also showed the presence of a sequence homolog to Smad Interaction Motives (SIM) found in DNA binding co-factors that control the affinity of receptor associated Smads for DNA (**Figure 23**). These elements led us to the hypothesis that PMEPA1 regulate TGF-β signaling and that membrane-bound and cytosolic isoforms might have different biological functions.

To assess the effect of PMEPA1 on TGF-β signaling pathway, we used a pGL3 reporter vector where luciferase expression is controlled by 9 CAGA boxes (Smad binding motifs) in dual-luciferase experiments. PMEPA1 knockdown using a shRNA against PMEPA1 express by pLKO.1 vector induced a significant decrease of $(CAGA)_9$ promoter activity suggesting that PMEPA1 could potentiate TGF-β signaling (**Figure 24A**). shPMEPA1 had no effect on the BRE4(Id1) promoter sensitive to Bone morphogenic protein (BMP)[31] when PC-3 cells were treated with BMP-7 (**Figure 24A**). BMPs are part of the TGF-β superfamily. BMPs are involved in bone formation and bone metastases including BMP-7[32;33]. The BMP pathway is similar to TGF-β pathway and the lack of effect of shPMEPA1 on it suggests that the effect of PMEPA1 knockdown is specific to TGF-β signaling. Similarly shPMEPA1 had no effect on the activity of the constitutively active promoter SV40 (**Figure 24A**). We tested then the effect of shPMEPA1 in other cell types. shPMEPA1 had not effect on TGF-β signaling in HepG2 cells (**Figure 24B**), which was expected since they do not express PMEPA1 even when treated with TGF-β (**Figure 5**). However, shPMEPA1 had no effect on TGF-β signaling in prostate (DU145), breast (MDA-MB-231) and lung (A549) cancer cells expressing PMEPA1 (**Figure 24B**). These results are suggesting that the effect of PMEPA1 on TGF-β pathway could be specific to PC-3 cells or an artifact due to the shRNA. We attempted to use siRNAs designed by Qiagen to knockdown PMEPA1 and confirm these results but could not validate them. We are in the process of validating 2 different siRNA

against PMEPA1 that where designed and developed by the laboratory of Dr. Srivastava[(34)].

We also tested the effect of the overexpression of specific isoforms of PMEPA1 on the $(CAGA)_9$ promoter activity. In PC-3 cells, the overexpression of PMEPA1a or PMEPA1b, the membrane-bound isoforms, induced a significant decrease of TGF-β signaling (**Figure 25**). The overexpression of the cytosolic isoform PMEPA1c increased $(CAGA)_9$ activity but not significantly (**Figure 25**). The non-significant effect of PMEPA1c overexpression could be due to the presence of the endogenous protein in PC-3 cells. Thus we tested the effect of PMEPA1 expression in HepG2 that are not expressing PMEPA1. When membrane-bound PMEPA1a and b were overexpressed in HepG2 cells, there was also a significant decrease of TGF-β signaling while overexpression of the cytosolic PMEPA1c had not effect (**Figure 26A**).

To further analyze the elements responsible for PMEPA1 function, we used site-directed mutagenesis (Stratagene) to neutralize the SIM, the 1st or 2nd PPxY domain or both of them. Mutation of the SIM reverted the inhibition of TGF-β signaling mediated by membrane-bound PMEPA1a and b (**Figure 26A**). Similarly, inactivation of both PPxY domains in PMEPA1a and PMEPA1b prevented the inhibition of TGF-β signaling (**Figure 26A**). Inactivation of only 1 of the 2 PPxY domains did not prevent TGF-β signaling inhibition mediated by PMEPA1a or PMEPA1b (**Figure 26B**). When we transfected decreasing decreasing quantities of pcDNA-PMEPA1a plasmid, we observed that inhibition of TGF-β signaling by membrane-bound PMEPA1a was dose-dependent (**Figure 27**). These results show that binding to either E3 ubiquitin ligase or Smad is necessary for membrane-bound PMEPA1 to inhibit TGF-β signaling, suggesting that PMEPA1 is a docking protein allowing the targeting of Smad for proteosomal degradation.

Mutations of SIM or PPxY domains in cytosolic PMEPA1c had little effect on $(CAGA)_9$ promoter activity (**Figure 26A**). We hypothesized then that PMEPA1c can compete with membrane-bound PMEPA1 and prevent their inhibition of TGF-β signaling and coexpressed membrane-bound PMEPA1a in HepG2 cells with increasing quantities of cytosolic PMEPA1c. Cytosolic PMEPA1c significantly decreased membrane-bound PMEPA1a mediated inhibition of TGF-β signaling in a dose-dependent manner (**Figure 28**).

Opposite to the absence of effect of shPMEPA1 on BMP signaling, overexpression of the membrane-bound PMEPA1a significantly inhibited the activity of a BMP sensitive promoter (**Figure 29**). The inhibition was not rescued by the cytosolic PMEPA1c.

Task 9: Determine the effect of PMEPA1 overexpression or knockdown on the activity of Smad proteins.

Since the SIM and the PPxY domains are required for membrane-bound PMEPA1 to inhibit TGF-β signaling, it suggests that PMEPA1 recruits E3 ubiquitin ligase and presents Smad protein for proteosomal degradation. Thus we tested the effect of proteosome inhibitors on the effect of membrane-bound PMEPA1. We used 2 different proteosome inhibitors, MG132 and lactacystin, both at concentrations that allowed to detect the accumulation of ubiquitinated proteins in HepG2 cells by Western-Blot (**Figure 30A**). We tested then the effect of proteosome inhibition on the $(CAGA)_9$ promoter activity induced by TGF-β in HepG2 cells, in the presence or absence of membrane-bound PMEPA1a. However the results were inconclusive since inhibition of the proteosome by lactacystin and MG132 decreased $(CAGA)_9$ promoter activity (**Figure 30B**). This inhibition of TGF-β signaling mediated by proteosome inhibitors prevented from clearly studying the inhibition mediated by PMEPA1a. Although it does not appear that, in these conditions, proteosome inhibitors affected the PMEPA1a-induced inhibition of TGF-β signaling (**Figure 30B**).

To directly study the effect of PMEPA1 on Smad proteins, first, we tested the interaction of Smad2/3 proteins with PMEPA1. Smad2 or Smad3 and membrane-bound PMEPA1 (a or b) were overexpressed in COS cells. Immunoprecipitation of Smad2/3 proteins allowed to detect the co-immunoprecipitation of PMEPA1 proteins (**Figure 31**). No signal was detected when cells were not transfected to express PMEPA1 or in the immunoprecipitation control (in absence of antibody) (**Figure 31**).

Additional experiments are required to confirm the interaction of PMEPA1 with Smad proteins. First we will perform the counter-experiment and immunoprecipitate PMEPA1 to test for Smad coimmunoprecipitation. Thus we validated the newly available mouse monoclonal antibody against human PMEPA1 (Abnova) for immunoprecipitation experiments (**Figure 32**). We will also test the effect of the inactivation of the SIM in PMEPA1 on Smad coimmunoprecipitation. Once PMEPA1-Smad2/3 interaction will be established, we will be able to test the ubiquitination level of Smad protein interacting with PMEPA1.

KEY RESEARCH ACCOMPLISHMENTS

1. The expression of the gene PMEPA1 is regulated by TGF-β in a dose- and time-dependent manner.
2. Membrane-bound isoform PMEPA1a and the cytosolic isoform PMEPA1c are the 2 isoforms of PMEPA1 induced by TGF-β in prostate cancer cells.
3. TGF-β regulates PMEPA1 expression through transcriptional control via Smad and non-Smad mechanisms. TGF-β regulates PMEPA1 promoter activity within a 1.5kb region, independently of the predicted Smad Binding Elements.
4. TGF-β increases PMEPA1 expression in different TGF-β sensitive prostate, breast and lung cancer cell lines.
5. Knockdown of PMEPA1 expression in PC-3 prostate cancer cells decreases bone metastases suggesting a decrease of TGF-β signaling, contrarily to our hypothesis.
6. Membrane-bound isoforms of PMEPA1 inhibit TGF-β and BMP signaling.
7. Smad interaction motif and PPxY domains are required for membrane-bound PMEPA1 to TGF-β signaling.
8. Membrane-bound isoforms of PMEPA1 interact with Smad2 and Smad3.
9. The cytosolic isoform PMEPA1c rescue inhibition of TGF-β signaling mediated by membrane-bound PMEPA1 isoforms. PMEPA1c does not rescue the inhibition of BMP signaling.

REPORTABLE OUTCOMES

Awards
2008 AIMM/ASBMR John Haddad Young Investigator award, American Society for Bone and Mineral Research.
2008 Noa Siris Schwartz Research Award, Bone and Cancer Foundation.

Publications
1. D. Javelaud, K.S. Mohammad, C.R. McKenna, **P. Fournier**, F. Luciani, M. Niewolna, J. Andre, V. Delmas, L. Larue, T.A. Guise, and A. Mauviel. *Stable overexpression of Smad7 in human melanoma cells impairs bone metastasis*. Cancer Research. **67**(5):2317-2324. 2007.
2. **PG. Fournier**, and TA. Guise. *BMP7: a new Bone Metastases Prevention?* American Journal of Pathology. **17**1(3):739-43. 2007.
3. LA. Kingsley, **PG. Fournier**, JM. Chirgwin, and TA. Guise. *Molecular biology of bone metastasis*. Molecular Cancer Therapeutics. **6**(10):2609-17. 2007.
4. **PGJ. Fournier**, F. Daubiné, M.W. Lundy, M.J. Rogers, F.H. Ebetino and P. Clézardin. *Lowering bone mineral affinity of bisphosphonates as a therapeutic strategy to optimize skeletal tumor growth inhibition in vivo.* Cancer Research. **68**(21):8945-8953. 2008.
5. LK. Dunn, KS. Mohammad, **PGJ. Fournier**, CR. McKenna, HW. Davis, M. Niewolna, XH. Peng, JM. Chirgwin and TA. Guise. *Hypoxia and TGF-β Drive Breast Cancer Bone Metastases through Parallel Signaling Pathways in Tumor Cells and the Bone Microenvironment*. PLoS ONE. *Submitted*.

Oral Presentations
1. **PGJ. Fournier**, GA. Clines, JM. Chirgwin, and TA. Guise. *TGF-β Promotes Prostate Cancer Bone Metastases and Increases the Expression of Pro-Osteolytic Genes and of the TGF-β Signaling Regulator PMEPA1*. Skeletal Complications of Malignancy V. Paget Foundation. Philadelphia, PA, USA. 2007.
2. **PGJ. Fournier**, GA. Clines, JM. Chirgwin, and TA. Guise. *TGF-β Promotes Prostate Cancer Bone Metastases and Increases the Expression of Pro-Osteolytic Genes and of the TGF-β Signaling Regulator PMEPA1*. The 25th Annual American Cancer Society Virginia Cancer Researchers Seminar, Richmond, VA, USA. 2007.

3. **PGJ. Fournier**. *Mechanisms and treatment of bone metastases - Role of TGF-β and use of bisphosphonates*. Invitation from A. Mauviel, INSERM U697, Hôpital Saint Louis, Paris, France. 2007.
4. **PGJ. Fournier**. *TGF-β Signaling and Bisphosphonates in Bone Metastases.* Invitation from G. van der Pluijm, Leiden University Medical Center, Netherlands. 2007.
5. **PGJ**. Fournier. TGF-β promotes prostate cancer bone metastases and increases the expression of pro-osteolytic genes and of the TGF-β signaling regulator PMEPA1. AIMM/ASBMR John Haddad Young Investigator Meeting. Snowmass Village, CO, USA. 2007.

Posters
1. **PGJ. Fournier**, GA. Clines, JM. Chirgwin, and TA. Guise. *TGF-β Promotes Prostate Cancer Bone Metastases and Increases Expression of Pro-Osteolytic Genes and of the TGF-β Signaling Regulator PMEPA1*. FASEB Summer Research Conferences. TGF-β Superfamily: Signaling and Development. Tucson, AZ, USA. 2007.
2. **PGJ. Fournier**, GA. Clines, JM. Chirgwin, and TA. Guise. *TGF-β Increases Osteolytic Prostate Cancer Bone Metastases and Expression of Pro-Metastatic Genes.* American Society for Bone and Mineral Research 29th annual meeting. Honolulu, HI, USA. 2007.
3. **PGJ. Fournier**, GA. Clines, JM. Chirgwin and TA. Guise, *Transforming Growth Factor-β (TGF-β) Promotes Prostate Cancer Bone Metastases: Increased Expression of Pro-Osteolytic Genes and of PMEPA1, a New TGF-β Signalling Regulator.* Eight Cancer Induced Bone Disease Conference. Cancer and Bone Society. Edinburgh, UK. 2008.
4. **PGJ. Fournier**, GA Clines, JM. Chirgwin and TA Guise. *TGF-β Activates Prostate Cancer Bone Metastases, Pro-Osteolytic Gene Expression and the New TGF-β Signaling Regulator PMEPA1.* Transforming growth factor-beta signaling and cancer: the 28th Sapporo Cancer Seminar. Sapporo, Japan. 2008.
5. **PGJ. Fournier**, GA Clines, JM. Chirgwin and TA Guise. Transforming Growth Factor-β (TGF-β) Activates Prostate Cancer Bone Metastases, Pro-Osteolytic Gene Expression and the New TGF-β Signaling Regulator PMEPA1. American Society for Bone and Mineral Research 30th annual meeting. Montréal, QC, Canada. 2008.
6. **PGJ Fournier**, KS Mohammad, CR McKenna, XH Peng, JM Chirgwin, TA Guise. *TGF-β Blockade Inhibits Osteolytic but not Osteoblastic Prostate Cancer Metastases.* American Society for Bone and Mineral Research 30th annual meeting. Montréal, QC, Canada. 2008.
7. **PGJ. Fournier**, GA. Clines, JM. Chirgwin and TA Guise. *Transforming Growth Factor-β (TGF-β) Activates Prostate Cancer Bone Metastases, Pro-Osteolytic Gene Expression and the New TGF-β Signaling Regulator PMEPA1.* Anita Roberts Symposium, TGF-Beta: Discovery and Promise. NIH-NCI, Bethesda, MD, USA. 2008.

Funding for future project
1. PGJ Fournier (PI)   09/2008-09/2009
   Bone and Cancer Foundation
   T Cells in Bone Metastases and Role of the Bone Microenvironment
   Role: PI

2. PGJ Fournier (PI)   09/2008-09/2009
   Research & Development Committee at the University of Virginia
   T Cells in Bone Metastases and Role of the Bone Microenvironment
   Role: PI

CONCLUSIONS

TGF-β provided by the bone microenvironment is a key factor in the development of bone metastases. Previous experiments have demonstrated that interference with TGF-β signaling in cancer cells decreases the development of bone metastases. TGF-β stimulates prostate cancer cell signaling and alters their

phenotype.

TGF-β signaling in cancer is however complex and can lead to the activation of numerous genes. We identified PMEPA1 as the most highly upregulated gene by TGF-β in PC-3 cells. TGF-β induced the expression of membrane-bound PMEPA1a and cytosolic PMEPA1c in different prostate, breast and lung cancer cell lines treated with TGF-β. Results about PMEPA1 in the literature are contradictory; some studies report that PMEPA1 expression is expressed in prostate cancer, some others that it is decreased. Also, little is know about PMEPA1 function. We showed that knockdown of PMEPA1 in PC-3 cells increased bone metastases in mice. This result is consistent with *in vitro* experiments showing that the membrane-bound isoform PMEPA1a in PC-3 decrease TGF-β signaling. This biological property of PMEPA1a was dependent on its interaction with E3 ubiquitin ligase and Smad protein, which suggest that membrane-bound PMEPA1 target Smad protein for proteosomal degradation. Interestingly the cytosolic isoform of PMEPA1, which is also induced by TGF-β, prevented PMEPA1a to inhibit TGF-β signaling. It is possible that PMEPA1c compete with PMEPA1a to bind Smads. Their different localization in cells could then explain their different properties. These results suggest that depending on which isoform is the most abundant in cells, PMEPA1 can provide a positive or negative feedback loop for TGF-β signaling.

LIST OF PERSONNEL RECEIVING PAY FROM THE RESEARCH EFFORT

Pierrick G. Fournier, Ph.D. (PI)

REFERENCES

1.   Fidler, I. J. 2003. *The pathogenesis of cancer metastasis: the 'seed and soil' hypothesis revisited.* Nat Rev Cancer **3**(6):453-8.
2.   Yoneda, T., Sasaki, A., and Mundy, G. R. 1994. *Osteolytic bone metastasis in breast cancer.* Breast Cancer Res Treat **32**(1):73-84.
3.   Mundy, G. R. 2002. *Metastasis to bone: causes, consequences and therapeutic opportunities.* Nat Rev Cancer **2**(8):584-93.
4.   Kang, Y., and Massague, J. 2004. *Epithelial-mesenchymal transitions: twist in development and metastasis.* Cell **118**(3):277-9.
5.   Desruisseau, S., Ghazarossian-Ragni, E., Chinot, O., et al. 1996. *Divergent effect of TGFbeta1 on growth and proteolytic modulation of human prostatic-cancer cell lines.* Int J Cancer **66**(6):796-801.
6.   Ananth, S., Knebelmann, B., Gruning, W., et al. 1999. *Transforming growth factor b1 is a target for the von Hippel-Lindau tumor suppressor and a critical growth factor for clear cell renal carcinoma.* Cancer Res **59**(9):2210-6.
7.   Thomas, D. A., and Massague, J. 2005. *TGF-beta directly targets cytotoxic T cell functions during tumor evasion of immune surveillance.* Cancer Cell **8**(5):369-80.
8.   Muraoka, R. S., Dumont, N., Ritter, C. A., et al. 2002. *Blockade of TGF-b inhibits mammary tumor cell viability, migration, and metastases.* J. Clin. Invest. **109**(12):1551-59.
9.   Yang, Y.-a., Dukhanina, O., Tang, B., et al. 2002. *Lifetime exposure to a soluble TGF-{beta} antagonist protects mice against metastasis without adverse side effects.* J. Clin. Invest. **109**(12):1607-15.
10.   Yin, J. J., Selander, K., Chirgwin, J. M., et al. 1999. *TGF-beta signaling blockade inhibits PTHrP secretion by breast cancer cells and bone metastases development.* J Clin Invest **103**(2):197-206.
11.   Dallas, S. L., Rosser, J. L., Mundy, G. R., et al. 2002. *Proteolysis of Latent Transforming Growth Factor-beta (TGF-b)-binding Protein-1 by Osteoclasts. A CELLULAR MECHANISM FOR RELEASE OF TGF-b FROM BONE MATRIX.* J. Biol. Chem. **277**(24):21352-60.
12.   Kang, Y., Siegel, P. M., Shu, W., et al. 2003. *A multigenic program mediating breast cancer metastasis to bone.* Cancer Cell **3**(6):537-49.
13.   Le Brun, G., Aubin, P., Soliman, H., et al. 1999. *Upregulation of endothelin-1 and its precursor by Il-1b, TNF-a, and TGF-b in the PC3 human prosate cancer cell line.* Cytokine **11**(2):157-62.
14.   Yin, J. J., Mohammad, K. S., Kakonen, S. M., et al. 2003. *A causal role for endothelin-1 in the pathogenesis of osteoblastic bone metastases.* PNAS **100**(19):10954-59.

15. Guise, T. A., Yin, J. J., Taylor, S. D., et al. 1996. *Evidence for a Causal Role of Parathyroid Hormone-related Protein in the Pathogenesis of Human Breast Cancer-mediated Osteolysis.* J. Clin. Invest. **98**(7):1544-49.

16. Giannini, G., Ambrosini, M. I., Di Marcotullio, L., et al. 2003. *EGF- and cell-cycle-regulated STAG1/PMEPA1/ERG1.2 belongs to a conserved gene family and is overexpressed and amplified in breast and ovarian cancer.* Mol Carcinog **38**(4):188-200.

17. Reichling, T., Goss, K. H., Carson, D. J., et al. 2005. *Transcriptional profiles of intestinal tumors in Apc(Min) mice are unique from those of embryonic intestine and identify novel gene targets dysregulated in human colorectal tumors.* Cancer Res **65**(1):166-76.

18. Jolliffe, C. N., Harvey, K. F., Haines, B. P., et al. 2000. *Identification of multiple proteins expressed in murine embryos as binding partners for the WW domains of the ubiquitin-protein ligase Nedd4.* Biochem J **351 Pt 3**:557-65.

19. Xu, L. L., Shi, Y., Petrovics, G., et al. 2003. *PMEPA1, an androgen-regulated NEDD4-binding protein, exhibits cell growth inhibitory function and decreased expression during prostate cancer progression.* Cancer Res **63**(15):4299-304.

20. Ingham, R. J., Gish, G., and Pawson, T. 2004. *The Nedd4 family of E3 ubiquitin ligases: functional diversity within a common modular architecture.* Oncogene **23**(11):1972-84.

21. Izzi, L., and Attisano, L. 2004. *Regulation of the TGFbeta signalling pathway by ubiquitin-mediated degradation.* Oncogene **23**(11):2071-8.

22. Seo, S. R., Lallemand, F., Ferrand, N., et al. 2004. *The novel E3 ubiquitin ligase Tiul1 associates with TGIF to target Smad2 for degradation.* Embo J **23**(19):3780-92.

23. Derynck, R., and Zhang, Y. E. 2003. *Smad-dependent and Smad-independent pathways in TGF-beta family signalling.* Nature **425**(6958):577-84.

24. Kakonen, S. M., Selander, K. S., Chirgwin, J. M., et al. 2002. *Transforming growth factor-beta stimulates parathyroid hormone-related protein and osteolytic metastases via Smad and mitogen-activated protein kinase signaling pathways.* J Biol Chem **277**(27):24571-8.

25. Kang, Y., He, W., Tulley, S., et al. 2005. *Breast cancer bone metastasis mediated by the Smad tumor suppressor pathway.* Proc Natl Acad Sci U S A **102**(39):13909-14.

26. Kim, I. Y., Ahn, H. J., Zelner, D. J., et al. 1996. *Genetic change in transforming growth factor beta (TGF-beta) receptor type I gene correlates with insensitivity to TGF-beta 1 in human prostate cancer cells.* Cancer Res **56**(1):44-8.

27. Zhang, Q., Rubenstein, J. N., Jang, T. L., et al. 2005. *Insensitivity to transforming growth factor-beta results from promoter methylation of cognate receptors in human prostate cancer cells (LNCaP).* Mol Endocrinol **19**(9):2390-9.

28. Guo, Y., and Kyprianou, N. 1998. *Overexpression of transforming growth factor (TGF) beta1 type II receptor restores TGF-beta1 sensitivity and signaling in human prostate cancer cells.* Cell Growth & Differentiation: The Molecular Biology Journal Of The American Association For Cancer Research **9**(2):185.

29. Zhao, H., Shiina, H., Greene, K. L., et al. 2005. *CpG methylation at promoter site -140 inactivates TGFbeta2 receptor gene in prostate cancer.* Cancer **104**(1):44-52.

30. Kuratomi, G., Komuro, A., Goto, K., et al. 2005. *NEDD4-2 (neural precursor cell expressed, developmentally down-regulated 4-2) negatively regulates TGF-beta (transforming growth factor-beta) signalling by inducing ubiquitin-mediated degradation of Smad2 and TGF-beta type I receptor.* Biochem J **386**(Pt 3):461-70.

31. Korchynskyi, O., and ten Dijke, P. 2002. *Identification and functional characterization of distinct critically important bone morphogenetic protein-specific response elements in the Id1 promoter.* J Biol Chem **277**(7):4883-91.

32. Buijs, J., T, Rentsch, C., A, van der Horst, G., et al. 2007. *BMP7, a Putative Regulator of Epithelial Homeostasis in the Human Prostate, is a Potent Inhibitor of Prostate Cancer Bone Metastasis In Vivo.* American Journal of Pathology

33. Fournier, P. G., and Guise, T. A. 2007. *BMP7: a new bone metastases prevention?* Am J Pathol **171**(3):739-43.

34. Li, H., Xu, L. L., Masuda, K., et al. 2008. *A feedback loop between the androgen receptor and a NEDD4-binding protein, PMEPA1, in prostate cancer cells.* J Biol Chem **283**(43):28988-95.

APPENDICES

1. Abstract from the Skeletal Complications of Malignancy V Meeting.

TGF-β promotes prostate cancer bone metastases and increases expression of pro-osteolytic genes and of the TGF-β signaling regulator PMEPA1

PGJ Fournier, GA Clines, JM Chirgwin, TA Guise. Medicine/Endocrinology, University of Virginia, Charlottesville, VA, USA

Prostate cancers commonly metastasize to bone and stimulate abnormal bone resorption and bone formation. Tumors which colonize bone are exposed to high concentrations of growth factors housed in bone matrix, such as insulin-like growth factors and transforming growth factor-β (TGF-β). These factors are released by osteoclastic resorption and fuel a vicious cycle of metastatic growth by changing the phenotype of the tumor cells. TGF-β is central to the pathogenesis of osteolytic metastases due to breast cancer and melanoma, but its role in prostate cancer bone metastases is less clear. We hypothesized that TGF-β would also promote prostate cancer bone metastases.

A specific inhibitor of the TGF-β type I receptor (TβRI) kinase, SD-208, decreased TGF-β-dependent Smad2 phosphorylation in PC-3 human prostate cancer cells *in vitro*. In vivo, PC-3 cells cause osteolytic bone metastases when inoculated into the left cardiac ventricle of male nude mice. Mice given 50mg/kg SD-208 daily had significantly decreased osteolytic bone metastases and increased survival compared to vehicle-treated mice when receiving drug from the time of tumor inoculation (prevention protocol). In a treatment protocol where mice receive drug from the time of detected osteolytic lesions, SD-208 at the same dose significantly decreased malignant osteolysis but did not improve survival. Therefore,TGF-β also promotes prostate cancer bone metastases.

To determine genes regulated by TGF-β, we analyzed PC-3 cells treated with TGF-β (24h, 5ng/mL) by Affymetrix gene array using DMT and dCHIP data analyses. Significantly upregulated genes included known TGF-β targets PTHrP, CTGF, MMP-13, TSP-1 and ADAM19, which function in bone remodeling or are dysregulated in cancer. The most increased gene was PMEPA1 (23.2-fold, $P<0.03$), a protein highly expressed in breast, colon and prostate cancers. Using real-time RT-PCR of RNA from PC-3 cells treated with TGF-β (5ng/mL, for 0 to 48h), we confirmed that PMEPA1 mRNA was rapidly induced and peaked at 24h (16.7-fold, $P<0.05$). TGF-β also increased PMEPA1 mRNA in prostate, breast and lung cancer lines. Treatment of PC-3 cells with SD-208, actinomycin D, or cycloheximide showed that TGF-β directly activates PMEPA1 transcription. TGF-β also increased PMEPA1 protein in PC-3 by Western blot; the induction was prevented by SD-208. We cloned and made deletion mutants in 3.7kb of the human PMEPA1 promoter, which contains 5 putative Smad-binding elements. Dual-luciferase assays and overexpression of Smads 2, 3 and 4 or inhibitory Smad7, indicated that PMEPA1 transcription is regulated by TGF-β via both Smad-dependent and -independent pathways.

PMEPA1 binds to the E3 ubiquitin ligase Nedd4, a relative of the Smurf proteins that inhibit TGF-β signaling, suggesting that PMEPA1 could regulate TGF-β signaling. Multiple PMEPA1 transcripts encode 3 protein isoforms with differing N-termini: 2 with a transmembrane domain, while the 3rd one is cytosolic. Sequences encoding each of the isoforms were expressed in A549 lung cancer cells to test their effects on the Smad-responsive (CAGA)$_9$ promoter. The membrane-bound PMEPA1 isoforms significantly inhibited the TGF-β-induced luciferase activity, while the cytosolic isoform did not. The membrane bound isoforms also reduced the Smad7-mediated inhibition of (CAGA)$_9$ promoter activity. The results suggest that membrane localization is required for the PMEPA1 inhibition of Smad-mediated TGF-β signaling.

Preliminary data suggest that cytosolic PMEPA1 is the most abundant TGF-β-induced isoform in PC-3 prostate cancer cells. We hypothesize that bone-derived TGF-β acts on metastatic prostate cancer cells to increase the non-inhibitory, cytosol isoform of PMEPA1, thereby potentiating TGF-β signaling and enhancing bone metastases.

2. Abstract from the 25th Annual American Cancer Society Virginia Cancer Researchers Seminar.

TGF-β promotes prostate cancer bone metastases and increases the expression of pro-osteolytic genes and of the TGF-β signaling regulator PMEPA1

PGJ Fournier, GA Clines, JM Chirgwin, TA Guise. Medicine/Endocrinology, University of Virginia, Charlottesville, VA, USA.

Prostate cancers commonly metastasize to bone stimulating abnormal bone resorption and bone formation. Tumors which colonize bone are exposed to high concentrations of growth factors. These are released during the osteoclastic resorption and fuel a vicious cycle of metastatic growth. Transforming growth factor-β (TGF-β) has been implicated as central in bone metastases from breast cancer and melanoma, but its role in prostate cancer bone metastases has been less studied.

We used an inhibitor specific of the TGF-β type I receptor (TβRI) kinase domain, SD-208, to test the role of TGF-β in prostate cancer bone metastases. SD-208 inhibited Smad2 phosphorylation induced by TGF-β in PC-3 prostate cancer cells *in vitro*. In a mouse bone metastases model, human PC-3 prostate cancer cells cause osteolytic bone metastases when inoculated into the left cardiac ventricle of male *nude* mice. Mice treated with SD-208, 50mg/kg/day, had significantly less osteolysis due to bone metastases and increased survival compared with vehicle-treated mice. This was evident when mice received drug at either the time of tumor inoculation (prevention setting) or at the time of established osteolytic lesions (treatment setting).

To determine downstream targets of TGF-β in prostate cancer, we analyzed PC-3 cells treated with TGF-β (24h, 5ng/mL) by Affymetrix gene array. Significantly upregulated genes included the known TGF-β targets PTHrP, CTGF, MMP-13, TSP-1 and ADAM19, which function in bone remodeling or are dysregulated in cancer.

The most increased gene was PMEPA1 (23.2-fold), a protein highly expressed in breast, colon and ovarian cancers. We validated that PMEPA1 mRNA was rapidly induced by TGF-β and peaked at 4 hours. TGF-β also increased PMEPA1 protein production in PC-3. PMEPA1 is expressed and up-regulated in other prostate, breast and lung cancer cells. Treating PC-3 cells with the classical actinomycin D or cycloheximide showed that TGF-β directly activates PMEPA1 transcription. Dual-Luciferase analysis of a 3.7kb fragment of PMEPA1 promoter and deletion fragments indicated that TGF-β regulates PMEPA1 transcription via Smad and non-Smad mechanisms. PMEPA1 interacts with the E3 ubiquitin ligase Nedd4 related to the Smurfs which inhibit TGF-β signaling by targeting Smads and TβRI for proteasomal degradation. A sequence homolog to the Smad Interaction Motif of DNA-binding cofactors was also identified in the C-terminus of PMEPA1 suggesting direct interaction with Smad proteins. PMEPA1 could then regulate TGF-β signaling. Using shRNAs we observed that PMEPA1 knock-down in PC-3 cells decreased TGF-β signaling.

We hypothesize that at sites of bone metastases PMEPA1 induced by bone-derived TGF-β will potentiate TGF-β signaling in cancer cells and further enhance bone metastases.

3. Abstract from the FASEB Summer Research Conferences. TGF-β Superfamily: Signaling and Development.

TGF-β promotes prostate cancer bone metastases and increases expression of pro-osteolytic genes and of the TGF-β signaling regulator PMEPA1

PGJ Fournier, GA Clines, JM Chirgwin, TA Guise. Medicine/Endocrinology, University of Virginia, Charlottesville, VA, USA.

Prostate cancers commonly metastasize to bone and stimulate abnormal bone resorption and bone formation. Tumors which colonize bone are exposed to high concentrations of growth factors housed in bone matrix, such as insulin like growth factors and transforming growth factor-β (TGF-β). These factors are released by osteoclastic resorption and fuel a vicious cycle of metastatic growth by changing the phenotype

of the tumor cells. TGF-β is central to the pathogenesis of osteolytic metastases due to breast cancer and melanoma, but its role in prostate cancer bone metastases is less clear. We hypothesized that TGF-β would also promote prostate cancer bone metastases.

A specific inhibitor of the TGF-β type I receptor (TβRI) kinase, SD-208, decreased TGF-β-dependent Smad2 phosphorylation in PC-3 human prostate cancer cells *in vitro*. In vivo, PC-3 cells cause osteolytic bone metastases when inoculated into the left cardiac ventricle of male nude mice. Mice given 50mg/kg SD-208 daily had significantly decreased osteolytic bone metastases and increased survival compared to vehicle-treated mice. This occurred when mice received drug either at the time of tumor inoculation (prevention setting) or at the time of established osteolytic lesions (treatment setting).

To determine genes regulated by TGF-β, we analyzed PC-3 cells treated with TGF-β (24h, 5ng/mL) by Affymetrix gene array andDMT and dCHIP data analyses. Significantly upregulated genes included known TGF-β targets PTHrP, CTGF, MMP-13, TSP-1 and ADAM19, which function in bone remodeling or are dysregulated in cancer. The most increased gene was PMEPA1 (23.2-fold, *P*<0.03), a protein highly expressed in breast, colon and prostate cancers. Using real-time RT-PCR of RNA from PC-3 cells treated with TGF-β (5ng/mL, for 0 to 48h), we confirmed that PMEPA1 mRNA was rapidly induced and peaked at 24h (16.7-fold, *P*<0.05). TGF-β also increased PMEPA1 mRNA in prostate, breast and lung cancer lines. Treatment of PC-3 cells with SD-208, actinomycin D, or cycloheximide showed that TGF-β directly activates PMEPA1 transcription. TGF-β also increased PMEPA1 protein in PC-3 by Western blot; the induction was prevented by SD-208. We cloned and made deletion mutants in 3.7kb of the human PMEPA1 promoter, which contains 5 putative Smad-binding elements. Dual-luciferase assays and overexpression of Smads 2, 3 and 4 or inhibitory Smad7, indicated that PMEPA1 transcription is regulated by TGF-β via both Smad-dependent and -independent pathways.

PMEPA1 binds to the E3 ubiquitin ligase Nedd4, which is related to the Smurf proteins that inhibit TGF-β signaling. PMEPA1 could then regulate TGF-β signaling. PMEPA1 transcripts encode 3 protein isoforms with differing N-termini: 2 with a transmembrane domain, while the 3rd one is cytosolic. Sequences encoding each of the isoforms were expressed in A549 lung cancer cells to test their effects on the Smad-responsive $(CAGA)_9$ promoter. The membrane-bound PMEPA1 isoforms significantly inhibited the TGF-β-induced luciferase activity, while the cytosolic isoform did not. The membrane bound isoforms also reduced the Smad7-mediated inhibition of $(CAGA)_9$ promoter activity. The results suggest that membrane localization is required for the PMEPA1 inhibition of Smad-mediated TGF-β signaling.

Preliminary data suggest that cytosolic PMEPA1 is the most abundant TGF-β-induced isoform in PC-3 prostate cancer cells. We hypothesize that bone-derived TGF-β acts on metastatic prostate cancer cells to increase the non-inhibitory, cytosol isoform of PMEPA1, thereby potentiating TGF-β signaling and enhancing bone metastases.

4. Abstract from the American Society for Bone and Mineral Research 29th annual meeting.

TGF-β increases osteolytic prostate cancer bone metastases and expression of pro-metastatic genes

PGJ Fournier, GA Clines, JM Chirgwin, TA Guise
Endocrinology, University of Virginia, Charlottesville, VA, USA

Prostate cancers commonly metastasize to bone, where high concentrations of TGF-β are released by osteoclastic resorption. TGF-β stimulates production of PTHrP, IL-11 and CTGF, which are central factors in bone metastases due to breast cancer and melanoma. We hypothesized that TGF-β would also promote prostate cancer bone metastases.

First, we showed that a specific inhibitor of the TGF-β type I receptor (TβRI) kinase, SD-208, inhibited TGF-β-dependent Smad2 phosphorylation in PC-3 prostate cancer cells *in vitro*. Mice were inoculated with PC-3 cells via the left cardiac ventricle. In both prevention and treatment protocols, SD-208 (50mg/kg/d) decreased osteolytic metastases and increased survival. To determine downstream targets of TGF-β in prostate cancer, we analyzed PC-3 cells treated with TGF-β (24h, 5ng/mL) by Affymetrix gene array with

DMT and dCHIP data analyses. Significantly upregulated genes included known TGF-β targets PTHrP, CTGF, MMP-13, TSP-1 and ADAM19, which function in bone remodeling or are dysregulated in cancer.

The most increased gene was PMEPA1 (23.2-fold, $P<0.03$), a protein highly expressed in breast, colon and prostate cancers. Using real-time qPCR of RNA from PC-3 cells treated with TGF-β (5ng/mL, for 0 to 48h), we confirmed that PMEPA1 mRNA was rapidly induced and peaked at 24h (16.7-fold, $P<0.05$). TGF-β also increased PMEPA1 mRNA in prostate, breast and lung cancer lines. PC-3 cells were treated with SD-208, the transcription inhibitor actinomycin D, or the translation inhibitor cycloheximide; the results showed that TGF-β directly activates PMEPA1 transcription. TGF-β also increased PMEPA1 protein production in PC-3 by Western blot; the induction was prevented by SD-208. We cloned and made deletion mutants in 3.7kb of the PMEPA1 promoter, which contains 5 putative Smad binding elements. Dual-luciferase assays and overexpression of Smad2, -3 and -4, indicated that PMEPA1 transcription is regulated by TGF-β via both Smad-dependent and independent pathways.

PMEPA1 interacts with the E3 ubiquitin ligase Nedd4, which is related to the Smurfs. These proteins inhibit TGF-β signaling by targeting Smads and TβRI for proteasomal degradation. PMEPA1 could prevent proteasomal inhibition of the TGF-β pathway by suppressing Nedd4/Smurf activity, leading to sustained TGF-β signaling in bone metastases. Our data indicate that TGF-β promotes osteolytic bone metastases by stimulating known prometastatic factors, as well as novel factors that may enhance TGF-β signaling in the tumor cell. Thus, TGF-β inhibitors should be effective treatments for osteolytic prostate cancer bone metastases.

5. Abstract from the 8th Cancer Induced Bone Disease Conference.

Transforming Growth Factor-β (TGF-β) Promotes Prostate Cancer Bone Metastases: Increased Expression of Pro-Osteolytic Genes and of PMEPA1, a New TGF-β Signalling Regulator

PGJ. Fournier, GA. Clines, JM. Chirgwin and TA. Guise. Medicine/Endocrinology, University of Virginia, Charlottesville, VA, USA.

TGF-β has a central role in breast cancer and melanoma metastases to bone. We hypothesized that TGF-β would also promote prostate cancer bone metastases.

A specific inhibitor of the TGF-β type I receptor kinase, SD-208, decreased Smad2 phosphorylation induced by TGF-β in PC-3 human prostate cancer cells. *In vivo* osteolytic bone metastases were caused by inoculating PC-3 cells in the left cardiac ventricle of athymic mice. SD-208 (50mg/kg/day) started at the time of tumor inoculation significantly decreased osteolytic bone metastases and increased mouse survival. When treatment began after osteolytic lesions were detected, the same dose of SD-208 significantly decreased bone destruction but did not improve survival.

To determine downstream targets of TGF-β in prostate cancer, we analyzed PC-3 cells treated ±TGF-β (5ng/mL) by Affimetrix gene array. Significantly upregulated genes included PTHrP, CTGF, MMP-13, TSP-1 and ADAM19, which function in bone remodeling or are dysregulated in cancer. The most increased gene was PMEPA1 (>20x), a protein highly expressed in breast, colon, prostate cancers. sqRT-PCR of RNA from PC-3 cells treated ±TGF-β and ±cycloheximide or ±actinomycin-D showed that TGF-β directly transcriptionally activates PMEPA1. Dual-luciferase analysis of a 3.7kb fragment of the human PMEPA1 promoter and deletion constructs showed that TGF-β regulates PMEPA1 transcription through Smad and non-Smad mechanisms. Western-Blot confirmed that TGF-β as low as 0.1ng/mL quickly and dose-dependently increased the production of the cytosolic isoform of PMEPA1 protein in PC-3.

PMEPA1 encodes PPxY domains which can interact with ubiquitin ligases like Smurf, and a Smad interaction motif, suggesting that PMEPA1 may regulate TGF-β signaling. shRNA knockdown of PMEPA1 significantly decreased TGF-β-induction of the synthetic Smad reporter (CAGA)$_9$. Thus PMEPA1 induced by bone-derived TGF-β could potentiate TGF-β signaling in cancer cells and enhance prostate cancer bone metastases.

6. Abstract from the 28th Sapporo Cancer Seminar.

TGF-β Activates Prostate Cancer Bone Metastases, Pro-Osteolytic Gene Expression and the New TGF-β Signaling Regulator PMEPA1

PGJ. Fournier, GA. Clines, JM. Chirgwin and TA. Guise. Medicine/Endocrinology, University of Virginia, Charlottesville, VA, USA.

Prostate cancers commonly metastasize to bone and stimulate abnormal bone resorption and bone formation. Tumors which colonize bone are exposed to high concentrations of growth factors housed in bone matrix, such as insulin like growth factors and transforming growth factor-β (TGF-β). These factors are released by osteoclastic resorption and fuel a vicious cycle of metastatic growth by changing the phenotype of the tumor cells. TGF-β is central to the pathogenesis of osteolytic metastases due to breast cancer and melanoma, but its role in prostate cancer bone metastases is less clear. We hypothesized that TGF-β would also promote prostate cancer bone metastases.

A specific inhibitor of the TGF-β type I receptor kinase, SD-208, decreased Smad2 phosphorylation induced by TGF-β in PC-3 human prostate cancer cells. Osteolytic bone metastases were caused by inoculating PC-3 cells in the left cardiac ventricle of athymic mice. SD-208 (50mg/kg/d po) begun at the time of tumor inoculation decreased osteolytic bone metastases (56% decrease, $P<0.05$) and increased survival (57 to 69 days median survival, $P<0.05$). When treatment began after osteolytic lesions were detected, SD-208 decreased bone destruction (47% decrease, $P<0.05$) without significantly improving survival (51 to 55 days, $P>0.1$).

We analyzed PC-3 cells treated ± TGF-β (5ng/mL) by Affimetrix gene array and sqRT-PCR. Significantly up-regulated genes included PTHrP, IL-11, CTGF and ADAM19, which can increase bone resorption, as well as MMP-13 and thrombospondin-1, two activators of TGF-β.

The most increased gene was PMEPA1 (>20x), a protein highly expressed in breast, colon and prostate cancers. sqRT-PCR of mRNA from PC-3 cells treated ±TGF-β and ±cycloheximide or ±actinomycin-D showed that TGF-β directly controls PMEPA1 transcription. Dual-luciferase experiments showed that a 3.7kb fragment of PMEPA1 promoter is activated by TGF-β. This fragment contains 5 consensus Smad binding elements, but mutagenesis showed that they are not involved in TGF-β induction. Analysis of promoter deletion constructs and overexpression of Smad2, 3 and 4 demonstrate that TGF-β induction of PMEPA1 promoter is mediated by a 1.2kb proximal fragment through both Smad and non-Smad mechanisms.

Western blotting confirmed that TGF-β quickly and dose-dependently increased the cytosolic isoform of PMEPA1 in PC-3 cells. PMEPA1 proteins contain 2 PPxY domains that can interact with Smurf ubiquitin ligases (which can regulate degradation of Smads and type I TGF-β receptor) and a Smad-interaction motif (found in DNA binding co-factors that control the affinity of Smads for DNA), suggesting that PMEPA1 regulates TGF-β signaling. shRNA knockdown of PMEPA1 significantly decreased TGF-β activation of the Smad reporter (CAGA)$_9$. PMEPA1 induced by bone-derived TGF-β could potentiate TGF-β signaling in cancer cells.

Our results show that TGF-β can promote PC-3 bone metastases through a transcriptional program that increases bone resorption and potentiates TGF-β signaling.

7. First abstract submitted to the American Society for Bone and Mineral Research 30th annual meeting.

Transforming Growth Factor-β (TGF-β) Activates Prostate Cancer Bone Metastases, Pro-Osteolytic Gene Expression and the New TGF-β Signaling Regulator PMEPA1.

PGJ. Fournier, GA. Clines, JM. Chirgwin and TA. Guise. Medicine/Endocrinology, University of Virginia, Charlottesville, VA, USA.

TGF-β increases breast cancer and melanoma bone metastases by activating pro-osteolytic genes (PTHrP, IL-11 or CTGF). We hypothesized that TGF-β would also promote prostate cancer bone metastases.

A specific inhibitor of the TGF-β type I receptor kinase, SD-208, decreased Smad2 phosphorylation induced by TGF-β in PC-3 human prostate cancer cells. Osteolytic bone metastases were caused by inoculating PC-3 cells in the left cardiac ventricle of athymic mice. SD-208 (50mg/kg/d po) begun at the time of tumor inoculation decreased osteolytic bone metastases (56% decrease, $P<0.05$) and increased survival (57 to 69 days median survival, $P<0.05$). When treatment began after osteolytic lesions were detected, SD-208 decreased bone destruction (47% decrease, $P<0.05$) without significantly improving survival (51 to 55 days, $P>0.1$).

We analyzed PC-3 cells treated ± TGF-β (5ng/mL) by Affimetrix gene array and sqRT-PCR. Significantly up-regulated genes included PTHrP, IL-11, CTGF and ADAM19, which can increase bone resorption, as well as MMP-13 and thrombospondin-1, two activators of TGF-β.

The most increased gene was PMEPA1 (>20x), a protein highly expressed in breast, colon and prostate cancers. sqRT-PCR of mRNA from PC-3 cells treated ±TGF-β and ±cycloheximide or ±actinomycin-D showed that TGF-β directly controls PMEPA1 transcription. Dual-luciferase experiments showed that a 3.7kb fragment of PMEPA1 promoter is activated by TGF-β. This fragment contains 5 consensus Smad binding elements, but mutagenesis showed that they are not involved in TGF-β induction. Analysis of promoter deletion constructs and overexpression of Smad2, 3 and 4 demonstrate that TGF-β induction of PMEPA1 promoter is mediated by a 1.2kb proximal fragment through both Smad and non-Smad mechanisms.

Western blotting confirmed that TGF-β quickly and dose-dependently increased the cytosolic isoform of PMEPA1 in PC-3 cells. PMEPA1 proteins contain 2 PPxY domains that can interact with Smurf ubiquitin ligases (which can regulate degradation of Smads and type I TGF-β receptor) and a Smad-interaction motif (found in DNA binding co-factors that control the affinity of Smads for DNA), suggesting that PMEPA1 regulates TGF-β signaling. shRNA knockdown of PMEPA1 significantly decreased TGF-β activation of the Smad reporter (CAGA)$_9$. PMEPA1 induced by bone-derived TGF-β could potentiate TGF-β signaling in cancer cells.

Our results show that TGF-β can promote PC-3 bone metastases through a transcriptional program that increases bone resorption and potentiates TGF-β signaling.

8. Second abstract submitted to the American Society for Bone and Mineral Research 30th annual meeting.

TGF-β Blockade Inhibits Osteolytic but not Osteoblastic Prostate Cancer Metastases.

PGJ Fournier, KS Mohammad, CR McKenna, XH Peng, JM Chirgwin, TA Guise. Medicine/Endocrinology, University of Virginia, Charlottesville, VA, USA.

Transforming growth factor-β (TGF-β) increases breast cancer and melanoma bone metastases by activating pro-osteolytic genes (PTHrP, IL-11 or CTGF). We hypothesized that TGF-β would also promote prostate cancer bone metastases.

A specific inhibitor of the TGF-β type I receptor kinase, SD-208, decreased Smad2 phosphorylation induced by TGF-β in PC-3 human prostate cancer cells. Osteolytic bone metastases were caused by inoculating PC-3 cells in the left cardiac ventricle of athymic mice. SD-208 (50mg/kg/d po) begun at the time of tumor inoculation decreased osteolytic bone metastases (56% decrease, P<0.05) and increased survival (57 to 69 days median survival, P<0.05). When treatment began after osteolytic lesions were detected, SD-208 decreased bone destruction (47% decrease, P<0.05) without significantly improving survival (51 to 55 days, P>0.1).

We analyzed PC-3 cells treated ± TGF-β (5ng/mL) by Affimetrix gene array and sqRT-PCR. Significantly up-regulated genes included PTHrP, IL-11, CTGF and ADAM19, which can increase bone resorption, as well as MMP-13 and thrombospondin-1, two activators of TGF-β.

The most increased gene was PMEPA1 (>20x), a protein highly expressed in breast, colon and prostate cancers. sqRT-PCR of mRNA from PC-3 cells treated ±TGF-β and ±cycloheximide or ±actinomycin-D

showed that TGF-β directly controls PMEPA1 transcription. Dual-luciferase experiments showed that a 3.7kb fragment of PMEPA1 promoter is activated by TGF-β. This fragment contains 5 consensus Smad binding elements, but mutagenesis showed that they are not involved in TGF-β induction. Analysis of promoter deletion constructs and overexpression of Smad2, 3 and 4 demonstrate that TGF-β induction of PMEPA1 promoter is mediated by a 1.2kb proximal fragment through both Smad and non-Smad mechanisms.

Western blotting confirmed that TGF-β quickly and dose-dependently increased the cytosolic isoform of PMEPA1 in PC-3 cells. PMEPA1 proteins contain 2 PPxY domains that can interact with Smurf ubiquitin ligases (which can regulate degradation of Smads and type I TGF-β receptor) and a Smad-interaction motif (found in DNA binding co-factors that control the affinity of Smads for DNA), suggesting that PMEPA1 regulates TGF-β signaling. shRNA knockdown of PMEPA1 significantly decreased TGF-β activation of the Smad reporter (CAGA)$_9$. PMEPA1 induced by bone-derived TGF-β could potentiate TGF-β signaling in cancer cells.

Our results show that TGF-β can promote PC-3 bone metastases through a transcriptional program that increases bone resorption and potentiates TGF-β signaling.

9. Abstract from the Anita Roberts Symposium, TGF-Beta: Discovery and Promise.

Transforming Growth Factor-β (TGF-β) Activates Prostate Cancer Bone Metastases, Pro-Osteolytic Gene Expression and the New TGF-β Signaling Regulator PMEPA1.

PGJ. Fournier, GA. Clines, JM. Chirgwin and TA. Guise. Medicine/Endocrinology, University of Virginia, Charlottesville, VA, USA.

TGF-β has a central role in breast cancer and melanoma bone metastases. We hypothesized that TGF-β would also promote prostate cancer bone metastases.

A specific inhibitor of the TGF-β type I receptor, SD-208 was tested in a mouse model. SD-208 (50mg/kg/day) started at the time of tumor inoculation significantly decreased osteolytic bone metastases caused by PC-3 prostate cancer cells in athymic mice and increased mouse survival. When treatment began after osteolytic lesions were detected, the same dose of SD-208 significantly decreased bone destruction but did not improve survival.

To determine downstream targets of TGF-β in prostate cancer, we analyzed PC-3 cells treated ±TGF-β by gene array. Significantly upregulated genes included PTHrP, CTGF, MMP-13, TSP-1 and ADAM19, which functions are dysregulated in bone remodeling and cancer. The most increased gene was PMEPA1 (>20x), a protein highly expressed in breast, colon, prostate cancers. sqRT-PCR of RNA from PC-3 cells treated ±TGF-β and ±cycloheximide or ±actinomycin-D showed that TGF-β directly transcriptionally activates PMEPA1. Dual-luciferase analysis of a fragment of the PMEPA1 promoter showed that TGF-β regulates PMEPA1 transcription through Smad and non-Smad mechanisms. Western-Blot confirmed that TGF-β as low as 0.1ng/mL quickly and dose-dependently increased the production of the cytosolic isoform of PMEPA1 protein in PC-3.

PMEPA1 interacts with R-Smads and HECT ubiquitin ligases, like Smurfs, suggesting that PMEPA1 regulates TGF-β signaling. Knockdown of PMEPA1 significantly decreased TGF-β-induction of the synthetic Smad reporter (CAGA)$_9$. Thus PMEPA1 induced by bone-derived TGF-β could potentiate TGF-β signaling in cancer cells and enhance prostate cancer bone metastases.

SUPPORTING DATA

cf pages 24 to 53
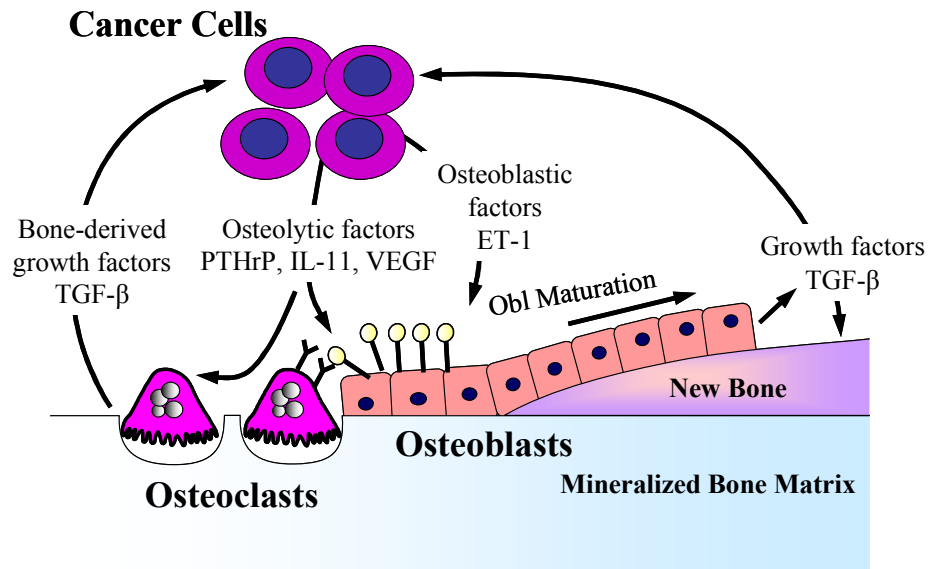
Figure 1. Tumor-bone cell interactions in the vicious cycle of bone metastases. Tumor stimulation of osteoblasts can increase both new bone formation and resorption. Tumor products, such as ET-1, stimulate osteoblasts proliferation. Immature osteoblasts respond to osteolytic cytokines, such as PTHrP, by expressing RANK ligand. RANK ligand stimulates bone resorption by osteoclasts, which release growth factors from mineralized matrix. Mature osteoblasts synthesize growth factors stimulate tumor cells. TGF-β is one of the major factors synthesized by osteoblasts, stored in mineralized bone matrix, and released by osteoclastic bone resorption**.**
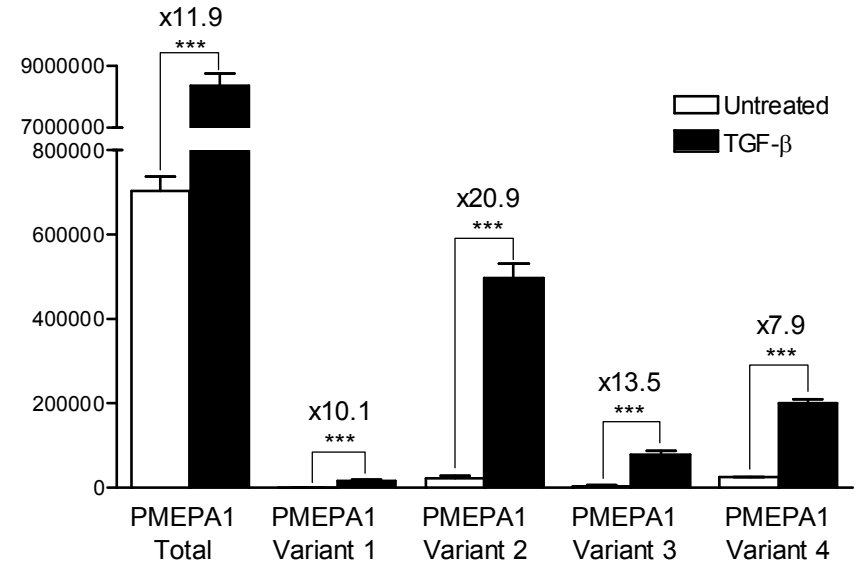
Figure 2. TGF-β increases the expression of all PMEPA1 variants in PC-3 prostate cancer cells. PC-3 cells were treated or not treated with TGF-β (5ng/mL, 24h) before extracting total RNA and preparing cDNA. Expression of each variant of PMEPA1 was quantified using real-time PCR and normalized to the endogenous ribosomal protein L32. Results are shown as the average ± SD of 3 independent experiments. ***, $P<0.001$ when compared to the untreated cells, using a non-parametric Mann-Whitney's U test.
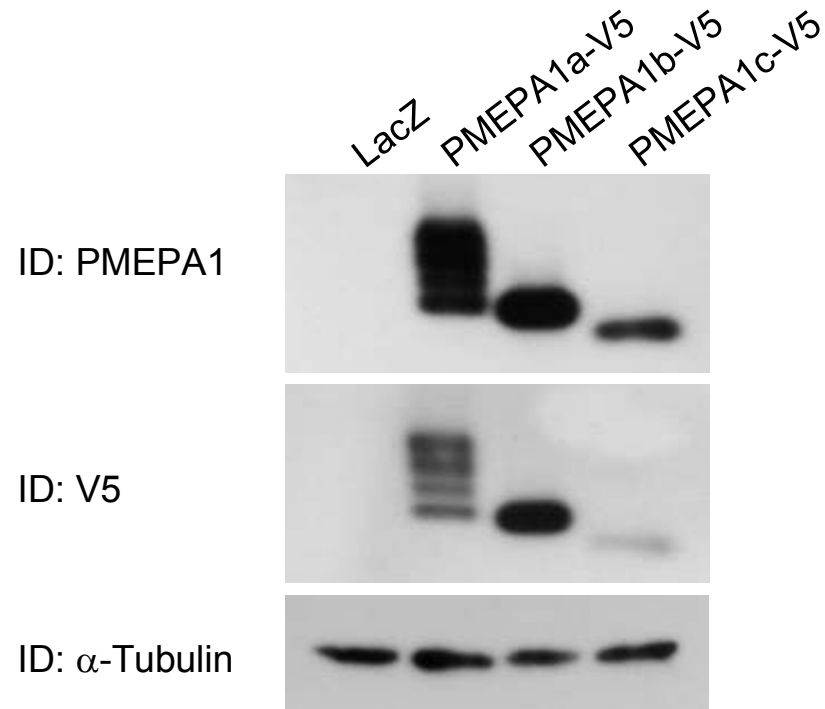
Figure 3. Validation of the antibody against PMEPA1. COS-1 were transfected with plasmid coding for LacZ, or the different isoforms of the PMEPA1 proteins tagged with V5. Protein lysates were analyzed by Western-blotting against PMEPA1. After stripping, the membrane was probed for the epitope V5 and for α-tubuline.
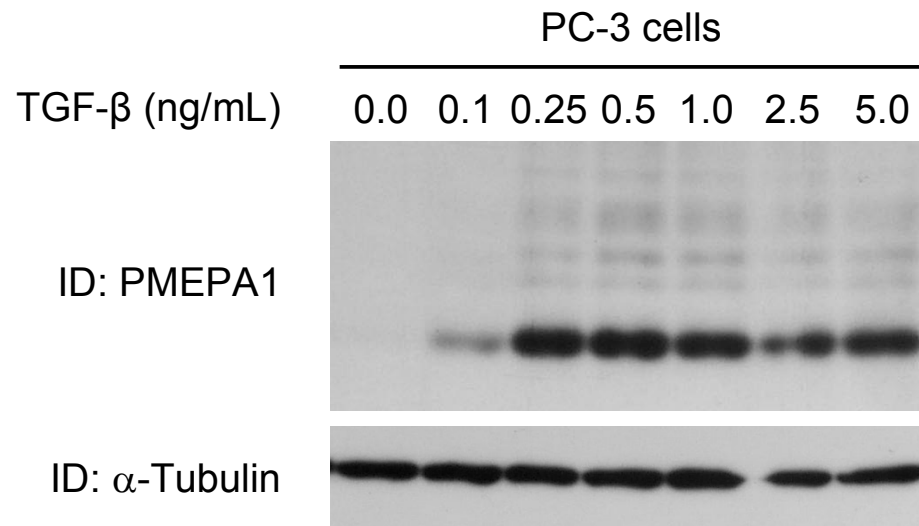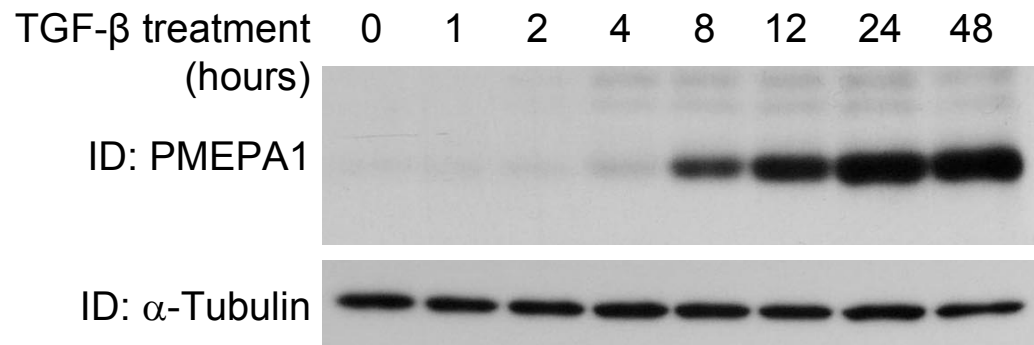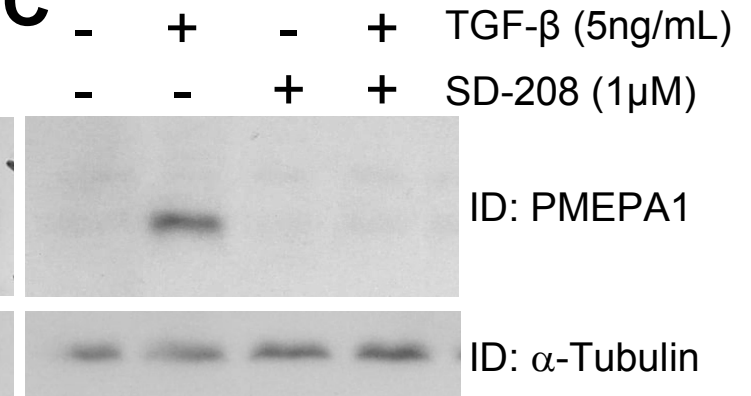
Figure 4. TGF-β induces a dose- and time-response increase of PMEPA1c protein in PC-3 cells. A. PC-3 cells were treated or not treated with 0.1 to 5.0ng/mL TGF-β for 24 hours before preparing protein lysates analyzed by Western-blotting. **B.** PC-3 cells were treated or not treated with 5ng/mL TGF-β from 1 to 48 hours before preparing protein lysates. **C.** PC-3 cells were pre-treated or not with the Tgfbr1 inhibitor SD-208(1μM) before being treated or not treated with TGF-β for 24 hours. Protein lysate were analyzed by Western-Blot to immunodetect PMEPA1. After stripping, the membrane was probed for α-Tubulin.

25
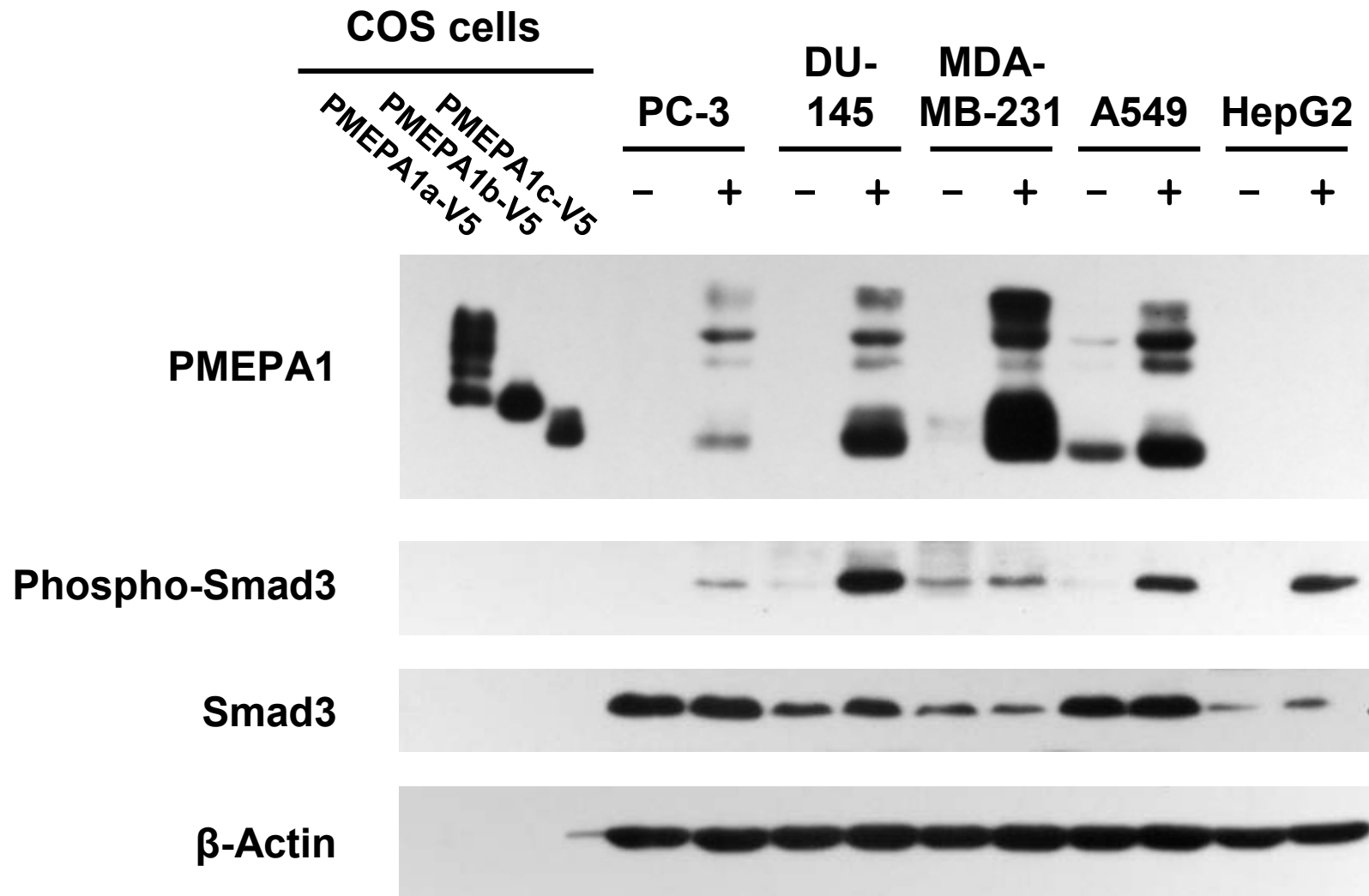
Figure 5. TGF-β induces the expression of cytosolic and membrane bound PMEPA1 in prostate, breast, lung cancer cells and hepatocarcinoma cells. Prostate (PC-3, DU-145), breast (MDA-MB-231) and lung (A549) cancer cells and hepatocarcinoma cells (HepG2) were grown until reaching cell layer reached near confluency. Cells were serum-starved for 4 hours and further cultivated in the presence or absence of TGF-β (5ng/mL) for 24 hours before preparing protein lysates. COS cells were transfected with a pcDNA expression vector coding for a specific isoform of PMEPA1 protein and protein lysates were prepared to be used a standards to identify which isoforms of PMEPA1 are expressed in cancer cells. Protein were analyzed by Western Blot to immunodetect PMEPA1, phosphorylated and total Smad3 and β-actin.
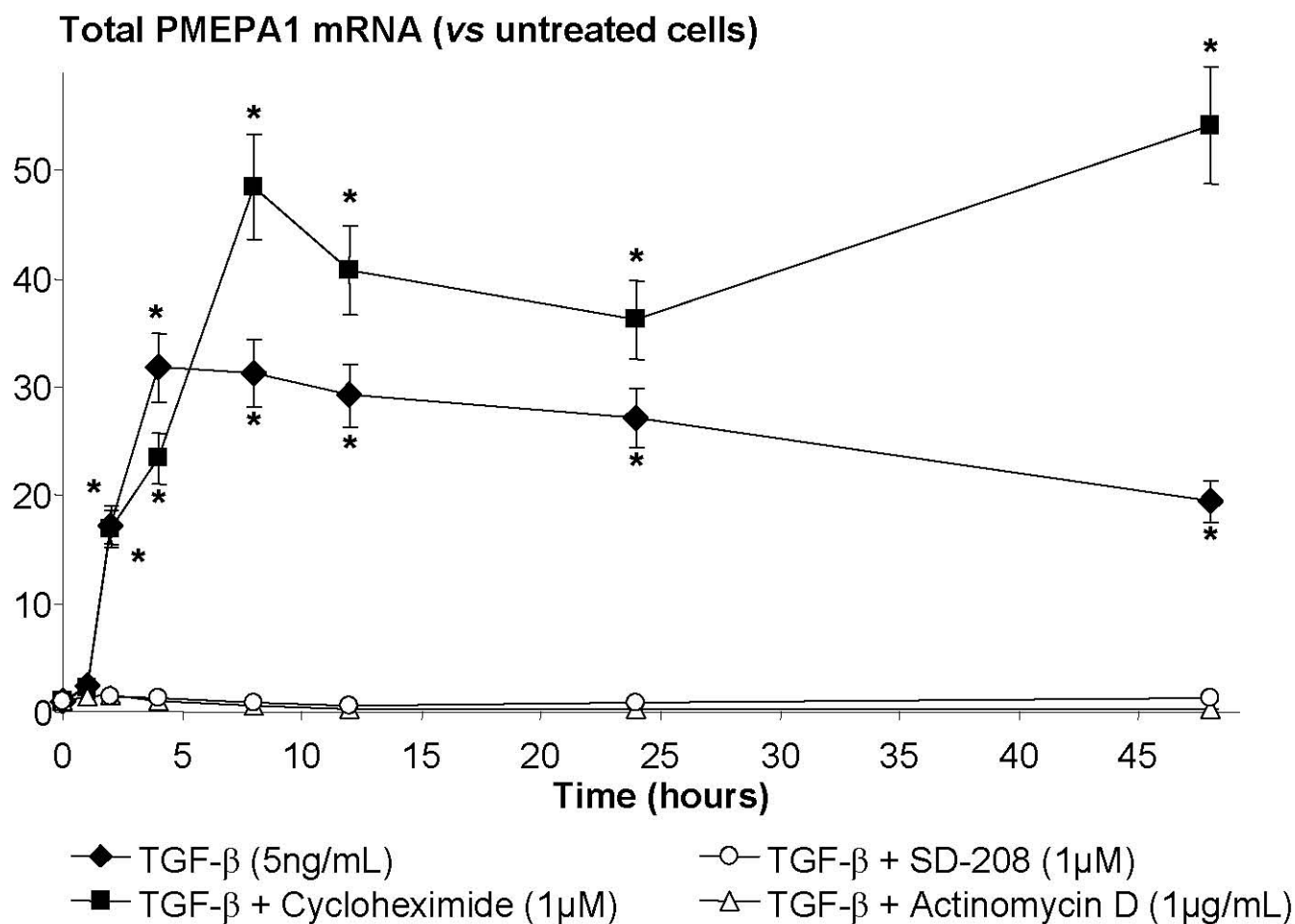
Figure 6. TGF-β increases PMEPA1 gene transcription. PC-3 cells were cultured until near confluency and starved overnight. Cell culture medium was then substituted with RPMI 1640-FBS (1%) and cells were treated or not treated with TGF-β for 0 to 48 hours, in the presence or absence of cycloheximide (translation inhibitor), actynomicin-D (transcription inhibitor) or SD-208 (Tgfbr1 inhibitor). Total RNA were extracted and cDNA were prepared. Total PMEPA1 expression was quantified by real-time PCR and normalized using the endogenous ribosomal protein L32 transcript, using the ΔΔCt method. All conditions were run in triplicate. The results represent the average (±SD) increase of PMEPA1 transcript induced by TGF-β and were analyzed using an unpaired Student's t test (*, $P<0.01$ when compared to untreated cells).
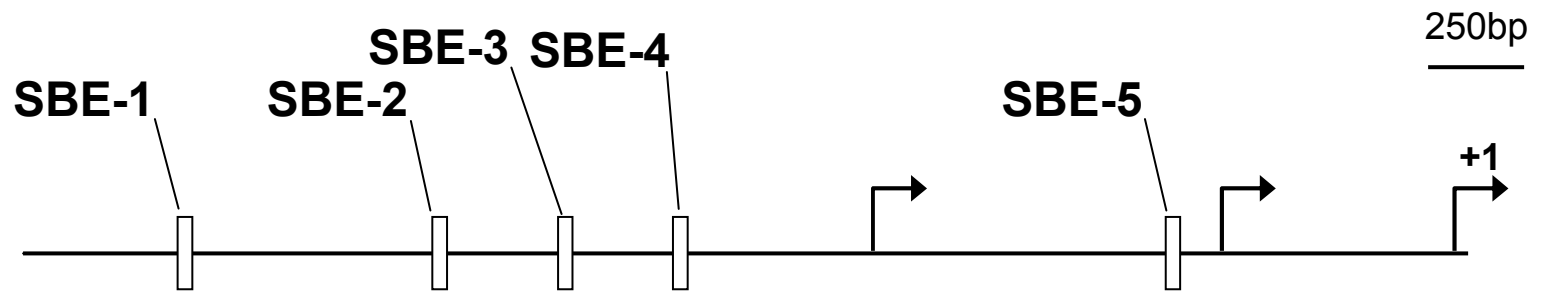
Figure 7. Schematization of a 3.7kb fragment of the PMEPA1 promoter.
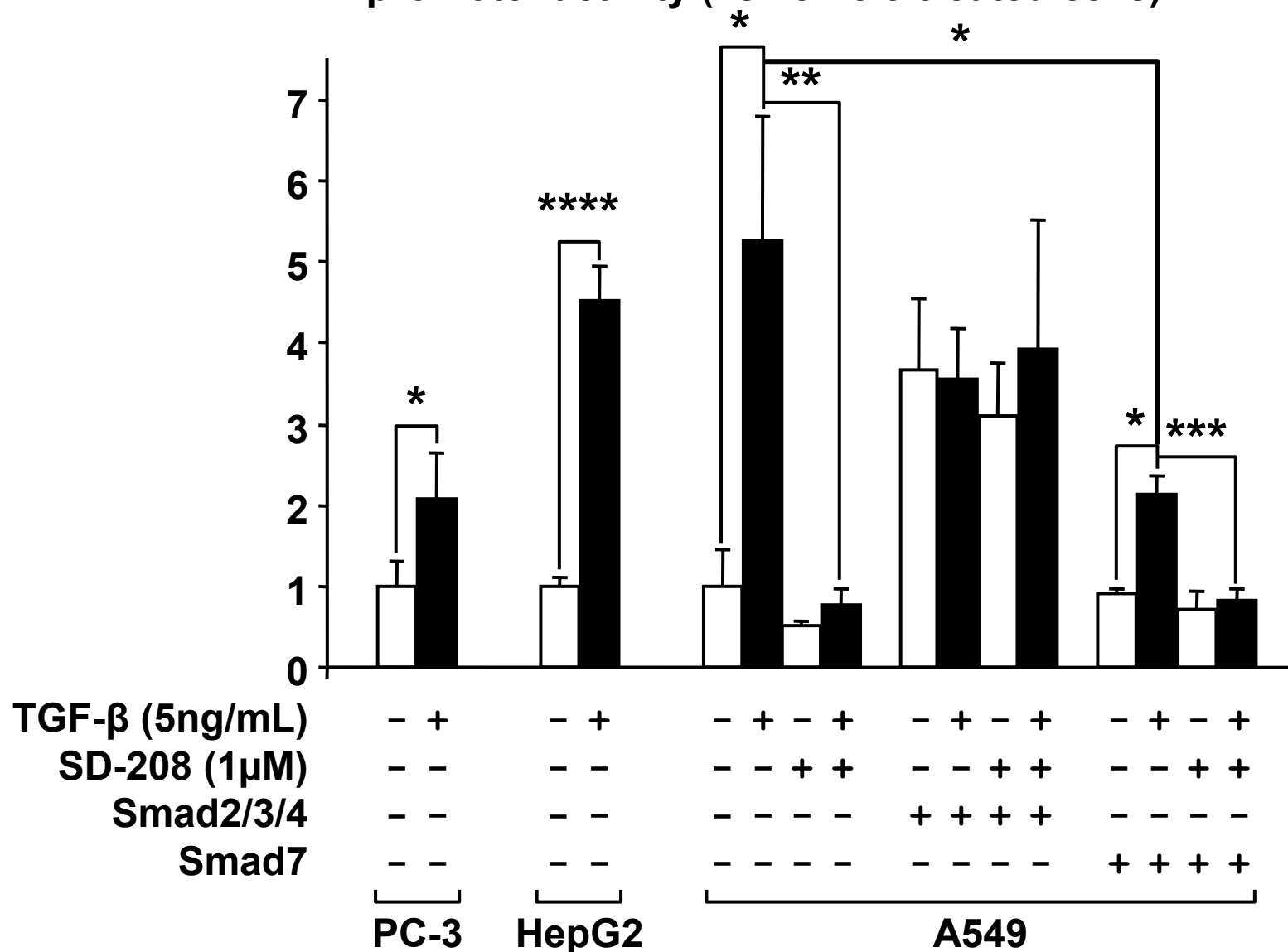
Figure 8. TGF-β-induction of PMEPA1 promotor activity is regulated by Smad proteins. ph*r*Luc-CMV plasmid and a pGL3-*f*Luc reporter plasmid containing the 3.7kb fragment of PMEPA1 promoter were transfected in PC-3, HepG2 or A549 cells with or without pCMV5 plasmids expressing Smad2/3/4 or Smad7. Cells were treated ± TGF-β and SD-208 for 24 hours before measuring dual-luciferase activity. Average ± SD of one representative experiment performed in quadruplicate. *P<0.05, **P<0.01, ***P<0.005, ****P<0.001, using an unpaired, two-tailed Student's *t* test.
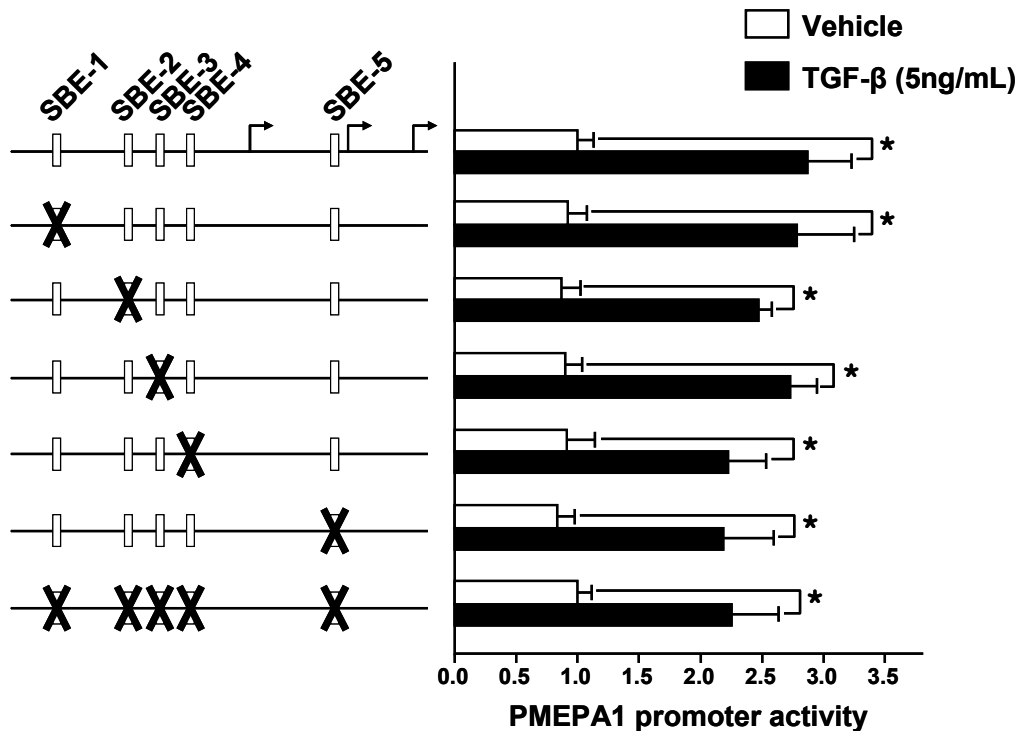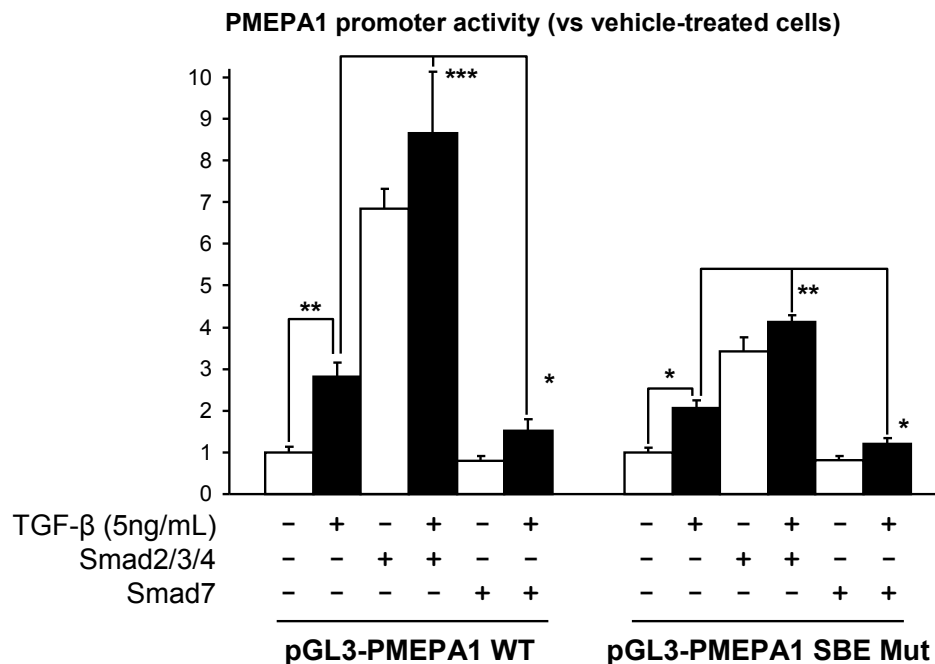
Figure 9. Mutation of the SBE in the PMEPA1 promoter does not decrease TGF-β responsiveness. A. ph*r*Luc-CMV plasmid and a pGL3-*f*Luc reporter plasmid containing the PMEPA1 promoter with or without mutated SBE (pictured by the crossed boxes) were transfected in A549 cells. *$P<0.05$, using a non-parametric Mann-Whintey's U test. **B.** A549 cells were transfected with phrLuc-CMV and a pGL3-PMEPA1 wild-type (WT) or where the five SBEs have been mutated (SBE Mut). Cells were treated ± TGF-β for 24 hours before measuring dual-luciferase activity. *$P<0.05$, **$P<0.01$, ***$P<0.005$, ****$P<0.001$, using an unpaired, two-tailed Student's *t* test.
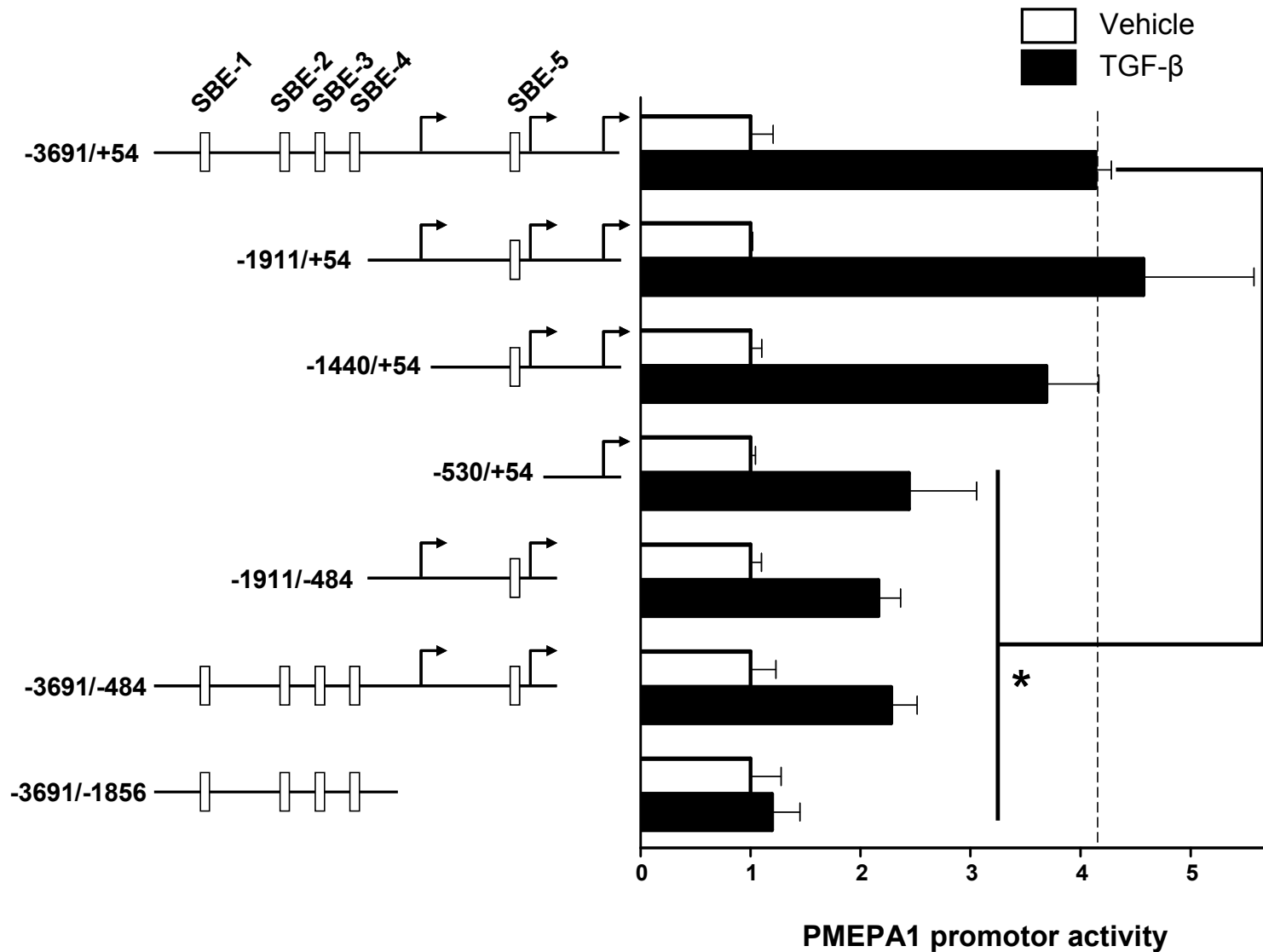
Figure 10. TGF-β-induction of PMEPA1 promoter is mediated within a 1.5kb proximal fragment of the promoter. A549 cells were transfected with a pGL3-fLuc reporter plasmid containing a fragment of the PMEPA1 promoter and a phrLuc-CMV plasmid, and treated ± TGF-β (5ng/mL, 24h) before measuring dual-luciferase activity. Average ± SD of one representative experiment performed in quadruplicate. * *P*<0.05, using a non-parametric Mann Whitney's *U* test.
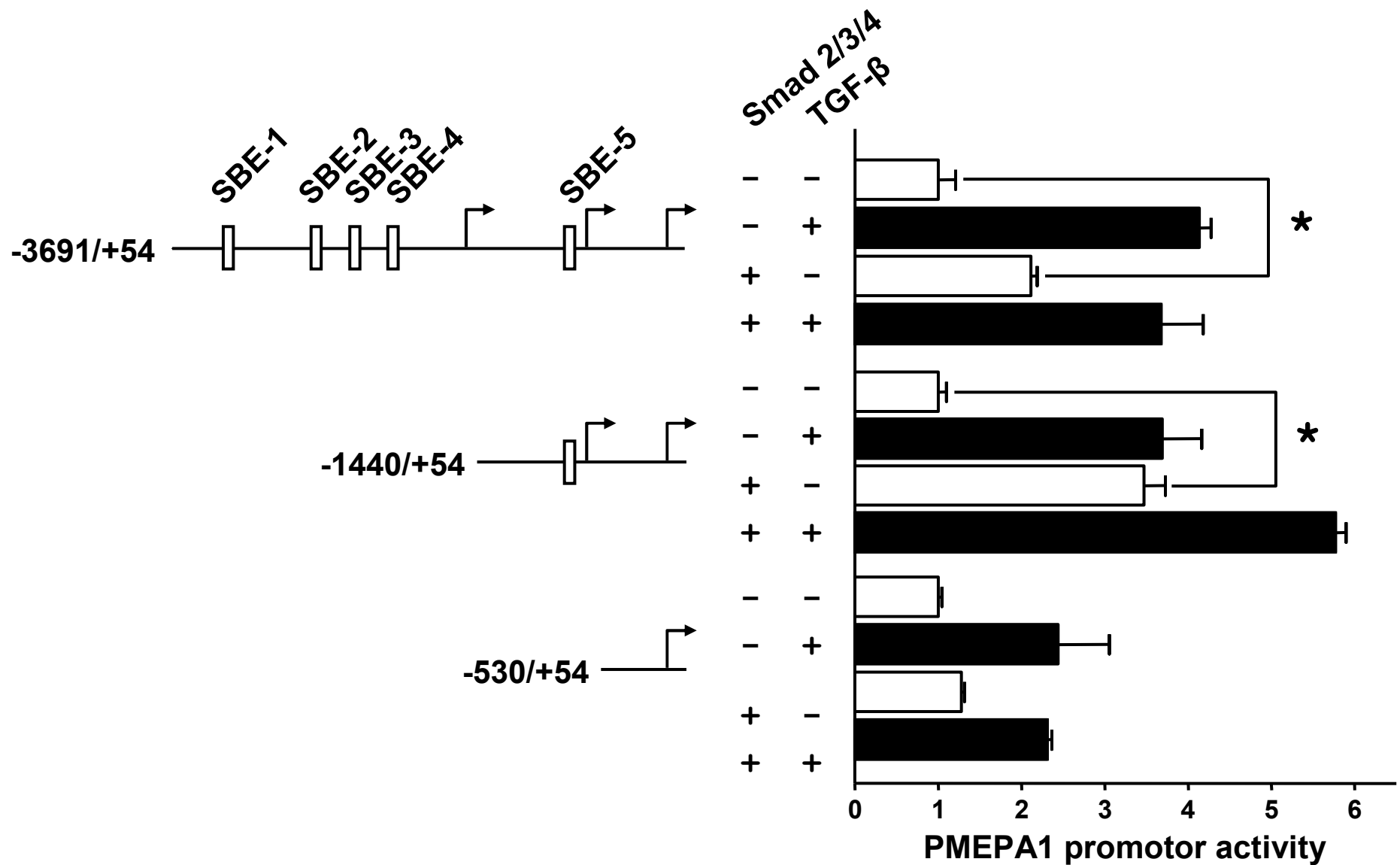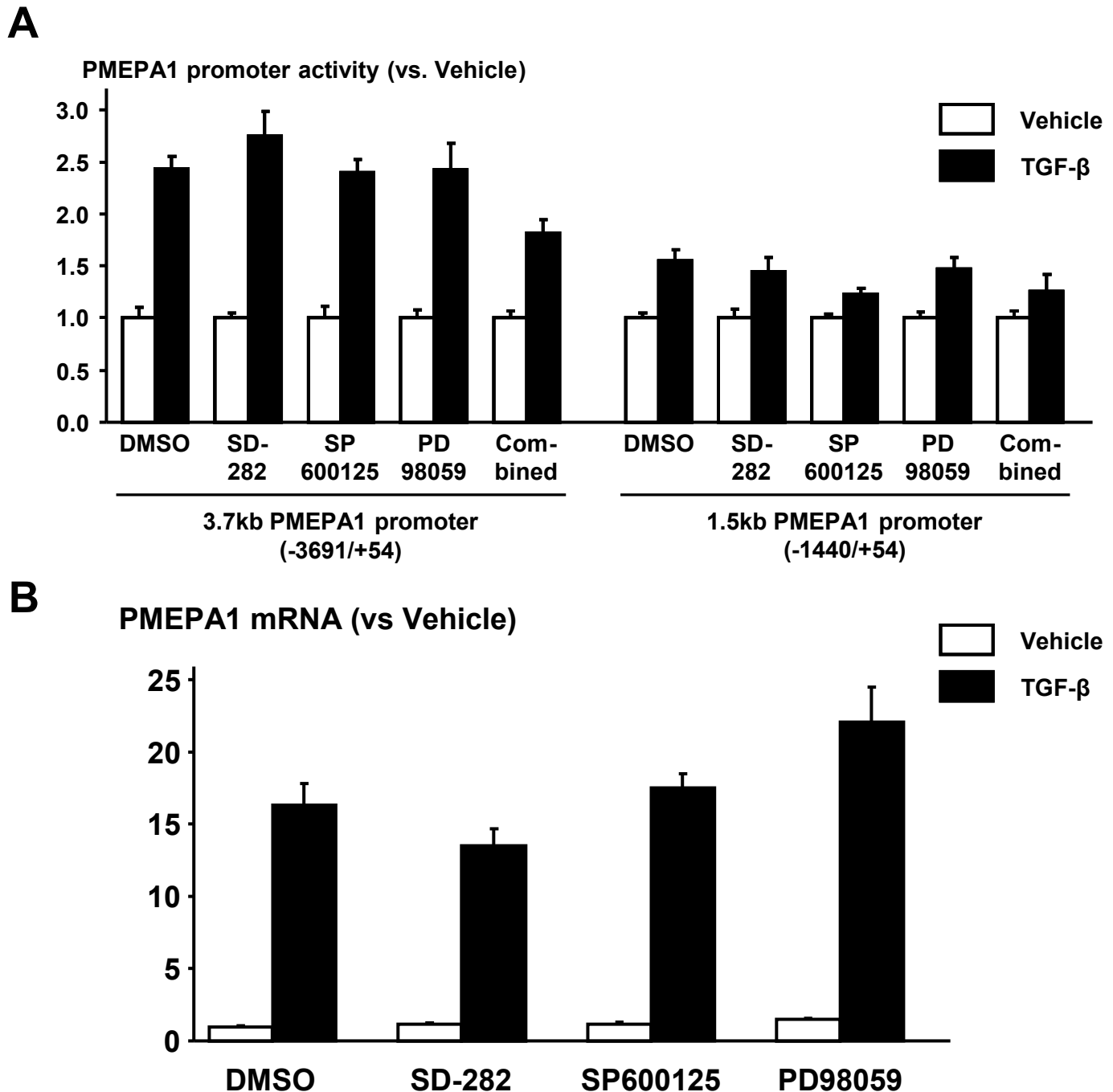
Figure 11. TGF-β-induction of PMEPA1 promoter is Smad and non-Smad regulated. A549 cells were transfected with a pGL3-fLuc reporter plasmid containing a fragment of the PMEPA1 promoter, a phrLuc-CMV plasmid and pCMV vectors expressing Smad2, 3 and 4 or an empty pCMV vector. Cells were treated ± TGF-β (5ng/mL, 24h) before measuring the dual-luciferase activity. Average ± SD of one representative experiment performed in quadruplicate. * $P<0.05$, using a non-parametric Mann Whitney's U test.

A

B

Figure 12. p38, JNK and MEK kinase inhibitors have no effect on PMEPA1 expression indced by TGF-β. A. A549 cells were transfected with a pGL3-fLuc reporter plasmid containing a fragment of the PMEPA1 promoter and a phrLuc-CMV plasmid. Cells were treated ± TGF-β (5ng/mL) in the presence or absence of SD-282 (1μM, p38 inhibitor), SP600125 (5μM, JNK inhibitor) and PD98059 (25μM, MEK inhibitor), alone or combined. Twenty-four hours later, the dual-luciferase activity was measured. Average ± SD of one representative experiment performed in quadruplicate. **B.**PC-3 cells were treated ± TGF-β (5ng/mL) in the presence or absence of SD-282 (1μM, p38 inhibitor), SP600125 (5μM, JNK inhibitor) and PD98059 (25μM, MEK inhibitor) for 24h. PMEPA1 mRNA levels were measured in triplicate by sqRT-PCR as described previously. The results represent the average (±SD) increase of PMEPA1 transcript induced by TGF-β.

A

	0 min	15 min	30 min	60 min
TGF-β (5ng/mL)	+ +	+ +	+ +	+ +
SD208 (1μM)	- +	- +	- +	- +

Phospho-Smad2

Smad2

B

(CAGA)₉ promoter activity

TGF-β (5ng/mL)	–	+	–	+
SD-208 (1μM)	–	–	+	+
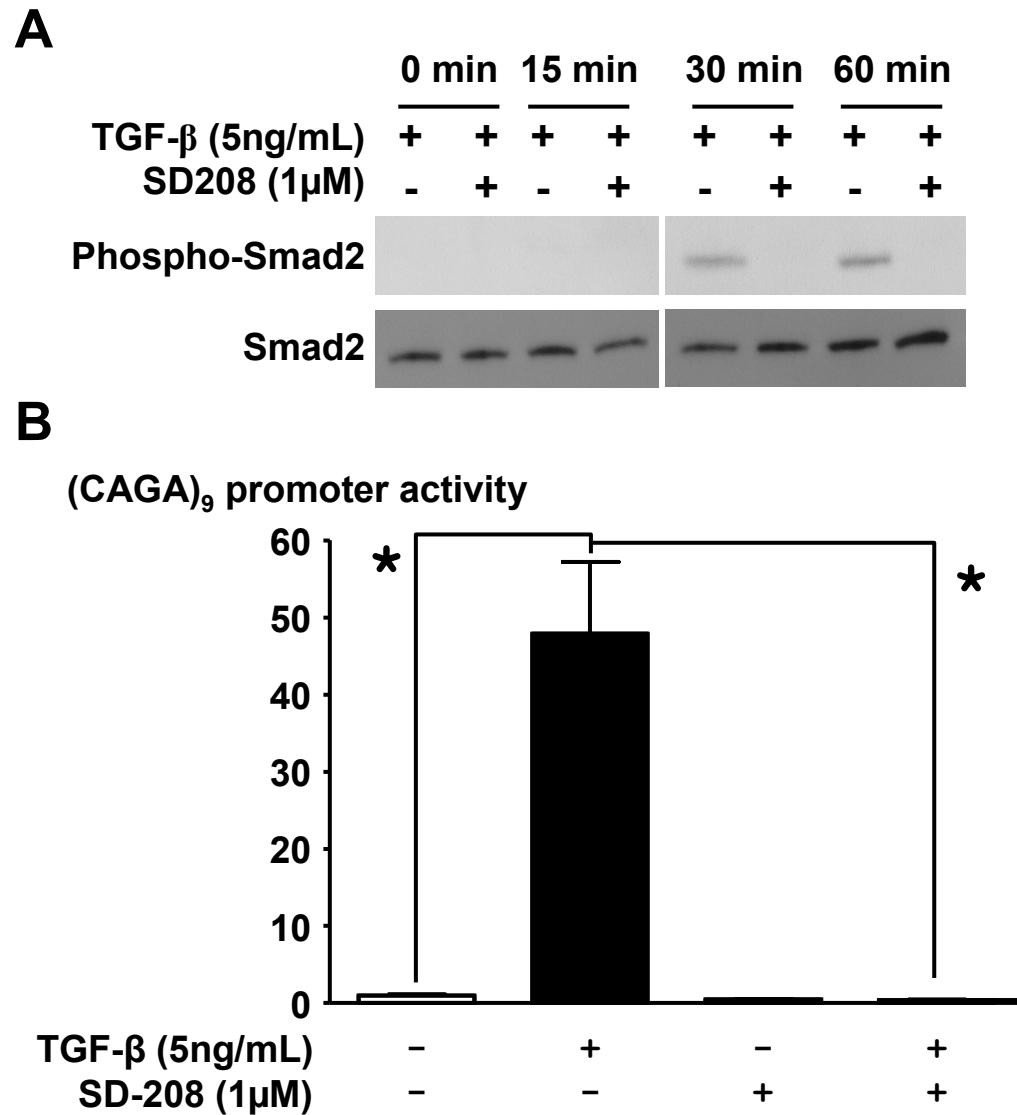
Figure 13. SD-208 inhibits TGF-β signaling in PC-3 cells. A. Immunoblotting detection of Smad2 and phospho-Smad2 on protein lysate from PC-3 cells treated or not with TGF-β, in the presence or absence of SD208. **B**. PC-3 cells were transfected with the pGL3 (CAGA)9-*f*Luc reporter construct sensitive to TGF-β and a *r*Luc vector. Cells were treated ± TGF-β (5ng/mL) for 24 hours before measuring dual-luciferase activity. *P<0.05 using a non-parametric Mann-Whitney's *U* test.

A

B

Osteolysis area (mm²)

P=0.0146

Relative human mRNA expression

SD-208   −   +   −   +

PMEPA1   PTHrP
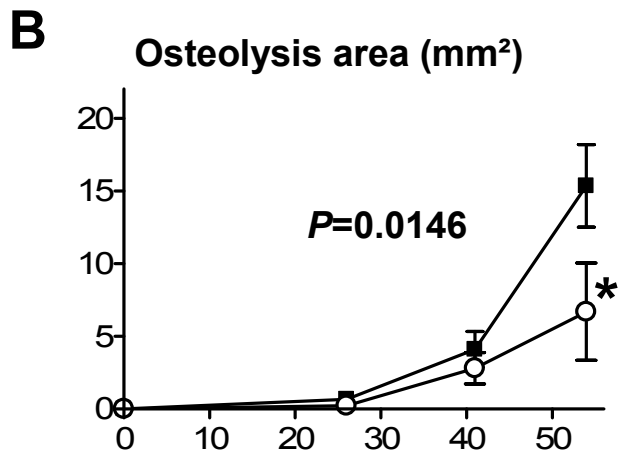
Figure 14. Inhibition of TGF-β signaling decrease bone destruction induced by PC-3 cells. A. Representative radiographies of tibia and distal femur of mice treated with vehicle or SD-208. Arrows indicate osteolytic area. **B.** Quantification of bone destruction. Results are expressed as the average osteolysis area ± SEM, and statistically analyzed using a 2-way ANOVA test.
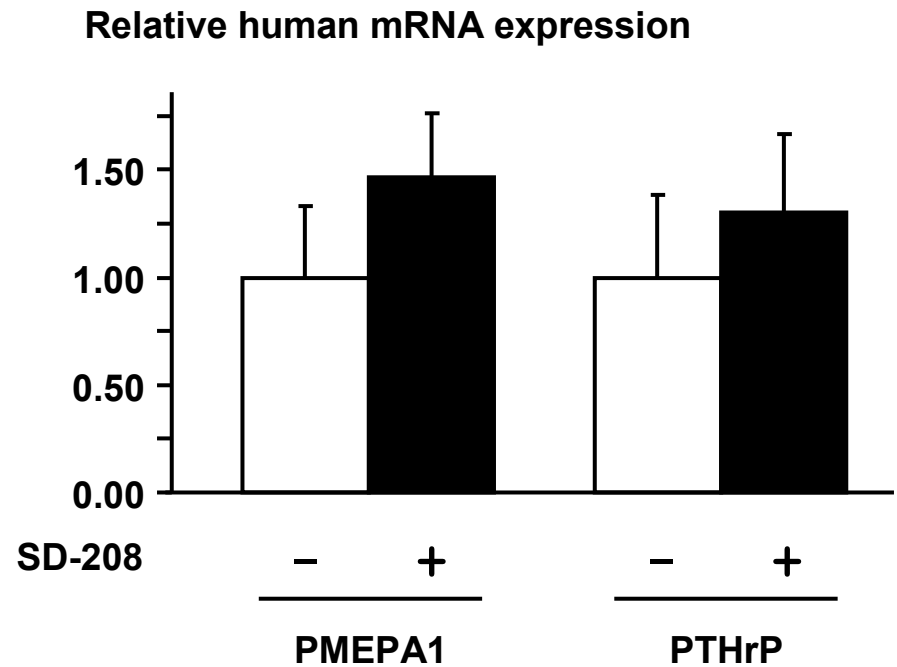
Figure 15. SD-208 (50mg/kg/day) does decrease human PMEPA1 or PTHrP mRNA at sites of bone metastases. Human gene expression was measured in bone marrow mRNA samples from mice with bone metastases from PC-3 cells treated or not treated with SD-208 (50mg/kg/day).

35

A

PMEPA1 mRNA relative expression

	PMEPA1a			PMEPA1b			PMEPA1c		
pLKO.1 empty	+	–	–	+	–	–	+	–	–
pLKO.1 shCtrl	–	+	–	–	+	–	–	+	–
pLKO.1 shPMEPA1	–	–	+	–	–	+	–	–	+

B

	PMEPA1a			PMEPA1b			PMEPA1c		
pLKO.1 empty	+	–	–	+	–	–	+	–	–
pLKO.1 shCtrl	–	+	–	–	+	–	–	+	–
pLKO.1 shPMEPA1	–	–	+	–	–	+	–	–	+

ID: PMEPA1

ID: α-Tubulin

C

pLKO.1 shCtrl   pLKO.1 shPMEPA1

500 200 100 50   500 200 100 50   ng plasmid/10^5 cells

ID: PMEPA1

ID: α-Tubulin
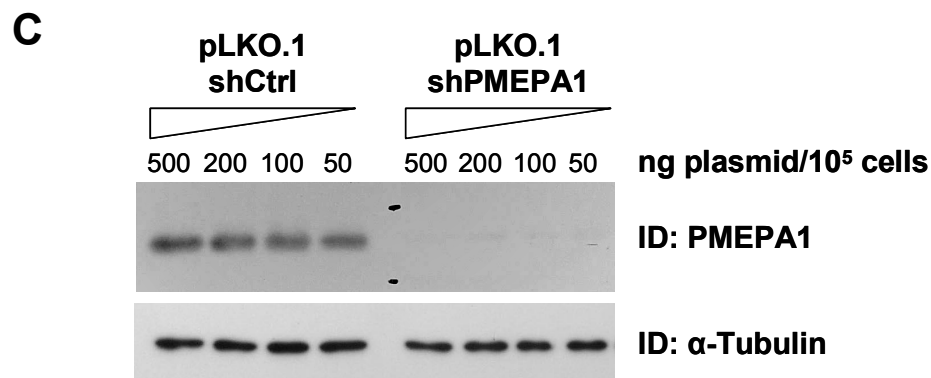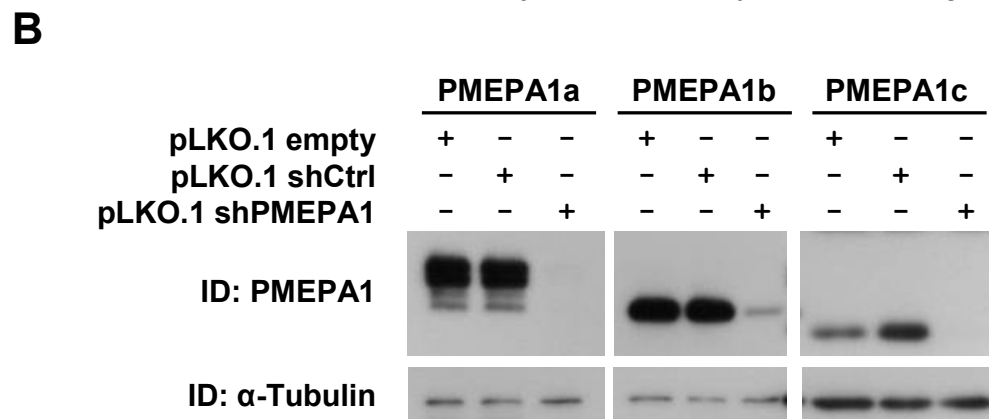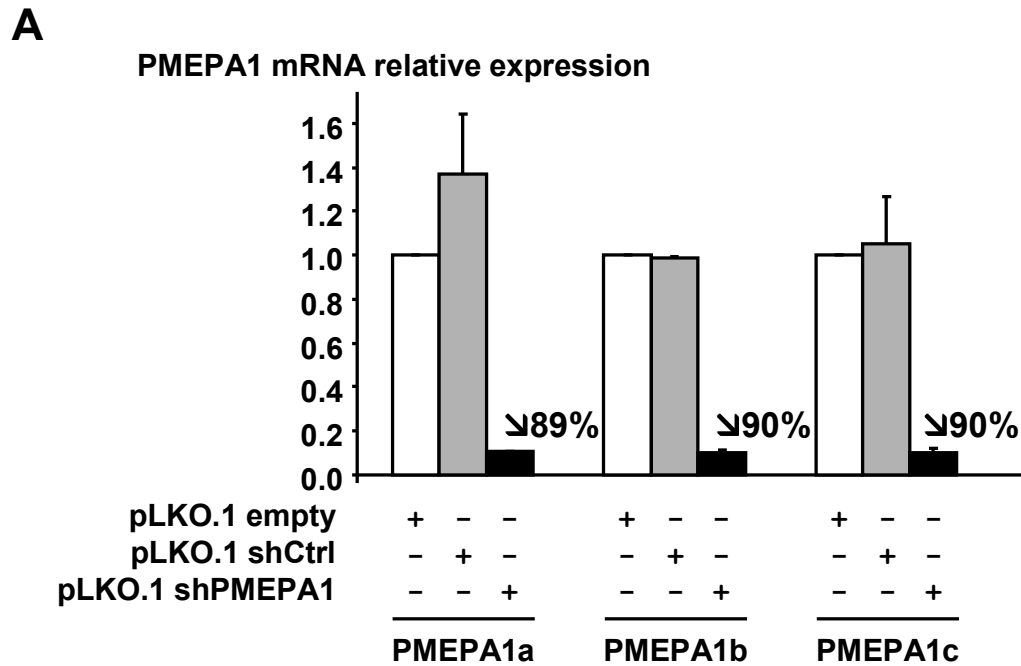
Figure 16. Validation of a short-hairpin RNA against PMEPA1. G COS7 cells were transfected with a pcDNA vector expressing a specific isoform of PMEPA1 with a V5 tag at the C-terminus and with an empty pLKO.1 vector or expressing a shRNA control (shCtrl) or a shRNA against PMEPA1 (shPMEPA1) (500ng/10^5 cells). Forty-eight hours later, total RNA was extracted to measure PMEPA1 mRNA levels using sqRT-PCR. **B.** Protein lysate were prepared to determine PMEPA1 protein levels using Western-blotting to detect PMEPA1 and α-Tubulin. **C.** COS7 were transfected to express PMEPA1c and with decreasing quantities of pLKO.1 vector (shCtrl or shPMEPA1). Protein lysate were prepared to determine PMEPA1 protein levels using Western-blotting to detect PMEPA1 and α-Tubulin.
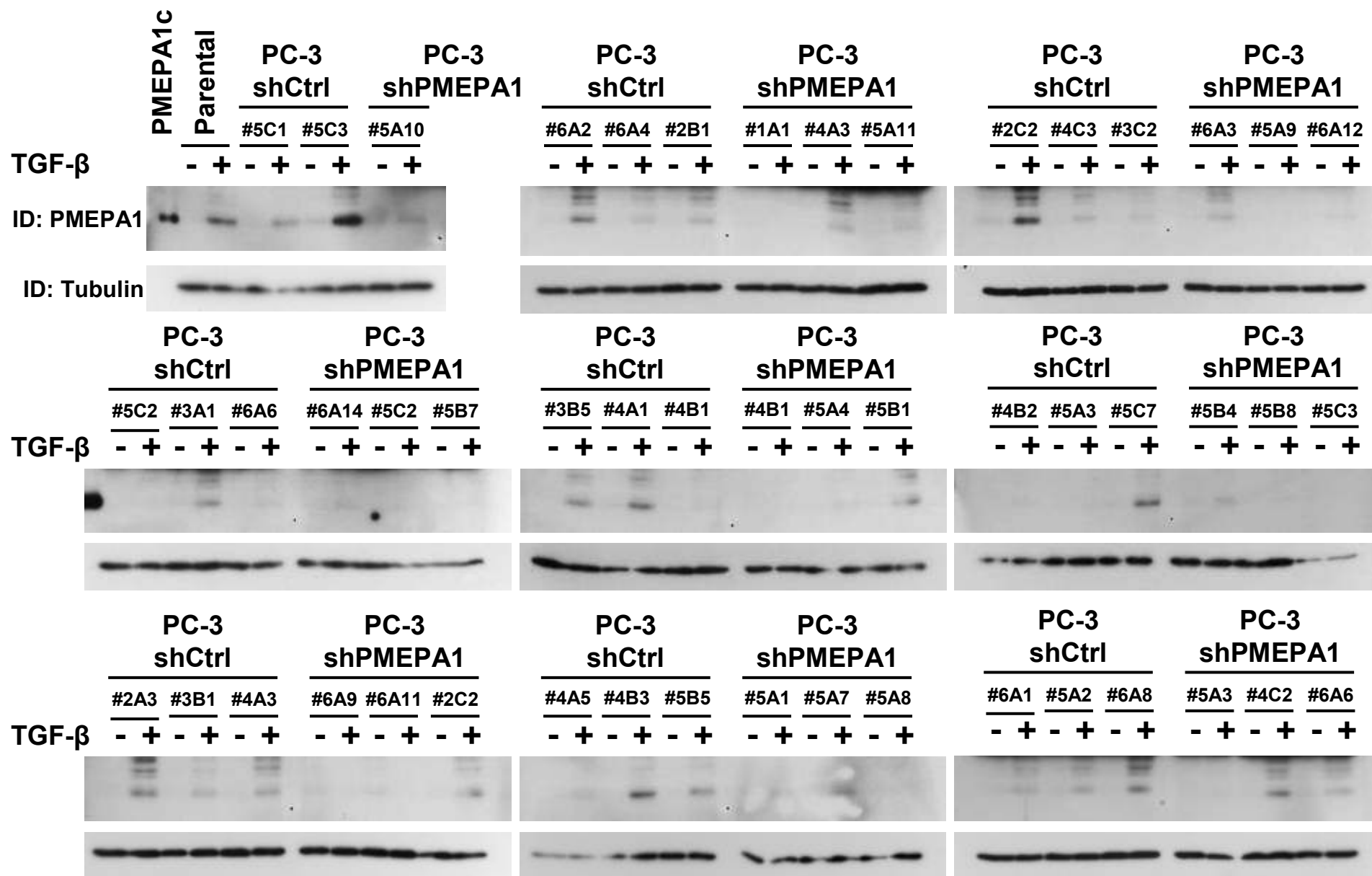
Figure 17. Selection of PC-3 clones knocked-down for PMEPA1 expression. PC-3 cells were transfected with a pLKO.1 vector expressing shCtrl or shPMEPA1. Transfected were selected in puromycin (250ng/mL) and single cell clones were isolated using cloning cylinders. After expansion, the cells were cultivated ± TGF-β (5ng/mL, 24h) and PMEPA1 expression was determined by Western-Blot.
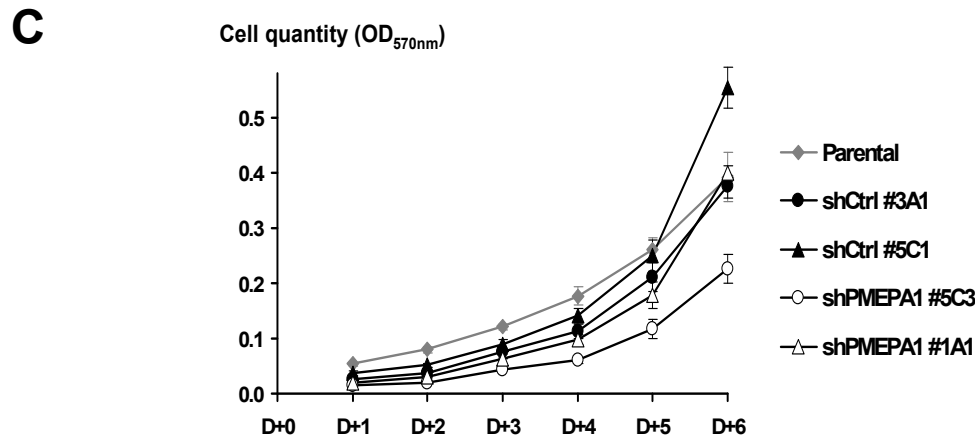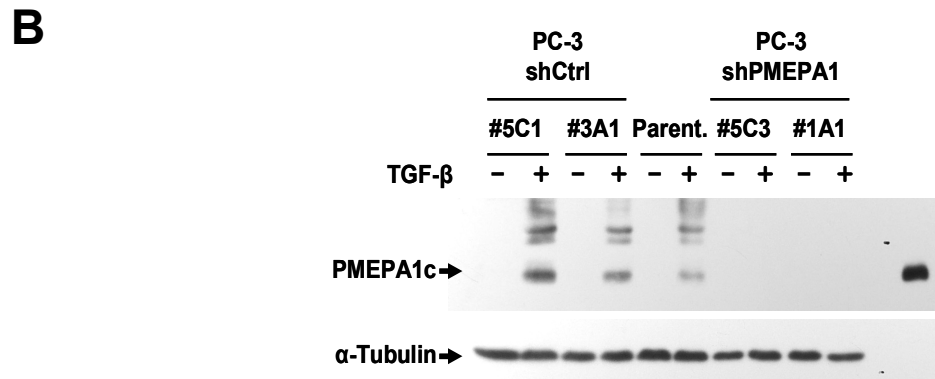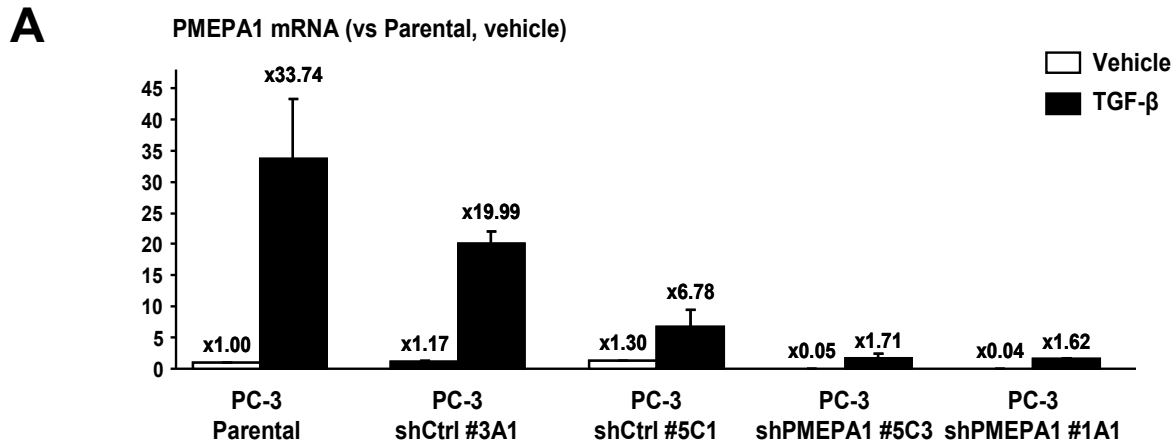
37

Figure 18. Stable knockdown of PMEPA1 expression in PC-3 prostate cancer cells. PC-3 parental cells were transfected with a pLKO.1 vector expressing a non-target shRNA (shCtrl) or an shRNA against PMEPA1 (shPMEPA1) and single cell clones were isolated after antibiotic selection (puromycin, 250pg/mL). Stability of the transfection was assessed by culturing PC-3 shCtrl clones (shCtrl #3A1 and #5C1) and PC-3 shPMEPA1 clones (shPMEPA1 #5C3 and #1A1) in absence of antibiotic during 75 days and by measuring the expression of PMEPA1 mRNA and protein in the presence or absence of TGF-β (5ng/mL, 24h). **A**. Total RNA was extracted and mean ± SEM expression of PMEPA1 was measured using semi-quantitative RT-PCR (n=3). **B**. Proteins were extracted from treated cells and PMEPA1 level was assayed by Western-blotting, α-tubulin was used as loading control. C. Parental and transfected PC-3 cells were seeded in 96 well-plate (500 cells per well) and cultured in complete medium for 6 days. Cells quantity was assessed using an MTT assay and results are represend as the average ± SEM optical density at 750nm (OD_{750nm}) of a sextuplicate.
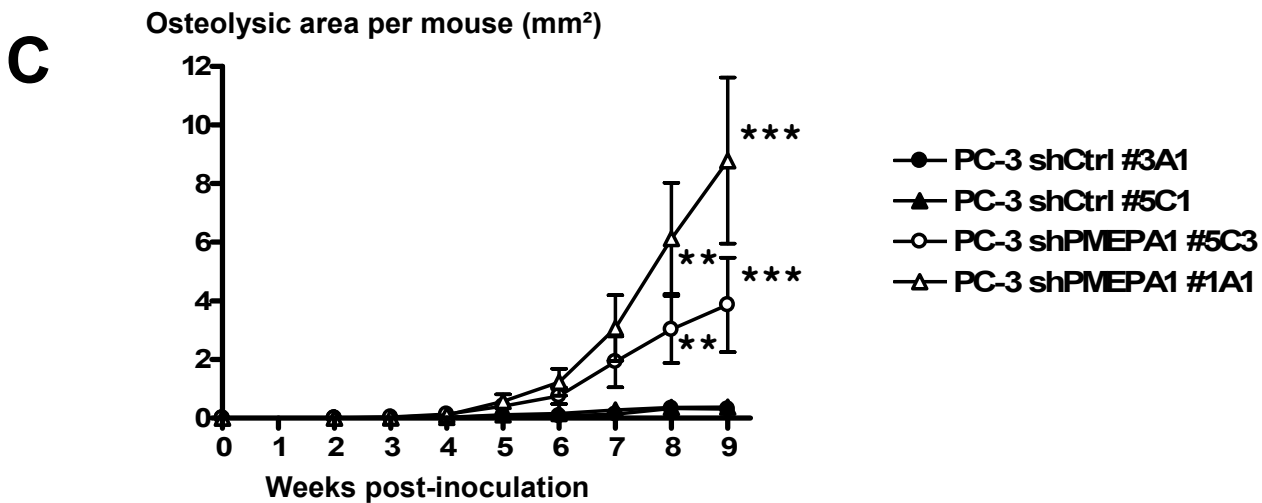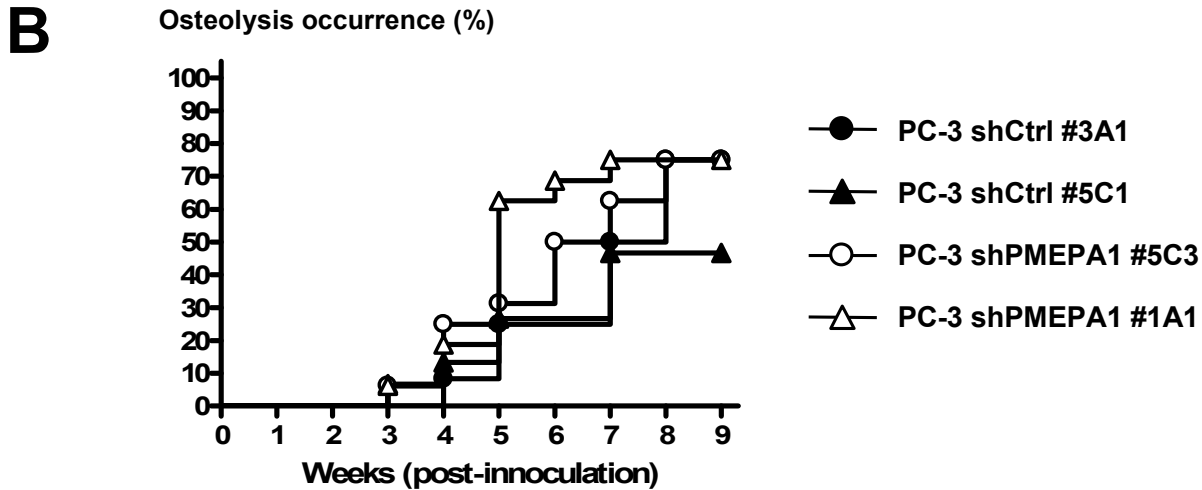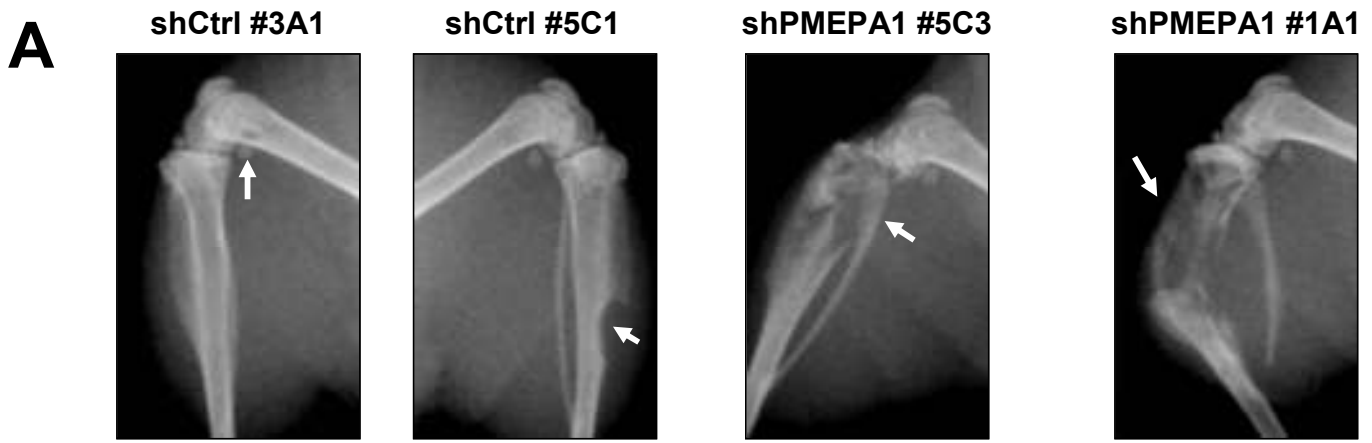
Figure 19. Knockdown of PMEPA1 in PC-3 prostate cancer cells increases osteolysic lesions in a mouse model of bone metastases. Four-week old, female Balb/C athymic mice received an intracardiac inoculation of PC-3 shCtr (#3A1 and #5C1) or shPMEPA1 (#5C3 and #1A1) in the left cardiac ventricle (10^5 cells in 100µL PBS, n=12 to 16 per group). The development of bone metastases was surveyed by radiographies. **A**. Representative radiographies of mouse hindlimbs 9 weeks after tumor cell inoculation. Arrow indicates osteolytic lesions. **B**. The occurence of osteolysis was analyzed using the method of Kaplan-Meyer. No significant differences were found between the different groups. **C.** Osteolytic areas were measured on x-ray and results are expressed as the average ± SEM osteolytic area per mouse. ** $P<0.01$ and *** $P<0.001$ vs shCtrl #3A1 or #5C1 using a 2-way ANOVA followed by a Bonferroni post-test.

A

(CAGA)₉ promoter activity
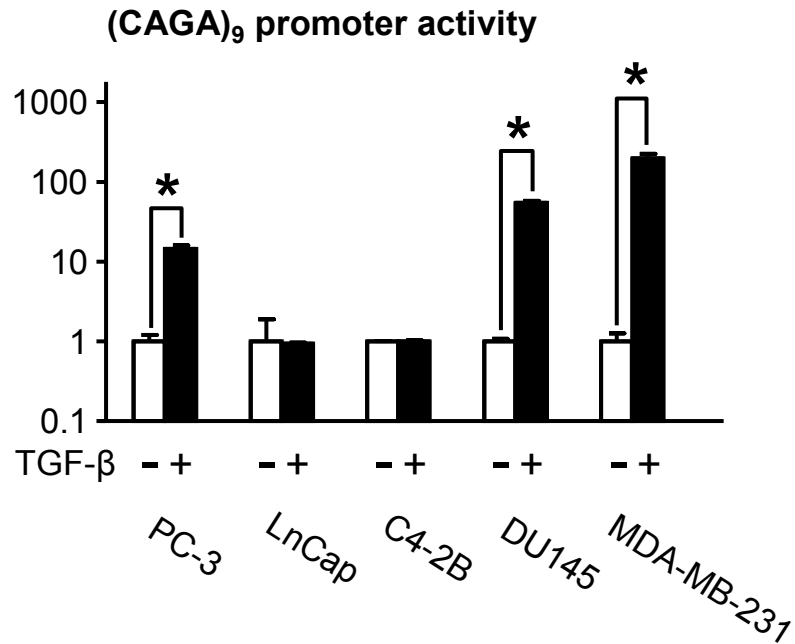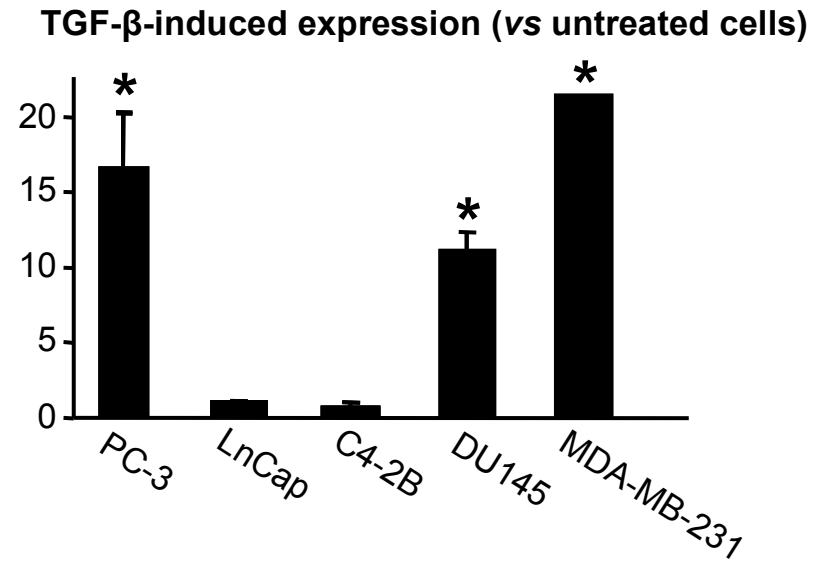

B

TGF-β-induced expression (*vs* untreated cells)

Figure 20. TGF-β increases PMEPA1 mRNA expression in TGF-β-sensitive cancer cells. A. TGF-β (5ng/mL, 24h) upregulates PMEPA1 mRNA expression in PC-3, DU145 and MDA-MB-231 cells but not in LnCap and C4-2B cells. PMEPA1 mRNA was quantified by real-time PCR as described previously. **B.** LnCap and C4-2B cells are not TGF-β sensitive. Cancer cells were transfected with the (CAGA)₉-*f*Luc reporter construct sensitive to TGF-β and a *r*Luc vector. Cells were treated ± TGF-β (5ng/mL) for 24 hours before measuring dual-luciferase activity. *P<0.01 using an unpaired, two-tailed Student's *t* test
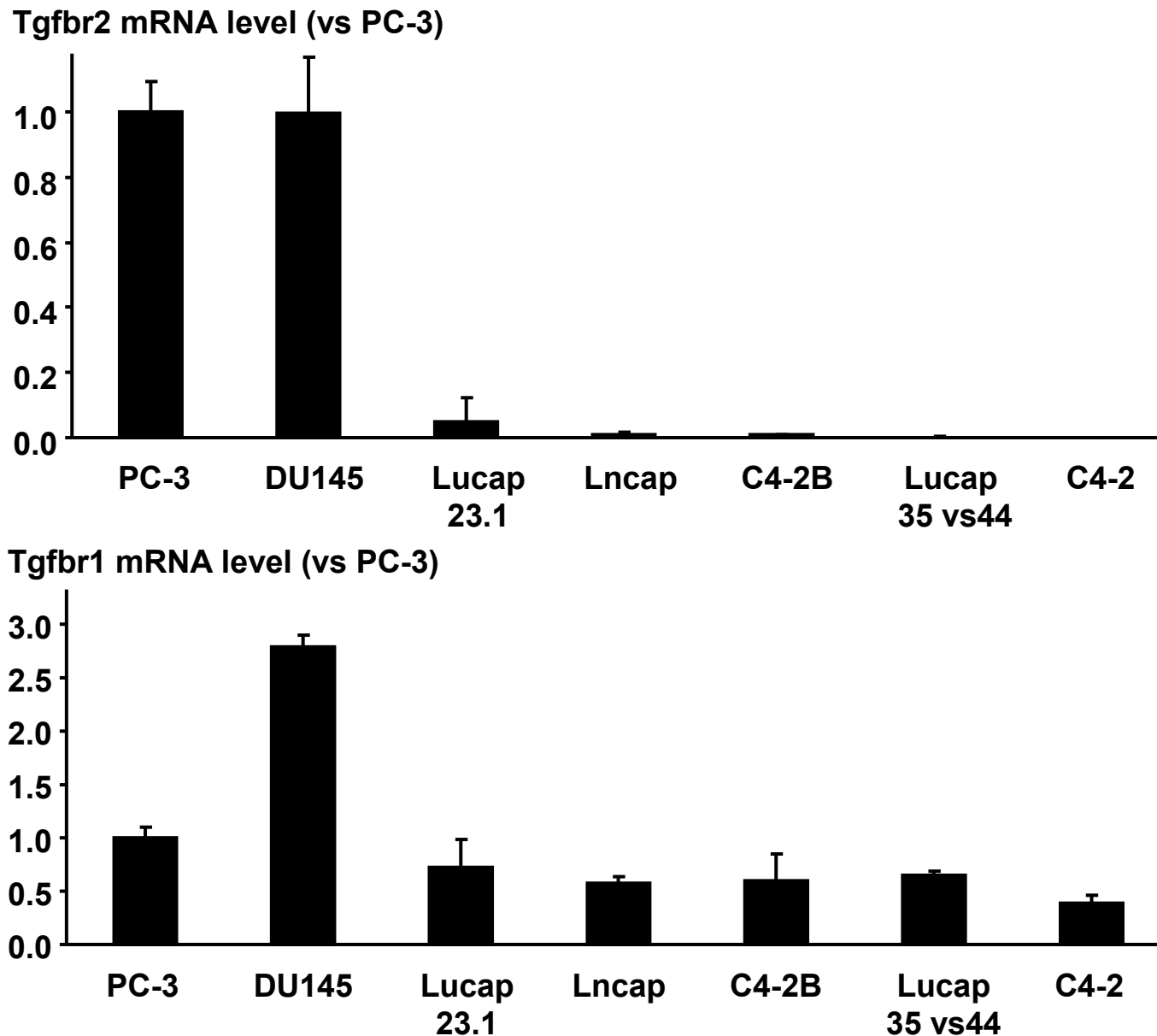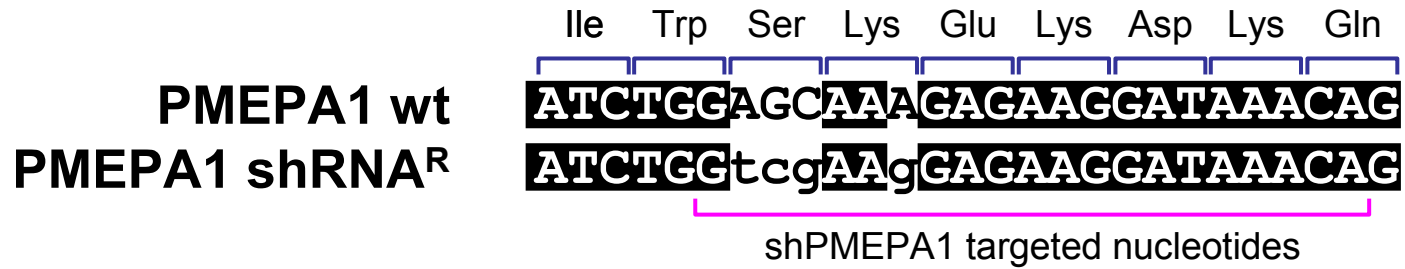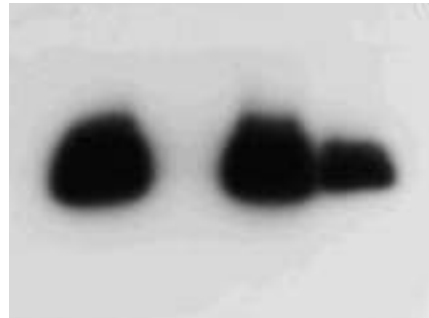
Figure 21. Expression of TGF-β receptor (Tgfbr) type 1 and 2 in prostate cancer cells. PC-3, DU145, LnCap, C4-2 and C4-2B human prostate cancer cells were grown in RPMI media. Lucap 23.1 and its androgen-independent derivative Lucap 35 vs44 human prostate cancer cells were maintained in SCID mice. Total RNA was extracted to measure Tgfbr1 and 2 expression by sqRT-PCR. Samples were analyzed in triplicates, and relative quantities are expressed as the average ± SEM against PC-3 cells.

A

	Ile	Trp	Ser	Lys	Glu	Lys	Asp	Lys	Gln

PMEPA1 wt ATCTGGAGCAAAGAGAAGGATAAACAG

PMEPA1 shRNA^R ATCTGGtcgAAgGAGAAGGATAAACAG

shPMEPA1 targeted nucleotides

B

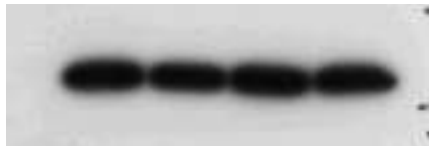| PMEPA1c-V5 wt	+	+	−	−
PMEPA1c-V5 shRNA^R	−	−	+	+
shControl	+	−	+	−
shPMEPA1	−	+	−	+

ID: PMEPA1

ID: αTubulin

Figure 22. Generation of a shRNA-resistant form of PMEPA1. A. Silent mutations introduced in the coding sequence of PMEPA1c at the site recognized by the shPMEPA1. **B**. pcDNA plasmid coding for the wild-type (wt) or the shRNA resistant (shRNA^R) PMEPA1c-V5 were cotransfected in COS7 cells with a pLKO.1 vector expressing a shControl or a shPMEPA1. Forty-eight hours later, protein lysates were prepared and analyzed using Western-blotting to detect PMEPA1 and αTubulin.
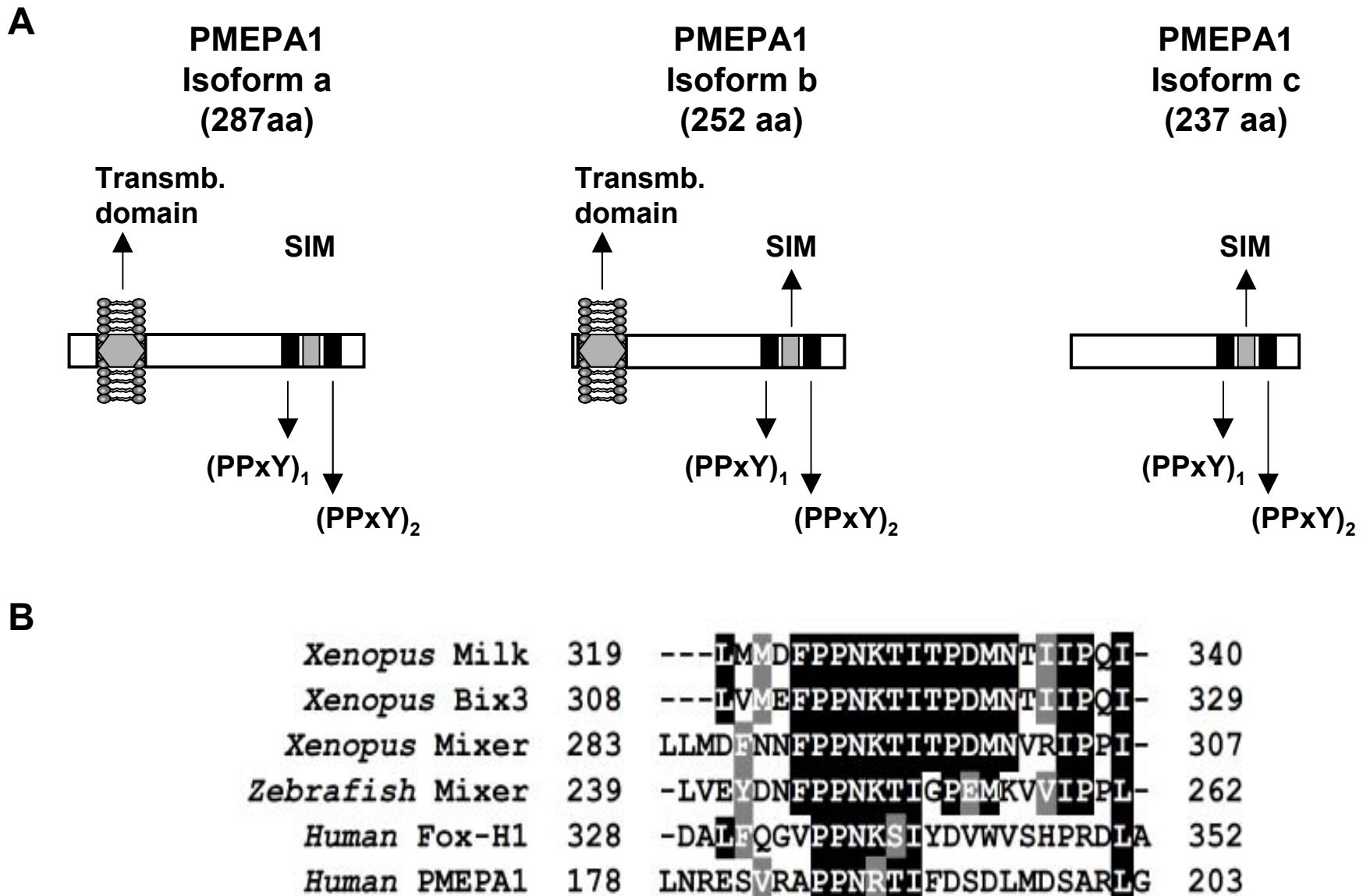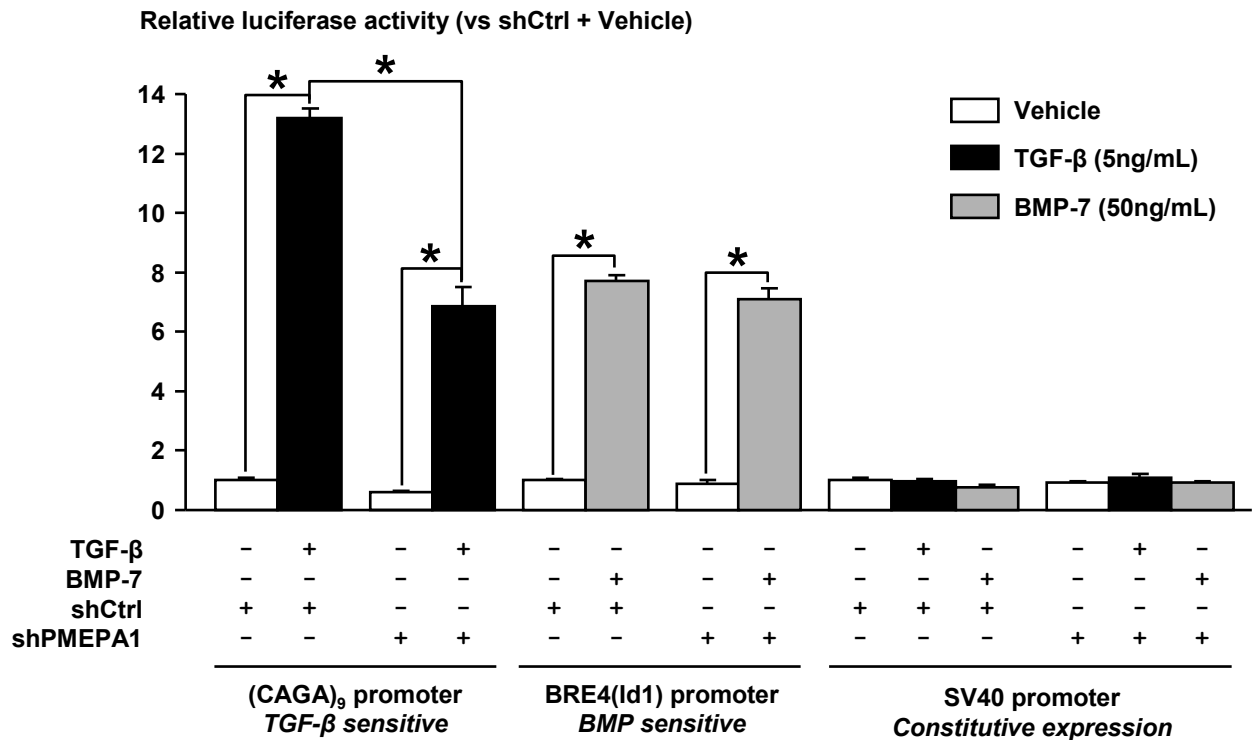
Figure 23. A. Schematization of PMEPA1 isoforms. **B.** Alignment of the Smad interaction motives of DNA-binding cofactors of R-Smads with human PMEPA1. Transmb., transmembrane; aa, amino acid; SIM, Smad interaction motif.

A

Relative luciferase activity (vs shCtrl + Vehicle)

Legend:
- ☐ Vehicle
- ■ TGF-β (5ng/mL)
- ▨ BMP-7 (50ng/mL)

Y-axis: 14, 12, 10, 8, 6, 4, 2, 0

TGF-β	–	+	–	+	–	–	–	–	–	+	–	–	+	–
BMP-7	–	–	–	–	–	+	–	+	–	–	+	–	–	+
shCtrl	+	+	–	–	+	+	–	–	+	+	+	–	–	–
shPMEPA1	–	–	+	+	–	–	+	+	–	–	–	+	+	+

(CAGA)₉ promoter — *TGF-β sensitive*   BRE4(Id1) promoter — *BMP sensitive*   SV40 promoter — *Constitutive expression*

B

(CAGA)₉ promoter activity (vs shCtrl + TGF-β)

Legend:
- ☐ Vehicle
- ■ TGF-β

Y-axis: 1.4, 1.2, 1.0, 0.8, 0.6, 0.4, 0.2, 0.0

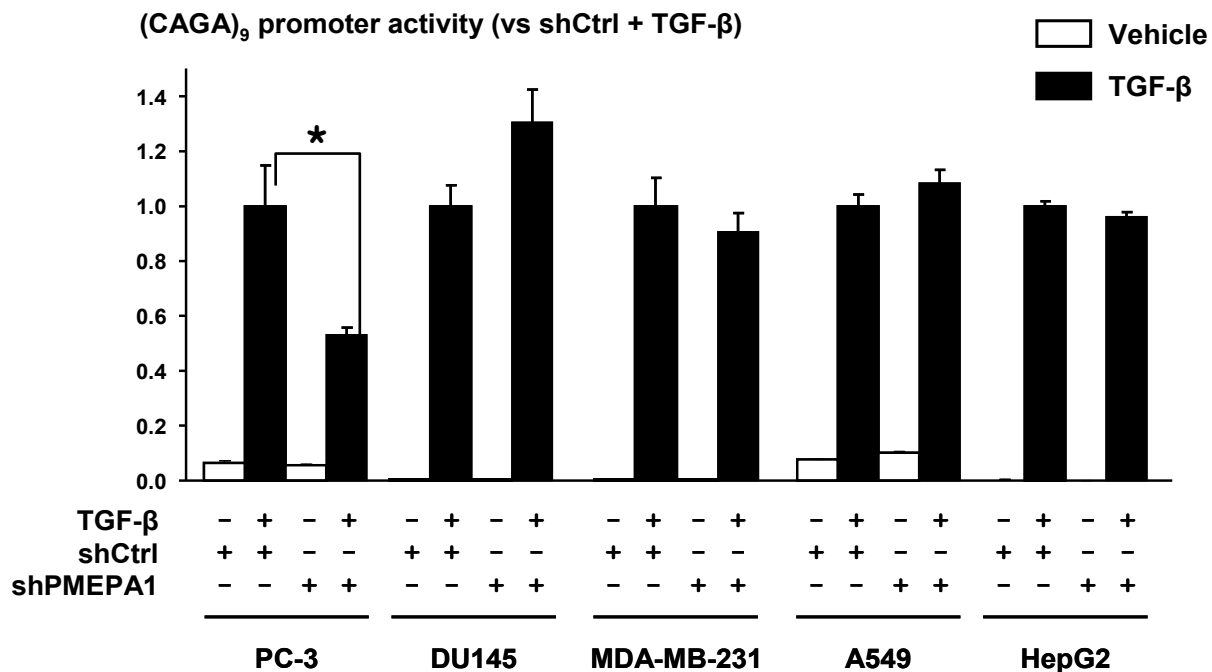|																				
TGF-β	–	+	–	+	–	+	–	+	–	+	–	+	–	+	–	+	–	+	–	+
shCtrl	+	+	–	–	+	+	–	–	+	+	–	–	+	+	–	–	+	+	–	–
shPMEPA1	–	–	+	+	–	–	+	+	–	–	+	+	–	–	+	+	–	–	+	+

PC-3   DU145   MDA-MB-231   A549   HepG2

Figure 24. PMEPA1 knockdown decreases TGF-β signaling specifically in PC-3 cells. A. PC-3 cells were cotransfected with a pGL3 reporter vector sensitive to TGF-β, (CAGA)9, BMP, BRE4(Id4) or constitutively active, SV40, phRL-CMV and a pLKO.1 vector expressing shCtrl or shPMEPA1. Cells were treated ± TGF-β (5ng/mL) or BMP-7 (50ng/mL) during 24h before measuring the dual-luciferase activity. **B.** Prostate (PC-3, DU145), breast (MDA-MB-231) and lung (A549) cancer cells and hepatocarcinoma cells (HepG2) were cotransfected with a pGL3-(CAGA)₉, phRL-CMV and a pLKO.1 vector expressing shCtrl or shPMEPA1. Cells were treated ± TGF-β (5ng/mL) or BMP-7 (50ng/mL) during 24h before measuring the dual-luciferase activity. Results represent the average ± SEM relative luciferase activity measured in quadruplicate. * $P<0.05$ using a Mann-Whitney's U test.

44

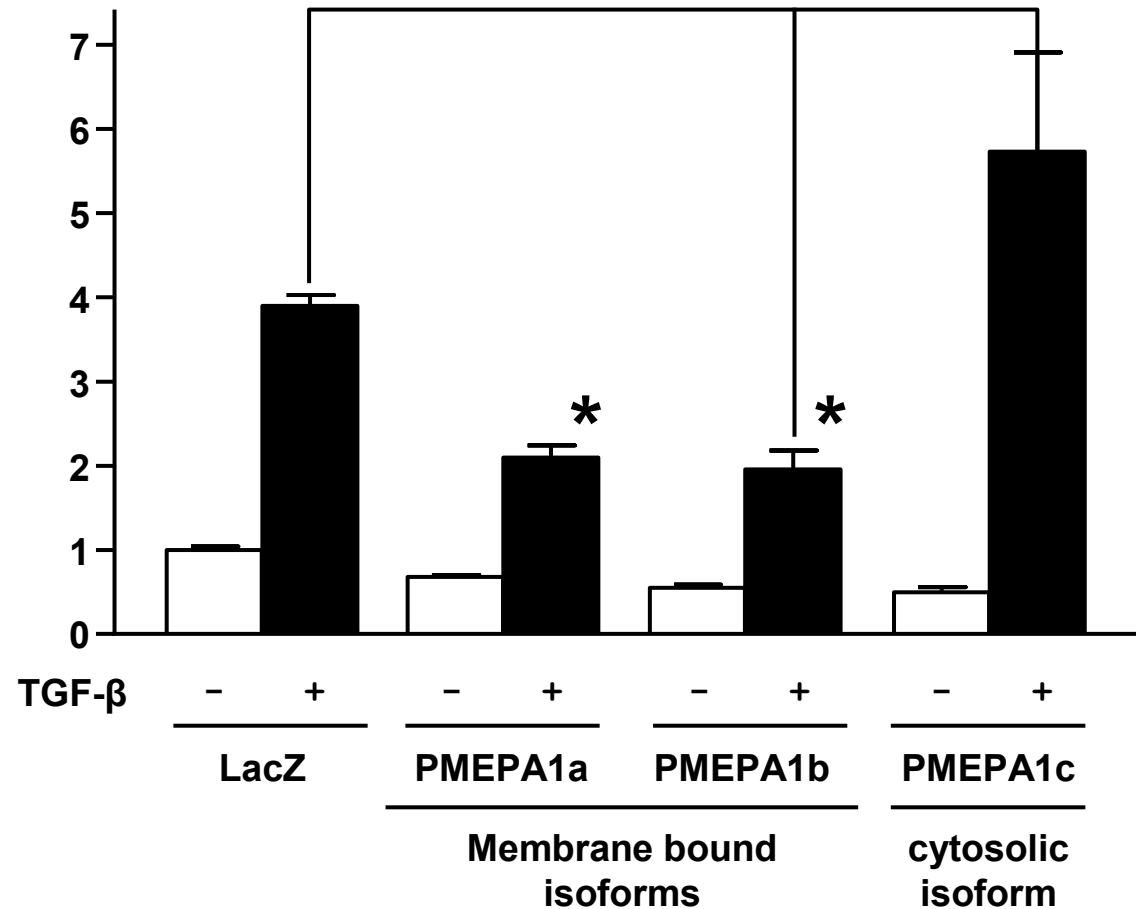**(CAGA)$_9$ promoter activity**
(vs LacZ + vehicle)

Figure 25. Effect of the overexpression of PMEPA1 isoforms on TGF-β signaling in prostate cancer cells. PC-3 cells were cotransfected with a pGL3- (CAGA)$_9$-fLuc vector, a phRL-CMV plasmid and a pcDNA plasmid expressing LacZ or the isoform a, b or c of PMEPA1. Cells were treated ± TGF-β (5ng/mL, 24h) before measuring dual-luciferase activity. Average ± SD of one representative experiment performed in quadruplicate. *$P<0.05$ using a non-parametric Mann-Whitney's U test.
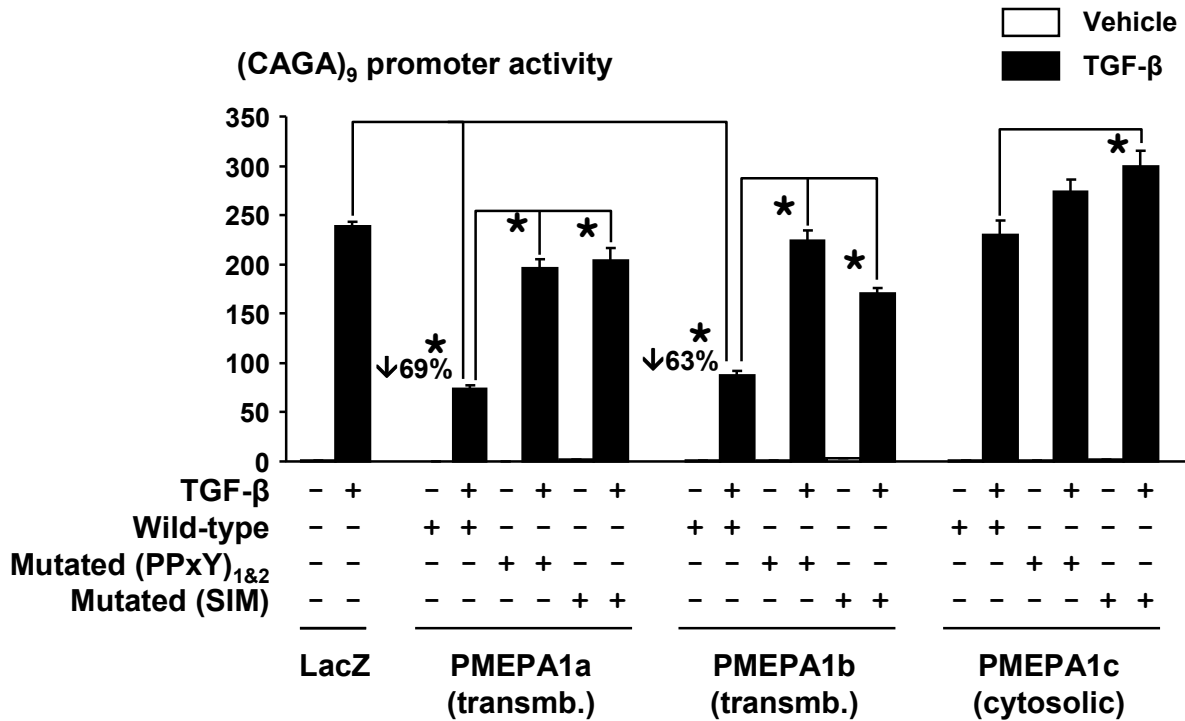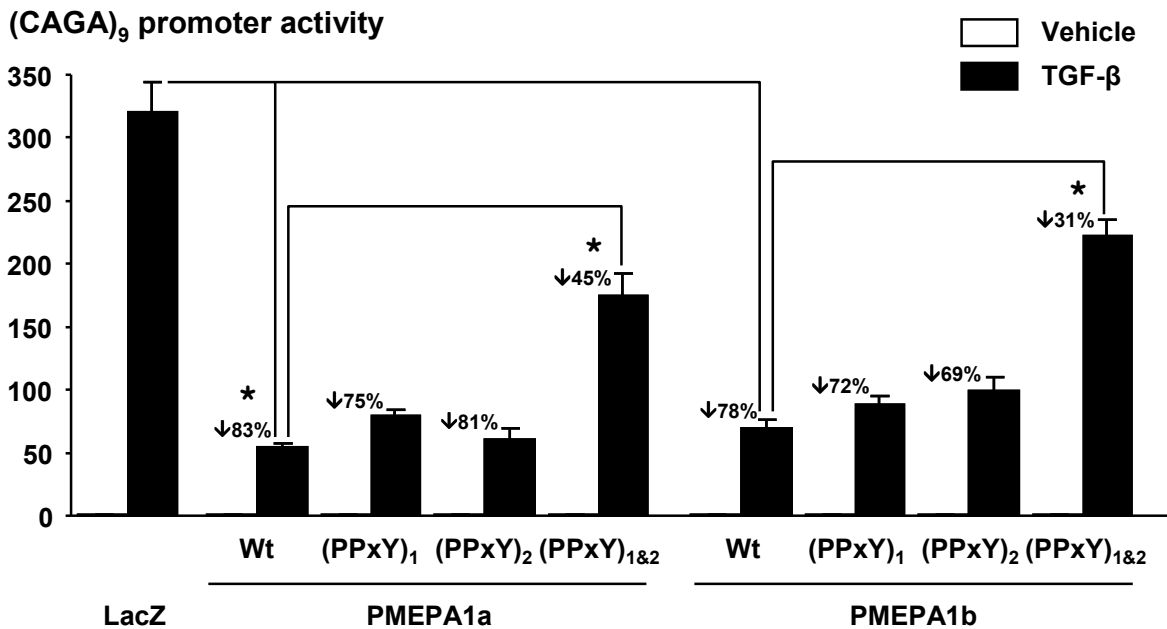
Figure 26. PPxY and SIM domains mediate the inhibition of TGF-β signaling mediated by membrane bound PMEPA1. HepG2 cells were cotransfected with a pGL3-(CAGA)$_9$-fLuc vector, a phRL-CMV plasmid and a pcDNA plasmid expressing LacZ or the isoform a, b or c of PMEPA1. Using site directed mutagenesis, PMEPA1 isoforms were mutated to neutralize the Smad interaction motif (SIM), the 1st, the 2nd or both PPxY domains. Cells were treated ± TGF-β (5ng/mL, 24h) before measuring dual-luciferase activity. Average ± SD of one representative experiment performed in quadruplicate. *$P<0.05$ using a non-parametric Mann-Whitney's U test.
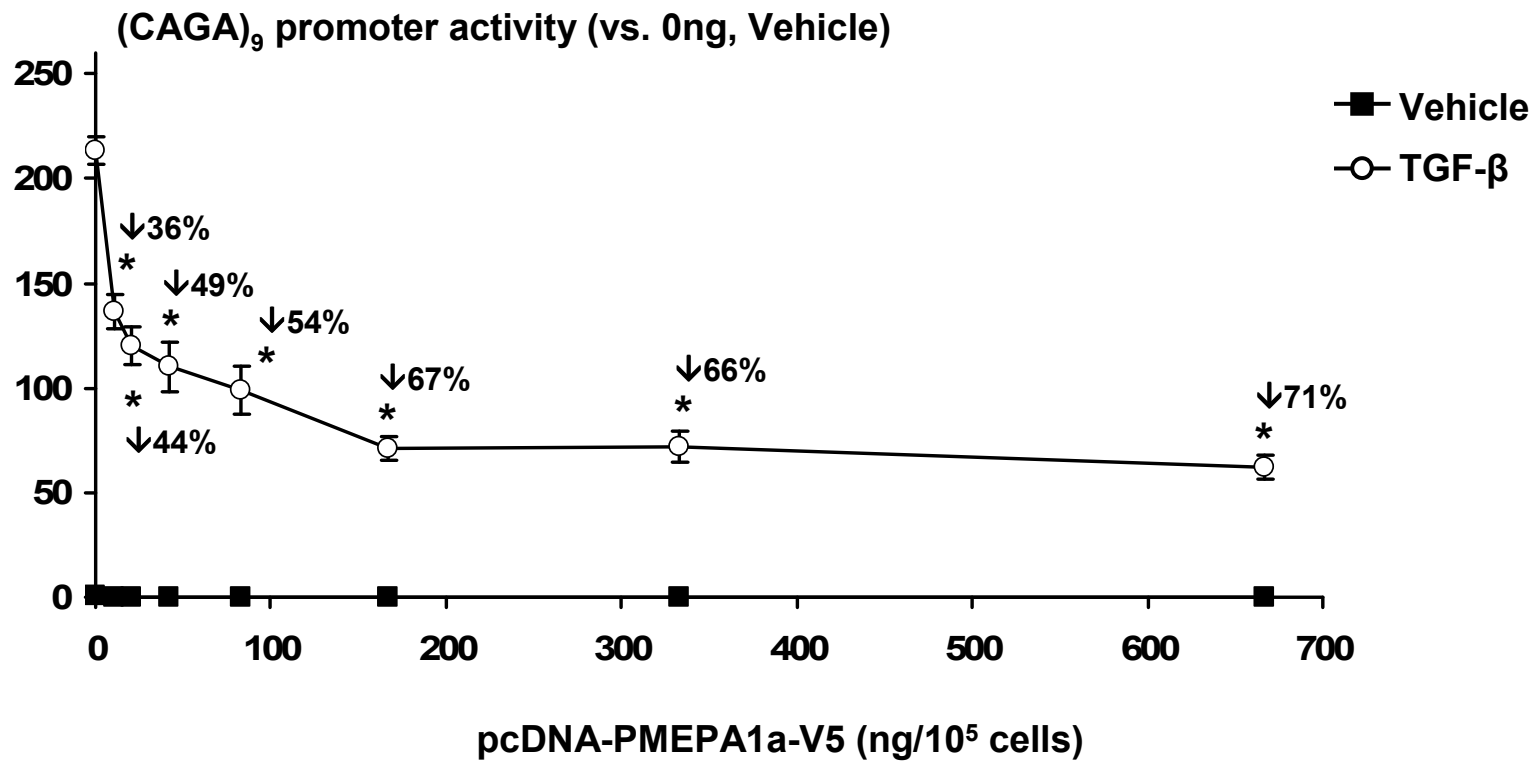
(CAGA)$_9$ promoter activity (vs. 0ng, Vehicle)

- ■ Vehicle
- ○ TGF-β

↓36% *
↓49% *
↓54% *
↓44% *
↓67% *
↓66% *
↓71% *

pcDNA-PMEPA1a-V5 (ng/10^5 cells)

Figure 27. Membrane-bound PMEPA1a inhibits TGF-β signaling in a dose-dependant manner. HepG2 cells were cotransfected with pGL3-(CAGA)$_9$-fLuc and phRL-CMV plasmids and decreasing quantities of pcDNA plasmid expressing the isoform a of PMEPA1. The total quantity of plasmid transfected was maintained constant using a pcDNA plasmid expressing LacZ. Cells were treated ± TGF-β (5ng/mL, 24h) before measuring dual-luciferase activity. Average ± SD of one representative experiment performed in quadruplicate. *$P<0.05$ when compared to cells not expressing PMEPA1a, using a non-parametric Mann-Whitney's *U* test. Values represent the decrease of luciferase activity compared to cells not expressing PMEPA1a and treated with TGF-β.
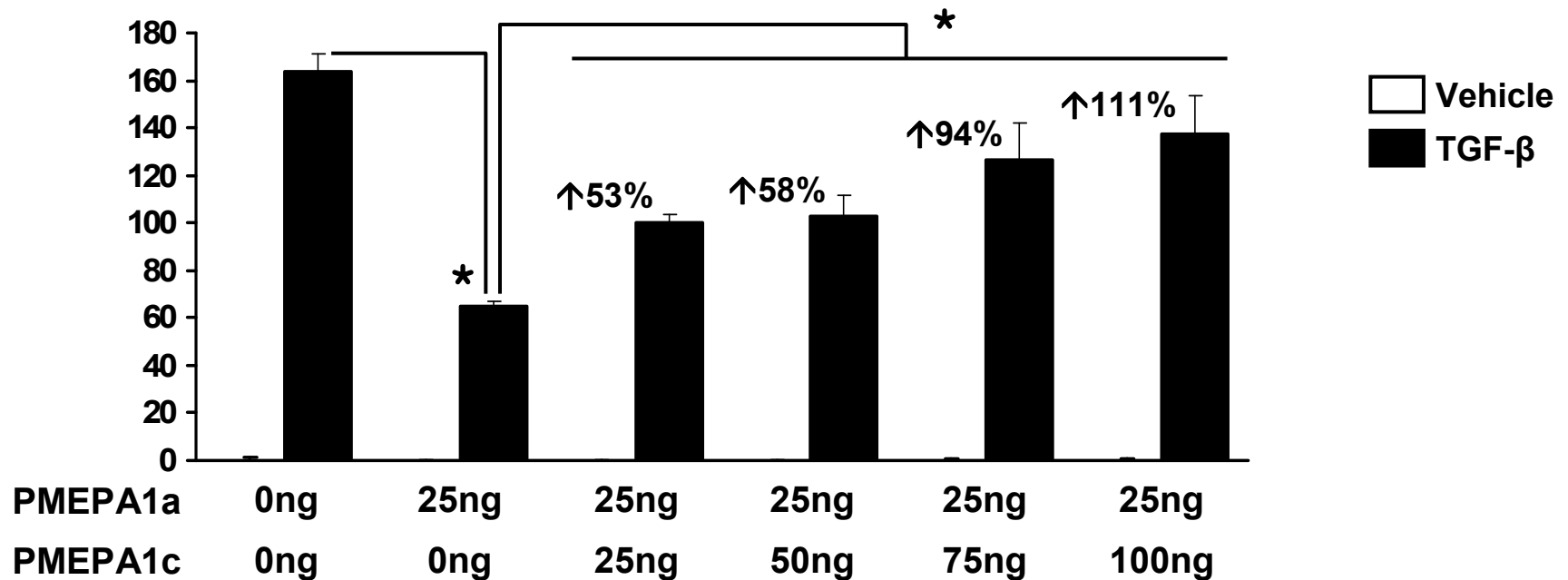
Figure 28. Cytosolic PMEPA1c reverts TGF-β signaling pathway inhibition mediated by membrane-bound PMEPA1a. HepG2 cells were cotransfected with pGL3-(CAGA)9-fLuc, phRL-CMV and pcDNA-PMEPA1a-V5 plasmids and increasing quantities of pcDNA plasmid expressing the isoform c of PMEPA1. The total quantity of plasmid transfected was maintained constant using a pcDNA plasmid expressing LacZ. Quantities of plasmid are expressed as ng/15000 cells. Cells were treated ± TGF-β (5ng/mL, 24h) before measuring dual-luciferase activity. Average ± SD of one representative experiment performed in quadruplicate. *P<0.05 using a non-parametric Mann-Whitney's *U* test. Values represent the increase of luciferase activity compared to cells expressing PMEPA1a only and treated with TGF-β.
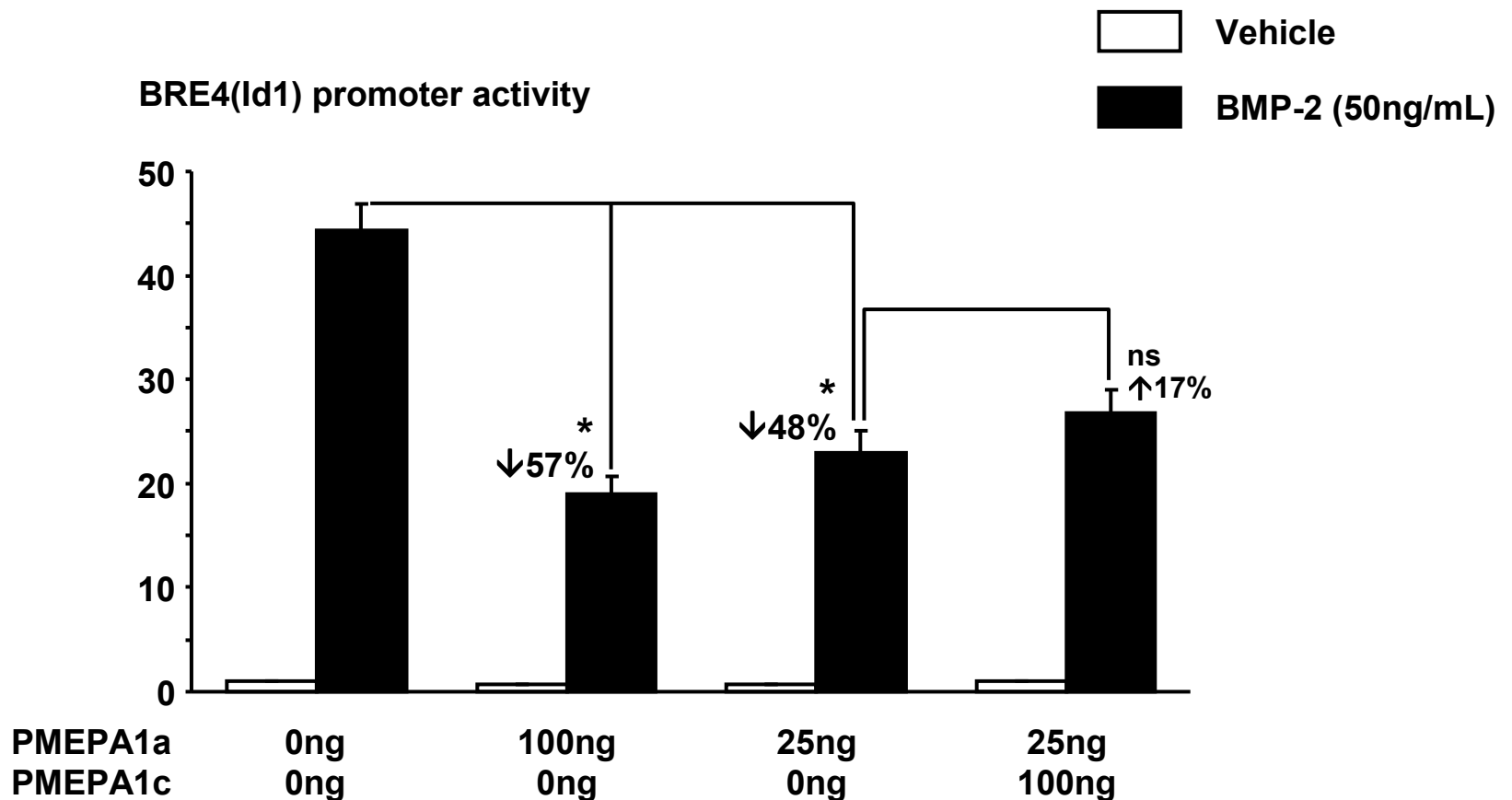
Figure 29. Membrane-bound PMEPA1a decrease BMP signaling pathway. HepG2 cells were cotransfected with pGL3-BRE4(Id1)-fLuc vector sensitive to BMP, phRL-CMV plasmid and pcDNA vectors to PMEPA1a and or PMEPA1c. The total quantity of plasmid transfected was maintained constant using a pcDNA plasmid expressing LacZ. Quantities of plasmid are expressed as ng/15000 cells. Cells were treated ± BMP-7 (50ng/mL, 24h) before measuring dual-luciferase activity. Average ± SD of one representative experiment performed in quadruplicate. *$P<0.05$ using a non-parametric Mann-Whitney's U test. ns, non significant.
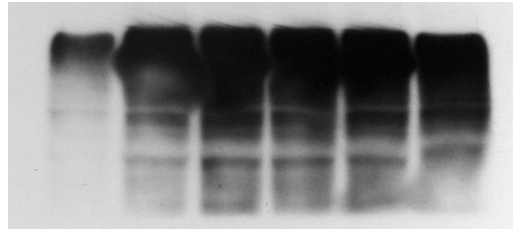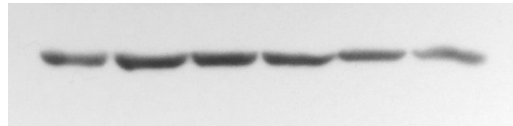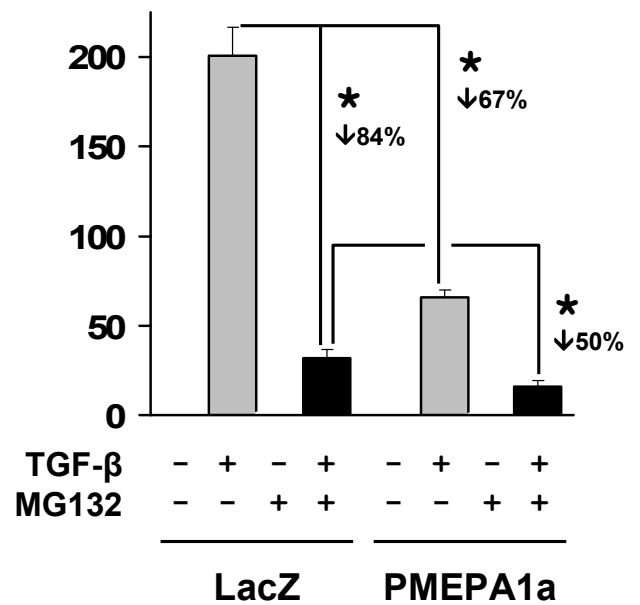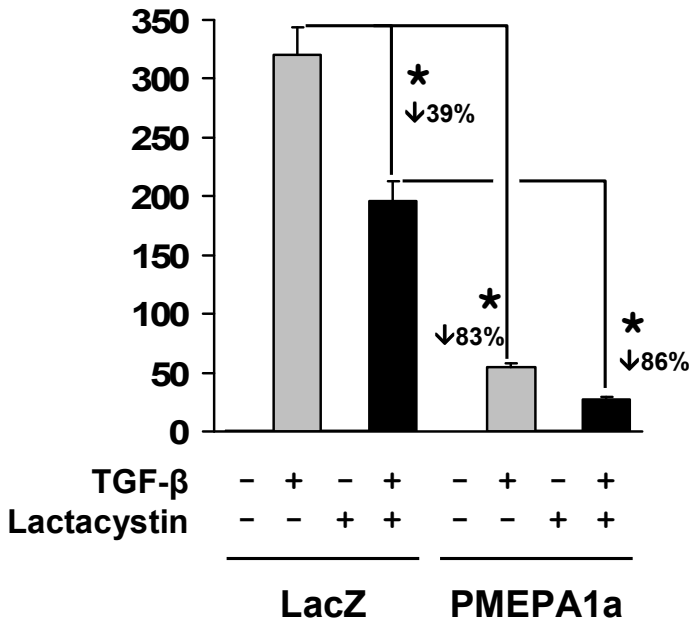
Figure 30. Effect of proteosome inhibitors on TGF-β signaling and membrane-bound PMEPA1. A. Subconfluent HepG2 cells were treated ± Lactacystin (5μM) or MG132 (1.25 to 10μM) during 24h. Protein lysates were prepared and ubiquitinated protein were immunodetect by Western-Blot with an antibody anti-ubiquitin. **B.** HepG2 cells were cotransfected with pGL3-(CAGA)9, phRL-CMV and a pcDNA vector expressing LacZ or membrane-bound PMEPA1. Cells were treated ± TGF-β (5ng/mL) in the presence or absence of Lactacystin (5μM) or MG132 (1.5μM). Twenty four hours later, the dual-luciferase activity was measured. Results are the average ± SEM of the relative promoter activity measured in quadruplicate. *, P<0.05 using a non-parametric Mann-Whitney's U test. Values indicate the decrease of promoter activity.
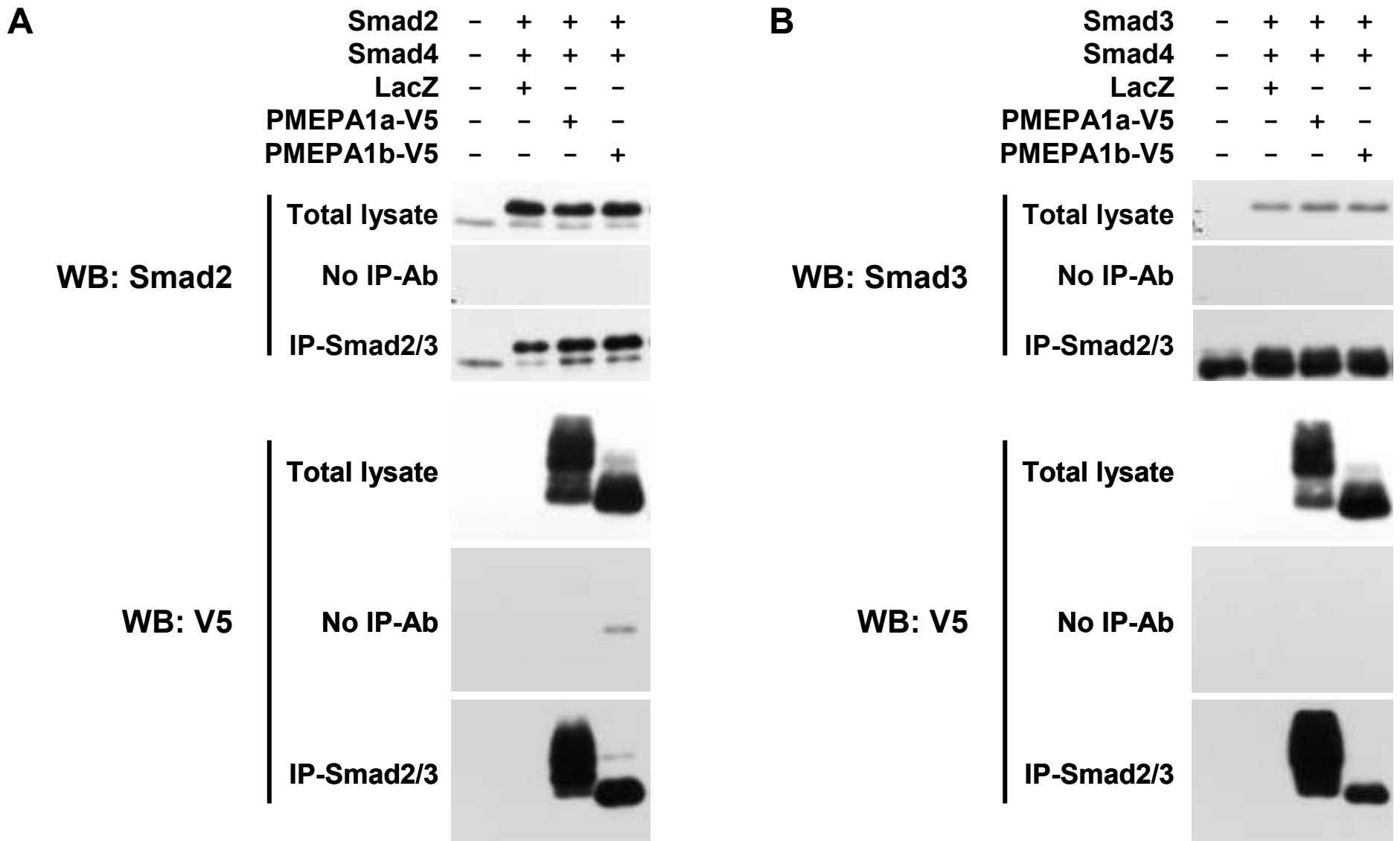
	Smad2	−	+	+	+
A	Smad4	−	+	+	+
	LacZ	−	+	−	−
	PMEPA1a-V5	−	−	+	−
	PMEPA1b-V5	−	−	−	+

	Smad3	−	+	+	+
B	Smad4	−	+	+	+
	LacZ	−	+	−	−
	PMEPA1a-V5	−	−	+	−
	PMEPA1b-V5	−	−	−	+

WB: Smad2 — Total lysate / No IP-Ab / IP-Smad2/3

WB: V5 — Total lysate / No IP-Ab / IP-Smad2/3

WB: Smad3 — Total lysate / No IP-Ab / IP-Smad2/3

WB: V5 — Total lysate / No IP-Ab / IP-Smad2/3

Figure 31. Membrane-bound PMEPA1 interact with Smad2 and 3. COS cells were cotransfected to express (**A**) Smad2 or (**B**) Smad3, Smad4 and LacZ, PMEPA1a-V5 or PMEPA1b-V5. Twenty-four hours later, cells were lyzed and we performed an immunoprecipitation with or without an antibody against Smad2/3 (Millipore) and protein G-Sepharose. Total lysates and immunoprecipitated proteins were analyzed by Western-Blot to immunodetect Smad2, Smad3 or the epitope tag V5 present at the C-terminus of transfected PMEPA1 proteins.
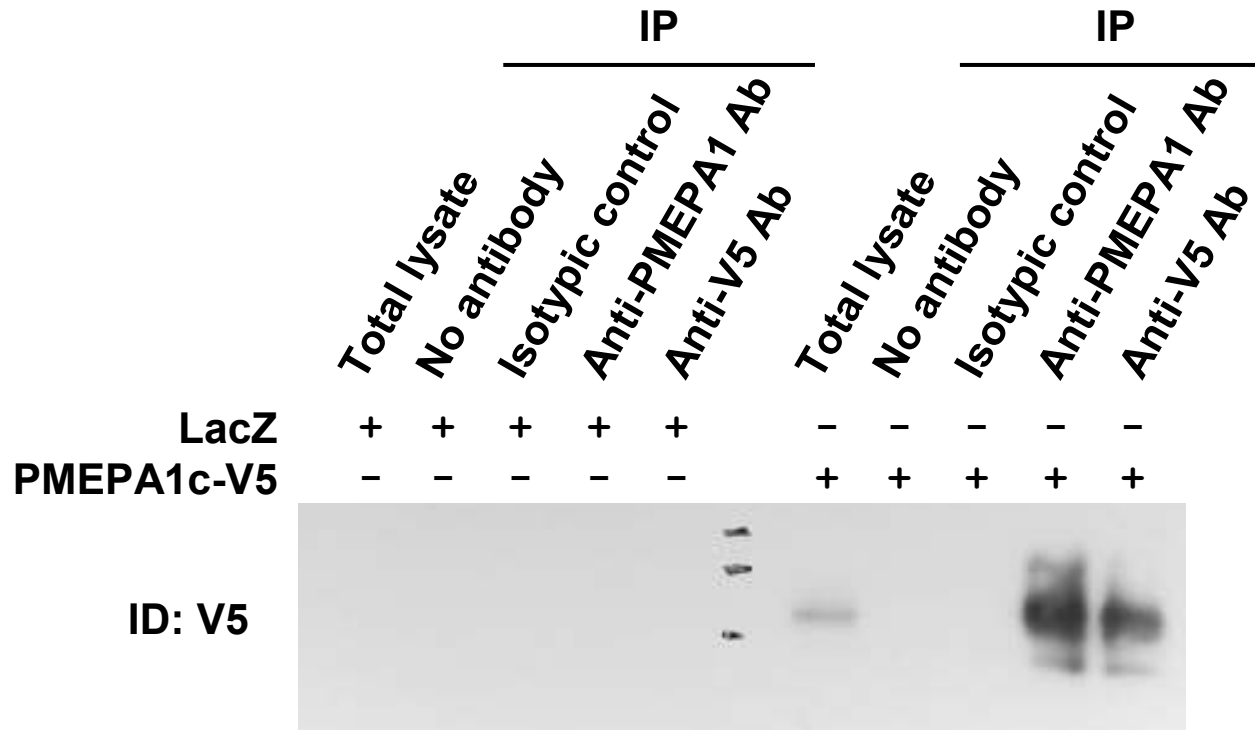
51

Figure 32. Validation of the mouse monoclonal antibody against PMEPA1 for immunoprecipitation. COS cells were transfected with a pcDNA plasmid expressing LacZ or PMEPA1c-V5. Forty-eight hours later, cells were lyzed and immunoprecipitation (IP) was performed using protein G-Sepharose in the absence of antibody or using an antibody against PMEPA1, against the epitope tag V5 or an isotypic control. Total lysate and immunoprecipitate were analyzed using Western-blotting to detect V5. PMEPA1 was detected only on total lysate or in immunoprecipitate where the anti-PMEPA1 antibody was used. No signal was detected in the absence of PMEPA1 expression (LacZ transfected cells).

Stable Overexpression of Smad7 in Human Melanoma Cells Impairs Bone Metastasis

Delphine Javelaud,[1] Khalid S. Mohammad,[2] Christopher R. McKenna,[2] Pierrick Fournier,[2] Flavie Luciani,[3] Maryla Niewolna,[2] Jocelyne André,[1] Véronique Delmas,[3] Lionel Larue,[3] Theresa A. Guise,[2] and Alain Mauviel[1]

[1]Institut National de la Sante et de la Recherche Medicale, U697, Paris, France; [2]University of Virginia, Charlottesville, Virginia; and [3]UMR146 Centre National de Recherche Scientifique, Orsay, France

Abstract

Melanoma has a propensity to metastasize to bone, where it is exposed to high concentrations of transforming growth factor-β (TGF-β). Because TGF-β promotes bone metastases from other solid tumors, such as breast cancer, we tested the role of TGF-β in melanoma metastases to bone. 1205Lu melanoma cells, stably transfected to overexpress the natural TGF-β/Smad signaling inhibitor Smad7, were studied in an experimental model of bone metastasis whereby tumor cells are inoculated into the left cardiac ventricle of nude mice. All mice bearing parental and mock-transfected 1205Lu cells developed osteolytic bone metastases 5 weeks post-tumor inoculation. Mice bearing 1205Lu-Smad7 tumors had significantly less osteolysis on radiographs and longer survival compared with parental and mock-transfected 1205Lu mice. To determine if the reduced bone metastases observed in mice bearing 1205Lu-Smad7 clones was due to reduced expression of TGF-β target genes known to enhance metastases to bone from breast cancer cells, we analyzed gene expression of osteolytic factors, parathyroid hormone-related protein (PTHrP) and interleukin-11 (IL-11), the chemotactic receptor CXCR4, and osteopontin in 1205Lu cells. Quantitative reverse transcription-PCR analysis indicated that *PTHrP, IL-11, CXCR4,* and osteopontin mRNA steady-state levels were robustly increased in response to TGF-β and that Smad7 and the TβRI small-molecule inhibitor, SB431542, prevented such induction. In addition, 1205Lu-Smad7 bone metastases expressed significantly lower levels of *IL-11, connective tissue growth factor,* and *PTHrP.* These data suggest that TGF-β promotes osteolytic bone metastases due to melanoma by stimulating the expression of prometastatic factors via the Smad pathway. Blockade of TGF-β signaling may be an effective treatment for melanoma metastasis to bone. [Cancer Res 2007;67(5):2317–24]

Introduction

Transforming growth factor-β (TGF-β) is a prototypic multifunctional cytokine whose broad modulatory activity affects numerous biological functions. At the organism level, these include, but are not limited to, control of immune functions, embryogenesis, carcinogenesis, and tissue responses to injury. At the cell level, TGF-β controls proliferation, migration, as well as extracellular matrix synthesis and degradation (1–5). The complexity of the role played by TGF-β in cancer and metastasis is underscored by the duality of this growth factor, depending on the stage of the disease (6–8). Thus, although the TGF-β signaling cascade functions as a tumor suppressor pathway in early carcinogenesis, mainly through the ability of TGF-β to inhibit the cell cycle, it paradoxically favors tumor progression during late-stage metastatic progression of tumors.

TGF-β signal transduction occurs via ligand-activated heterotetrameric serine/threonine kinase receptors (TβRI and TβRII) on the cell surface, which phosphorylate the cytoplasmic proteins Smad2 and Smad3. These receptor-regulated Smads (R-Smads) are ligand-specific and, on activation, associate with Smad4, a common partner to all receptor-regulated Smads activated by the various ligands of the TGF-β family. R-Smad/Smad4 heterocomplexes then translocate into the cell nucleus to regulate target gene transcription (5, 9). The inhibitory Smad, Smad7, interferes with Smad signaling by various means: (*a*) it binds activated TβRI to prevent phosphorylation of Smad2/3; (*b*) it recruits E3 ubiquitin-ligases, such as Smurf1, Smurf2, and WWP1, to the activated TGF-β receptor complexes, leading to their proteasomal degradation; and (*c*) it interacts with GADD34, the regulatory subunit of the protein phosphatase PP1, thereby recruiting it to TβRI to inactivate the latter (10–12).

The effect of TGF-β on melanoma progression is just beginning to unravel. Malignant melanomas secrete high amounts of TGF-β, whose autocrine and paracrine effects contribute directly and indirectly to tumor progression (13). Indeed, we identified previously that melanoma cell–derived TGF-β results in high, ligand-dependent, constitutive Smad3-driven transcriptional activity (14). In addition, we identified that overexpression of Smad7 inhibits melanoma cell matrix metalloproteinase (MMP)-2 and MMP-9 production, dramatically impairs their invasive capacity *in vitro*, reduces anchorage-independent growth, and delays s.c. tumor growth in nude mice (15). These findings underscore the notion that intact, or exacerbated, Smad signaling occurs throughout tumor progression in melanoma cells.

In experimental models of metastasis, it has been shown that TGF-β is essential for breast cancer cells to form bone metastases (16, 17). Furthermore, the release of TGF-β from the bone matrix on activation of osteoclasts by soluble factors, such as parathyroid hormone-related protein (PTHrP) derived from cancer cells, further exacerbates the latter and enhances the growth of metastases, thereby establishing what has been viewed as a vicious cycle orchestrated by TGF-β (18, 19).

In this report, we show that Smad7 overexpression delays the establishment and growth of melanoma bone metastases in a

---

mouse model. In addition, we determine that inhibition of the Smad cascade in melanoma cells represses the expression of a panel of TGF-β–dependent genes that was identified previously as critical for the establishment of bone metastases by breast cancer cells (17).

Materials and Methods

Cell Cultures and Reagents

Melanoma cell lines WM239-A, WM1341-D, WM983-A, WM793, WM983-B, WM852, and 1205Lu, kind gifts from Dr. M. Herlyn (Wistar Institute, Philadelphia, PA), have been described previously (14, 20, 21). They were grown in a composite medium (W489) consisting of three parts of MCDB153 and one part of L15 supplemented with 4% FCS and antibiotics. Melanoma cell lines Dauv-1, 888-mel, 501-mel, SK-28, and FO-1 have been described previously (22). They were grown in RPMI 1640 supplemented with 10% FCS and antibiotics. Human lung fibroblasts (WI-26) were grown in DMEM containing 10% FCS and antibiotics. Generation of Smad7-expressing clones (S7.a and S7.c) and mock-transfected cells has been described previously (15). All cells were grown at 37°C in a humidified atmosphere of 5% CO_2. The Smad3/Smad4–specific reporter plasmid (CAGA)$_9$-luc (23) was a gift from S. Dennler (Institut National de la Sante et de la Recherche Medicale U697, Paris, France). The pRL-TK vector was from Promega (Madison, WI). TGF-β$_1$ was purchased from R&D Systems, Inc. (Minneapolis, MN). The ALK5/TβRI inhibitor SB431542 was from Sigma-Aldrich (St. Louis, MO).

Biochemical Methods

Protein extraction and Western blotting were done as described previously (24). Anti-Smad3 and anti–β-actin were from Zymed (San Francisco, CA) and Sigma-Aldrich, respectively. The rabbit anti–phospho-Smad2/Smad3 antibody (25) was a generous gift from E. Leof (Mayo Clinic College of Medicine, Rochester, MN). Secondary antimouse and antirabbit horseradish peroxidase–conjugated antibodies were from Santa Cruz Biotechnology Inc. (Santa Cruz, CA).

Generation of Melanoma Cell Conditioned Medium

Cells (3 × 10^6) of each cell type were plated in a 150-mm tissue culture dish and cultured in 16 mL W489 medium without FCS for 72 h. Supernatants were then collected and floating cells were removed by centrifugation (420 g, 5 min). The corresponding cell layers were lysed and total protein concentration was determined to normalize each conditioned medium.

Cells Transfections and Luciferase Assays

Melanoma cells were seeded in 24-well plates and transfected at approximately 70% to 80% confluency with the polycationic compound Fugene (Roche Diagnostics, Indianapolis, IN) in fresh medium containing 1% FCS. TGF-β was added 4 h post-transfection. WI-26 fibroblasts were seeded in 24-well plates and transfected at approximately 70% to 80% confluency with Jet-PEI (Polyplus-Transfection, Illkirch, France) in fresh W489 medium without FCS. Conditioned media were added 4 h post-transfection. Following a 16-h incubation, cells were rinsed twice with PBS and lysed in passive lysis buffer (Promega). Luciferase activities were determined with a Dual-Glo luciferase assay kit according to the manufacturer's protocol (Promega).

Animal Experiments

The animal protocols for bone metastasis experiments were approved by the Institutional Animal Care and Use Committee at the University of Virginia (Charlottesville, VA) and were in accordance with the NIH Guide for the Care and Use of Laboratory Animals. Athymic female nude mice 4 weeks of age were housed in laminar flow isolated hoods. Water supplemented with vitamin K and autoclaved mouse chow were provided *ad libitum*. Radiographs were taken under mouse anesthesia mixture (30% ketamine and 20% xylazine in 0.9% NaCl). Tumor inoculation into the left cardiac ventricle was done on anesthetized mice positioned ventral side up as described previously (26). Briefly, the left cardiac ventricle was punctured percutaneously using a 26-gauge needle attached to a 1-mL

syringe containing suspended tumor cells. Visualization of bright red blood entering the hub of the needle in a pulsatile fashion indicated a correct position in the left cardiac ventricle. Tumor cells (10^5 in 0.1 mL PBS) were inoculated slowly over 1 min. Mice were followed by radiography for the development of bone lesions throughout the experiments. Mice were X-rayed in a prone and lateral position using a Digital Faxitron MX-20 with digital camera (Faxitron X-ray, Wheeling, IL) as described previously (26). Radiographs where taken at ×1 magnification and when a lesion was suspected, additional images with higher magnification (×4) were taken. Images were saved and lesion areas were measured and analyzed using MetaMorph software (Molecular Devices, Downingtown. PA).

Bone histology. Forelimb and hind limb bones were removed from mice at the time of experimental termination. Tissues were fixed in 10% neutral buffered formalin for 48 h, decalcified in 10% EDTA for 2 weeks, processed
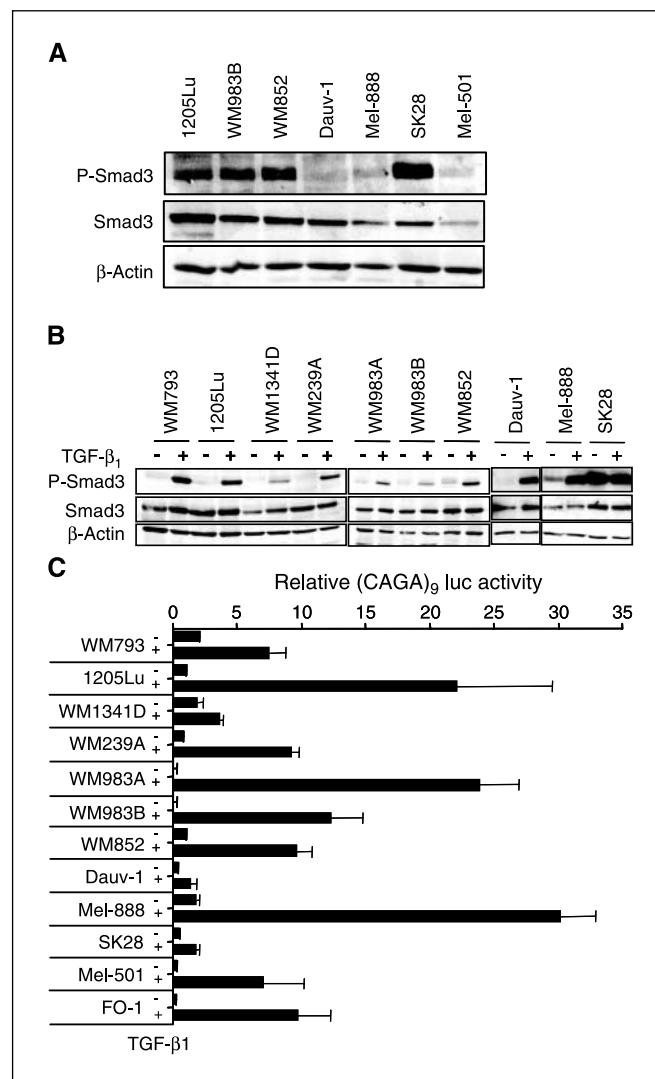

Figure 1. *A,* total protein extracts (60 μg) from unstimulated cultured melanoma cell lines were analyzed by Western blotting for phospho-Smad3 content. An anti–β-actin antibody was used for normalization. *B,* subconfluent melanoma cell cultures were incubated for 6 h in medium containing 1% serum. TGF-β1 (10 ng/mL) was added to the cultures 20 min before cell lysis for Western analysis (30 μg/lane) with specific antibodies directed against phospho-Smad3, Smad3, or β-actin. *C,* subconfluent melanoma cell cultures were transfected with 0.4 μg (CAGA)$_9$-luc vector together with 0.2 μg pRL-TK *Renilla* luciferase expression vector. Four hours post-transfection, cultures were left untreated or stimulated with TGF-β (10 ng/mL). Luciferase activities were measured in cell extracts 16 h post-transfection. *Columns,* mean of three independent experiments; *bars,* SE.

using an automated tissue processor (Excelsior, Thermoelectric), and embedded in paraffin. The sections were stained with H&E with orange G and phloxine to visualize new bone.

RNA Extraction and Gene Expression Analysis

In vitro experiments. Total RNA was isolated using an RNeasy kit (Qiagen GmbH, Hilden Germany).

In vivo experiments. The femur and tibiae from mice were dissected and cleaned from adhering tissues. The cartilage ends were cut off and the tumor cells in the marrow cavity were flushed out using cold PBS in a syringe with a sterile needle. After centrifugation, cells were resuspended in RNAlater (Qiagen) and total RNA was isolated with Trizol (Invitrogen, San Diego, CA) according to the manufacturer's instructions. Genomic DNA contaminations were eliminated by DNase I treatment. One microgram of RNA from each sample was reverse transcribed using the Thermoscript kit (Invitrogen) following the manufacturer's instructions. The resulting cDNAs were then processed for real-time PCR using SYBR Green technology. Reactions were carried out in a 7300 Real-time PCR System (Applied Biosystems) for 40 cycles (95°C for 15 sec/60°C for 1 min) after an initial 10-min incubation at 95°C.

Primers used for *in vitro* experiments were as follows *TGF-β1* (sense, 5′-ctctccgacctgccacaga-3′; antisense, 5′-aacctagatgggcgcgatct-3′); *TGF-β2* (sense, 5′-ccfcccactttctacagaccc-3′; antisense, 5′-gcgctgggtgggagatgttaa-3′); *TGF-β3* (sense, 5′-ctggccctgctgaactttg-3′; antisense, 5′-aaggtggtgcaagtgga-caga-3′); *CXCR4* (sense, 5′-cagtggccgacctcctctt-3′; antisense, 5′-cagtttgc-cacggcatca-3′); *interleukin-11* (*IL-11*; sense, 5′-actgctgctgctgaagactc-3′; antisense, 5′-ccacccctgctcctgaaata-3′); *PTHrP* (sense, 5′-tttacggcgac-gattcttcc-3′; antisense, 5′-ttcttcccaggtgtcttgag-3′); and *osteopontin* (sense, 5′-aggcagagcacagcatcgt-3′; 5′-ttggctgagaaggctgcaa-3′). Primers used for *in vivo* experiments were as follows: *IL-11* (sense, 5′-tgaagactcggctgtgacc-3′; antisense, 5′-cctcacggaaggactgtctc-3′); *PTHrP* (sense, 5′-actcgctctgcctggt-taga-3′; antisense, 5′-ggaggtgtcagacaggtggt-3′); and *connective tissue growth factor* (*CTGF*; sense, 5′-gctaccacatttcctacctagaaatca-3′; antisense, 5′-gacagtccgtcaaaacagattgtt-3′).

Target gene expression was normalized against the endogenous control genes *cyclophylin A* (sense, 5′-caaatgctggacccaacaca-3′; antisense, 5′-tgccatc-caaccactcagtct-3′) or *glyceraldehyde-3-phosphate dehydrogenase* (*GAPDH*; sense, 5′-gctcctcctgttcgacagtca-3′; antisense, 5′-accttccccatggtgtctga-3′). Data were analyzed using Applied Biosystems Sequence Detections Software (version 1.2.1).

Statistical Analyses

Differences in osteolytic lesion areas between groups were determined by one-way ANOVA and two-way ANOVA. Kaplan-Meier survival curve data were analyzed by log-rank test. All results were expressed as mean ± SE, and $P < 0.05$ was considered significant (GraphPad prism).

Results and Discussion

The role of TGF-β in melanoma progression and metastasis is controversial. Using a specific Smad-dependent transcription assay as well as Smad/DNA interaction assays based on our original characterization of *hCOL7A1* as a Smad3/Smad4 gene target (27), we showed previously that human melanoma cells secrete active TGF-β and exhibit both high constitutive, ligand-induced, Smad signaling (14). Subsequently, others have shown that TGF-β that is produced by melanoma cells contributes to peritumoral stroma remodeling, providing a survival advantage to melanoma cells (28). Contrasting with these results, it has also been proposed that the oncoproteins c-Ski and SnoN, known to interfere with Smad signaling (29), are expressed at high levels in melanoma cells and may be responsible for the lack of growth-inhibitory activity of TGF-β in these cells (30, 31). Recently, we showed that overexpression of Smad7 in melanoma cells inhibits endogenous constitutive Smad signaling, reduces MMP secretion, and delays tumorigenicity both *in vitro* and in a model of
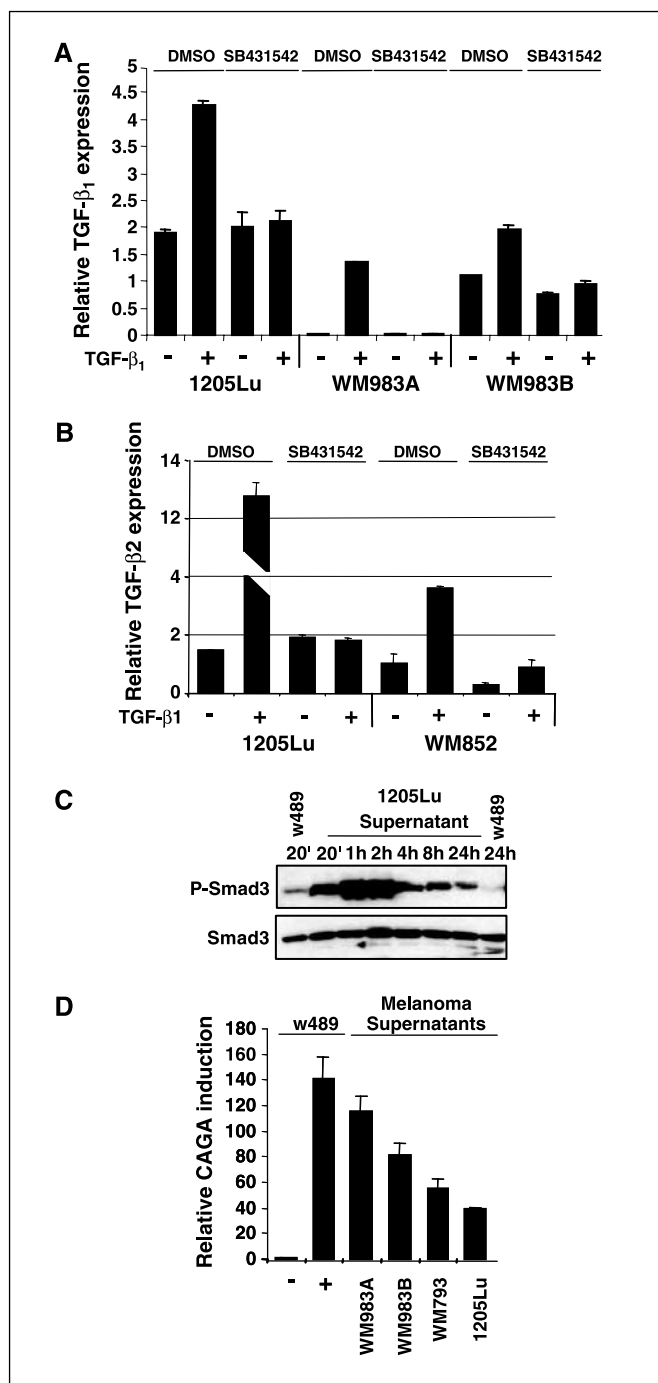

Figure 2. Subconfluent melanoma cell cultures were preincubated for 6 h in medium containing 1% serum before stimulation with TGF-β1 (10 ng/mL) in the absence or presence of 5 μmol/L SB431542 (or DMSO) added 1 h before addition of the growth factor. Total RNA was analyzed by quantitative RT-PCR with primers specific for *TGF-β1* (*A*) or *TGF-β2* (*B*). Values are corrected for *cyclophilin A* mRNA levels in the same samples. *C,* subconfluent WI-26 human lung fibroblast cultures were incubated for 24 h in medium containing 0% serum, following which an equivalent volume of either W489 unconditioned or 1205Lu melanoma cell conditioned medium was added. WI-26 cell layers were then lysed for Western analysis with specific antibodies directed against phospho-Smad3 and Smad3. *D,* subconfluent WI-26 fibroblast cultures were transfected with 0.4 μg (CAGA)₉-luc vector together with 0.2 μg pRL-TK *Renilla* luciferase expression vector in W489 medium without serum. Four hours post-transfection, cultures were left untreated (−) or stimulated with TGF-β (10 ng/mL) (+) or an equivalent volume of various melanoma cell conditioned medium. Luciferase activities were measured in cell extracts 20 h later. Results are expressed as relative reporter activation. *Columns,* mean of three independent experiments; *bars,* SE.

subcutaneous tumor formation in nude mice (15). These apparently contradictory results about the role of autocrine TGF-β signaling in melanoma cells led us to reevaluate the activation status of Smad signaling obtained in several available melanoma cell lines. Most transcriptional responses to TGF-β in the adult are mediated by Smad3/Smad4, although it is generally accepted that Smad2 is critical during embryonic life (9). We thus focused our attention on Smad3/Smad4 status and activation. As shown in Fig. 1A, the various cell lines tested exhibited variable basal levels of P-Smad3, a marker of TGF-β receptor activation (Fig. 1A). In all cases, exogenously added TGF-β further induced a dramatic elevation of P-Smad3 levels, indicative of functional TGF-β receptor complexes (Fig. 1B). Transient cell transfection experiments with the Smad3/Smad4–specific reporter construct (CAGA)$_9$-lux (23) indicated that most cell lines responded to exogenous TGF-β with a robust transcriptional response (Fig. 1C), indicative of functional TGF-β/Smad signal transduction cascade all the way from the cell membrane to the nucleus. These results are in full agreement with our initial observations (14) and consistent with the accepted concept of an autocrine and oncogenic role for TGF-β in late-stage carcinogenesis (reviewed in refs. 32, 33).

TGF-β expression is often increased in tumor cells and has been correlated with the advanced stage of melanoma progression (34). We thus wanted to determine whether an autoregulatory loop controlled TGF-β expression in melanoma cells. First, using quantitative real-time PCR, we determined that all melanoma cell lines available in the laboratory expressed the three TGF-β isoforms (data not shown). *TGF-β1* expression was predominant, with relative expression levels 10- to 20-fold higher than those for *TGF-β3* (data not shown). *TGF-β2* was expressed at very low levels (100- to 1,000-fold less than TGF-β1). These results are consistent with previously published observations (35). Incubation of some of these cell lines, selected based on their robust Smad-specific transcriptional response to TGF-β (see Fig. 1C) with exogenous TGF-β1 for 24 h led to a consistently observed increase in the expression of *TGF-β1,* which was totally abrogated by the ALK5 inhibitor SB431542 (Fig. 2A). Expression of *TGF-β2* mRNA was also induced by TGF-β1 treatment (Fig. 2B); however, it only occurred in 50% of the cell lines tested (data not shown). Again, incubation with the ALK5 inhibitor SB431542 led to a complete abrogation of *TGF-β2* induction by exogenous TGF-β1. Of note, no modulation of *TGF-β3* expression was observed after either TGF-β1 or SB431542 treatment in any of the cell lines tested (data not shown), suggesting its independence from Smad signaling.

To determine whether melanoma cells secrete active TGF-β that could induce stroma activation, melanoma cell culture supernatants were studied for their capacity to activate the Smad pathway in fibroblasts in culture. Incubation of WI-26 human lung fibroblasts with conditioned medium from four distinct melanoma cell lines exhibiting constitutive Smad3/Smad4 activation and TGF-β1 expression induced both rapid and sustained Smad3 phosphorylation in WI-26 cells (Fig. 2C) and potent transactivation of the transfected (CAGA)$_9$-lux construct (Fig. 2D). Incubation with W489 unconditioned medium did not induce any of these TGF-β–specific responses. Together, these results emphasize the fact that ligand-dependent constitutive activation of the Smad pathway in melanoma cells translates into production of active TGF-β that is highly capable of inducing both autocrine and paracrine (stromal) responses.
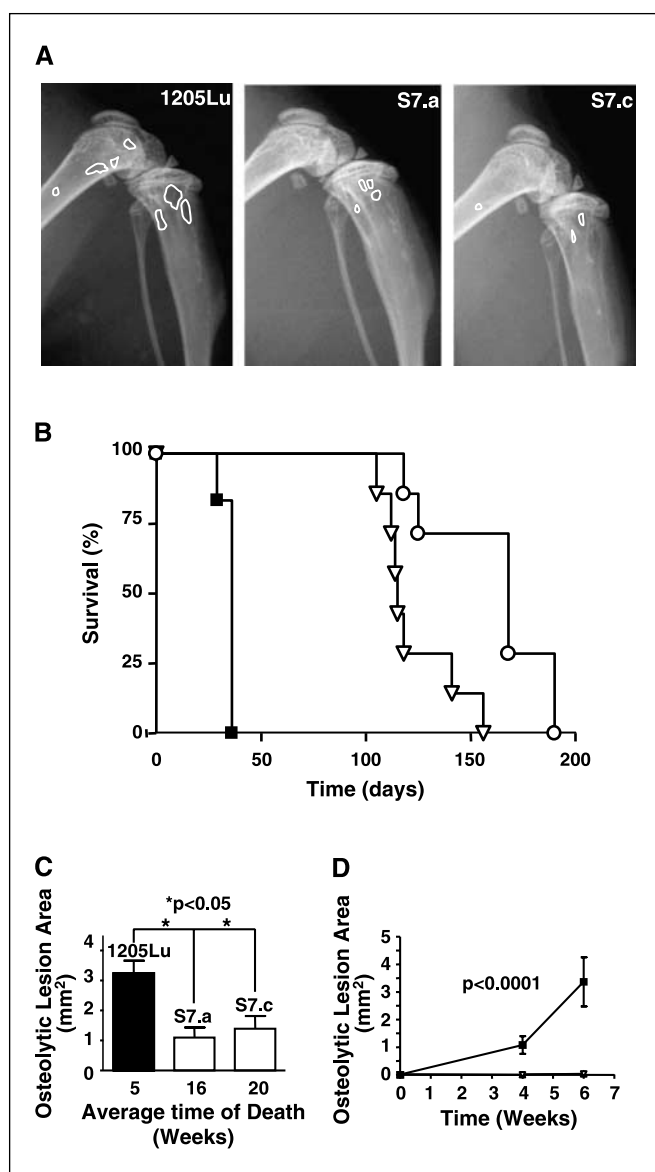

Figure 3. *A,* representative X-ray radiography of the hind limbs of mice, 5 wks (parental, *n* = 6) or 14 wks (clones S7.a and S7.b, seven mice each) post-tumor cell inoculation. Osteolytic lesions are highlighted with white lines. Note the dramatic difference in both size and number of lesions generated by parental 1205Lu cells versus Smad7-overexpressing clones. *B,* survival of mice bearing S7.a (▽) and S7.c (○) tumors was significantly longer than that of mice bearing parental 1205Lu cells (■). *C,* osteolytic lesion area (mm^2) on radiographs was measured by computerized image analysis of forelimbs and hind limbs at the time of death: 5 wks postinoculation for parental 1205Lu cells, 16 and 20 wks postinoculation for S7.a and S7.c clones, respectively. *Columns,* mean (*n* = 7); *bars,* SE. *D,* osteolytic lesion area (mm^2) on radiographs was measured by computerized image analysis of forelimbs and hind limbs at 4 and 6 wks postinoculation for both pcDNA transfected 1205Lu cells (*n* = 11; ■) and clones overexpressing Smad7 (12 mice for each clone; ▲ and ▼). *Points,* mean; *bars,* SE. Note that lesion area was so small in both Smad7-overexpressing 1205Lu-bearing mice that the data lines are indistinguishable from the X axis.

It is expected from our data on the expression of the three TGF-β isoforms (see above) that TGF-β1 and TGF-β3 represent the majority of constitutively produced isoforms capable of driving Smad signaling in melanoma cells even in the presence of a TβRI inhibitor. Furthermore, TGF-β1 and TGF-β2 are likely to be

induced further in tissue environments rich in TGF-β, such as in late-stage cancer progression.

We showed previously that TGF-β promotes bone metastases from solid tumors, such as breast cancer (16, 17, 19). Thus, given our recent data linking autocrine TGF-β signaling to melanoma aggressiveness (15), we decided to test the role of autocrine TGF-β signaling in melanoma metastases to bone by overexpressing the inhibitory Smad7 in a cell line with high endogenous Smad activity. For this purpose, we used 1205Lu cells as (*a*) they exhibit high autonomous, ligand-induced, constitutive TGF-β/Smad signaling; (*b*) they exhibit a strong transcriptional response to exogenous TGF-β; (*c*) they are highly invasive in a Matrigel assay; and (*d*) they are highly tumorigenic *in vivo* (15). Furthermore, we showed previously that Smad7 overexpression in 1205Lu melanoma cells reduces MMP-2 and MMP-9 production as well as their capacity to invade Matrigel and to establish subcutaneous tumors in nude mice (15).

In a proof-of-concept experiment, parental 1205Lu cells rapidly established bone metastases in a model of bone metastasis whereby tumor cells are inoculated into the left cardiac ventricle of nude mice. Reasons for using the model include the facts that (*a*) no model exists whereby primary melanoma tumors metastasize to bone; (*b*) the left cardiac ventricle model was established with melanoma lines (36); and (*c*) the relevance to bone metastases has been consistently shown in the literature (37, 38). Specifically, this model addresses the process of metastasis from entry of tumor cells into the arterial circulation to the establishment of bone metastasis and tumor-bone interactions.

Bone metastases seemed to be mostly osteolytic, but some osteoblastic lesions were also found (Supplementary Fig. S1). In addition, soft tissue metastases to various organs, adrenal glands, lungs, liver, and skin, appeared in all test mice (*n* = 6) 5 to 10 weeks post-tumor inoculation (data not shown).

Next, 1205Lu melanoma cells were stably transfected with pcDNA-Smad7. In the first experiment, Smad7-overexpressing clones were compared with parental 1205Lu. All mice (*n* = 6) inoculated with parental 1205Lu cells developed osteolytic bone metastases 5 weeks post-tumor inoculation (Fig. 3*A, left*) as well as metastases to adrenal glands and kidney (data not shown). All mice

Table 1. Modulation of osteolytic factor gene expression by TGF-β in melanoma cells

	Cell	DMSO		SB431542	
		UT	TGF-β	UT	TGF-β
IL-11	1205Lu	0.55 ± 0.03	19.28 ± 2.06	0.32	0.46 ± 0.07
	Fold induction		35		1.1
	WM983A	0.02	1.36 ± 0.01	0.02 ± 0.005	0.02 ± 0.01
	Fold induction		68		1
	WM983B	0.05 ± 0.03	1.66 ± 0.15	0.52 ± 0.14	0.46 ± 0.13
	Fold induction		31.9		0.9
	WM852	2.7 ± 0.41	11.9 ± 3.5	1.6 ± 0.1	0.4 ± 0.1
	Fold induction		4.4		0.25
PTHrP	*1205Lu	0.41 ± 0.005	1.12 ± 0.2	0.41 ± 0.01	0.33 ± 0.25
	Fold induction		2.69		0.8
	WM983A	0.08	0.41 ± 0.01	0.03 ± 0.005	NA
	Fold induction		5.1		
	WM983B	0.08 ± 0.005	0.31 ± 0.03	0.12 ± 0.02	0.13 ± 0.01
	Fold induction		3.9		1.1
	WM852	2.98	8.91	1.62	1.98
	Fold induction		3		1.22
CXCR4	*1205Lu	0.04	0.43	0.01	NA
	Fold induction				
	WM983A	1.47 ± 0.03	35.4 ± 9.1	2.12 ± 0.015	2.01 ± 0.35
	Fold induction		24.1		0.9
	WM983B	1.38	14.37	0.78	1.49
	Fold induction		10.4		1.9
	WM852	0.26 ± 0.03	0.59 ± 0.04	0.37 ± 0.03	0.33 ± 0.07
	Fold induction		2.2		0.9
OPN	1205Lu	0.65 ± 0,0.8	4.65 ± 0.19	0.67 ± 0.03	1.04 ± 0.03
	Fold induction		7.1		1.5
	WM983B	69.9 ± 2.4	155.3 ± 7.5	92.6 ± 2.9	88.8 ± 1.3
	Fold induction		2.2		0.9
	WM852	0.64	11.09 ± 0.16	0.38 ± 0.01	0.25 ± 0.02
	Fold induction		1.7		0.65

NOTE: Subconfluent melanoma cell cultures were preincubated for 6 h in W489 medium without serum before stimulation with TGF-β1 (10 ng/mL) in the absence or presence of 5 μmol/L SB431542 (or DMSO) added 1 h before addition of the growth factor. Total RNA was analyzed by quantitative RT-PCR with primers specific for *IL-11, PTHrP, CXCR4*, and osteopontin. Values are corrected for *cyclophilin A* mRNA levels in the same samples and expressed as fold induction relative to untreated cultures, after 8 (*) or 24 h of incubation, depending on the peak of gene expression induced by TGF-β. Abbreviations: UT, untreated; OPN, osteopontin; NA, not amplified.
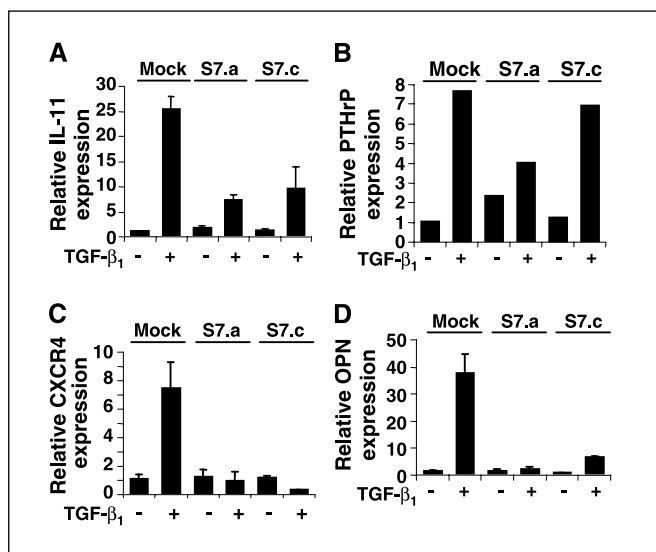
Figure 4. Subconfluent melanoma cell cultures (mock transfected and clones S7.a and S7.c) were preincubated for 6 h in medium containing 1% serum before stimulation with TGF-β1. Twenty-four hours later, RNA was extracted and analyzed by quantitative RT-PCR with primers specific for *IL-11* (*A*), *PTHrP* (*B*), *CXCR4* (*C*), and osteopontin (*OPN; D*). Values are corrected for *cyclophilin A* mRNA levels in the same samples.

bearing parental tumor cells had to be euthanized by week 5. In contrast, only 1 of 14 mice bearing Smad7-transfected 1205Lu cells (2 different clones, 7 mice for each group) had osteolytic bone lesions on radiographs 10 weeks post-tumor inoculation (Fig. 3*A, middle* and *right*), and only 5 of 14 had been euthanized after 15 weeks. The remaining animals were euthanized after 19 weeks because they all exhibited severe cachexia. Together, mice bearing Smad7-overexpressing 1205Lu tumors had significantly longer survival compared with mice bearing parental 1205Lu (Fig. 3*B*). Quantitative computerized image analysis of osteolytic lesion area on radiographs indicated that at time of experiment termination (19 weeks), mice bearing Smad7-overexpressing 1205Lu had markedly less bone destruction than the mice inoculated with parental 1205Lu tumor cells after only 5 weeks (Fig. 3*C*). This was remarkable in light of the fact that the mice bearing Smad7-overexpressing 1205Lu melanoma were euthanized 16 to 20 weeks following tumor inoculation compared with 5 weeks for mice bearing parental 1205Lu melanoma.

In a separate experiment, mice inoculated with Smad7-over-expressing 1205Lu melanoma cells (12 mice for each Smad7-overexpressing 1205Lu clone) were compared with mice inoculated with an empty vector-transfected control 1205Lu clone (11 mice) for the early establishment of bone metastases. For this purpose, the osteolytic lesion area was measured by X-ray 4 and 6 weeks following intracardiac injection of the tumor cells. As shown in Fig. 3*D*, whereas 10 of 11 mice injected with pcDNA-transfected tumor cells (EV) developed osteolytic metastases clearly detectable by X-ray as early as 4 weeks postinoculation, none of the 24 mice inoculated with either of the Smad7-transfected clones had detectable bone lesions after 6 weeks.

Taken together, these experiments show (*a*) that 1205Lu-Smad7 tumors cause significantly less and delayed bone metastases than parental and mock-transfected cells and (*b*) that mice bearing these Smad7 tumors live longer.

The contribution of TGF-β to bone metastasis of breast cancer cells has been ascribed to what has been viewed as a vicious cycle

whereby tumors homing favorably to bone secrete osteolytic factors, such as PTHrP and IL-11. The latter activate osteoblasts and osteoclasts to cause the degradation of the bone matrix and subsequent release of soluble factors, including TGF-β, which in turn exacerbates tumor cells to produce more osteoclast-activating factors (19). A signature of TGF-β–inducible genes was identified, comprising *CTGF, CXCR4* and *IL-11,* which, when overexpressed in nonmetastatic cells, induced them to metastasize to bone (17, 39). We thus screened several melanoma cell lines for their expression of TGF-β–dependent target genes known to enhance metastases to bone from breast cancer cells (i.e., the osteolytic factors PTHrP and IL-11, the chemotactic receptor CXCR4, as well as CTGF and osteopontin). Quantitative reverse transcription-PCR (RT-PCR) analysis indicated that *PTHrP, IL-11, CXCR4,* and *osteopontin* mRNA steady-state levels were robustly increased in all cell lines treated with TGF-β *in vitro* (Table 1). The small-molecule inhibitor ALK5/TβRI, SB431542, efficiently prevented the induction of *PTHrP, IL-11, CXCR4,* and *osteopontin* by TGF-β in all cell lines tested and inhibited the basal expression levels of those genes, suggesting a role for autocrine TGF-β signaling in controlling their basal level of expression.

Next, we examined whether Smad7 overexpression modulated the expression of bone metastasis–specific genes in 1205Lu cells *in vitro* and *in vivo*. As shown in Fig. 4, stable Smad7 over-expression significantly reduced the extent of activation of *IL-11* (Fig. 4*A*), *CXCR4* (Fig. 4*B*), *OPN* (Fig. 4*C*) and, to a lesser extent, *PTHrP* (Fig. 4*D*) gene expression by TGF-β in two distinct clones. To determine whether such down-regulation of bone metastasis–specific genes by Smad7 occurred *in vivo*, RNA was extracted from bone and s.c. metastases that developed in mice after intracardiac inoculation of either mock- or Smad7-transfected 1205Lu melanoma cells. Semiquantitative RT-PCR was used to determine the respective steady-state mRNA levels for *IL-11, PTHrP, CTGF,* and *GAPDH* using primers specific for the human orthologue of each gene. Gene
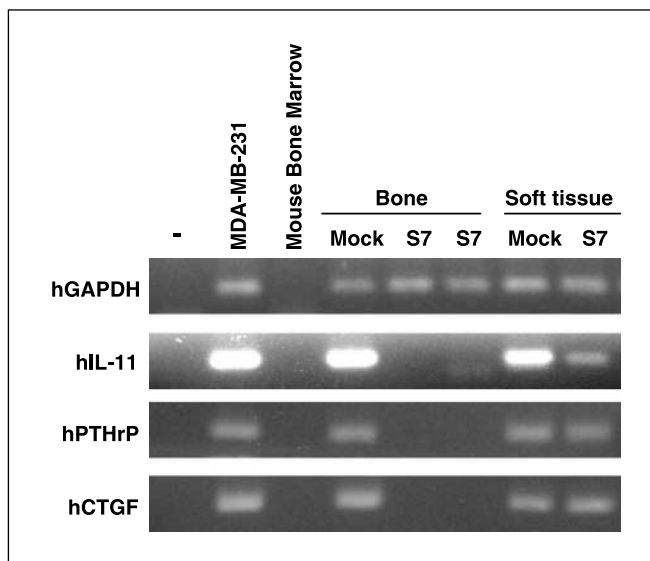

Figure 5. RNA was extracted from either bone or soft tissue (s.c.) metastatic lesions derived from mock and Smad7 (*S7*) inoculated tumor cells and analyzed by semiquantitative RT-PCR with primers specific for human *IL-11* (*hIL-11*), human *PTHrP* (*hPTHrP*), human *CTGF* (*hCTGF*), or human GAPDH (*hGAPDH*). *Left lane,* PCRs run without cDNA templates. As a positive control, we used mRNA from cultured human breast adenocarcinoma cell line MDA-MB-231, known to express the genes of interest. Mouse bone marrow RNA was used as a negative control to ascertain the species specificity of the primers.

expression of bone metastases genes *IL-11, PTHrP*, and *CTGF* in RNA derived from melanoma tumors differed depending on the metastatic site and whether the tumors expressed Smad7. As shown in Fig. 5, bone metastases from both Smad7 clones expressed little or no *IL-11, PTHrP*, and *CTGF*, whereas a bone metastasis from mock-transfected 1205Lu cells expressed these genes, all shown previously to drive the capacity of the latter to form bone metastases by MDA-MB-231 breast cancer (17). In contrast, *IL-11, PTHrP*, and *CTGF* were expressed in s.c. metastases regardless of whether the tumors overexpressed Smad7. One explanation for this differential expression may be due to different concentrations of TGF-β in the respective microenvironments. In bone, where TGF-β concentrations are high, Smad7 blocks the induction of bone metastases genes. In the s.c. site, *PTHrP* and *CTGF* may be induced by growth factors, which do not signal through the TGF-β/Smad pathway. Thus, Smad7 does not block their induction. Together, these data suggest that attenuation of TGF-β signaling by Smad7 results in tissue-specific regulation of genes involved in the process of bone metastasis by melanoma cells. It is thus likely that the pathophysiology of melanoma metastases to bone is similar to breast cancer and that extinguished *IL-11, CTGF*, and *PTHrP* expression likely contributes to the reduced capacity of Smad7-expressing clones to form bone metastases.

We showed previously that expression of a dominant-negative TβRII by MDA-MB-231 resulted in a reduced capacity for these aggressive breast cancer cells to form bone metastases due to lesser bone destruction, less tumor with fewer associated osteoclasts, and prolonged animal survival compared with controls (26). PTHrP, produced by tumor cell under the control of TGF-β signaling, was identified as critical for bone destruction. More recently, using both functional imaging of the Smad pathway in a mouse xenograft model and immunohistochemical analysis of human breast cancer bone metastases, Kang et al. (40) provided evidence for active Smad signaling in both human and mouse bone metastatic lesions. Depletion of Smad4 using RNA interference showed that the Smad pathway contributes to the formation of osteolytic bone metastases by MDA-MB-231 breast cancer cells by controlling the expression of *IL-11, CXCR4*, and *CTGF* (41), thus reinforcing previous observations (40). Together, these studies suggest that a limited, yet highly significant gene signature is indicative of the bone metastasis potential of breast cancer cells. Many of these genes are regulated by TGF-β via the Smad signaling pathway. Consistent with these collective findings, our results show that targeting endogenous TGF-β/Smad signaling in melanoma cells by mean of Smad7 overexpression is sufficient to dramatically delay bone metastasis formation in a mouse model of tumor cell inoculation in the left cardiac ventricle. Smad7 overexpression was shown to reduce the expression of the TGF-β/Smad–dependent bone metastasis signature genes, *PTHrP, IL-11, CTGF, osteopontin*, or *CXCR4*. We do not provide functional evidence for a causal role for each of these target genes in the melanoma metastatic process to bone. Yet, our results are consistent with the hypothesis that TGF-β may promote melanoma bone metastases via mechanisms similar to those identified in breast cancer metastasis.

The TGF-β/Smad pathway has also been implicated in other aspects of metastases. For example, Smad4 knockdown has reduced bone metastases due to MDA-MB-231 via interference with epithelial to mesenchymal transition (41). Moreover, it was shown recently that adenoviral delivery of Smad7 to JygMC(A) breast cancer cells significantly impairs their capacity to metastasize to lung and liver, possibly by altering their adhesive and migratory properties (42). TGF-β blockade has been effective to reduce breast cancer metastases to bone and other sites in mouse models (41, 43–47). In concordance, our results support the notion that blockade, or attenuation, of intracellular TGF-β signaling may be beneficial for the treatment of melanoma, another aggressive solid tumor able to generate bone metastases.

Acknowledgments

References

1. Roberts AB, Russo A, Felici A, Flanders KC. Smad3: a key player in pathogenetic mechanisms dependent on TGF-β. Ann N Y Acad Sci 2003;995:1–10.
2. Cohen MM Jr. TGF β/Smad signaling system and its pathologic correlates. Am J Med Genet 2003;116A:1–10.
3. Verrecchia F, Mauviel A. Transforming growth factor-β signaling through the Smad pathway: role in extracellular matrix gene expression and regulation. J Invest Dermatol 2002;118:211–5.
4. Chen W, Wahl SM. TGF-β: receptors, signaling pathways, and autoimmunity. Curr Dir Autoimmun 2002;5:62–91.
5. Javelaud D, Mauviel A. Mammalian transforming growth factor-βs: Smad signaling and physio-pathological roles. Int J Biochem Cell Biol 2004;36:1161–5.
6. Akhurst RJ. TGF-β antagonists: why suppress a tumor suppressor? J Clin Invest 2002;109:1533–6.
7. Siegel PM, Massague J. Cytostatic and apoptotic actions of TGF-β in homeostasis and cancer. Nat Rev Cancer 2003;3:807–21.
8. Wakefield LM, Roberts AB. TGF-β signaling: positive and negative effects on tumorigenesis. Curr Opin Genet Dev 2002;12:22–9.
9. Shi Y, Massague J. Mechanisms of TGF-β signaling from cell membrane to the nucleus. Cell 2003;113:685–700.
10. Nakao A, Okumura K, Ogawa H. Smad7: a new key player in TGF-β-associated disease. Trends Mol Med 2002;8:361–3.
11. Shi W, Sun C, He B, et al. GADD34-PP1c recruited by Smad7 dephosphorylates TGFβ type I receptor. J Cell Biol 2004;164:291–300.
12. Komuro A, Imamura T, Saitoh M, et al. Negative regulation of transforming growth factor-β (TGF-β) signaling by WW domain-containing protein 1 (WWP1). Oncogene 2004;23:6914–23.
13. Krasagakis K, Garbe C, Zouboulis CC, Orfanos CE. Growth control of melanoma cells and melanocytes by cytokines. Recent Results Cancer Res 1995;139:169–82.
14. Rodeck U, Nishiyama T, Mauviel A. Independent regulation of growth and SMAD-mediated transcription by transforming growth factor β in human melanoma cells. Cancer Res 1999;59:547–50.
15. Javelaud D, Delmas V, Moller M, et al. Stable overexpression of Smad7 in human melanoma cells inhibits their tumorigenicity *in vitro* and *in vivo*. Oncogene 2005;24:7624–9.
16. Yin JJ, Selander K, Chirgwin JM, et al. TGF-β signaling blockade inhibits PTHrP secretion by breast cancer cells and bone metastases development. J Clin Invest 1999;103:197–206.
17. Kang Y, Siegel PM, Shu W, et al. A multigenic program mediating breast cancer metastasis to bone. Cancer Cell 2003;3:537–49.
18. Mundy GR. Metastasis to bone: causes, consequences, and therapeutic opportunities. Nat Rev Cancer 2002;2:584–93.
19. Kozlow W, Guise TA. Breast cancer metastasis to bone: mechanisms of osteolysis and implications for therapy. J Mammary Gland Biol Neoplasia 2005;10:169–80.
20. Rodeck U, Melber K, Kath R, et al. Constitutive expression of multiple growth factor genes by melanoma cells but not normal melanocytes. J Invest Dermatol 1991;97:20–6.
21. MacDougall JR, Kobayashi H, Kerbel RS. Responsiveness

of normal, dysplastic melanocytes and melanoma cells from different lesional stages of disease progression to the growth inhibitory effects of TGF-β. Mol Cell Diff 1993;1:21–40.

22. Moore R, Champeval D, Denat L, et al. Involvement of cadherins 7 and 20 in mouse embryogenesis and melanocyte transformation. Oncogene 2004;23:6726–35.

23. Dennler S, Itoh S, Vivien D, ten Dijke P, Huet S, Gauthier JM. Direct binding of Smad3 and Smad4 to critical TGF β-inducible elements in the promoter of human plasminogen activator inhibitor-type 1 gene. EMBO J 1998;17:3091–100.

24. Javelaud D, Laboureau J, Gabison E, Verrecchia F, Mauviel A. Disruption of basal JNK activity differentially affects key fibroblast functions important for wound healing. J Biol Chem 2003;278:24624–8.

25. Daniels CE, Wilkes MC, Edens M, et al. Imatinib mesylate inhibits the profibrogenic activity of TGF-β and prevents bleomycin-mediated lung fibrosis. J Clin Invest 2004;114:1308–16.

26. Guise TA, Yin JJ, Taylor SD, et al. Evidence for a causal role of parathyroid hormone-related protein in the pathogenesis of human breast cancer-mediated osteolysis. J Clin Invest 1996;98:1544–9.

27. Vindevoghel L, Lechleider RJ, Kon A, et al. SMAD3/4-dependent transcriptional activation of the human type VII collagen gene (COL7A1) promoter by transforming growth factor β. Proc Natl Acad Sci U S A 1998;95:14769–74.

28. Berking C, Takemoto R, Schaider H, et al. Transforming growth factor-β1 increases survival of human melanoma through stroma remodeling. Cancer Res 2001;61:8306–16.

29. Xu W, Angelis K, Danielpour D, et al. Ski acts as a co-repressor with Smad2 and Smad3 to regulate the response to type β transforming growth factor. Proc Natl Acad Sci U S A 2000;97:5924–9.

30. Reed JA, Bales E, Xu W, Okan NA, Bandyopadhyay D, Medrano EE. Cytoplasmic localization of the oncogenic protein ski in human cutaneous melanomas *in vivo*: functional implications for transforming growth factor β signaling. Cancer Res 2001;61:8074–8.

31. Medrano EE. Repression of TGF-β signaling by the oncogenic protein SKI in human melanomas: consequences for proliferation, survival, and metastasis. Oncogene 2003;22:3123–9.

32. Gold LI. The role for transforming growth factor-β (TGF-β) in human cancer. Crit Rev Oncog 1999;10:303–60.

33. Derynck R, Akhurst RJ, Balmain A. TGF-β signaling in tumor suppression and cancer progression. Nat Genet 2001;29:117–29.

34. Krasagakis K, Tholke D, Farthmann B, Eberle J, Mansmann U, Orfanos CE. Elevated plasma levels of transforming growth factor (TGF)-β1 and TGF-β2 in patients with disseminated malignant melanoma. Br J Cancer 1998;77:1492–4.

35. Krasagakis K, Kruger-Krasagakes S, Fimmel S, et al. Desensitization of melanoma cells to autocrine TGF-β isoforms. J Cell Physiol 1999;178:179–87.

36. Arguello F, Baggs RB, Frantz CN. A murine model of experimental metastasis to bone and bone marrow. Cancer Res 1988;48:6876–81.

37. Bakewell SJ, Nestor P, Prasad S, et al. Platelet and osteoclast β₃ integrins are critical for bone metastasis. Proc Natl Acad Sci U S A 2003;100:14205–10.

38. Ohno H, Kubo K, Murooka H, et al. A c-fms tyrosine kinase inhibitor, Ki20227, suppresses osteoclast differentiation and osteolytic bone destruction in a bone metastasis model. Mol Cancer Ther 2006;5:2634–43.

39. Minn AJ, Kang Y, Serganova I, et al. Distinct organ-specific metastatic potential of individual breast cancer cells and primary tumors. J Clin Invest 2005;115:44–55.

40. Kang Y, He W, Tulley S, et al. Breast cancer bone metastasis mediated by the Smad tumor suppressor pathway. Proc Natl Acad Sci U S A 2005;102:13909–14.

41. Deckers M, van Dinther M, Buijs J, et al. The tumor suppressor Smad4 is required for transforming growth factor β-induced epithelial to mesenchymal transition and bone metastasis of breast cancer cells. Cancer Res 2006;66:2202–9.

42. Azuma H, Ehata S, Miyazaki H, et al. Effect of Smad7 expression on metastasis of mouse mammary carcinoma JygMC(A) cells. J Natl Cancer Inst 2005;97:1734–46.

43. Yang YA, Dukhanina O, Tang B, et al. Lifetime exposure to a soluble TGF-β antagonist protects mice against metastasis without adverse side effects. J Clin Invest 2002;109:1607–15.

44. Bandyopadhyay A, Agyin JK, Wang L, et al. Inhibition of pulmonary and skeletal metastasis by a transforming growth factor-β type I receptor kinase inhibitor. Cancer Res 2006;66:6714–21.

45. Nam JS, Suchar AM, Kang MJ, et al. Bone sialoprotein mediates the tumor cell-targeted prometastatic activity of transforming growth factor β in a mouse model of breast cancer. Cancer Res 2006;66:6327–35.

46. Muraoka RS, Dumont N, Ritter CA, et al. Blockade of TGF-β inhibits mammary tumor cell viability, migration, and metastases. J Clin Invest 2002;109:1551–9.

47. Arteaga CL. Inhibition of TGFβ signaling in cancer therapy. Curr Opin Genet Dev 2006;16:30–7.

Commentary

BMP7: A New *Bone Metastases Prevention?*

Pierrick G.J. Fournier and Theresa A. Guise

From the Department of Internal Medicine, Division of Endocrinology and Metabolism, University of Virginia, Charlottesville, Virginia

Prostate cancer is the most frequently diagnosed cancer in men and a leading cause of cancer death. More than 218,000 cases will occur in 2007, and prostate cancer will lead to more than 27,000 deaths.[1] Although the 5-year survival rate is excellent for localized stages (100%), the relative survival rapidly decreases to 33% when prostate cancer metastasizes.[1] Cancer cells from prostate primary tumors commonly colonize bones, and postmortem analyses show that 65 to 75% of patients with advanced disease have bone metastases.[2] Scientific knowledge of bone metastasis pathophysiology has increased in recent years, but effective therapy for this devastating complication of cancer remains suboptimal. In this issue of *The American Journal of Pathology*, Buijs and colleagues[3] shed more light into pathophysiology of bone metastases. More importantly, they apply this knowledge to develop novel therapy for bone metastases using bone morphogenetic protein 7 (BMP7).

In the bone microenvironment, tumor cells interact with bone cells to disrupt normal bone remodeling, causing abnormal new bone formation or bone destruction, characteristic of osteoblastic and osteolytic metastases, respectively (Figure 1). This imbalance increases patient morbidity from pathological fractures, intractable bone pain, spinal cord compression, and hypercalcemia. As noted by Stephen Paget in the 19th century, bone osteotropism of cancers, such as prostate, have been attributed to the characteristics of these cells as seeds to survive and grow in the fertile soil of the bone microenvironment.[4] Mineralized bone matrix is a major storehouse of growth factors, such as transforming growth factor-β (TGF-β), which is released and activated by tumor stimulation of osteoclastic bone resorption. These cancer cells, stimulated by TGF-β, secrete more osteolytic factors such as parathyroid hormone-related protein (PTHrP), interleukin (IL)-6, and IL-11 that can in turn further stimulate osteoclastic resorption and increase more TGF-β release from bone. TGF-β plays a central role in this feed-forward stimulation of osteoclastic bone resorption, referred to as the vicious cycle of bone me-

tastasis.[5–7] The TGF-β signaling pathway in tumor cells represents a promising therapeutic target; different modalities to block TGF-β signaling are under investigation in mice and in humans. Buijs and colleagues[3] demonstrate that, in prostate cancer cells, BMP7, also known as osteogenic protein-1 (OP-1), is an antagonist of the TGF-β pathway and can inhibit osteolytic metastases attributable to prostate cancer.

The TGF-β superfamily encompasses BMPs and TGF-β. TGF-β1, TGF-β2, and TGF-β3 isoforms have a high homology, possess similar biological functions, and bind the type I (also known as ALK5) and II TGF-β receptors.[8] The serine/threonine kinase activity of the heterotetrameric receptor complex phosphorylates the receptor-associated Smad2 and Smad3, which when associated with the Co-Smad, Smad4, and co-activators or co-repressors control targeted gene expression to regulate cell growth, differentiation, and migration.[8] TGF-β receptors can also activate Smad-independent signaling in cells through mitogen activated protein kinase kinase and other pathways. TGF-β has a complex role in malignancy. On one hand, it is a tumor suppressor and inhibits growth of epithelial cells. On the other hand, TGF-β promotes invasion and metastasis in transformed cells. Thus, it is considered to be both tumor suppressor and inducer in the early and late stage of the pathology, respectively.[8] BMPs activate a combination of type I receptors (type IA and IB BMP receptors and type IA activin receptor) and type II receptors (type II BMP receptor, and type II and IIB activin receptors). The serine/threonine activity of these BMP receptors activates Smad1, Smad5, and Smad8, which associate with Smad4 and transcription factors to participate in gene transcription regulation. The core Smad complexes,
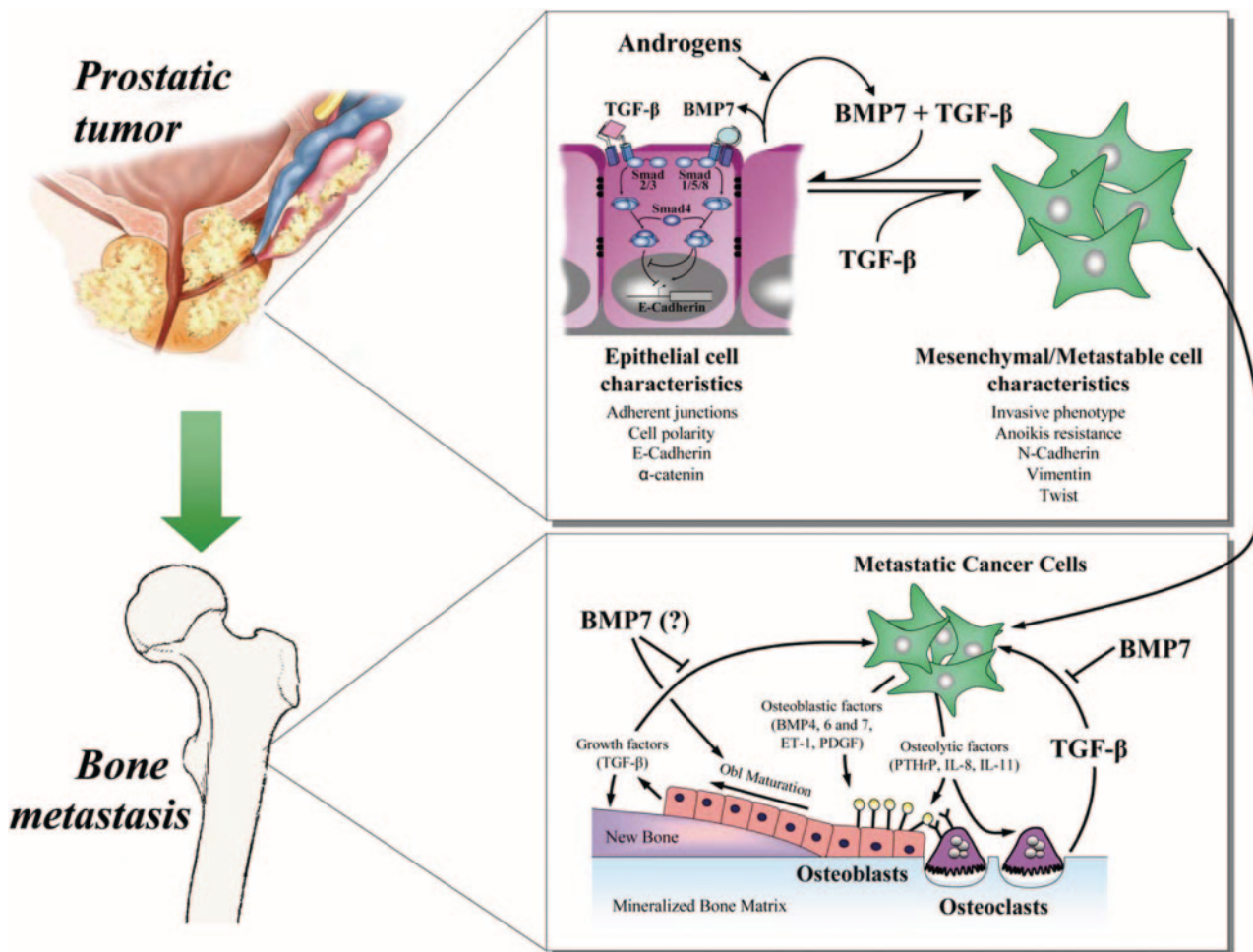
Figure 1. Role of BMP7 in prostate cancer progression and in bone metastases. Top: In the prostate gland, androgens stimulate the production of BMP7 by normal epithelial cells. Through Smad1/5/8, specifics of BMP signaling, BMP7 represses EMT via different mechanisms including the regulation of E-cadherin expression. BMP7, combined with TGF-β, which signals through Smad2/3, further increases E-cadherin expression and then more efficiently prevents EMT and cancer progression. In the later stage of the disease, BMP7 ceases to act on cancer cells, potentially because of the loss of androgen-induced production of BMP7 after anti-androgen therapy. TGF-β alone represses E-cadherin expression and favors EMT. Cancer cells then acquire a metastatic potential (metastable cells) and can disseminate through the bloodstream to other organs, including bones. Bottom: At sites of bone metastases, cancer cells produce osteolytic factors such as PTHrP, IL-8, or IL-11 that increase bone resorption by directly acting on osteoclasts and their precursors or via the osteoblasts through production of RANK ligand. Growth factors released from resorbed mineralized bone matrix, such as TGF-β, promote tumor growth in bone by enhancing the production of tumor factors that stimulate bone resorption and bone formation. Cancer cells can also induce osteoblast maturation and new bone formation by production of endothelin-1 (ET-1); platelet-derived growth factor (PDGF); and BMP4, -6, or -7. Mature osteoblasts secrete growth factors such as TGF-β that may fuel the progression of bone metastases. BMP7, used as a therapeutic agent, can inhibit TGF-β signaling and progression of this vicious cycle of tumor growth of bone metastases.

based on their composition, bind different DNA motifs: the Smad-binding elements (SBE) are targeted by TGF-β and BMP pathways, whereas the CAGA motives and the BMP-response elements are specific of TGF-β and BMP pathways, respectively. Using a CAGA-luciferase construct, Buijs and colleagues[3] showed that BMP7 inhibits the luciferase activity induced by TGF-β and therefore the TGF-β pathway in prostate cancer cells *in vitro*. The effects of BMP7 were tested in immunodeficient mice inoculated with the highly aggressive PC-3M-Pro4 human prostate cancer cells expressing the firefly luciferase directly into the tibia or into the left cardiac ventricle to induce bone metastases detectable by bioluminescence. In cancer cells *in vivo*, BMP7 treatment triggered BMP pathway activity as shown by the nuclear accumulation of phosphorylated Smad1 on sections of bone metastases. This was associated with decreased tumor burden. The effect of BMP7 was bone-specific because it had no

effect on orthotopic prostate cancer tumors. Thus, BMP7 could be used as a TGF-β antagonist in the treatment of osteolytic metastases from prostate cancer. These data are consistent with those derived from breast cancer and melanoma bone metastases in which inhibition of TGF-β signaling by either small-molecule inhibitors or overexpression of the inhibitory Smad7 reduced bone metastases.[9–11] Whether BMP7 inhibits TGF-β signaling *in vivo* as it does *in vitro* is not conclusively demonstrated by Buijs and colleagues.[3] This would require demonstration that BMP7 reduced luciferase activity of PC-3M-Pro4 prostate cancer cells that stably express a TGF-β-specific, CAGA-controlled luciferase vector *in vivo*.

The development of bone metastases also depends on primary tumor expression of factors such as chemokine receptor CXCR4, integrin $\alpha_V\beta_3$, and MMPs that facilitate the journey of cancer cells from the primary site to bone.[6] Detachment of tumor cells from the primary site is con-

sidered a first step of the metastatic cascade and controversially considered to reproduce epithelial-to-mesenchymal transition (EMT). EMT occurs in embryonic development during the migration and differentiation of cells away from the neural crest to form bone, smooth muscle cells, peripheral neurons and glia, and melanocytes. Epithelial cells undergoing EMT lose their polarity and cell-to-cell contacts, undergo cytoskeleton remodeling, and acquire mesenchymal and migration phenotypes that can be related to the transition from localized to invasive tumor (Figure 1). This progression is associated with the decreased expression of epithelial markers, such as E-cadherin, and the increase of mesenchymal markers, such as N-cadherin or vimentin. By signaling through the Smad pathway, TGF-β is a well-known inducer of EMT. TGF-β can increase the expression of N-cadherin in mammary epithelial cells[12] and repress the expression of E-cadherin in mammary and renal epithelial cells.[12,13] Conversely, in the same renal epithelial cells, BMP7 enhanced E-cadherin expression and antagonized TGF-β repression through a Smad-dependent mechanism.[13] This phenomenon seems to be analogous to the BMP7-inhibition of the TGF-β pathway in prostate cancer cells. Buijs and colleagues[3] show that BMP7 induced E-cadherin promoter activity in prostate cancer cells, and its expression in prostate cancer cells *in vitro* was correlated with the E-cadherin ratio and inversely correlated with aggressiveness. Consequently, prostate cancer cells had a decreased BMP7 expression compared with normal epithelial prostatic cells when the expression of BMP7 was compared in matched normal epithelial and malignant prostate cancer cells from patients using laser microdissection or immunohistochemistry methods.[3] Although E-cadherin expression in prostate cancer is inversely correlated with the Gleason score, BMP7 expression in prostate cells did not reach a significant inverse correlation with the Gleason score because of statistical limitation. These findings describe a model whereby BMP7 expressed in normal epithelial cells induces E-cadherin expression and contributes to maintenance of an epithelial state, whereas during cancer progression BMP7 expression is lost and E-cadherin expression is decreased leading to EMT and metastasis (Figure 1). In such a model, BMP7 treatment of the primary tumor would prevent metastasis development. This effect could be further potentiated in prostate cancer cells by an environment rich in TGF-β because the combination of BMP7 and TGF-β induced a higher increase of E-cadherin and decrease of vimentin expression than each growth factor alone (Figure 1).[3] This up-regulation, however, was not detected in renal epithelial cells[13] and may be cell-specific for reasons that remain to be explained. Buijs and colleagues[3] did not notice any effect of BMP7 on the local spreading of orthotopically implanted PC-3M-Pro4 cells, but such an inhibition may occur during micrometastatic deposit in the bone marrow in prostate and breast cancer bone metastases.

Despite the significance of these findings, limitations of the models prevent complete extrapolation to the human situation. First, the models (intracardiac inoculation or direct injection into bone) do not reproduce the entire metastatic process, and orthotopic inoculation of PC-3M-Pro4 does not lead to distant metastases. Second, the cell lines used *in vivo*, derived from PC-3, do not express androgen receptor or respond to androgens. Finally, PC-3 and its derivatives cause osteolytic bone metastases, unlike the osteoblastic lesions that occur in men with prostate cancer.

To study the relative role of BMP7 inhibition of EMT in metastases to distant sites of bone and other organs requires an animal model in which tumor cells metastasize from the primary site to bone. That said, there are very few and limited models that recapitulate the events of the entire metastatic cascade attributable to prostate or breast cancer. Inoculation of the 4T1 murine breast cancer cells into the mammary gland results in formation of a primary tumor that disseminates to the lung, the adrenal glands, and to bone. Using this model, Muraoka and colleagues[14] showed that inhibition of TGF-β signaling with a soluble type II receptor significantly reduced metastases. However, these investigators did not study EMT or bone metastases; such studies would be highly relevant, given the findings of Buijs and colleagues[3] reported here. Another relevant model that recapitulates the metastatic cascade and shows enhanced metastasis with increased TGF-β signaling uses a genetically engineered expression of an oncogenic version of the Neu receptor tyrosine kinase (c-Neu) under the control of the mouse mammary tumor virus (MMTV) in mouse mammary gland. Here, mammary tumors spontaneously develop and later metastasize to lung.[15] Overexpression of a constitutively active form of the TGF-β type I receptor [either MTV/TβRI(AAD) or MMTV-TβRI(S223/225)] increased metastasis formation,[15,16] whereas impairment of the TGF-β pathway in mammary cells with a dominant-negative form of the TGF-β type II receptor lacking its kinase cytoplasmic domain [MMTV/TβRII(ΔCyt)] decreased the frequency of metastasis to the lungs.[15] Analysis of endogenous expression of BMP7 and EMT markers, as well as testing the effects of a BMP7 treatment could answer questions about BMP7 antagonism of TGF-β-induced EMT and metastasis. However, because bone metastases do not develop in this model, it would not be useful to study such events in the bone microenvironment.

BMP7 expression in prostate cells is androgen-dependent because orchidectomy decreased BMP7 expression whereas testosterone and dihydrotestosterone increased it.[17,18] Further, Buijs and colleagues[3] show that BMP7 expression is reduced in prostate cancer cell lines that lack androgen receptor. These observations raise several questions relative to androgen regulation of BMP7: i) Is BMP7 expression correlated with androgen independence? ii) Could the evolution of prostate cancer to metastatic dissemination after hormonal therapy be linked to the loss of androgen-induced BMP7 expression and loss of epithelial phenotype maintenance? iii) How does androgen deprivation therapy affect this process? iv) Are there bone-specific implications?

Most patients with prostate cancer metastases to bone have osteoblastic lesions on radiographs. However, osteoclastic bone resorption is clearly evident and contributes to pathophysiology of bone metastasis in this set-

ting. The bone resorption marker N-telopeptide is increased in prostate cancer patients with bone metastases and is a stronger predictor of death than prostate-specific antigen,[19] and bisphosphonates improve skeletal morbidity in patients with osteoblastic disease.[20] The model used by Buijs and colleagues,[3] PC-3M-Pro4, a subclone of PC-3, is similar to MDA-MB-231 breast cancer or B16F10 melanoma in that it causes osteolytic bone metastases in mice. Although this model lacks the osteoblastic component evident in humans with prostate cancer bone metastases, important information can be gleaned regarding the role of BMP7 in osteolytic prostate cancer bone metastases. Nonetheless, the effect of BMP7 on bone metastases should be evaluated in known osteoblastic models such as those induced by ZR-75-1 breast cancer[21] and LuCap 23.1 or C4-2B prostate cancer. As the authors suggest, BMP7 could trigger different effects with different bone metastasis phenotypes. Depending on the cell type, BMP7 can induce EMT as assessed by E-cadherin expression in the parental prostate cancer cell line PC-3 or have no effect in other prostate cancer cells.[22] BMPs can also protect some prostate cancer cells (LnCap, C4-2B) from apoptosis[22] or induce the apoptosis of myeloma cells, which are known to induce osteolysis.[23] In other bone metastasis models, BMPs have been shown to induce bone metastases.[24–26] Noggin inhibits BMP signaling by binding BMP ligands, and when Noggin was overexpressed in PC-3 or LAPC-9 prostate cancer cells, there was a decrease of osteolytic and osteoblastic lesions, respectively.[25,26] This positive effect of BMPs in the osteoblastic process could be related to an increase of BMP7 expression at sites of osteoblastic prostate cancer metastases.[27] BMPs induce the differentiation of cells from the osteoblast lineage and enhance osteoblast activity; BMP7-knockout mice have a smaller skeleton and decreased bone mineralization.[28] Thus, BMP7 at sites of bone metastases could potentially promote the osteoblastic reaction and enhance osteoblastic bone metastasis. This distinction would be important to confirm in animal models before proceeding to clinical trials.

Overall, Buijs and colleague[3] provide a role for BMP7 expression in the maintenance of epithelial behavior in the prostate (Figure 1). In normal epithelial cells, BMP7 and TGF-β concur to induce the expression of E-cadherin, repress vimentin synthesis, and prevent EMT. In later stage, because of loss of expression of BMP7 by cancer cells and/or resistance of these cells to the BMP7 secreted by surrounding normal epithelial cells, malignant cells lose the expression of E-cadherin under the influence of TGF-β, which then induces EMT and leads to metastatic spreading. This model re-emphasizes the double-edged-sword properties and the complexity of TGF-β and members of the TGF-β superfamily in cancer biology. It also provides a rationale for further investigation of BMP7 in the prevention of osteolytic bone metastases attributable to prostate cancer. This effect is bone-specific, and whether it is dependent on the bone metastasis phenotype remains to be studied. Buijs and colleagues[3] offer interesting and clinically relevant perspectives for the therapeutic use of BMP7, but they also

raise numerous questions regarding its role at the different stages of prostate cancer that exemplify the promises but also the versatility of the members of the TGF-β superfamily.

References

1. Jemal A, Siegel R, Ward E, Murray T, Xu J, Thun MJ: Cancer statistics, 2007. CA Cancer J Clin 2007, 57:43–66
2. Coleman RE: Metastatic bone disease: clinical features, pathophysiology and treatment strategies. Cancer Treat Rev 2001, 27:165–176
3. Buijs JT, Rentsch CA, van der Horst G, van Overveld PGM, Schwaninger R, Henriquez NV, Papapoulos SE, Pelger RCM, Vukicevic S, Cecchini MG, Löwik CWGM, van der Pluijm G: BMP7, a putative regulator of epithelial homeostasis in the human prostate, is a potent inhibitor of prostate cancer bone metastasis in vivo. Am J Pathol 2007, 171:1047–1057
4. Fidler IJ: The pathogenesis of cancer metastasis: the 'seed and soil' hypothesis revisited. Nat Rev Cancer 2003, 3:453–458
5. Kang Y, He W, Tulley S, Gupta GP, Serganova I, Chen CR, Manova-Todorova K, Blasberg R, Gerald WL, Massague J: Breast cancer bone metastasis mediated by the Smad tumor suppressor pathway. Proc Natl Acad Sci USA 2005, 102:13909–13914
6. Kang Y, Siegel PM, Shu W, Drobnjak M, Kakonen SM, Cordon-Cardo C, Guise TA, Massague J: A multigenic program mediating breast cancer metastasis to bone. Cancer Cell 2003, 3:537–549
7. Yin JJ, Selander K, Chirgwin JM, Dallas M, Grubbs BG, Wieser R, Massague J, Mundy GR, Guise TA: TGF-β signaling blockade inhibits PTHrP secretion by breast cancer cells and bone metastases development. J Clin Invest 1999, 103:197–206
8. Massagué J, Gomis RR: The logic of TGFβ signaling. FEBS Lett 2006, 580:2811–2820
9. Bandyopadhyay A, Agyin JK, Wang L, Tang Y, Lei X, Story BM, Cornell JE, Pollock BH, Mundy GR, Sun LZ: Inhibition of pulmonary and skeletal metastasis by a transforming growth factor-β type I receptor kinase inhibitor. Cancer Res 2006, 66:6714–6721
10. Javelaud D, Mohammad KS, McKenna CR, Fournier P, Luciani F, Niewolna M, Andre J, Delmas V, Larue L, Guise TA, Mauviel A: Stable overexpression of Smad7 in human melanoma cells impairs bone metastasis. Cancer Res 2007, 67:2317–2324
11. Stebbins EG, Mohammad KS, Niewolna M, McKenna CR, Mison AP, Schimmoller F, Murphy A, Chakravarty S, Dugar S, Higgins LS, Wong DH, Guise TA: SD-208, a small molecule inhibitor of transforming growth factor-β receptor I kinase reduces breast cancer metastases to bone and improves survival in a mouse model. J Bone Miner Res 2005, 20:S55
12. Deckers M, van Dinther M, Buijs J, Que I, Lowik C, van der Pluijm G, ten Dijke P: The tumor suppressor Smad4 is required for transforming growth factor β-induced epithelial to mesenchymal transition and bone metastasis of breast cancer cells. Cancer Res 2006, 66:2202–2209
13. Zeisberg M, Hanai J, Sugimoto H, Mammoto T, Charytan D, Strutz F, Kalluri R: BMP-7 counteracts TGF-β1-induced epithelial-to-mesenchymal transition and reverses chronic renal injury. Nat Med 2003, 9:964–968
14. Muraoka RS, Dumont N, Ritter CA, Dugger TC, Brantley DM, Chen J, Easterly E, Roebuck LR, Ryan S, Gotwals PJ, Koteliansky V, Arteaga CL: Blockade of TGF-β inhibits mammary tumor cell viability, migration, and metastases. J Clin Invest 2002, 109:1551–1559
15. Muraoka RS, Koh Y, Roebuck LR, Sanders ME, Brantley-Sieders D, Gorska AE, Moses HL, Arteaga CL: Increased malignancy of Neu-induced mammary tumors overexpressing active transforming growth factor beta1. Mol Cell Biol 2003, 23:8691–8703
16. Siegel PM, Shu W, Cardiff RD, Muller WJ, Massague J: Transforming growth factor beta signaling impairs Neu-induced mammary tumorigenesis while promoting pulmonary metastasis. Proc Natl Acad Sci USA 2003, 100:8430–8435
17. Masuda H, Fukabori Y, Nakano K, Shimizu N, Yamanaka H: Expression of bone morphogenetic protein-7 (BMP-7) in human prostate. Prostate 2004, 59:101–106
18. Thomas R, Anderson WA, Raman V, Reddi AH: Androgen-dependent

gene expression of bone morphogenetic protein 7 in mouse prostate. Prostate 1998, 37:236–245

19. Coleman RE, Major P, Lipton A, Brown JE, Lee K-A, Smith M, Saad F, Zheng M, Hei YJ, Seaman J, Cook R: Predictive value of bone resorption and formation markers in cancer patients with bone metastases receiving the bisphosphonate zoledronic acid. J Clin Oncol 2005, 23:4925–4935

20. Saad F, Gleason DM, Murray R, Tchekmedyian S, Venner P, Lacombe L, Chin JL, Vinholes JJ, Goas JA, Chen B: A randomized, placebo-controlled trial of zoledronic acid in patients with hormone-refractory metastatic prostate carcinoma. J Natl Cancer Inst 2002, 94:1458–1468

21. Yin JJ, Mohammad KS, Kakonen SM, Harris S, Wu-Wong JR, Wessale JL, Padley RJ, Garrett IR, Chirgwin JM, Guise TA: A causal role for endothelin-1 in the pathogenesis of osteoblastic bone metastases. Proc Natl Acad Sci USA 2003, 100:10954–10959

22. Yang S, Zhong C, Frenkel B, Reddi AH, Roy-Burman P: Diverse biological effect and Smad signaling of bone morphogenetic protein 7 in prostate tumor cells. Cancer Res 2005, 65:5769–5777

23. Ro TB, Holt RU, Brenne AT, Hjorth-Hansen H, Waage A, Hjertner O, Sundan A, Borset M: Bone morphogenetic protein-5, -6 and -7 inhibit growth and induce apoptosis in human myeloma cells. Oncogene 2004, 23:3024–3032

24. Dai J, Keller J, Zhang J, Lu Y, Yao Z, Keller ET: Bone morphogenetic protein-6 promotes osteoblastic prostate cancer bone metastases through a dual mechanism. Cancer Res 2005, 65:8274–8285

25. Feeley BT, Gamradt SC, Hsu WK, Liu N, Krenek L, Robbins P, Huard J, Lieberman JR: Influence of BMPs on the formation of osteoblastic lesions in metastatic prostate cancer. J Bone Miner Res 2005, 20:2189–2199

26. Feeley BT, Krenek L, Liu N, Hsu WK, Gamradt SC, Schwarz EM, Huard J, Lieberman JR: Overexpression of noggin inhibits BMP-mediated growth of osteolytic prostate cancer lesions. Bone 2006, 38:154–166

27. Masuda H, Fukabori Y, Nakano K, Takezawa Y, Suzuki TC, Yamanaka H: Increased expression of bone morphogenetic protein-7 in bone metastatic prostate cancer. Prostate 2003, 54:268–274

28. Jena N, Martin-Seisdedos C, McCue P, Croce CM: BMP7 null mutation in mice: developmental defects in skeleton, kidney, and eye. Exp Cell Res 1997, 230:28–37

Molecular Biology of Bone Metastasis

Lauren A. Kingsley, Pierrick G.J. Fournier, John M. Chirgwin, and Theresa A. Guise

University of Virginia Department of Medicine, Division of Endocrinology, Charlottesville, Virginia

Abstract

Metastasis is a final stage of tumor progression. Breast and prostate cancer cells preferentially metastasize to bone, wherein they cause incurable osteolytic and osteoblastic lesions. The bone matrix is rich in factors, such as transforming growth factor-β and insulin-like growth factors, which are released into the tumor microenvironment by osteolysis. These factors stimulate the growth of tumor cells and alter their phenotype, thus promoting a vicious cycle of metastasis and bone pathology. Physical factors within the bone microenvironment, including low oxygen levels, acidic pH, and high extracellular calcium concentrations, may also enhance tumor growth. These elements of the microenvironment are potential targets for chemotherapeutic intervention to halt tumor growth and suppress bone metastasis. [Mol Cancer Ther 2007;6(10):2609–17]

Introduction

Breast and prostate cancer are a leading cause of cancer death among women and men — second only to lung cancer. Mammography and prostate-specific antigen testing have improved early detection and treatment of these cancers, slowing their increase in incidence over the past decade and increasing the 5-year survival rate to 98% for breast cancer and 100% for prostate cancer when detected at the earliest stages. However, the breast cancer survival rate drops dramatically to 83% for patients initially diagnosed with regional spread and to 26% for those with distant metastases. Prostate cancer survival rate drops to 33% with distant metastases (1).

The skeleton is a preferred site for breast and prostate cancer metastasis. Within the skeleton, metastases present as two types of lesions: osteoblastic or osteolytic. These lesions result from an imbalance between osteoblast-mediated bone formation and osteoclast-mediated bone resorption. Osteoblastic lesions, characteristic of prostate cancer, are caused by an excess of osteoblast activity relative to resorption by osteoclasts, leading to abnormal bone formation. In breast cancer, osteolytic lesions are found in 80% of patients with stage IV metastatic disease (2). The lesions are characterized by increased osteoclast activity and net bone destruction (3).

Breast cancer bone lesions span a spectrum in which the majority are osteolytic, but up to 15% are osteoblastic or mixed (2). Although bone metastases are classified by their radiographic appearance, most patients have evidence of abnormal bone resorption and formation. For example, autopsy examination of prostate cancer bone metastases found marked phenotypic heterogeneity both within a particular lesion and between lesions from a single patient (4). Both osteoblastic and osteolytic bone metastases lead to numerous skeletal complications, including bone pain, hypercalcemia, pathologic fractures, and spinal cord and nerve compression syndromes (5). Such complications increase morbidity and diminish quality of life in these patients.

Metastasis to bone occurs in the late stages of tumor progression and is a multistep process. Cancer cells first detach from the primary tumor and migrate locally to invade blood vessels. Once in the bloodstream, cancer cells are attracted to preferred sites of metastasis through site-specific interactions between tumor cells and cells in the target tissue (3). Tumor cells that metastasize to the skeleton adhere to the endosteal surface and colonize bone. The bone microenvironment is composed of osteoblasts, osteoclasts, and the mineralized bone matrix, plus many other cell types. It is highly favorable for tumor invasion and growth. Crosstalk between tumor cells and the microenvironment promotes a vicious cycle of tumor growth and bone destruction (2, 6). This vicious cycle is shown in Fig. 1. Tumor cells secrete factors which stimulate osteoclast-mediated bone destruction and the consequent release of numerous factors immobilized within the bony matrix that act on cancer cells, promoting a more aggressive tumor phenotype and potentiating cancer spread and bone destruction.

Crosstalk between tumor and bone activates numerous signaling pathways which drive the vicious cycle. In prostate cancer bone metastasis, for example, Wnt proteins released by tumor cells stimulate osteoblasts and have autocrine effects on tumor proliferation (7). An inhibitor of Wnt signaling, Dkk-1, can regulate metastatic progression by opposing osteogenic Wnts early in metastasis and
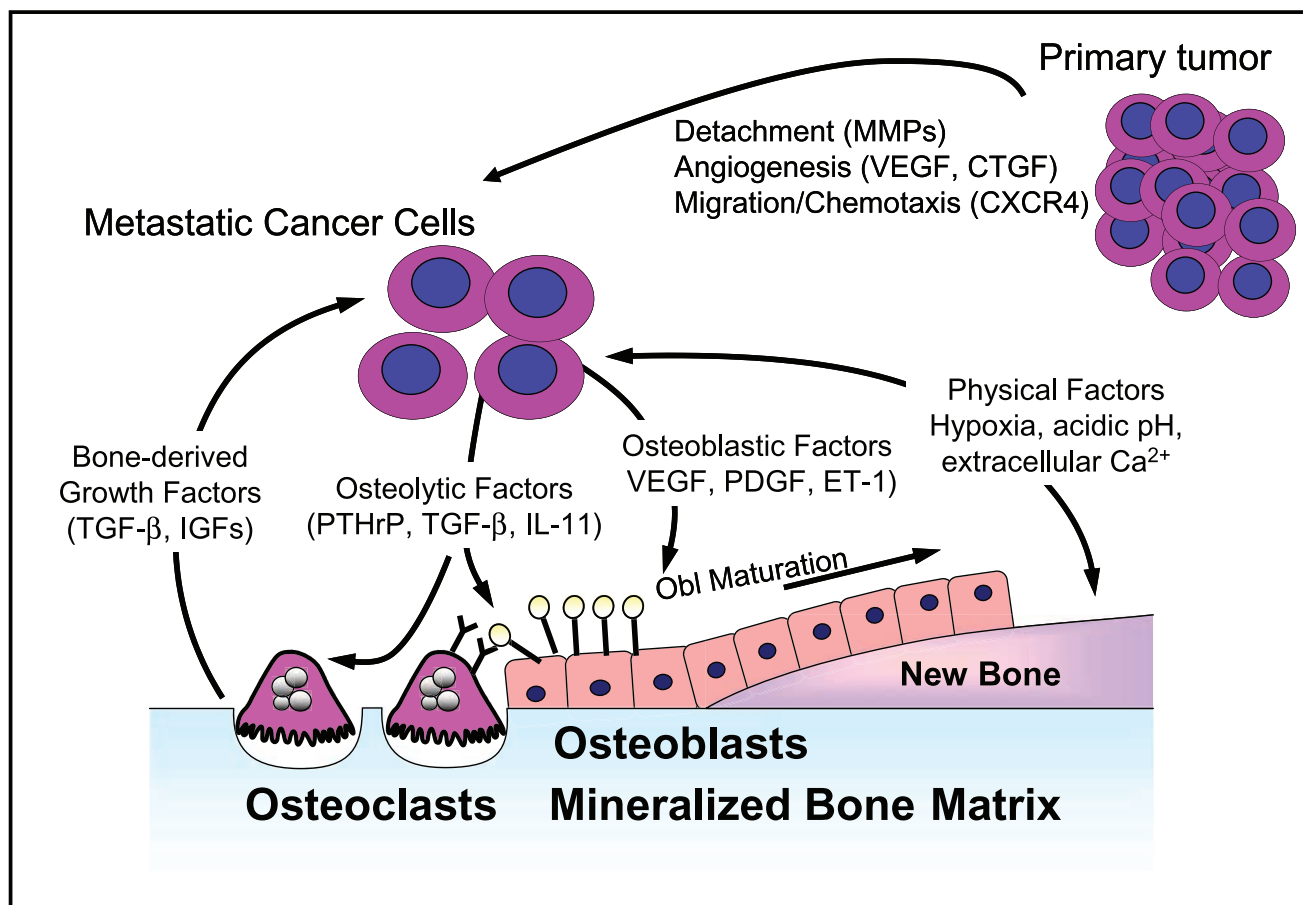
Figure 1. The vicious cycle of bone metastases. Factors, such as MMPs, chemokine receptor 4 (*CXCR4*), vascular endothelial growth factor (*VEGF*), and connective tissue growth factor (*CTGF*), target metastatic tumor cells to bone and facilitate survival within the bone microenvironment. Physical factors within the bone microenvironment, including hypoxia, acidic pH, and extracellular Ca^{2+}, and bone-derived growth factors, such as TGF-β and IGFs, activate tumor expression of osteoblast-stimulatory factors, including vascular endothelial growth factor, platelet-derived growth factor (*PDGF*), and ET-1. Osteoclast-stimulatory factors, including PTHrP, TGF-β, and IL-11, can also be increased. These factors stimulate bone cells, which in turn release factors that promote tumor growth in bone.

controlling the phenotypic switch from osteolytic to osteoblastic lesions later in metastasis.

Tumor cells and bone cells may rely on the same signaling pathways and transcription factors to facilitate their cooperative interactions at sites of metastases. This phenomenon has been suggested to represent "osteomimicry" on the part of the tumor cells (8). For example, metastatic breast cancer cells express bone sialoprotein (9) under control of Runx2 and MSX2 transcription factors, which are also important regulators of osteoblast functions. Runx2 activity in both cancer cells and osteoblasts stimulates the production and release of angiogenic factors andmatrix metalloproteinase (MMP) into the microenvironment and up-regulates adhesion proteins, which allow tumor and bone cells to bind (10). Runx2 expression by cancer cells may also support tumor-induced osteoclastogenesis. Expression of similar surface proteins and secreted factors allows for coexistence of these two cell types and promotes the growth of metastatic lesions.

We believe that the bone microenvironment plays a critical role in the vicious cycle by altering the phenotype of tumor cells to give highly aggressive metastatic lesions. The bone matrix is rich in growth factors, such as transforming growth factor-β (TGF-β), insulin-like growth factor-I (IGF-I), and IGF-II, which are released by osteolysis and can stimulate bone and tumor cell proliferation. Physical properties of the bone matrix, including low oxygen content, acidic pH, and high extracellular calcium concentration, create an environment favorable for tumor growth. Hypoxia, acidosis, and high calcium, plus growth factors, such as TGF-β and IGFs, combine to drive the vicious cycle of bone metastasis (Fig. 2).

Growth Factors as Mediators of the Bone Microenvironment

The destruction of bone by osteoclasts releases calcium and growth factors from the matrix. Ninety percent of the protein

released consists of collagen; among the remaining 10% are IGFs, TGF-β, fibroblast growth factor, platelet-derived growth factor, and bone morphogenetic proteins (11). All of these factors can act on metastatic cells. Although termed ''growth'' factors, they need not increase tumor burden by direct stimulation of cancer cell proliferation. They can also act indirectly to promote angiogenesis and increase tumor production of osteolytic and osteoblastic factors, which remodel the skeleton to accommodate tumor growth.

TGF-β is not the most abundant growth factor in bone, but it has the best established role in osteolytic metastases. TGF-β binds to a heterodimeric receptor and can activate the canonical Smad signaling pathway or Smad-independent pathways through extracellular signal-regulated kinase 1/2, p38 mitogen-activated protein kinase, and c-Jun-NH$_2$ kinase (12). TGF-β is deposited in the bone matrix by osteoblasts and released and activated during osteoclastic resorption (13). It regulates bone development and remodeling (for review, ref. 14). Advanced cancers often escape growth inhibition by TGF-β, and this factor mediates metastases by activating epithelial-mesenchymal transition and tumor cell invasion, increasing angiogenesis and suppressing immune surveillance of tumor cells (15).

In 75% of patients with biopsied bone metastases, tumor cells stained positive for phosphorylated Smad2 localized to the nucleus (16). When MDA-MB-231 cells transduced with a retroviral vector expressing a reporter gene under the control of a TGF-β–sensitive promoter, micro–positron emission tomography imaging showed reporter activation only in bone and not in adrenal metastases (16), demonstrating that Smad signaling was activated when the tumor cells were in bone. Knockdown of Smad4 (16), engineered expression of the inhibitory Smad7 (17), or introduction of a dominant-negative TGF-β type II receptor (TβRII Δcyt; ref. 18) dramatically decreased bone metastases in breast or melanoma models. Small-molecule inhibitors of TGF-β type I receptor kinase give similar results in mouse models (19–21).

TGF-β may stimulate bone metastases by inducing proosteolytic gene expression in cancer cells, with parathyroid hormone–related protein (PTHrP) having a central role. PTHrP is expressed by osteolytic breast and prostate cancer cell lines, such as MDA-MB-231, MDA-MB-435, and PC-3 (18, 22). Its expression is higher at sites of bone metastases compared with nonosseous metastases (23). Among factors released from bone during resorption, only
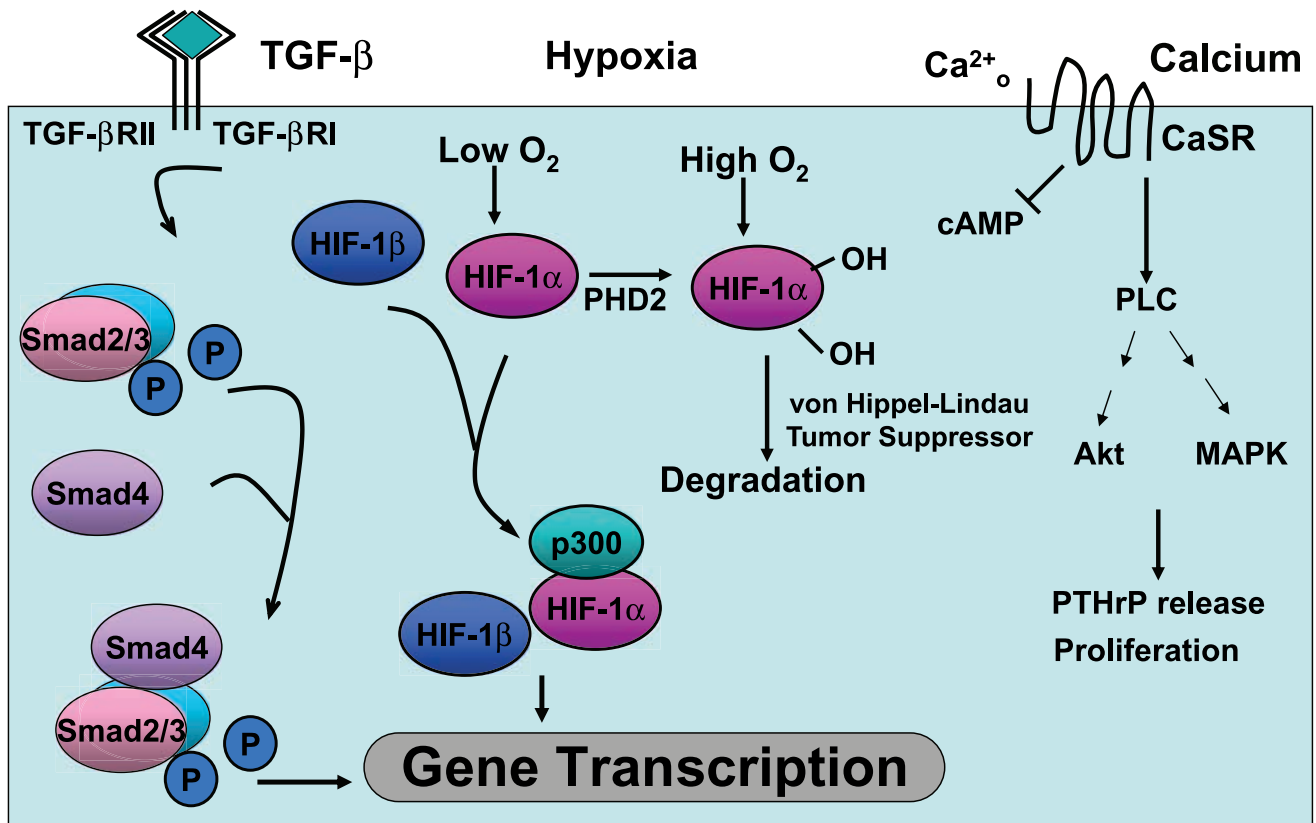

Figure 2. Signaling pathways in bone metastases. The bone microenvironment up-regulates signaling pathways within tumor cells, including the TGF-β, hypoxia, and calcium signaling pathways, enabling survival and tumor growth in bone. TGF-β binding to its receptor activates the Smad signaling pathway to mediate gene transcription. In the hypoxic bone microenvironment, HIF-1α is stabilized and mediates the transcription of hypoxia-responsive genes. Extracellular calcium stimulates the CaSR to stimulate tumor-cell proliferation and result in PTHrP release.

TGF-β increased PTHrP production (18), which occurred via Smad-dependent and Smad-independent pathways (24). This induction was prevented by the expression of TβRII Δcyt in MDA-MB-231 cells (18, 24). These cells gave decreased bone metastases in mice, which could be reversed by overexpression of PTHrP or a constitutively active type I receptor subunit (24). Neutralizing antibodies against PTHrP (22) or inhibitors of its gene transcription (25) decreased osteolytic metastases and tumor burden in cancer models. TGF-β–induced PTHrP increases osteoblastic production of RANK ligand, which stimulates osteoclast formation and activity and promotes bone metastases (26–28). The consequent increase in bone resorption releases more bone matrix factors to act on cancer cells, sustaining a vicious cycle.

PTHrP is not the only factor regulated by TGF-β. Cyclooxygenase-2 is expressed in 87% of the bone metastases from patients (29). Its expression by MDA-MB-231 cells is higher in bone metastases than in cells growing orthotopically. TGF-β increases cyclooxygenase-2 expression in osteoblasts, bone marrow stromal cells, and breast cancer cells, whereas, as an inhibitor of bone resorption, the bisphosphonate risedronate reduced cyclooxygenase-2 immunostaining in bone (29). Media conditioned by TGF-β–treated MDA-MB-231 cells support osteoclast formation, a response blocked by the cyclooxygenase-2 inhibitor NS-398. The inhibitors NS-398, nimesulide, and MF-tricyclic decreased the number of osteoclasts at the tumor-bone interface, as well as skeletal tumor burden in mice inoculated with MDA-MB-231 cells (29, 30). Cyclooxygenase-2 expression in bone-seeking subclones of MDA-MB-231 cells correlates with increased production of interleukin-8 (IL-8; ref. 30). IL-8 induces osteoclast formation and activity independent of the RANK ligand pathway (31) and can also induce IL-11 (32). IL-11 can act on osteoclasts via RANK ligand (33) and by regulation of granulocyte macrophage colony-stimulating factor (34). However, overexpression of IL-11 does not increase bone metastases in the absence of other prometastatic factors, such as osteopontin, connective tissue growth factor, or chemokine receptor 4 (35). IL-11, connective tissue growth factor, chemokine receptor 4, and MMP-1 are all up-regulated in the gene signature of breast cancer cells capable of forming osteolytic bone metastases (35). Osteopontin is a protein secreted by osteoblasts and involved in bone matrix mineralization (36). Its expression is regulated by Runx2 (37), which is increased by TGF-β in breast cancer cells (38). Cancer cells that cause bone metastases often secrete the proteases MMP-9 and MMP-13, which are regulated by Runx2 (10, 38), and cathepsin K (39). These proteases are involved in bone resorption and osteoclast recruitment (40), and cathepsin K is essential for normal bone turnover. Cancer cells express a number of osteoblasts markers, such as osteopontin, bone sialoprotein, and osteocalcin (8), which are regulated by Runx2 in both osteoblasts and cancer cells (37, 41, 42).

IGF-I and IGF-II are the most abundant proteins in bone and important in bone development (for review, ref. 43).

IGF signaling is also important in cancer and metastases; it promotes transformation and angiogenesis, induces cell proliferation and invasion, and is antiapoptotic (44). Both IGFs act through the IGF-IR to maintain cell growth. Their specific contributions to bone metastases are surprisingly untested. Different bone-seeking subclones of MDA-MB-231 cells had altered sensitivity to IGF-I in migration and anchorage-independent growth assays, perhaps due to increased expression of IGF-IR compared with parental cells (45, 46). In biopsies from prostate cancer patients with bone metastases, IGF-IR was frequently increased, as was the receptor substrate IRS-1 (47). Stable overexpression of IGF-IR in neuroblastoma cells increased tumor growth and osteolysis when the cells were directly injected in the tibia of mice (48). Similar results were obtained using MDA-MB-231 cells expressing of a dominant-negative IGF-IR, which decreased bone metastases (49). When MDA-PCA-2b prostate cancer cells were injected into human bone grafts in NOD/SCID mice, neutralizing antibodies against human IGF-I or mouse or human IGF-II, but not against mouse IGF-I, decreased development of bone lesions (50). However, engineered overexpression of IGF-I had no effect on two models of prostate cancer bone metastases (51). The development of skeletal metastases depends on the reactions of the cancer cells to the bone microenvironment, whose milieu consists of more than growth factors. It is also characterized by low pO_2, low pH, and high Ca^{2+}.

Physical Properties of the Bone Microenvironment

Hypoxia

Hypoxia is a major contributor to tumor metastasis, regulating secreted products that drive tumor-cell proliferation and spread. Hypoxia also contributes to resistance to radiation and chemotherapy in primary tumors. Solid tumors are particularly susceptible to hypoxia because they proliferate rapidly, outgrowing the malformed tumor vasculature, which is unable to meet the increasing metabolic demands of the expanding tumor.

Bone is a hypoxic microenvironment capable of potentiating tumor metastasis and growth. Hypoxia regulates normal marrow hematopoiesis and chondrocyte differentiation. The medullary cavity oxygen pressure in humans is estimated to be 5% O_2 (52). Cancer cells capable of surviving at low oxygen levels can thrive in the hypoxic bone microenvironment and participate in the vicious cycle of bone metastasis.

Hypoxic signaling is mediated by hypoxia-inducible factor-1 (HIF-1; ref. 53). This transcription factor is a heterodimer of HIF-1α and HIF-1β. HIF-1α expression is regulated in response to oxygen levels, whereas HIF-1β is constitutively expressed. Under normoxic conditions, oxygen-dependent prolyl hydroxylases modify HIF-1α at specific residues within the oxygen-dependent degradation domain. Hydroxylated HIF-1α is recognized and targeted for proteosomal degradation by the von Hippel-Lindau tumor suppressor, which is a component of an E3

ubiquitin-protein ligase (54). When oxygen levels are low, HIF-1α is no longer targeted for degradation by prolyl hydroxylases and instead, heterodimerizes with HIF-1β. The HIF-1 heterodimer enters the nucleus where it binds to hypoxia-response elements in DNA and mediates the transcription of numerous hypoxia-response genes.

Hypoxic signaling is increased in cancer cells exposed to low oxygen levels in the primary tumor. Hypoxia-response genes regulated by HIF-1 include glycolytic enzymes, glucose transporters, and vascular endothelial growth factor, which is important for angiogenesis. Other genes are expressed in a cell-type specific manner, including ones involved in tissue remodeling/migration/invasion, apoptosis, stress responses, proliferation/differentiation, and growth factor/cytokine function (55). Many are also prometastatic, suggesting a role for hypoxia signaling in the vicious cycle of bone metastasis.

In 13 different human cancers, including lung, breast, prostate, and colon, HIF-1α was overexpressed in two thirds of all the regional lymph node and bone metastases examined, including 69% of metastases versus 29% of primary tumors among the breast cancers (56). HIF-1α overexpression was correlated with advanced tumor stage (57), suggesting that increased HIF-1α is associated with a more aggressive and metastatic tumor phenotype.

In vitro, HIF-1α overexpression correlated with increased invasive potential of human prostate cancer cells, as well as enhanced expression of vimentin, cathepsin D, and MMP-2, which are important for cell migration and invasion, and decreased levels of E-cadherin, which is responsible for maintenance of cell-cell contacts and adhesion (58). Vimentin and E-cadherin are involved in epithelial-mesenchymal transition early in metastatic progression. Through upregulation of these proteins, HIF-1 alters the phenotype of tumor cells to increase their metastatic capability.

HIF-1α increases the transcription of factors that could accelerate the vicious cycle of skeletal metastases. MET, a receptor tyrosine kinase that binds hepatocyte growth factor, is overexpressed in advanced breast cancer and is associated with invasion and metastasis. MET expression is mediated by HIF-1α under hypoxic conditions. HIF-1α and MET cooverexpression in primary tumor samples from breast cancer patients who had undergone modified radical mastectomy was independently correlated with metastasis and decreased 10-year disease-free survival (59). HIF-1 also regulates the expression of other factors, including adrenomedullin, chemokine receptor 4, and connective tissue growth factor, with known roles in carcinogenesis and tumor metastasis (35, 55, 60, 61).

Under normoxic conditions, HIF-1α stabilization is regulated by numerous growth factors and cytokines through the phosphatidylinositol-3-kinase/protein kinase B (Akt) and the mitogen-activated protein kinase pathways (62). Growth factors, such as IGFs, fibroblast growth factor, epidermal growth factor (EGF), and tumor necrosis factor-α, have been shown to stabilize HIF-1α. Expression of these factors by tumor cells is associated with enhanced proliferation and tumor spread. Hypoxia and growth factor signaling pathways may synergistically promote the vicious cycle of skeletal metastasis.

Several studies have shown crosstalk between hypoxia and growth factor signaling pathways. In normoxic conditions, the EGF receptor (EGFR) signaling pathway activates HIF-1α–mediated transcription of survivin, a protein which increases apoptotic resistance of human breast cancer cells, thus contributing to a more aggressive cancer phenotype (63). Crosstalk also occurs between the HIF-1α and TGF-β signaling pathways: TGF-β increases hypoxic signaling by selectively inhibiting prolyl hydroxylase 2 and decreasing HIF-1α degradation (64). As discussed previously, TGF-β is important in osteolytic bone metastases, and these results show that TGF-β potentiates HIF-1 signaling within the hypoxic bone microenvironment.

As a regulator of tumor progression and metastasis, the hypoxia signaling pathway is an important chemotherapeutic target. Inhibiting this pathway may prevent the development of HIF-mediated resistance to chemotherapy and radiation therapy. A number of small molecule inhibitors of hypoxia signaling are under development. One such inhibitor is 2-methoxyestradiol, a poorly estrogenic estrogen metabolite and microtubule-depolymerizing agent with antiangiogenic and antitumorigenic properties (65). 2-Methoxyestradiol decreases HIF-1α levels and vascular endothelial growth factor mRNA expression *in vitro* and induces apoptosis of tumor cells (66, 67). 2-Methoxyestradiol is currently being evaluated in phases I and II clinical trials for the treatment of multiple types of cancer, and more potent analogues with improved antiangiogenic and antitumor effects are being developed (68). Other small molecule antihypoxic agents include inhibitors of topoisomerase I and II, such as camptothecin and GL331, and inhibitors of phosphatidylinositol-3-kinase, such as LY294002 — all of which have been shown to inhibit HIF-mediated gene transcription (62). Because HIF-1 crosstalks with multiple signaling pathways, inhibiting hypoxia signaling alone may be inadequate to halt tumor growth and spread (69). However, small molecule inhibitors could be useful in combination with other therapies to halt the vicious cycle of metastasis.

Acidic pH

Acidosis of the bone microenvironment also potentiates the vicious cycle of bone metastasis. Extracellular pH is tightly regulated within bone and has significant effects on osteoblast and osteoclast function. Extracellular acidification results in increased osteoclast resorption pit formation, with osteoclasts being maximally stimulated at pH levels of <6.9 (70). Osteoblast mineralization and bone formation is significantly impaired by acid (71). The combined effect on osteoclasts and osteoblasts is the release of alkaline bone mineral from the skeleton, compensating for systemic acidosis.

Tumor metastasis leads to localized regions of acidosis within the skeleton (70). Increased glycolysis and lactic acid production by proliferating cancer cells and decreased buffering capacity of the interstitial fluid contribute to the

acidic microenvironment within primary tumors (72). The acid-mediated tumor invasion hypothesis states that altered glucose metabolism in cancer cells stimulates cancer cell proliferation and results in a more invasive tumor phenotype (73). Acidosis alters cellular dynamics at the interface between the tumor and normal tissue, promoting apoptosis in adjacent normal cells and facilitating extracellular matrix degradation through the release of proteolytic enzymes. Unlike normal cells, cancer cells have compensatory mechanisms to allow proliferation and metastasis even at low extracellular pH and thus are not susceptible to acid-induced apoptosis.

Hypoxia further promotes acidosis within tumor cells through HIF-mediated overexpression of glycolytic enzymes and increased lactic acid production (74). Together, hypoxia and pH regulatory mechanisms control survival and proliferation of tumor cells. Apoptosis of E1a/Ras-transformed mouse embryo fibroblasts is mediated by hypoxia-induced acidosis rather than as a direct effect of hypoxia exposure (75).

Tumor acidosis promotes the release and activation of proteins, such as cathepsins B, D, and L and MMPs, which degrade the extracellular matrix and facilitate metastasis (73). Cathepsin B is a cysteine proteases expressed by tumor cells, which is activated in an acidic microenvironment and could participate in the vicious cycle of bone metastasis (76). It is expressed at low levels in primary prostate tumors; however, bone metastatic lesions express high levels of activated cathepsin B, suggesting that protease activity is modulated by interactions between tumor cells and the bone microenvironment (77).

Hypoxia-mediated acidosis also activates numerous stress signaling cascades within tumor cells, including the nuclear factor-κB and activator protein-1 pathways, which in turn regulate the transcription of prometastatic factors, such as IL-8, a cytokine important for cell motility, proliferation, and angiogenesis (78). IL-8 expression is induced by prolonged hypoxia and decreased intracellular pH in pancreatic and prostate cancer cells (79). Its overexpression correlates with increasing tumor grade and metastasis in many cancers, including breast and prostate.

Both hypoxia and acidosis have been implicated in resistance of cancer cells to radiation and chemotherapy. Extracellular acidity contributes to chemotherapeutic resistance via a pH gradient that prevents the intracellular accumulation of weakly basic drugs, such as Adriamycin (74). Tumor acidosis is a direct consequence of hypoxia exposure. Thus, therapeutic approaches, which target hypoxia signaling may exert their beneficial effects by correcting pH in cancer cells, making them more susceptible to conventional radiation and chemotherapy.

Extracellular Calcium

Calcium released from the mineralized bone matrix contributes to the vicious cycle of metastasis by several mechanisms. Calcium is the primary inorganic component of the bone matrix and, in the bone microenvironment, levels are maintained within a narrow physiologic range ($\sim$1.1-1.3 mmol/L; ref. 80). Active osteoclastic bone resorption causes extracellular calcium (Ca^{2+}_o) levels to rise up to 8 to 40 mmol/L (81).

Calcium effects are mediated through the extracellular calcium-sensing receptor (CaSR), a G protein–coupled receptor, which, in the presence of high Ca^{2+}_o, inhibits cyclic AMP and activates phospholipase C (82). The CaSR is expressed in normal tissues and is overexpressed in several types of cancer, including breast and prostate cancer (83, 84). The CaSR regulates secretion of PTHrP, whose role in osteolytic bone metastases is discussed previously (83). In normal mammary epithelium, the CaSr responds to low Ca^{2+}_o by increasing PTHrP, which activates bone resorption and release of bone matrix calcium. PTHrP production from these cells is decreased by high Ca^{2+}_o or CaSR agonists (85). Unlike normal mammary epithelial cells, breast cancer cells secrete increased levels of PTHrP in response to known agonists of the CaSR: high Ca^{2+}_o, spermine, and neomycin (83). Similar effects were observed in prostate cancer cells (84). Expression of a dominant-negative form of the CaSR in prostate cancer cells prevented Ca^{2+}_o-stimulated PTHrP release, whereas TGF-β pretreatment increased basal and Ca^{2+}_o-stimulated PTHrP (84). Thus, the vicious cycle of bone metastasis includes contributions by the CaSR: TGF-β and Ca^{2+}_o released during osteolysis activate the CaSR to increase PTHrP release, perpetuating osteolysis and bone matrix destruction.

Ca^{2+}_o has also been shown to specifically induce proliferation of PC-3 and C4-2B prostate cancer cells known to metastasize to the skeleton at concentrations of 2.5 mmol/L but does not affect LNCaP prostate epithelial cells, which do not form bone metastases (86). This effect is likely mediated by the CaSR, as knockdown of the CaSR by shRNA decreased PC-3 cell proliferation *in vitro* and inhibited the formation of bone metastases in mice. Clinically, overexpression of cytoplasmic CaSR in breast cancer tumor samples is positively correlated with the bone metastases rather than visceral metastases, suggesting that the CaSR may be a good potential marker for predicting bone metastases (87).

The CaSR activates Akt signaling to promote PC-3 cell attachment *in vitro*. Similarly, bone matrix calcium may act through this receptor to help cancer cells localize to and attach to bone during metastasis. The CaSR also signals in part through the mitogen-activated protein kinase signaling pathway to stimulate PTHrP release. Inhibitors of mitogen-activated protein/extracellular signal-regulated kinase kinase, p38 mitogen-activated protein kinase, protein kinase C, and c-Jun-NH$_2$ kinase prevented CaSR-stimulated PTHrP release by HEK293 and H-500 Leydig cancer cells in response to high Ca^{2+}_o (88, 89). Increased phosphorylation of EFK1/2, p38 mitogen-activated protein kinase, and SEK1 (upstream of c-Jun-NH$_2$ kinase) was observed in response to Ca^{2+}_o activation of the CaSR (88, 89).

G protein–coupled receptors, of which the CaSR is one, transactivate tyrosine kinase receptors and activate mitogen-activated protein kinase signaling cascades (90). The CaSR may interact with the EGFR signaling pathway to

stimulate PTHrP release. High Ca^{2+}_o resulted in delayed phosphorylation of extracellular signal-regulated kinase in PC-3 cells (91). An inhibitor of the EGFR kinase or an EGFR-neutralizing antibody prevented extracellular signal-regulated kinase phosphorylation and reduced PTHrP secretion, supporting a mechanism whereby the CaSR transactivates EGFR, resulting in extracellular signal-regulated kinase phosphorylation and increased PTHrP release. Such a mechanism may explain the finding that EGF induced PTHrP in prostatic epithelial cells (92). Inhibitors of the EGFR, such as gefitinib or PKI166, reduced osteoclastogenesis (93) and malignant osteolysis, as well as the growth of cancer cells in bone (94, 95), suggesting that the EGFR may be an important target in the vicious cycle of bone metastasis.

Two classes of therapeutic agents targeting the CaSR have been developed. Calcimimetics, including cinacalcet, increase the affinity of the CaSR for Ca^{2+}_o, which in turn inhibits release of PTH or PTHrP and leads to lower serum calcium levels. Calcimimetics have been approved for the treatment of hyperparathyroidism in end-stage renal disease and for parathyroid cancer (96). A second class of drugs which targets the CaSR is the calcilytics. Calcilytic agents have been proposed as an anabolic therapy for osteoporosis and act similarly to injectable PTH, though these drugs have not yet been approved for clinical use (96). By preventing calcium-stimulated activation of the CaSR and release of PTHrP by tumor cells, calcimimetics and calcilytics may interrupt the vicious cycle and are potentially useful for the prevention and treatment of bone metastases.

Conclusion

Crosstalk between tumor cells and the bone microenvironment promotes a vicious cycle of bone metastasis. This crosstalk occurs via multiple factors and signaling pathways. The bone microenvironment contains numerous physical factors, such as hypoxia, acidosis, and extracellular calcium, and growth factors, like TGF-β, which have been implicated in this vicious cycle. These factors activate signaling pathways in cancer cells, promoting a more aggressive tumor phenotype. Whereas much is understood about the effects of these factors in cancer cells at the primary tumor site, continued research is necessary to further elucidate their role in skeletal metastasis. Understanding the interactions between tumor and bone may help to identify potential targets for chemotherapeutic intervention to halt tumor growth and bone metastasis.

References

1. Jemal A, Siegel R, Ward E, Murray T, Xu J, Thun MJ. Cancer statistics, 2007. CA Cancer J Clin 2007;57:43 – 66.

2. Kozlow W, Guise TA. Breast cancer metastasis to bone: mechanisms of osteolysis and implications for therapy. J Mammary Gland Biol Neoplasia 2005;10:169 – 80.

3. Kakonen SM, Mundy GR. Mechanisms of osteolytic bone metastases in breast carcinoma. Cancer 2003;97:834 – 9.

4. Roudier MP, True LD, Higano CS, et al. Phenotypic heterogeneity of end-stage prostate carcinoma metastatic to bone. Hum Pathol 2003;34: 646 – 53.

5. Coleman RE. Skeletal complications of malignancy. Cancer 1997;80: 1588 – 94.

6. Yoneda T, Hiraga T. Crosstalk between cancer cells and bone microenvironment in bone metastasis. Biochem Biophys Res Commun 2005;328:679 – 87.

7. Hall CL, Kang S, MacDougald OA, Keller ET. Role of Wnts in prostate cancer bone metastases. J Cell Biochem 2006;97:661 – 72.

8. Koeneman KS, Yeung F, Chung LW. Osteomimetic properties of prostate cancer cells: a hypothesis supporting the predilection of prostate cancer metastasis and growth in the bone environment. Prostate 1999; 39:246 – 61.

9. Barnes GL, Javed A, Waller SM, et al. Osteoblast-related transcription factors Runx2 (Cbfa1/AML3) and MSX2 mediate the expression of bone sialoprotein in human metastatic breast cancer cells. Cancer Res 2003;63: 2631 – 7.

10. Pratap J, Javed A, Languino LR, et al. The Runx2 osteogenic transcription factor regulates matrix metalloproteinase 9 in bone metastatic cancer cells and controls cell invasion. Mol Cell Biol 2005;25:8581 – 91.

11. Mohan S, Baylink DJ. Bone growth factors. Clin Orthop Relat Res 1991;263:30 – 48.

12. Derynck R, Zhang YE. Smad-dependent and Smad-independent pathways in TGF-β family signalling. Nature 2003;425:577 – 84.

13. Dallas SL, Rosser JL, Mundy GR, Bonewald LF. Proteolysis of latent transforming growth factor-β (TGF-β)-binding protein-1 by osteoclasts. A cellular mechanism for release of TGF-β from bone matrix. J Biol Chem 2002;277:21352 – 60.

14. Janssens K, ten Dijke P, Janssens S, Van Hul W. Transforming growth factor-β1 to the bone. Endocr Rev 2005;26:743 – 74.

15. Elliott RL, Blobe GC. Role of transforming growth factor β in human cancer. J Clin Oncol 2005;23:2078 – 93.

16. Kang Y, He W, Tulley S, et al. Breast cancer bone metastasis mediated by the Smad tumor suppressor pathway. Proc Natl Acad Sci U S A 2005; 102:13909 – 14.

17. Javelaud D, Mohammad KS, McKenna CR, et al. Stable overexpression of smad7 in human melanoma cells impairs bone metastasis. Cancer Res 2007;67:2317 – 24.

18. Yin JJ, Selander K, Chirgwin JM, et al. TGF-β signaling blockade inhibits PTHrP secretion by breast cancer cells and bone metastases development. J Clin Invest 1999;103:197 – 206.

19. Bandyopadhyay A, Agyin JK, Wang L, et al. Inhibition of pulmonary and skeletal metastasis by a transforming growth factor-β type I receptor kinase inhibitor. Cancer Res 2006;66:6714 – 21.

20. Ehata S, Hanyu A, Fujime M, et al. Ki26894, a novel transforming growth factor-b; type I receptor kinase inhibitor, inhibits *in vitro* invasion and *in vivo* bone metastasis of a human breast cancer cell line. Cancer Sci 2007;98:127 – 33.

21. Stebbins EG, Mohammad KS, Niewolna M, et al. SD-208, a small molecule inhibitor of tranforming growth factor-b receptor I kinase reduces breast cancer metastases to bone and improves survival in a mouse model [abstract]. J Bone Miner Res 2005;20:S55.

22. Guise TA, Yin JJ, Taylor SD, et al. Evidence for a causal role of parathyroid hormone-related protein in the pathogenesis of human breast cancer-mediated osteolysis. J Clin Invest 1996;98:1544 – 9.

23. Powell G, Southby J, Danks J, et al. Localization of parathyroid hormone-related protein in breast cancer metastases: increased incidence in bone compared with other sites. Cancer Res 1991;51:3059 – 61.

24. Kakonen SM, Selander KS, Chirgwin JM, et al. Transforming growth factor-β stimulates parathyroid hormone-related protein and osteolytic metastases via Smad and mitogen-activated protein kinase signaling pathways. J Biol Chem 2002;277:24571 – 8.

25. Gallwitz WE, Guise TA, Mundy GR. Guanosine nucleotides inhibit different syndromes of PTHrP excess caused by human cancers *in vivo*. J Clin Invest 2002;110:1559 – 72.

26. Kitazawa S, Kitazawa R. RANK ligand is a prerequisite for cancer-associated osteolytic lesions. J Pathol 2002;198:228 – 36.

27. Kondo H, Guo J, Bringhurst FR. Cyclic adenosine monophosphate/ protein kinase A mediates parathyroid hormone/parathyroid hormone-related protein receptor regulation of osteoclastogenesis and expression of

RANKL and osteoprotegerin mRNAs by marrow stromal cells. J Bone Miner Res 2002;17:1667 – 79.

28. Pollock JH, Blaha MJ, Lavish SA, Stevenson S, Greenfield EM. *In vivo* demonstration that parathyroid hormone and parathyroid hormone-related protein stimulate expression by osteoblasts of interleukin-6 and leukemia inhibitory factor. J Bone Miner Res 1996;11:754 – 9.

29. Hiraga T, Myoui A, Choi ME, Yoshikawa H, Yoneda T. Stimulation of cyclooxygenase-2 expression by bone-derived transforming growth factor-β enhances bone metastases in breast cancer. Cancer Res 2006; 66:2067 – 73.

30. Singh B, Berry JA, Shoher A, Ayers GD, Wei C, Lucci A. COX-2 involvement in breast cancer metastasis to bone. Oncogene 2007. doi: 10.1038/sj.onc.1210154.

31. Bendre MS, Margulies AG, Walser B, et al. Tumor-derived interleukin-8 stimulates osteolysis independent of the receptor activator of nuclear factor-κB ligand pathway. Cancer Res 2005;65:11001 – 9.

32. Singh B, Berry JA, Shoher A, Lucci A. COX-2 induces IL-11 production in human breast cancer cells. J Surg Res 2006;131:267 – 75.

33. Horwood NJ, Elliott J, Martin TJ, Gillespie MT. Osteotropic agents regulate the expression of osteoclast differentiation factor and osteoprotegerin in osteoblastic stromal cells. Endocrinology 1998;139:4743.

34. Morgan H, Tumber A, Hill PA. Breast cancer cells induce osteoclast formation by stimulating host IL-11 production and downregulating granulocyte/macrophage colony-stimulating factor. Int J Cancer 2004; 109:653 – 60.

35. Kang Y, Siegel PM, Shu W, et al. A multigenic program mediating breast cancer metastasis to bone. Cancer Cell 2003;3:537 – 49.

36. Gehron Robey P, Boskey AL. Extracellular Matrix and Biomineralization of Bone. 5th ed. In: Favus MJ, editor. Primer on the Metabolic Bone Diseases and Disorders of Mineral Metabolism. Washington (DC): American Society for Bone and Mineral Research; 2003. p. 38 – 46.

37. Sato M, Morii E, Komori T, et al. Transcriptional regulation of osteopontin gene *in vivo* by PEBP2αA/CBFA1 and ETS1 in the skeletal tissues. Oncogene 1998;17:1517 – 25.

38. Selvamurugan N, Kwok S, Partridge NC. Smad3 interacts with JunB and Cbfa1/Runx2 for transforming growth factor-β1-stimulated collagenase-3 expression in human breast cancer cells. J Biol Chem 2004;279:27764 – 73.

39. Brubaker KD, Vessella RL, True LD, Thomas R, Corey E. Cathepsin K mRNA and protein expression in prostate cancer progression. J Bone Miner Res 2003;18:222 – 30.

40. Delaisse JM, Andersen TL, Engsig MT, Henriksen K, Troen T, Blavier L. Matrix metalloproteinases (MMP) and cathepsin K contribute differently to osteoclastic activities. Microsc Res Tech 2003;61:504 – 13.

41. Roca H, Phimphilai M, Gopalakrishnan R, Xiao G, Franceschi RT. Cooperative interactions between RUNX2 and homeodomain protein-binding sites are critical for the osteoblast-specific expression of the bone sialoprotein gene. J Biol Chem 2005;280:30845 – 55.

42. Yeung F, Law WK, Yeh CH, et al. Regulation of human osteocalcin promoter in hormone-independent human prostate cancer cells. J Biol Chem 2002;277:2468 – 76.

43. Dupont J, Holzenberger M. Biology of insulin-like growth factors in development. Birth Defects Res Part C Embryo Today 2003;69:257 – 71.

44. Baserga R, Peruzzi F, Reiss K. The IGF-1 receptor in cancer biology. Int J Cancer 2003;107:873 – 7.

45. Jackson JG, Zhang X, Yoneda T, Yee D. Regulation of breast cancer cell motility by insulin receptor substrate-2 (IRS-2) in metastatic variants of human breast cancer cell lines. Oncogene 2001;20:7318 – 25.

46. Yoneda T, Williams PJ, Hiraga T, Niewolna M, Nishimura R. A bone-seeking clone exhibits different biological properties from the MDA-MB-231 parental human breast cancer cells and a brain-seeking clone *in vivo* and *in vitro*. J Bone Miner Res 2001;16:1486 – 95.

47. Hellawell GO, Turner GD, Davies DR, Poulsom R, Brewster SF, Macaulay VM. Expression of the type 1 insulin-like growth factor receptor is up-regulated in primary prostate cancer and commonly persists in metastatic disease. Cancer Res 2002;62:2942 – 50.

48. van Golen CM, Schwab TS, Kim B, et al. Insulin-like growth factor-I receptor expression regulates neuroblastoma metastasis to bone. Cancer Res 2006;66:6570 – 8.

49. Hiraga T, Myoui A, Williams PJ, Mundy GR, Yoneda T. Suppression of

IGF signaling propagation and NF-kB activation reduces bone metastases in breast cancer [abstract]. J Bone Miner Res 2001;16:S200.

50. Goya M, Miyamoto SI, Nagai K, et al. Growth inhibition of human prostate cancer cells in human adult bone implanted into nonobese diabetic/severe combined immunodeficient mice by a ligand-specific antibody to human insulin-like growth factors. Cancer Res 2004;64: 6252 – 8.

51. Rubin J, Fan X, Rahnert J, et al. IGF-I secretion by prostate carcinoma cells does not alter tumor-bone cell interactions *in vitro* or *in vivo*. Prostate 2006;66:789 – 800.

52. Asosingh K, De Raeve H, de Ridder M, et al. Role of the hypoxic bone marrow microenvironment in 5T2MM murine myeloma tumor progression. Haematologica 2005;90:810 – 7.

53. Harris AL. Hypoxia - a key regulatory factor in tumour growth. Nat Rev Cancer 2002;2:38 – 47.

54. Semenza GL. HIF-1 and tumor progression: pathophysiology and therapeutics. Trends Mol Med 2002;8:S62 – 7.

55. Le QT, Denko NC, Giaccia AJ. Hypoxic gene expression and metastasis. Cancer Metastasis Rev 2004;23:293 – 310.

56. Zhong H, De Marzo AM, Laughner E, et al. Overexpression of hypoxia-inducible factor 1α in common human cancers and their metastases. Cancer Res 1999;59:5830 – 5.

57. Bos R, Zhong H, Hanrahan CF, et al. Levels of hypoxia-inducible factor-1 α during breast carcinogenesis. J Natl Cancer Inst 2001;93: 309 – 14.

58. Luo Y, He DL, Ning L, et al. Over-expression of hypoxia-inducible factor-1α increases the invasive potency of LNCaP cells *in vitro*. BJU Int 2006;98:1315 – 9.

59. Chen HH, Su WC, Lin PW, Guo HR, Lee WY. Hypoxia-inducible factor-1α correlates with MET and metastasis in node-negative breast cancer. Breast Cancer Res Treat 2007;103:167 – 75.

60. Garayoa M, Martinez A, Lee S, et al. Hypoxia-inducible factor-1 (HIF-1) up-regulates adrenomedullin expression in human tumor cell lines during oxygen deprivation: a possible promotion mechanism of carcinogenesis. Mol Endocrinol 2000;14:848 – 62.

61. Higgins DF, Biju MP, Akai Y, Wutz A, Johnson RS, Haase VH. Hypoxic induction of Ctgf is directly mediated by Hif-1. Am J Physiol Renal Physiol 2004;287:F1223 – 32.

62. Powis G, Kirkpatrick L. Hypoxia inducible factor-1α as a cancer drug target. Mol Cancer Ther 2004;3:647 – 54.

63. Peng XH, Karna P, Cao Z, Jiang BH, Zhou M, Yang L. Cross-talk between epidermal growth factor receptor and hypoxia-inducible factor-1α signal pathways increases resistance to apoptosis by up-regulating survivin gene expression. J Biol Chem 2006;281:25903 – 14.

64. McMahon S, Charbonneau M, Grandmont S, Richard DE, Dubois CM. Transforming growth factor β1 induces hypoxia-inducible factor-1 stabilization through selective inhibition of PHD2 expression. J Biol Chem 2006;281:24171 – 81.

65. Mooberry SL. New insights into 2-methoxyestradiol, a promising antiangiogenic and antitumor agent. Curr Opin Oncol 2003;15:425 – 30.

66. Mooberry SL. Mechanism of action of 2-methoxyestradiol: new developments. Drug Resist Updat 2003;6:355 – 61.

67. Mabjeesh NJ, Escuin D, LaVallee TM, et al. 2ME2 inhibits tumor growth and angiogenesis by disrupting microtubules and dysregulating HIF. Cancer Cell 2003;3:363 – 75.

68. Tinley TL, Leal RM, Randall-Hlubek DA, et al. Novel 2-methoxyestradiol analogues with antitumor activity. Cancer Res 2003;63:1538 – 49.

69. Melillo G. Inhibiting hypoxia-inducible factor 1 for cancer therapy. Mol Cancer Res 2006;4:601 – 5.

70. Arnett T. Regulation of bone cell function by acid-base balance. Proc Nutr Soc 2003;62:511 – 20.

71. Brandao-Burch A, Utting JC, Orriss IR, Arnett TR. Acidosis inhibits bone formation by osteoblasts *in vitro* by preventing mineralization. Calcif Tissue Int 2005;77:167 – 74.

72. Raghunand N, Gatenby RA, Gillies RJ. Microenvironmental and cellular consequences of altered blood flow in tumours. Br J Radiol 2003;76 Spec No 1:S11 – 22.

73. Gatenby RA, Gawlinski ET, Gmitro AF, Kaylor B, Gillies RJ. Acid-mediated tumor invasion: a multidisciplinary study. Cancer Res 2006;66: 5216 – 23.

74. Shannon AM, Bouchier-Hayes DJ, Condron CM, Toomey D. Tumour hypoxia, chemotherapeutic resistance and hypoxia-related therapies. Cancer Treat Rev 2003;29:297 – 307.

75. Schmaltz C, Hardenbergh PH, Wells A, Fisher DE. Regulation of proliferation-survival decisions during tumor cell hypoxia. Mol Cell Biol 1998;18:2845 – 54.

76. Webb SD, Sherratt JA, Fish RG. Alterations in proteolytic activity at low pH and its association with invasion: a theoretical model. Clin Exp Metastasis 1999;17:397 – 407.

77. Podgorski I, Linebaugh BE, Sameni M, et al. Bone microenvironment modulates expression and activity of cathepsin B in prostate cancer. Neoplasia 2005;7:207 – 23.

78. Xie K, Huang S. Regulation of cancer metastasis by stress pathways. Clin Exp Metastasis 2003;20:31 – 43.

79. Shi Q, Xiong Q, Le X, Xie K. Regulation of interleukin-8 expression by tumor-associated stress factors. J Interferon Cytokine Res 2001;21: 553 – 66.

80. Dvorak MM, Siddiqua A, Ward DT, et al. Physiological changes in extracellular calcium concentration directly control osteoblast function in the absence of calciotropic hormones. Proc Natl Acad Sci U S A 2004; 101:5140 – 5.

81. Berger CE, Rathod H, Gillespie JI, Horrocks BR, Datta HK. Scanning electrochemical microscopy at the surface of bone-resorbing osteoclasts: evidence for steady-state disposal and intracellular functional compartmentalization of calcium. J Bone Miner Res 2001;16: 2092 – 102.

82. Chattopadhyay N. Effects of calcium-sensing receptor on the secretion of parathyroid hormone-related peptide and its impact on humoral hypercalcemia of malignancy. Am J Physiol Endocrinol Metab 2006;290:E761 – 70.

83. Sanders JL, Chattopadhyay N, Kifor O, Yamaguchi T, Butters RR, Brown EM. Extracellular calcium-sensing receptor expression and its potential role in regulating parathyroid hormone-related peptide secretion in human breast cancer cell lines. Endocrinology 2000;141:4357 – 64.

84. Sanders JL, Chattopadhyay N, Kifor O, Yamaguchi T, Brown EM. Ca(2 +)-sensing receptor expression and PTHrP secretion in PC-3 human prostate cancer cells. Am J Physiol Endocrinol Metab 2001;281: E1267 – 74.

85. VanHouten J, Dann P, McGeoch G, et al. The calcium-sensing receptor regulates mammary gland parathyroid hormone-related protein production and calcium transport. J Clin Invest 2004;113:598 – 608.

86. Liao J, Schneider A, Datta NS, McCauley LK. Extracellular calcium as a candidate mediator of prostate cancer skeletal metastasis. Cancer Res 2006;66:9065 – 73.

87. Mihai R, Stevens J, McKinney C, Ibrahim NB. Expression of the calcium receptor in human breast cancer-a potential new marker predicting the risk of bone metastases. Eur J Surg Oncol 2006;32:511 – 5.

88. MacLeod RJ, Chattopadhyay N, Brown EM. PTHrP stimulated by the calcium-sensing receptor requires MAP kinase activation. Am J Physiol Endocrinol Metab 2003;284:E435 – 42.

89. Tfelt-Hansen J, MacLeod RJ, Chattopadhyay N, et al. Calcium-sensing receptor stimulates PTHrP release by pathways dependent on PKC, p38 MAPK, JNK, and ERK1/2 in H-500 cells. Am J Physiol Endocrinol Metab 2003;285:E329 – 37.

90. Wetzker R, Bohmer FD. Transactivation joins multiple tracks to the ERK/MAPK cascade. Nat Rev Mol Cell Biol 2003;4:651 – 7.

91. Yano S, Macleod RJ, Chattopadhyay N, et al. Calcium-sensing receptor activation stimulates parathyroid hormone-related protein secretion in prostate cancer cells: role of epidermal growth factor receptor transactivation. Bone 2004;35:664 – 72.

92. Cramer SD, Peehl DM, Edgar MG, Wong ST, Deftos LJ, Feldman D. Parathyroid hormone-related protein (PTHrP) is an epidermal growth factor-regulated secretory product of human prostatic epithelial cells. Prostate 1996;29:20 – 9.

93. Normanno N, De Luca A, Aldinucci D, et al. Gefitinib inhibits the ability of human bone marrow stromal cells to induce osteoclast differentiation: implications for the pathogenesis and treatment of bone metastasis. Endocr Relat Cancer 2005;12:471 – 82.

94. Kim SJ, Uehara H, Karashima T, Shepherd DL, Killion JJ, Fidler IJ. Blockade of epidermal growth factor receptor signaling in tumor cells and tumor-associated endothelial cells for therapy of androgen-independent human prostate cancer growing in the bone of nude mice. Clin Cancer Res 2003;9:1200 – 10.

95. Weber KL, Doucet M, Price JE, Baker C, Kim SJ, Fidler IJ. Blockade of epidermal growth factor receptor signaling leads to inhibition of renal cell carcinoma growth in the bone of nude mice. Cancer Res 2003;63:2940 – 7.

96. Brown EM. Clinical lessons from the calcium-sensing receptor. Nat Clin Pract Endocrinol Metab 2007;3:122 – 33.

Lowering Bone Mineral Affinity of Bisphosphonates as a Therapeutic Strategy to Optimize Skeletal Tumor Growth Inhibition *In vivo*

Pierrick G.J. Fournier,[1,2] Florence Daubiné,[1,2] Mark W. Lundy,[4] Michael J. Rogers,[3] Frank H. Ebetino,[4] and Philippe Clézardin[1,2]

[1]Institut National de la Santé et de la Recherche Médicale, Research Unit UMR 664, Faculté de Médecine Laennec, Lyon, France; [2]Université Claude Bernard Lyon 1, Villeurbanne, France; [3]Institute of Medical Sciences, Aberdeen, United Kingdom; and [4]Procter and Gamble Pharmaceuticals, Mason, Ohio

Abstract

Bisphosphonates bind avidly to bone mineral and are potent inhibitors of osteoclast-mediated bone destruction. They also exhibit antitumor activity *in vitro*. Here, we used a mouse model of human breast cancer bone metastasis to examine the effects of risedronate and NE-10790, a phosphonocarboxylate analogue of the bisphosphonate risedronate, on osteolysis and tumor growth. Osteolysis was measured by radiography and histomorphometry. Tumor burden was measured by fluorescence imaging and histomorphometry. NE-10790 had a 70-fold lower bone mineral affinity compared with risedronate. It was 7-fold and 8,800-fold less potent than risedronate at reducing, respectively, breast cancer cell viability *in vitro* and bone loss in ovariectomized animals. We next showed that risedronate given at a low dosage in animals bearing human B02-GFP breast tumors reduced osteolysis by inhibiting bone resorption, whereas therapy with higher doses also inhibited skeletal tumor burden. Conversely, therapy with NE-10790 substantially reduced skeletal tumor growth at a dosage that did not inhibit osteolysis, a higher dosage being able to also reduce bone destruction. The *in vivo* antitumor activity of NE-10790 was restricted to bone because it did not inhibit the growth of subcutaneous B02-GFP tumor xenografts nor the formation of B16-F10 melanoma lung metastases. Moreover, NE-10790, in combination with risedronate, reduced both osteolysis and skeletal tumor burden, whereas NE-10790 or risedronate alone only decreased either tumor burden or osteolysis, respectively. In conclusion, our study shows that decreasing the bone mineral affinity of bisphosphonates is an effective therapeutic strategy to inhibit skeletal tumor growth *in vivo*. [Cancer Res 2008;68(21):8945–53]

Introduction

Cancer cells that metastasize to the skeleton are, on their own, rarely able to destroy bone (1). Instead, they stimulate the function of bone-degrading cells, the osteoclasts, leading to the formation of osteolytic lesions (1). In this respect, bisphosphonate drugs are potent inhibitors of osteoclast-mediated bone resorption, and have shown clinical utility in the palliative treatment of patients with osteolytic metastases (2).

Chemically, bisphosphonates are all characterized by two phosphonate groups linked to a central carbon atom, forming a P-C-P structure (3). Two chains (called R_1 and R_2) are covalently bound to the carbon atom of the common P-C-P structure. This common backbone and the R_1 side chain (preferably a hydroxyl group) allow bisphosphonates to bind avidly to hydroxyapatite crystals in the skeleton (3). The R_2 side chain determines the potency of bisphosphonates to inhibit osteoclast-mediated bone resorption (3). Bisphosphonates that lack a nitrogen functional group in the R_2 side chain (e.g., etidronate or clodronate) cause the intracellular accumulation of nonhydrolyzable, cytotoxic ATP analogues that subsequently induce osteoclast apoptosis (3). Bisphosphonates with an R_2 side chain containing a nitrogen atom either in an alkyl chain (e.g., pamidronate, alendronate, ibandronate) or within a heterocyclic ring (e.g., risedronate or zoledronate) target osteoclast farnesyl diphosphate (FPP) synthase, a key enzyme in the mevalonate pathway, and inhibit its activity to varying degrees, depending on the overall molecular structure of these nitrogen-containing bisphosphonates (4). The inhibition of FPP synthase activity by nitrogen-containing bisphosphonates leads to impaired prenylation and prevents correct function of small GTPases that are essential for osteoclast activity (3).

There is now extensive *in vivo* preclinical evidence that bisphosphonates can reduce skeletal tumor burden and inhibit the formation of bone metastases in animal models (5). Several mechanisms have been proposed to explain these observations. For example, bisphosphonates may render the bone a less favorable microenvironment for tumor cell colonization by reducing osteoclast-mediated bone resorption, which, in turn, deprives tumor cells of bone-derived growth factors that are required for tumor cell proliferation (5). In addition, bisphosphonates seem to have direct antitumor effects (5). They have been shown to inhibit tumor cell adhesion, invasion, and proliferation, and they induce apoptosis of a variety of human tumor cell lines *in vitro* (5). Inhibition of the prenylation of small GTPases in tumor cells is thought to be responsible for many of the observed *in vitro* antitumor effects of nitrogen-containing bisphosphonates (5). However, whereas bisphosphonates clearly exhibit a direct antitumor potential, these drugs that are used for the treatment of patients with skeletal metastases to date have shown no convincing antitumor effects (2). Thus, it is important to define new strategies to optimize the direct antitumor properties of bisphosphonates *in vivo*.

We have previously shown that soluble bisphosphonates are significantly more potent than mineral-bound bisphosphonates at inhibiting tumor cell adhesion to bone *in vitro* (6). Moreover, it has been recently reported that osteoclasts internalize bisphosphonates from bone, whereas nonresorbing breast cancer cells only take up small amounts of these bisphosphonates that become

available due to their natural desorption from the bone surface (7). Overall, these findings (6, 7) suggest that the higher the affinity of a bisphosphonate is for bone mineral, the more limited their direct antitumor potential is *in vivo*. Therefore, we reasoned that a bisphosphonate possessing weak bone mineral affinity could be released in higher concentration near the bone mineral surface and might act directly on tumor cells that reside in the bone marrow.

To address this question, we used a phosphonocarboxylate analogue of risedronate, NE-10790, in which one of the phosphonate groups of the P-C-P moiety is replaced with a carboxyl group. NE-10790 has a low bone mineral affinity and a poor antiresorptive activity *in vitro* and in the Schenk growing rat model (8, 9). In addition, this compound inhibits breast and prostate cancer cell invasion and induces apoptosis of myeloma cells *in vitro* (10, 11). At the molecular level, NE-10790 does not inhibit FPP synthase activity but blocks Rab geranylgeranyl transferase in several cell types, including osteoclasts, macrophages, and myeloma cells (11, 12). Here, using a mouse model of human breast cancer bone metastasis, we compared the effects of risedronate and NE-10790 on osteolysis and skeletal tumor growth.

Materials and Methods

Cell lines. MDA-MB-231, MDA-MB-435s, MCF-7, Hs 578T, T-47D, and ZR-75-1 human breast cancer cell lines were obtained from the American Type Culture Collection-LGC Promochem. The MDA-MB-231/B02 human breast cancer cell line is a subpopulation of the MDA-MB-231 cancer line that was selected for the high efficiency with which it metastasizes to bone after i.v. inoculation (13). Tumor cells were routinely cultured in RPMI 1640 (Invitrogen) or α-MEM (Invitrogen) supplemented with 10% (v/v) heat-inactivated FCS (Invitrogen) and 1% (v/v) penicillin/streptomycin (Invitrogen) in a humidified atmosphere of 5% CO_2 in air.

Drugs and reagents. Risedronate [2-(3-pyridinyl)1-hydroxyethylidene-bisphosphonic acid] and NE-10790 [2-(3-pyridinyl)1-hydroxyethylidene-1,1-phosphonocarboxylic acid] were obtained from Procter and Gamble Pharmaceuticals. These drugs were resuspended in PBS or cell culture medium and stored at 4°C. All transgeranylgeraniol (GGOH) was purchased from Sigma-Aldrich, diluted at (10^{-1} mol/L) in absolute ethanol, and stored at -20°C.

Measurement of the bone mineral affinity of risedronate and NE-10790. Binding affinity constants (K_L) for the adsorption of risedronate and NE-10790 were calculated from kinetic studies on hydroxyapatite crystal growth using Langmuir isotherm plots, as previously described (14, 15).

Cell viability assay. Cell viability was determined using a 3-(4,5-dimethylthiazol-2-yl)-2,5-diphenyltetrazolium bromide (MTT) assay, as previously described (13, 16). Because the doubling time varies from one cell line to another, B02-GFP, MDA-MB-231, MDA-MB-435s, MCF-7, Hs 578T, T-47D, and ZR-75-1 cells were seeded in 96-well plates at different cell densities (5×10^2, 10^4, 8×10^3, 5×10^2, 6×10^3, 8×10^3, and 4×10^3 cells per well, respectively) to ensure similar growth rates. Twenty-four hours later, growing cells were washed and further cultured for 6 d in complete medium in the presence or absence of increasing concentrations of drugs and in the presence or absence of GGOH (10 μmol/L). The half-maximal inhibitory concentration (IC_{50}) of each drug was calculated using a nonlinear curve fit (Logistic 4PL) with Softmax v2.22 software (Molecular Devices).

Cytokine array. A commercial antibody-based protein microarray designed to detect 79 growth factors, cytokines, and chemokines (RayBio Human Cytokine Array V, RayBiotech) was used. Experiments were carried out following manufacturer's instructions. Array membranes were blocked with the saturated buffer for 1 h and then incubated for 2 h with the conditioned medium (1 mL) from cultured B02-GFP breast cancer cells or the supernatant of bone marrow cells collected after flushing the hind limbs from naive animals and animals with bone metastases that had been treated or not treated with drugs. After washing, membranes were incubated for 2 hs with a cocktail of 79 biotinylated antibodies. Membranes were then washed and incubated for an additional 2 h with a peroxidase-labeled streptavidin solution. Detection of immunoreactive spots was carried out using an enhanced chemiluminescence detection system (GE Healthcare).

Measurement of cytokine production by ELISA. Breast cancer cells (B02-GFP, MDA-MB-231, MDA-MB-435s, MCF-7, Hs578T, T47D, and ZR-75-1) were seeded in 24-well and 96-well plates at a cell density used for the cell viability assay. Growing cells were cultured for 2 d in complete α-MEM in the presence or absence of drugs. After washing to remove drugs, tumor cells were further cultured for another 2 d, at which time the 96-well and 24-well plates were used for cell counting and measurement of cytokine production, respectively. For the measurement of cytokines, cell culture supernatants containing protease inhibitors (aprotinin and leupeptin; 1 μg/mL) were centrifuged (1,000 $\times$ *g*, 5 min, 4°C) and then stored at -20°C until use. The measurement of human interleukin-6 (IL-6), IL-8, and MCP-1 was performed by ELISA (Module Set Bender MedSystems, AbCys SA). Results were expressed as nanograms per milliliter per 10^6 cells. Cell culture supernatants used for measurement of cytokine production were also tested in the osteoclastogenesis assay.

***In vitro* osteoclastogenesis assay.** Experiments were carried out using 8-wk-old female OF1 mice (Charles River Laboratories), as previously described (16). Briefly, bone marrow cells were flushed from hind limbs and then seeded in 12-well plates at a density of 180,000 cells per well in complete α-MEM supplemented with murine macrophage-colony stimulating factor (M-CSF, 25 ng/mL; PreproTech), receptor activator of nuclear receptor factor κB ligand (RANKL; 0.5% v/v) and the conditioned media from B02-GFP cells previously treated with the vehicle, risedronate, or NE-10790. After 6 d of culture, differentiated osteoclasts were enumerated under a light microscope on the basis of multinuclearity (cells with more than three nuclei) and tartrate-resistant acid phosphatase (TRAP) activity using a commercial kit (Sigma). Results were expressed as the number of osteoclasts per square centimeter.

Animal studies. All procedures involving animals, including housing and care, method of euthanasia, and experimental protocols were conducted in accordance with a code of practice established by the ethical committees in Lyon (France) and Mason (Ohio). These studies were routinely inspected by the attending veterinarian to ensure continued compliance with the proposed protocols. Four-week-old female BALB/c homozygous (*nu/nu*) athymic mice and 4-wk-old C57BL/6 mice were obtained from Charles River. Sham-operated or ovariectomized 3-mo-old female Sprague-Dawley rats were obtained from Simonsen Laboratories.

For bone loss experiments, rats were sham-operated or ovariectomized at 3 mo of age, allowed to lose bone for 7 d, and then treated for 35 d. During treatment, the vehicle (PBS), risedronate (1.4 μg/kg body weight), or NE-10790 (3,700, 12,350 or 37,000 μg/kg body weight) was given s.c. to animals daily. Bone mineral density was measured on the proximal tibiae using single-photon absorptiometry. Results were expressed in milligrams per square centimeter.

For bone metastasis experiments, we specifically used B02 cells that had been stably transfected with the gene encoding green fluorescent protein to detect tumor cells in live animals using noninvasive fluorescence imaging. The characteristics of the B02-GFP cell line were described elsewhere (17). B02-GFP cells (5×10^5 in 100 μL of PBS) were injected into the tail vein of nude mice anesthetized with 130 mg/kg ketamin and 8.8 mg/kg xylazin. Based on an average body weight of 20 g for 4-wk-old mice, risedronate (5–150 μg/kg body weight) or NE-10790 (20–37,000 μg/kg body weight) was given daily to animals by s.c. injection beginning on the day of tumor cell inoculation (day 0), and continuing until the end of the protocol (day 35). All doses of each drug were given by s.c. injection in 100 μL PBS (vehicle). Control mice received a daily treatment with vehicle only. On day 35 after tumor cell inoculation, radiographs of anesthetized mice were taken with the use of MIN-R2000 films (Kodak) in an MX-20 cabinet X-ray system (Faxitron X-Ray Corporation). Osteolytic lesions were identified on radiographs as radiolucent lesions in the bone. The area of the osteolytic lesions was measured using a Visiolab 2000 computerized image analysis system (Explora Nova), and the extent of bone destruction per animal was

Figure 1. *A,* antiresorptive potencies of risedronate and NE-10790 in an animal model of bone loss caused by ovariectomy. The bone mineral density of tibiae from female rats 35 d after ovariectomy was statistically significantly decreased when compared with that observed with sham-operated animals. The treatment of ovariectomized animals with a daily dose of 1.4 μg/kg risedronate prevented bone loss, whereas much higher doses of NE-10790 were required to reach this end point. *Columns,* mean of six animals per group; *bars,* SD. *, $P < 0.05$. *B,* effects of risedronate and NE-10790 on viability of B02-GFP breast cancer cells *in vitro*. B02-GFP cells were cultured in complete medium and then treated with increasing concentrations of each drug for 6 d. Cell viability was measured using an MTT assay. The viability of untreated cells was set to 100% (control), and results were expressed as a percentage of the control. Half-maximal inhibitory concentrations (IC_{50}) for risedronate and NE-10790 were 0.37 and 2.74 mmol/L, respectively. *C,* effect of 10 μmol/L geranylgeraniol (GGOH) on viability of B02-GFP cells upon treatment with risedronate (IC_{50}; 0.37 mmol/L), NE-10790 (IC_{50}; 2.74 mmol/L), or the vehicle (*Ctrl*). *Columns,* mean of two separate experiments; *bars,* SD. *, $P < 0.05$.
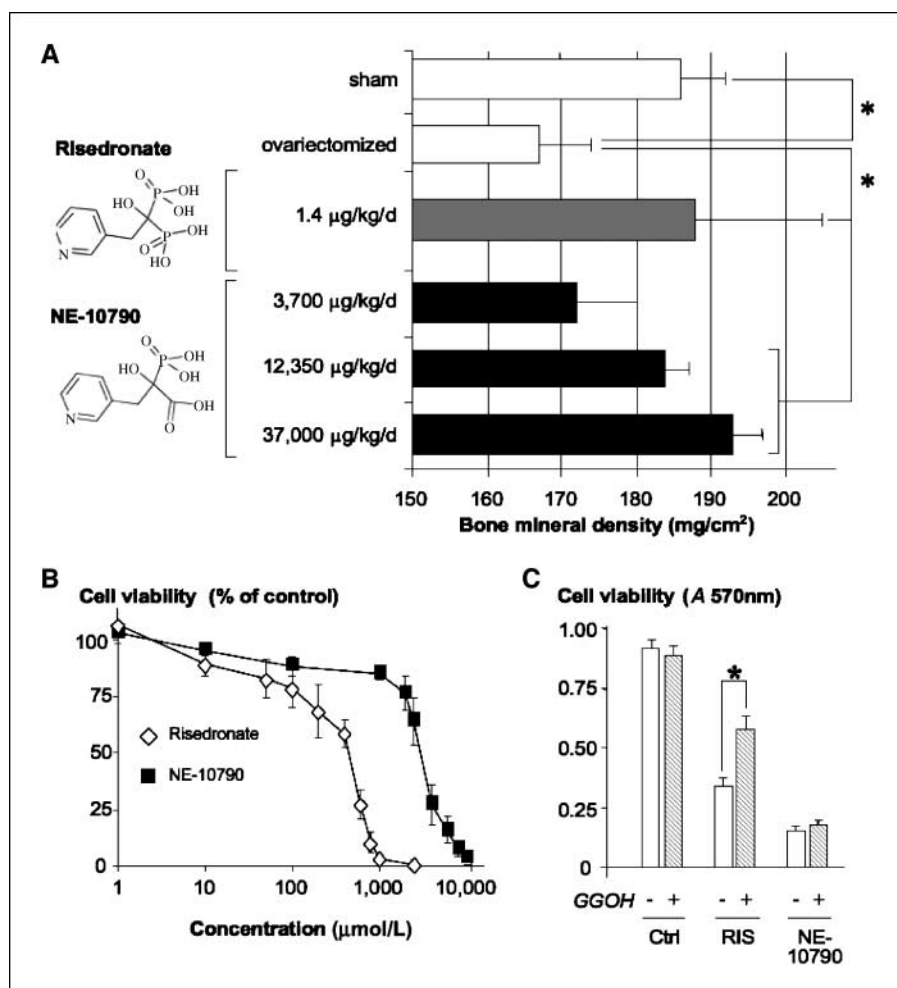
expressed in square millimeters, as described previously (13, 16, 17). Animals analyzed by radiography were also examined by noninvasive, whole-body fluorescence imaging using a fluorescence scanning system (FluorImager, Molecular Dynamics). Tumor burden in animals was identified on scanned images as fluorescent spots. The area of fluorescent spots was measured using an ImageQuant computerized image analysis system (Molecular Dynamics), and the extent of tumor burden per animal was expressed in square millimeters, as described previously (16, 17). Anesthetized mice were killed by cervical dislocation after radiography and fluorescence imaging on day 35.

Bone histology and histomorphometry. Bone histology and histomorphometric analysis of bone tissue sections were performed as previously described (13, 16, 17). Briefly, metastatic animals treated with the vehicle, risedronate, or NE-10790 were killed on day 35 after tumor cell inoculation, and both hind limbs from each animal were dissected, fixed in 80% (v/v) alcohol, dehydrated, and embedded in methylmethacrylate. A microtome (Polycut E, Reichert-Jung) was used to cut 7-μm-thick sections of undecalcified long bones, and the sections were stained with Goldner's trichrome (13, 16, 17). Histologic and histomorphometric analyses were performed on Goldner's trichrome-stained longitudinal medial sections of tibial metaphysis with the use of Visiolab 2000 computerized image analysis system, as described previously (13, 16, 17). The *in situ* detection of osteoclasts was performed on TRAP-stained longitudinal medial sections of tibial metaphysis with the use of a commercial kit (Merck). Osteoclast number (Oc.N/BS) and resorption surface (Oc.S/BS) were calculated as, respectively, the ratio of TRAP-positive cells (Oc.N) and TRAP-positive trabecular bone surface (Oc.S) to the total trabecular bone surface using Visiolab 2000 computerized image analysis system (16).

Statistical analysis. All data were analyzed with the use of StatView v5.0 software (version 5.0; SAS Institute, Inc.). Pairwise comparisons were carried out by performing nonparametric Mann-Whitney U test. P values of <0.05 were considered statistically significant. All statistical tests were two-sided.

Results

Structure-activity relationships of risedronate and NE-10790. Phosphonate groups of the P-C-P structure are responsible for the strong affinity of bisphosphonates for bone mineral (3). NE-10790 is a phosphonocarboxylate analogue of risedronate in which one of the phosphonate groups is replaced with a carboxyl group (Fig. 1*A*). The affinity constant (K_L) for the adsorption of NE-10790 on hydroxyapatite crystals was measured using an experimental procedure similar to that previously described for risedronate (13, 14). Compared with risedronate (K_L = 2.2 μmol/L), we observed that modifications to the P-C-P moiety resulted in a 73-fold decrease in bone mineral affinity for NE-10790 (K_L = 0.03 μmol/L; ref. 14).

We then studied antiresorptive potencies of risedronate and NE-10790 in an animal model of bone loss caused by ovariectomy. The treatment of ovariectomized animals with increasing doses of NE-10790 (3,700–37,000 μg/kg) showed that the lowest effective dose (LED) required to prevent bone loss was 12,350 μg/kg (Fig. 1*A*). By contrast, risedronate had a LED of 1.4 μg/kg (Fig. 1*A*). NE-10790

was, therefore, 8,800-fold less potent than risedronate as an inhibitor of osteoclast-mediated bone resorption *in vivo*.

We next examined the potencies of risedronate and NE-10790 at inhibiting the viability of B02-GFP breast cancer cells *in vitro*. Risedronate reduced the number of viable B02-GFP cells in a time-dependent (data not shown) and dose-dependent manner (Fig. 1*B*) with a half-maximal inhibitory concentration (IC_{50}) of 0.37 mmol/L (Supplementary Table S1). NE-10790 (IC_{50} = 2.74 mmol/L) was 7-fold less potent than risedronate at reducing tumor cell viability (Fig. 1*B* and Supplementary Table S1). These effects of risedronate and NE-10790 on tumor cell viability were not restricted to B02-GFP cells because similar results were obtained with MDA-MB-231, MDA-MB-435s, MCF-7, Hs578T, T-47D, and ZR-75-1 breast cancer cell lines (Supplementary Table S1). Risedronate is known for its ability to inhibit protein prenylation by acting as a potent inhibitor of FPP synthase (3). NE10790 does not inhibit FPP synthase but, instead, inhibits Rab geranylgeranyl transferase, an enzyme downstream of FPP synthase in the mevalonate pathway required

for protein prenylation (11). Cell viability experiments were therefore conducted in the presence of exogenous geranylgeraniol (GGOH), an intermediate of the mevalonate pathway downstream of FPP synthase but upstream of Rab geranylgeranyl transferase. As shown in Fig. 1*C*, the inhibitory effect of risedronate on B02-GFP cell viability was overcome by replenishing tumor cells with 10 μmol/L GGOH (Fig. 1*C*). As expected, GGOH did not prevent the inhibitory effect of NE-10790 (Fig. 1*C*).

Effects of risedronate and NE-10790 on the formation of breast cancer bone metastases. We used a mouse model of bone metastasis in which we have previously shown that the bisphosphonate zoledronate, given s.c. at a daily dose of 150 μg/kg, markedly inhibits osteolysis and skeletal tumor burden in animals bearing B02-GFP breast cancer cells (15). The same dosing regimen was therefore chosen to compare the effects of risedronate and NE-10790 on the formation of B02-GFP breast cancer bone metastases.

Radiographical analysis on day 35 after tumor cell injection revealed that metastatic animals treated with risedronate had
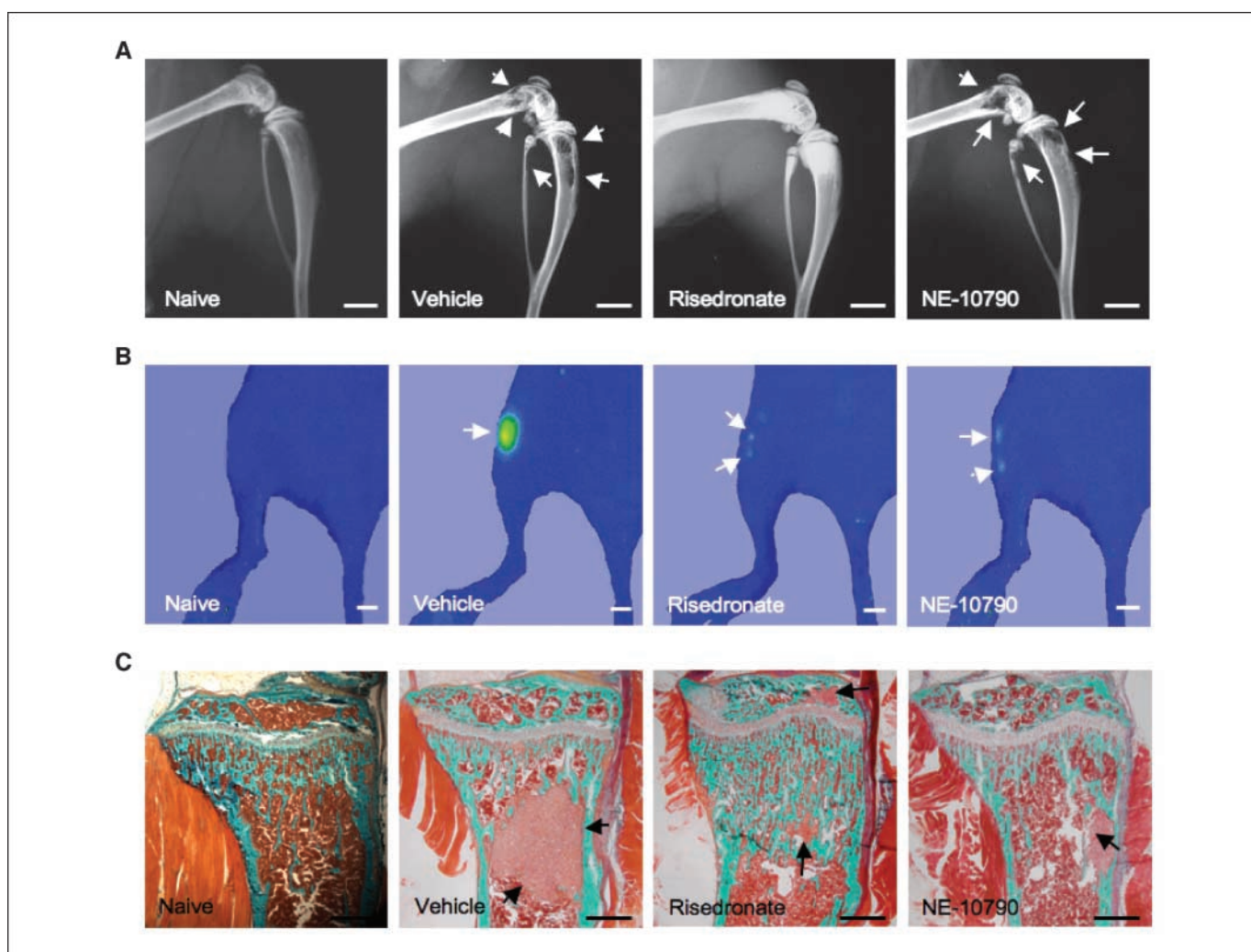
Figure 2. Radiography, fluorescence imaging, and histology of hind limbs from nude mice treated with risedronate or NE-10790. Mice inoculated with B02-GFP breast cancer cells were treated daily with 150 μg/kg risedronate or NE-10790, beginning on the day of tumor cell inoculation (day 0) and continuing until the end of the protocol (day 35). Control mice received a daily treatment with the vehicle only. Naive mice were animals that had not been inoculated with tumor cells. *A*, radiographs of hind limbs. *B*, scanned fluorescent images of hind limbs. *C*, micrographs of Goldner's trichrome-stained tibial metaphysis. All images were obtained from metastatic mice on day 35 after tumor cell inoculation or from aged-matched naive animals. The images shown are examples that best illustrate the effects of the treatments. Osteolytic lesions and tumor burden on representative radiographs and fluorescent images, respectively, are indicated by white arrows. *Scale bar,* 1 cm. For histologic tissue sections, bone is stained green whereas bone marrow and tumor cells (*black arrows*) are stained red. *Scale bar,* 0.5 mm.

Table 1. Effects of risedronate and NE-10790 on the extent of osteolytic lesions and skeletal tumor burden in animals bearing B02-GFP breast cancer cells

Treatment*	No. mice	Radiography (mm^2/mouse)	Fluorescence (mm^2/mouse)	Histomorphometry[†]		
				No. legs	BV/TV (%)	TB/STV (%)
Naive	5	0	0	4	28.4 ± 2[‡]	0
Vehicle	28	5.6 ± 0.9	13.7 ± 2.2	9	20.8 ± 1.8	22.6 ± 6.5
Risedronate	16	0.3 ± 0.1[‡]	8.3 ± 2.3[‡]	7	48.1 ± 2[‡]	5.6 ± 3.5[§]
NE-10790	20	4.3 ± 0.8	4.1 ± 1.3[‡]	7	24.4 ± 1.1	4.6 ± 2.1[§]

Abbreviations: BV/TV, bone volume–tissue volume ratio; TB/STV, tumor burden–soft tissue volume ratio.
*Drug administration was initiated from the time of tumor cell inoculation (day 0) to the end of the protocol (day 35). All measurements were made 35 d after tumor cell injection. Results are the mean ± SE of three separate experiments. Risedronate and NE-10790 were given at a daily dose of 150 μg/kg s.c. from days 0 to 35. PBS was used as vehicle. Naive are age-matched animals that had not been injected with tumor cells.
[†] Histomorphometry was performed on legs with bone metastasis.
[‡] $P < 0.05$, compared with the vehicle-treated group. Statistical pairwise comparisons were made using Mann-Whitney U test.
[§] $P < 0.005$, compared with the vehicle-treated group. Statistical pairwise comparisons were made using Mann-Whitney U test.

osteolytic lesions that were 95% smaller than those of tumor-bearing mice treated with the vehicle (Fig. 2A; Table 1). By contrast, NE-10790 did not inhibit bone destruction (Fig. 2A; Table 1). Noninvasive fluorescence imaging on day 35 after tumor cell injection showed that these metastatic animals treated with risedronate or NE-10790 also had a statistically significantly lower tumor burden than animals treated with the vehicle (Fig. 2B). In this respect, risedronate and NE-10790 decreased tumor burden by 40% and 70%, respectively, compared with vehicle (Table 1).

Histomorphometric analysis of hind limbs with metastases showed that mice treated with risedronate had a bone volume (BV)–tissue volume (TV) ratio that was significantly higher than vehicle-treated mice and mice that had not been injected with tumor cells, indicating a complete prevention of bone loss by the bisphosphonate (Fig. 2C; Table 1). TRAP staining of bone tissue sections of metastatic legs from mice treated with risedronate showed a statistically significant inhibition of the osteoclast number (Oc.N) and active-osteoclast resorption surface (Oc.S) per trabecular bone surface (BS) when compared with vehicle (Fig. 3). By contrast, the BV/TV, Oc.N/BS, and Oc.S/BS ratios for mice treated with NE-10790 did not statistically significantly differ from those observed with vehicle-treated mice (Table 1; Figs. 2C and 3). Yet, mice treated with NE-10790 had a tumor burden (TB)–soft tissue volume (STV) ratio decreased by 75% compared with vehicle (Table 1). Risedronate also reduced the TB/STV ratio by 80%, compared with vehicle (Table 1).

Aside from our observation that these compounds decreased skeletal B02-GFP tumor burden at a dosage of 150 μg/kg/d (Fig. 2B and C; Table 1), we found that the same dosing regimen of NE-10790 or risedronate did not inhibit the growth of s.c. B02-GFP tumor xenografts in animals (Supplementary Fig. S1A). Moreover, risedronate and NE-10790 (used at a dosage of 350 μg/kg/d) did not inhibit the formation of B16-F10 pulmonary metastases in animals (Supplementary Fig. S1B).

A head-to-head comparison of the effects of risedronate and NE-10790 on bone metastasis formation was next conducted using increasing doses of each of these compounds. Radiographical analysis and fluorescence imaging of animals on day 35 after B02-GFP tumor cell injection revealed that risedronate and NE-10790

inhibited both osteolysis and tumor burden in a dose-dependent manner (Fig. 3). The LED of risedronate that inhibited osteolysis (15 μg/kg/d) did not inhibit tumor burden (Fig. 3A and B), indicating that risedronate first inhibited osteoclast-mediated bone resorption and then skeletal tumor growth. Conversely, the LED of NE-10790 that inhibited tumor burden (150 μg/kg/d) did not inhibit osteolysis (Figs. 2 and 3A and B). A higher dose of NE-10790 (37,000 μg/kg/d) did, however, inhibit osteolysis, as judged by radiography and TRAP staining of metastatic bone tissue sections (Fig. 3).

Effects of risedronate and NE-10790 on the production of osteoclast-stimulatory cytokines by breast cancer cells. *In vitro* B02-GFP cells produced several cytokines, chemokines, and growth factors as detected by RayBio human cytokine antibody arrays (Gro, GM-CSF, IL-6, IL-8, MCP-1, IGFBP-1, VEGF, TIMP-1, and TIMP-2; Fig. 4A). The effects of risedronate and NE-10790 on production of these factors were investigated. B02-GFP cells were cultured for 2 days in the presence of risedronate or NE-10790 using a concentration that induced a 50% reduction in cell viability. After washing to remove drugs, tumor cells were further cultured for another 2 days, at which time conditioned media were collected and incubated with a cytokine antibody array membrane. Compared with vehicle, several cytokines were differentially expressed in the conditioned medium from cells treated with risedronate or NE-10790, including osteoclast-stimulatory cytokines IL-6, IL-8, and MCP-1 (Supplementary Fig. S2). These results were confirmed by ELISA. NE-10790 and, to a lower extent, risedronate stimulated the production of IL-8, IL-6, and MCP-1 by B02-GFP cells when compared with that observed with the conditioned medium from vehicle-treated cells (Fig. 4B).

Ex vivo experiments, using human cytokine antibody arrays and ELISA, were next conducted to measure human cytokine levels in the bone marrow of metastatic hind limbs from animals treated with a daily dose of 150 μg/kg risedronate, NE-10790, or the vehicle. Several human cytokines/growth factors were produced in the bone marrow of metastatic legs from vehicle-treated animals (Fig. 4C), among which human IL-8 was the most abundant. No human IL-8 was detected in the bone marrow cell supernatant of bones from age-matched animals that had not been inoculated with B02-GFP

cells (naive animals; Fig. 4*D*), further indicating that the detection of human IL-8 was solely inherent to the presence of human tumor cells in the bone marrow. Furthermore, human IL-8 amounts in bone marrow cell supernatants of metastatic bones from risedronate-treated and NE-10790–treated animals were increased 2-fold to 3-fold compared with vehicle-treated animals (Fig. 4*D*).

After the observation that risedronate and NE-10790 stimulated the production of osteoclast-stimulatory cytokines by tumor cells, conditioned media used to measure human cytokine levels were tested for their ability to stimulate osteoclastogenesis *in vitro*. These conditioned media did not, however, induce the development of mature osteoclasts *in vitro* (Fig. 5). Additional experiments were therefore conducted in the presence of RANKL and M-CSF, which are two hematopoietic factors both necessary and sufficient to induce osteoclastogenesis (18). Compared with the conditioned medium from vehicle-treated tumor cells, the conditioned medium collected from NE-10790–treated B02-GFP cells statistically significantly enhanced the differentiation of osteoclasts induced by RANKL + M-CSF (Fig. 5). By contrast, the conditioned medium from risedronate-treated cells did not promote RANKL + M-CSF-induced osteoclastogenesis *in vitro* (Fig. 5).

Effect of a combined treatment with risedronate and NE-10790 on breast cancer bone metastases. Results obtained with risedronate and NE-10790 on breast cancer bone metastasis

formation brought us to the question of whether risedronate might maximize the antitumor activity of NE-10790 when used in combination. As shown in Supplementary Fig. S3, the combination of risedronate (used at its lowest antiresorptive effective dose) with NE-10790 (used at its lowest antitumor effective dose) statistically significantly decreased both osteolysis and skeletal tumor burden when compared with the vehicle-treated animals, whereas risedronate or NE-10790 alone at these doses only decreased either osteolysis or tumor burden, respectively. The use of NE-10790 in combination with risedronate did not further decrease the extent of osteolytic lesions when compared with risedronate alone (1.4 ± 0.4 versus 1.9 ± 1.3 mm^2, respectively; Supplementary Fig. S3*A*). Similarly, the antitumor efficacy observed in combining NE-10790 with risedronate did not differ statistically significantly from that obtained with NE-10790 alone (3.7 ± 1.4 versus 4.1 ± 1.3 mm^2, respectively; Supplementary Fig. S3*B*).

Discussion

Our results first show that the bisphosphonate risedronate given at a low dosage in an animal model of breast cancer bone metastasis inhibited osteolysis by inhibiting bone resorption, whereas therapy with higher dosages also inhibited skeletal tumor burden. These results are in agreement with previous preclinical findings (19), showing that zoledronate therapy with a long dosing
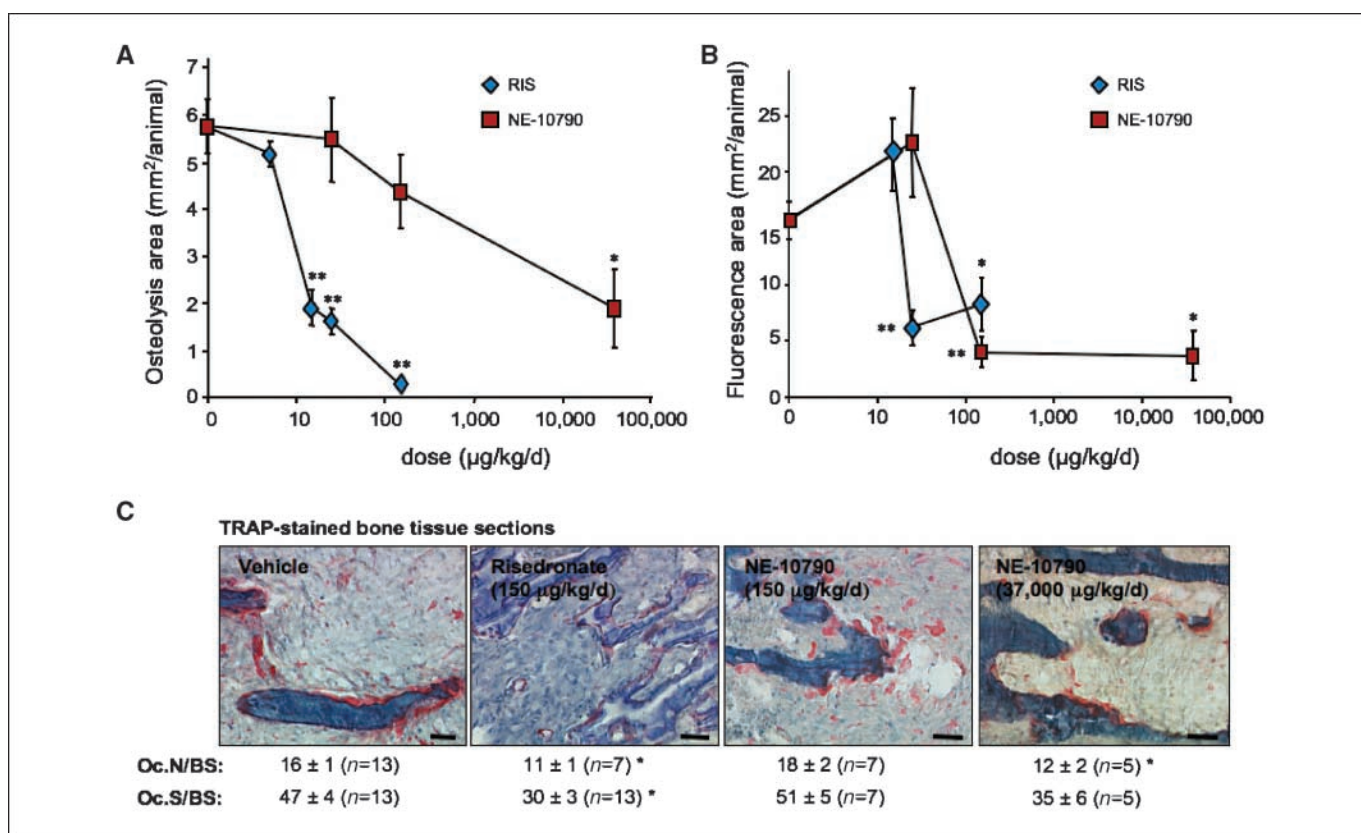

Figure 3. Dose-response effect of risedronate (*RIS*) and NE-10790 on the extent of bone destruction (*A*) and tumor burden (*B*) in animals bearing B02-GFP breast cancer cells, as judged by radiography and fluorescence imaging, respectively. Daily doses of risedronate were 5, 15, 25, or 150 μg/kg. Daily doses of NE-10790 were 25, 150, or 37,000 μg/kg. Radiographical and fluorescent data were obtained on day 35 after tumor cell inoculation. Results are the mean ± SE of 5 to 10 animals per group. * and **, $P < 0.05$ and 0.005, respectively, when compared with animals treated with the vehicle. *C*, effects of different dosing regimens of risedronate and NE-10790 on the recruitment of osteoclasts at the bone metastatic site. All micrographs were obtained from metastatic mice on day 35 after tumor cell inoculation. The images shown are examples that best illustrate the effects of the treatments. The *in situ* detection of osteoclasts on bone tissue sections was performed after TRAP staining. Osteoclasts are stained red. *Oc.N/BS*, osteoclast number per millimeter of bone surface; *Oc.S/BS*, osteoclast surface relative to bone surface ratio (%). *Points*, mean of *n* animals; *bars*, SE. *, $P < 0.05$ compared with vehicle.
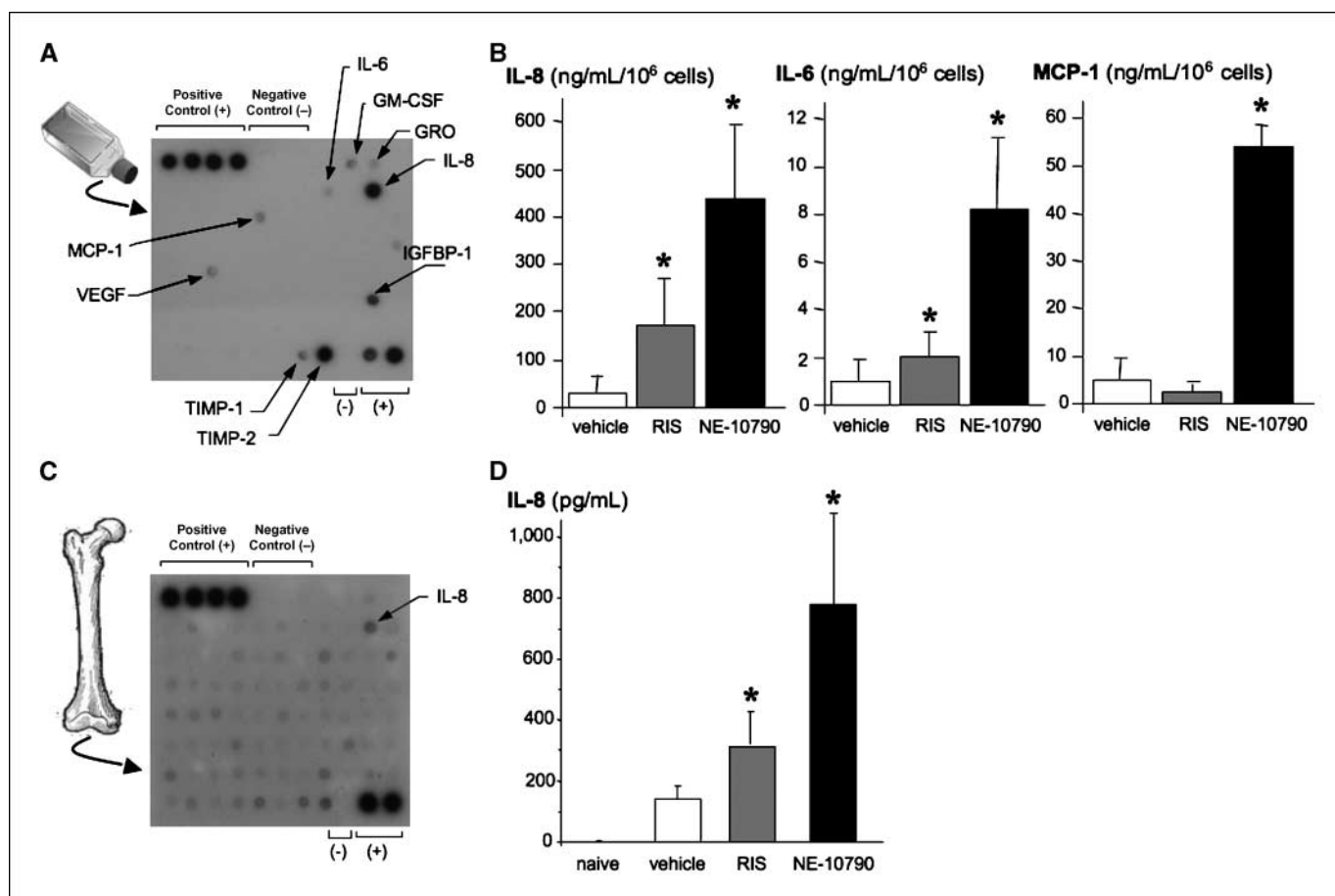
Figure 4. Effects of risedronate and NE-10790 on production of osteoclast-stimulatory cytokines by B02-GFP breast cancer cells *in vitro* and *ex vivo*. *A,* detection of cytokines, chemokines, and growth factors produced by cultured, untreated B02-GFP breast cancer cells using an antibody-based protein microarray. Immunoreactive spots were detected with an enhanced chemiluminescence detection system. *B,* ELISA quantification of the amounts of IL-8, IL-6, and MCP-1 produced in the conditioned media from B02-GFP breast cancer cells treated with the vehicle, risedronate (*RIS*; IC$_{50}$, 0.37 mmol/L), or NE-10790 (IC$_{50}$, 2.7 mmol/L). *Columns,* mean of three separate experiments; *bars,* SD. *, $P < 0.05$ compared with vehicle-treated cells. *C,* detection of human cytokines, chemokines, and growth factors produced in the bone marrow cell supernatant of bones from animals on day 35 after B02-GFP tumor cell inoculation. *D,* ELISA quantification of the amount of human IL-8 produced in bone marrow cell supernatants of bones from animals that were treated with a daily dose of 150 μg/kg risedronate or NE-10790 from days 0 to 35. Control mice received a daily treatment with the vehicle only. Naive mice were animals that had not been inoculated with tumor cells. *Columns,* mean of three animals per group; *bars,* SE. *, $P < 0.05$ compared with vehicle-treated animals.

interval inhibits osteolysis, whereas a therapy with more frequent dosing intervals reduces both osteolysis and skeletal tumor burden. It is possible that the antitumor activity of bisphosphonates (as exemplified here by risedronate) in preclinical models of bone metastasis is explained by the inhibition of osteoclast-mediated bone resorption which, in turn, deprives tumor cells of bone-derived growth factors that are required for tumor growth. However, if a bisphosphonate treatment decreased skeletal tumor burden solely by reducing bone loss, we would have expected the lower dosage of risedronate to have inhibited skeletal tumor growth more than what we observed. Similarly, zoledronate therapy with a long dosing interval would have also inhibited skeletal tumor burden (19). Thus, there must be additional reasons explaining the limited antitumor activity of these drugs *in vivo*. We have previously shown that mineral-bound bisphosphonates are significantly less potent than soluble bisphosphonates at inhibiting breast and prostate cancer cell adhesion to bone *in vitro* (6). We therefore surmised that, irrespective of the antiresorptive properties of bisphosphonates, the rapid uptake of these drugs in bone might limit their ability to act directly on tumor cells that reside in the bone marrow. Conversely, bisphosphonates with a low bone

mineral affinity should be more readily released from the bone surface, enabling a more prolonged exposure of the bone marrow to these drugs and a direct effect on tumor cells. To address this important question, we examined the effects of NE-10790 on osteolysis and skeletal tumor growth.

Our results show that, compared with risedronate, NE-10790 poorly inhibited osteoclast-mediated bone resorption in animal models of bone loss caused by ovariectomy or cancer. These results were in complete agreement with a previous report showing that NE-10790 is 8,000-fold less potent than risedronate at inhibiting bone resorption in the Schenk rat growing model (8). Conversely, NE-10790 is only 100-fold less potent than risedronate at inhibiting osteoclastic resorption *in vitro* (9, 12). The difference in antiresorptive potency between *in vitro* and *in vivo* studies is likely explained by the low bone mineral affinity of NE-10790 which, in turn, limits the skeletal uptake of the drug *in vivo*. Our results also show that a continuous treatment with NE-10790, at a dosage that did not inhibit osteolysis, produced meaningful antitumor effects in a mouse model of breast cancer bone metastasis. Moreover, the *in vivo* antitumor activity of NE-10790 was restricted to bone because the dosing regimen of NE-10790 that reduced
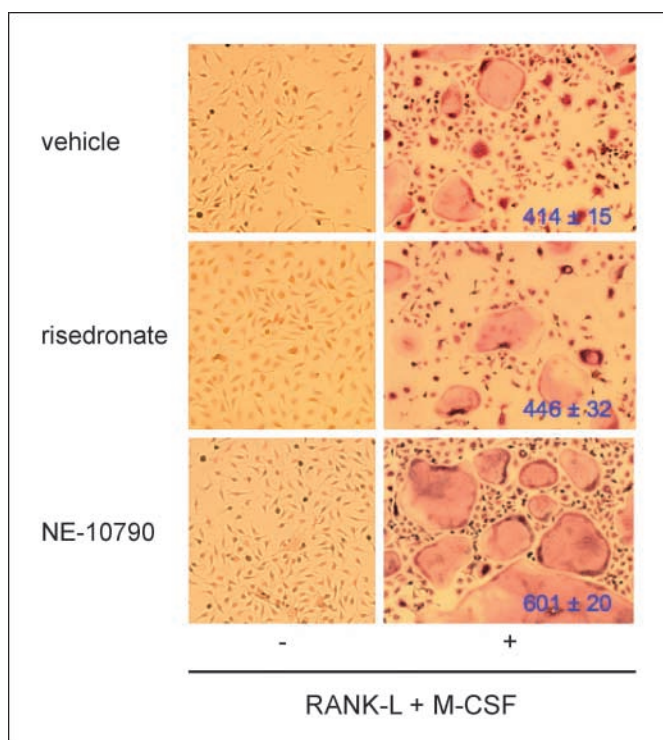
Figure 5. Effect of the conditioned medium from B02 breast cancer cells treated with a drug (risedronate or NE-10790) or the vehicle on osteoclast differentiation. Mononuclear cells were isolated from the bone marrow, and then incubated with or without RANKL + M-CSF and the conditioned medium (diluted 1:5 in complete medium) from B02-GFP cells trated with the vehicle, risedronate (IC_{50}, 0.37 mmol/L), or NE-10790 (IC_{50}, 2.7 mmol/L). Osteoclasts were observed in the presence of RANK-L and M-CSF only. Differentiated osteoclasts were enumerated under a light microscope as a function of multinucleation (more than three nuclei) and TRAP staining. Representative TRAP-stained osteoclasts are shown for each treatment, and the osteoclast number (cell/cm^2) is indicated in blue. Results are the mean ± SD of three separate experiments. The number of osteoclasts in the NE-10790–treated group is statistically significantly higher than the vehicle-treated or risedronate-treated group ($P < 0.01$, Mann-Whitney U test).

skeletal B02-GFP tumor burden did not inhibit the s.c. growth of B02-GFP tumor xenografts nor the formation of B16-F10 melanoma lung metastases. Thus, our results strongly suggest that, after a transient accumulation in bone, NE-10790 was released from bone mineral, enabling a direct effect of the drug on breast cancer cells that reside in the bone marrow.

How did NE-10790 inhibit skeletal tumor burden in our mouse model of bone metastasis? NE-10790 specifically inhibits Rab geranylgeranyl transferase (Rab GGTase or GGTase-2) in several cell types, including osteoclasts, macrophages, and myeloma cells (11, 12). In addition, NE-10790 induces apoptosis of myeloma cells (11) and inhibits breast cancer cell invasion *in vitro* (10). We found that NE-10790 also inhibited the viability of breast cancer cell lines and that GGOH (an intermediate of the mevalonate pathway upstream of Rab GGTase) did not prevent the inhibitory effect of NE-10790 on viability of breast cancer cells. Moreover, NE-10790 inhibited the prenylation of Rab6 (geranylgeranylated by Rab GGTase) but not that of Rap1a (geranylgeranylated by GGTase-1) in B02-GFP breast cancer cells.[5] These results are in line with the

observation that NE-10790 disrupts the prenylation and membrane localization of several Rab proteins (Rab5, Rab6, and Rab27a) in J774 macrophages (20). Evidence is emerging that Rab GGTase plays an important role in cancer cell proliferation and aggressiveness *in vivo* (21, 22). Our results provide some support for a role of prenylated Rab GGTase in breast cancer bone metastasis. They also suggest that NE-10790 (and potentially to some extent, risedronate and other bisphosphonates, depending on their bone mineral affinity), by preventing Rab prenylation in breast cancer cells, reduced both the invasion and viability of tumor cells, leading to inhibition of skeletal tumor burden.

Whereas NE-10790 was decreasing skeletal tumor growth, it concomitantly stimulated the production of osteoclast-stimulatory cytokine IL-8 by tumor cells resident in the bone marrow. Tumor-derived IL-8 mediates osteolysis in experimental breast cancer bone metastasis (23). These findings (23) may explain why tumor-bearing animals treated with NE-10790 had osteolytic lesions despite a substantial reduction of skeletal tumor burden. Molecular mechanisms through which NE-10790 stimulates IL-8 production by breast cancer cells are unknown. Cyclooxygenase-2 (COX-2) overexpression in MDA-MB-231 breast cancer cells causes an increase production of IL-8 (24). GGTI-286, a selective inhibitor of geranylgeranyltransferases, increases COX-2 expression in smooth muscle cells (25). It is therefore possible that NE-10790 stimulates COX-2 expression in breast cancer cells. Whatever the molecular mechanisms are, a higher dosage of NE-10790 inhibited osteoclast-mediated bone resorption, thereby counteracting the osteoclast-stimulatory effect of tumor-derived IL-8. The risk associated with IL-8 production by NE-10790–treated tumor cells was also minimized when using NE-10790 in combination with risedronate. Moreover, the combination of NE-10790 with risedronate inhibited both osteolysis and skeletal tumor burden, whereas NE-10790 or risedronate used as a single-agent therapy only decreased either tumor burden or osteolysis, respectively. Our results are reminiscent of those obtained in combining bisphosphonates with chemotherapeutic agents for the treatment of animals with bone metastases, in which drug combinations were shown to provide a greater benefit compared with either drug alone (4, 26). These experimental findings (refs. 4, 26 and this study) are therefore in line with current clinical studies investigating the utility of bisphosphonates as adjuvant therapy for the prevention of bone metastases in several large-scale clinical trials in multiple cancer types (27). For example, it was recently reported that the addition of zoledronate to adjuvant endocrine therapy for premenopausal women with endocrine-responsive breast cancer significantly prolonged the disease-free and relapse-free survival by 35% over a 5-year period (28). Our results suggest that the use of risedronate and NE-10790 in combination with standard cytotoxic and/or endocrine treatments may represent another promising approach to obtain clinically meaningful antitumor effects.

In conclusion, our study shows for the first time that decreasing the bone mineral affinity of bisphosphonates is an effective therapeutic strategy to inhibit skeletal tumor growth in a mouse model of breast cancer bone metastasis. We believe that such compounds with a low bone mineral affinity will open new exciting ways for optimizing antitumor activity of bisphosphonates in oncology.

Disclosure of Potential Conflicts of Interest

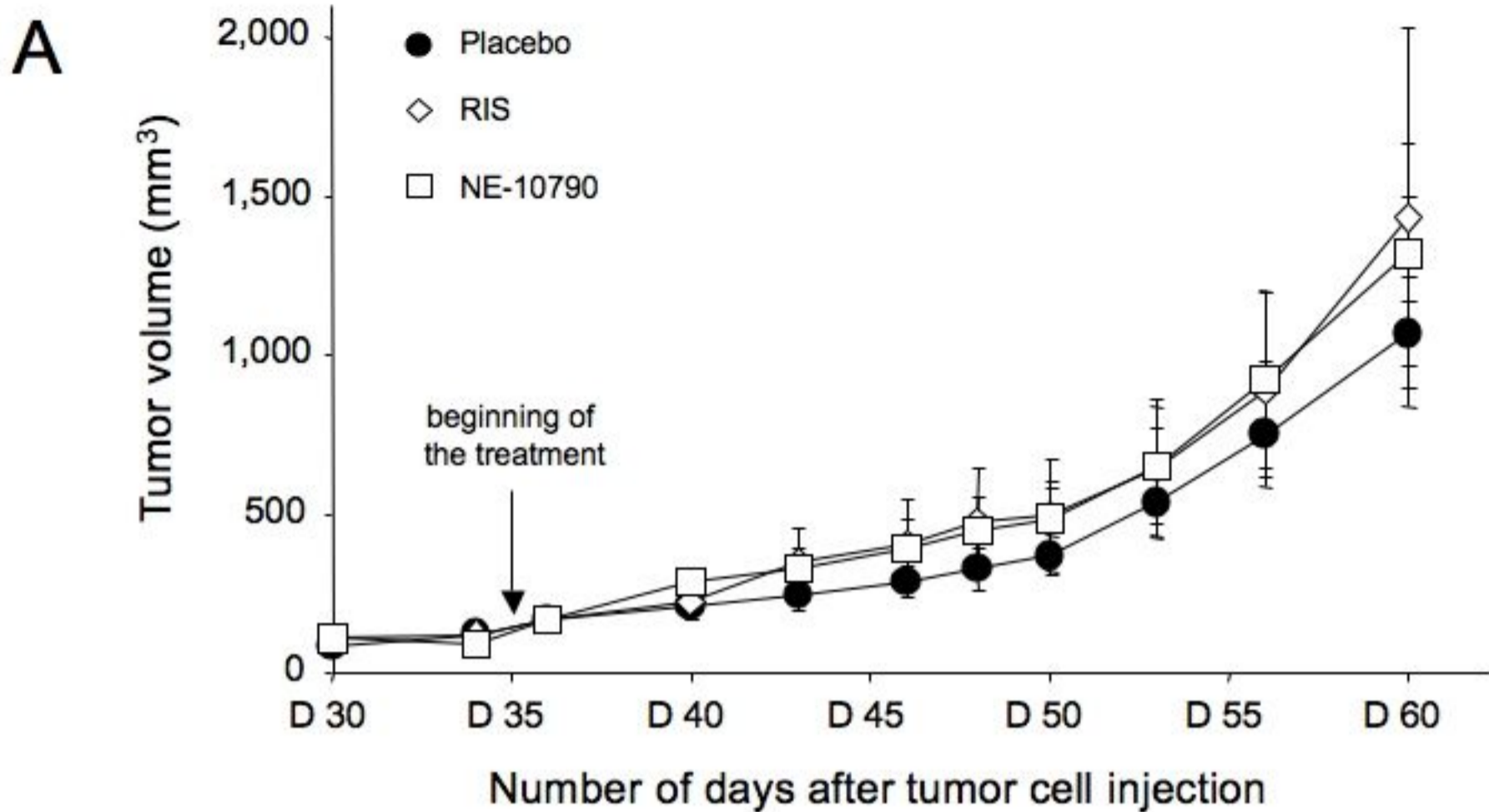[5] S. Gordon and M. Rogers, unpublished results.
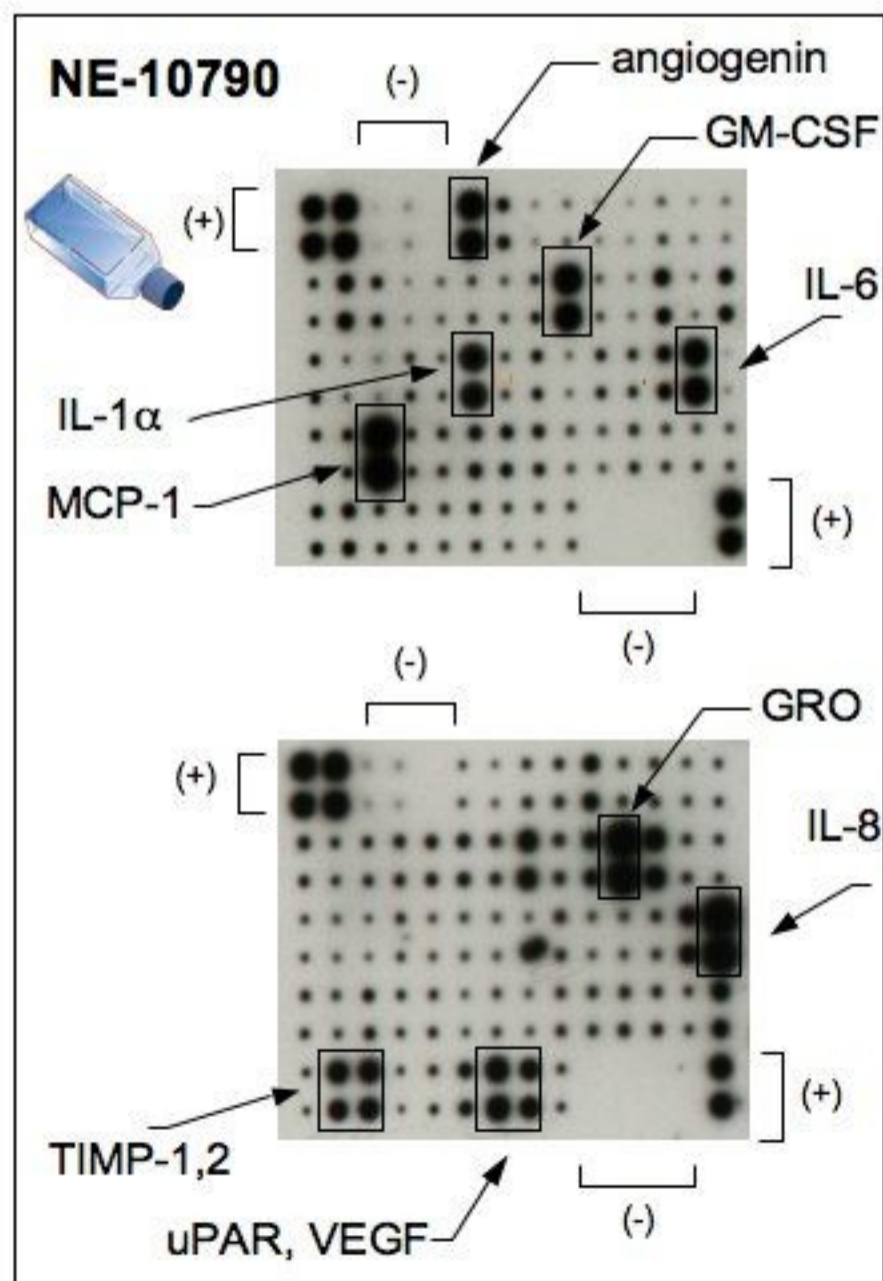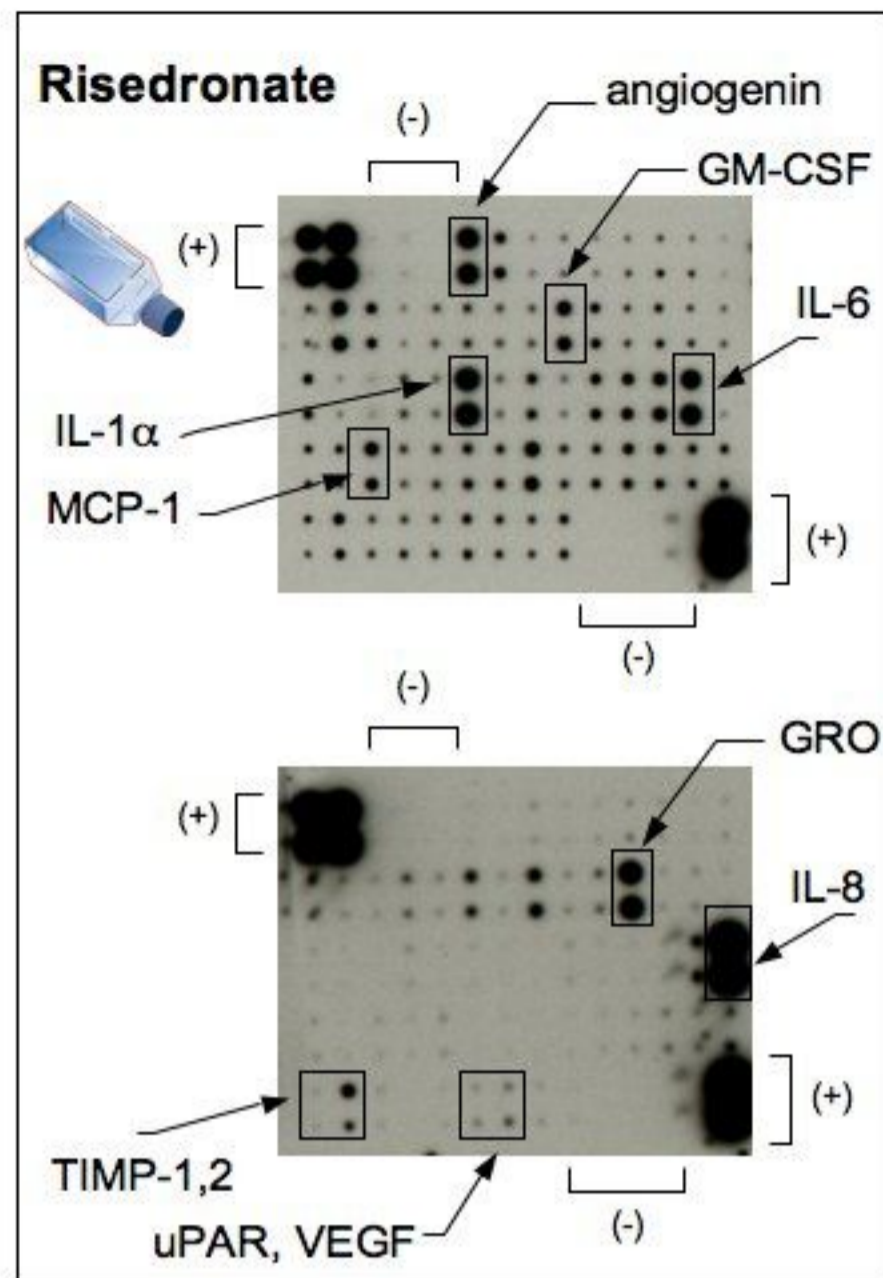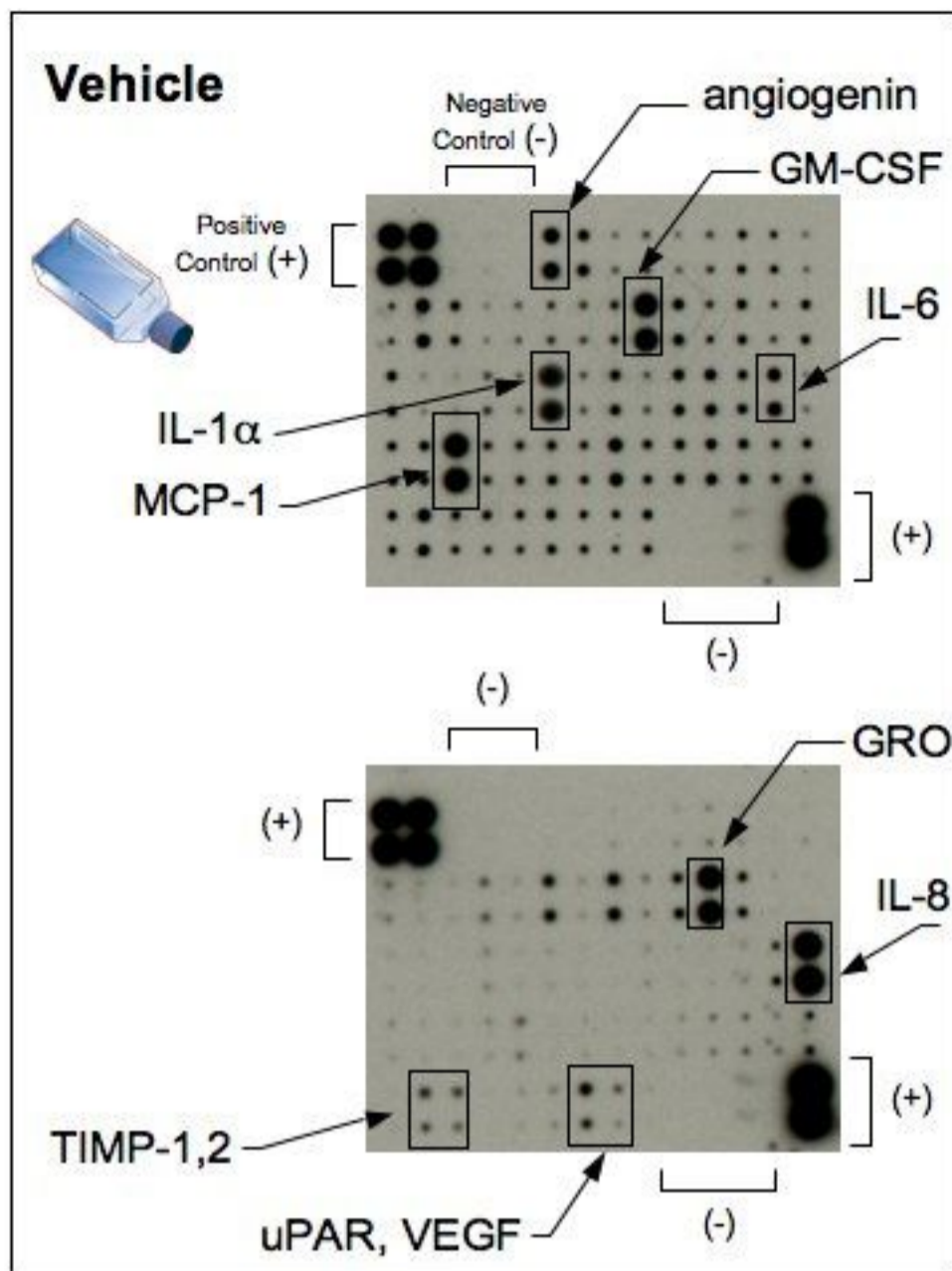
Acknowledgments

References

1. Clezardin P, Teti A. Bone metastasis: pathogenesis and therapeutic implications. Clin Exp Metastasis 2007;24:599–608.

2. Coleman RE. Risks and benefits of bisphosphonates. Br J Cancer 2008;98:1736–40.

3. Coxon FP, Thompson K, Rogers MJ. Recent advances in understanding the mechanism of action of bisphosphonates. Curr Opin Pharmacol 2006;6:307–12.

4. Dunford JE, Kwaasi AA, Rogers MJ, et al. Structure-activity relationsgips among the nitrogen containing bisphosphonates in clinical use and other analogues: time-dependent inhibition of human farnesyl pyrophosphate synthase. J Med Chem 2008;51:2187–95.

5. Stresing V, Daubine F, Benzaid I, Mönkkönen H, Clezardin P. Bisphosphonates in cancer therapy. Cancer Lett 2007;257:16–35.

6. Boissier S, Magnetto S, Frappart L, et al. Bisphosphonates inhibit prostate and breast carcinoma cell adhesion to unmineralized and mineralized bone extracellular matrices. Cancer Res 1997;57:3890–94.

7. Coxon FP, Thompson K, Roelofs AJ, Ebetino FH, Rogers MJ. Visualizing mineral binding and uptake of bisphosphonate by osteoclasts and non-resorbing cells. Bone 2008;42:848–60.

8. Ebetino FH, Bayless AV, Amburgey J, Ibbotson KJ, Dansereau S, Ebrahimpour A. Elucidation of a pharmacophore for the bisphosphonate mechanism of bone antiresorptive activity. Phosphorus, Sulfur, Silicon 1996;109:217–20.

9. van Beek ER, Löwik CWGM, Ebetino FH, Papapoulos SE. Binding and antiresorptive properties of heterocycle-containing bisphosphonate analogs: structure-activity relationship. Bone 1998;23:437–42.

10. Boissier S, Ferreras M, Peyruchaud O, et al. Bisphosphonates inhibit breast and prostate carcinoma cell invasion, an early event in the formation of bone metastases. Cancer Res 2000;60:2949–54.

11. Roelofs AJ, Hulley PA, Meijer A, Ebetino FH, Russell RGG, Shipman CM. Selective inhibition of Rab prenylation by a phosphonocarboxylate analogue of risedronate induces apoptosis, but not S-phase arrest, in human myeloma cells. Int J Cancer 2006;119:1254–61.

12. Coxon FP, Helfrich MH, Larijani B, et al. Identification of a novel phosphonocarboxylate inhibitor of Rab geranylgeranyl transferase that specifically prevents Rab prenylation in osteoclasts and macrophages. J Biol Chem 2001;276:48213–22.

13. Pécheur I, Peyruchaud O, Serre CM, et al. Integrin $\alpha(v)\beta3$ expression confers on tumor cells a greater propensity to metastasize to bone. FASEB J 2002;16:1266–8 (10.1096/fj.01–0911fje).

14. Nancollas GH, Tang R, Phipps RJ, et al. Novel insights into actions of bisphosphonates on bone: differences in interactions with hydroxyapatite. Bone 2006;38:617–27.

15. Ebetino FH, Emmerling P, Barnett B, Nancollas GH. Differentiation of hydroxyapatite affinity of bisphosphonate analogs for mechanism of action studies [abstract SA305]. J Bone Miner Res 2004;19:s157.

16. Boucharaba A, Serre CM, Guglielmi J, Bordet JC, Clezardin P, Peyruchaud O. The type 1 lysophosphatidic acid receptor is a target for therapy in bone metastases. Proc Natl Acad Sci U S A 2006;103:9643–8.

17. Peyruchaud O, Winding B, Pecheur I, Serre CM, Delmas P, Clezardin P. Early detection of bone metastases in a murine model using fluorescent human breast cancer cells: application to the use of the bisphosphonate zoledronic acid in the treatment of osteolytic lesions. J Bone Miner Res 2001;16:2027–34.

18. Teitelbaum SL. Bone resorption by osteoclasts. Science 2000;289:1504–8.

19. Daubine F, Le Gall C, Gasser J, Green J, Clezardin P. Antitumor effects of clinical dosing regimens of bisphosphonates in experimental breast cancer bone metastasis. J Natl Cancer Inst 2007;99:322–30.

20. Coxon FP, Ebetino FH, Mules EH, Seabra MC, McKenna CE, Rogers MJ. Phosphonocarboxylate inhibitors of Rab geranylgeranyl transferase disrupt the prenylation and membrane localization of Rab proteins in osteoclasts *in vitro* and *in vivo*. Bone 2005;37:349–58.

21. Lackner MR, Kindt RM, Carroll PM, et al. Chemical genetics identifies Rab geranylgeranyl transferase as an apoptotic target for farnesyl transferase inhibitors. Cancer Cell 2005;7:325–36.

22. Cheng KW, Lahad JP, Gray JW, Mills GB. Emerging role of Rab GTPases in cancer and human disease. Cancer Res 2005;65:2516–9.

23. Bendre MS, Margulies AG, Walser B, et al. Tumor-derived interleukin-8 stimulates osteolysis independent of the receptor activator of nuclear factor-κB ligand pathway. Cancer Res 2005;65:11001–9.

24. Singh B, Berry JA, Vincent LE, Lucci A. Involvement of IL-8 in COX-2-mediated bone metastases from breast cancer. J Surg Res 2006;134:44–51.

25. Degraeve F, Bolla M, Blaie S, et al. Modulation of COX-2 expression by statins in human aortic smooth muscle cells. J Biol Chem 2001;276:46849–55.

26. Ottewell PD, Deux B, Monkkonen H, et al. Differential effect of doxorubicin and zoledronic acid on intraosseous versus extraosseous breast tumor growth *in vivo*. Clin Cancer Res 2008;14:4658–66.

27. Lipton A. Emerging role of bisphosphonates in the clinic. Antitumor activity and prevention of metastasis to bone. Cancer Treat Rev 2008;34:S25–30.

28. Gnant M, Mlineritsch B, Schippinger W, et al. Adjuvant ovarian suppression combined with tamoxifen or anastrozole, alone or in combination with zoledronic acid, in premenopausal women with hormone-responsive, stage I and II breast cancer: first efficacy results from ABCSG-12 [abstract LBA4]. J Clin Oncol 2008;26.

Figure S1: (*A*) Effect of risedronate (RIS) and NE-10790 on growth of subcutaneous breast cancer xenografts in nude mice. B02 cells were inoculated subcutaneously into the right flank of animals. On day 35, at the time tumor xenografts became palpable, animals were treated subcutaneously with a daily dose of 150 μg/kg RIS or NE-10790 until the end of the protocol (day 60). Control animals (placebo) were treated with the vehicle only. None of the drugs inhibited the growth of B02 breast cancer cells *in vivo*. Results are the mean ± SD of 5 animals per group. (*B*) Effect of risedronate (RIS) and NE-10790 on lung metastasis formation. B16-F10 melanoma cells were injected intravenously to C57BL/6 mice. RIS or NE-10790 (at a dosage of 350 μg/kg/day) was administered to animals by subcutaneous injection beginning on the day of tumor cell inoculation (day 0), and continuing until the end of the protocol (day 14). Control animals (placebo) were treated with the vehicle only. Visible pigmented melanoma lung metastases were enumerated, and results presented as dot plots (bars indicate the mean values). *Inset:* images shown are examples that best illustrate metastatic lungs in each group. None of the drugs inhibited B16 F10 lung metastasis. Results are the mean ± SD of 6 animals per group.

Figure S2: Effects of risedronate and NE-10790 on production of osteoclast-stimulatory cytokines by B02-GFP breast cancer cells *in vitro*. B02-GFP cells were cultured for 2 days in the presence of risedronate or NE-10790, using a concentration that induced a 50% reduction in cell viability. After washing to remove drugs, tumor cells were further cultured for another 2 days, at which time conditioned media were collected and incubated with a set of two antibody-based protein microarray membranes (RayBio Human Cytokine Array VI and VII, RayBiotech) designed to detect 120 growth factors, cytokines and chemokines. Detection of immunoreactive spots was carried out using an enhanced chemiluminescence detection system (ECL, GE Healthcare, Orsay, France).
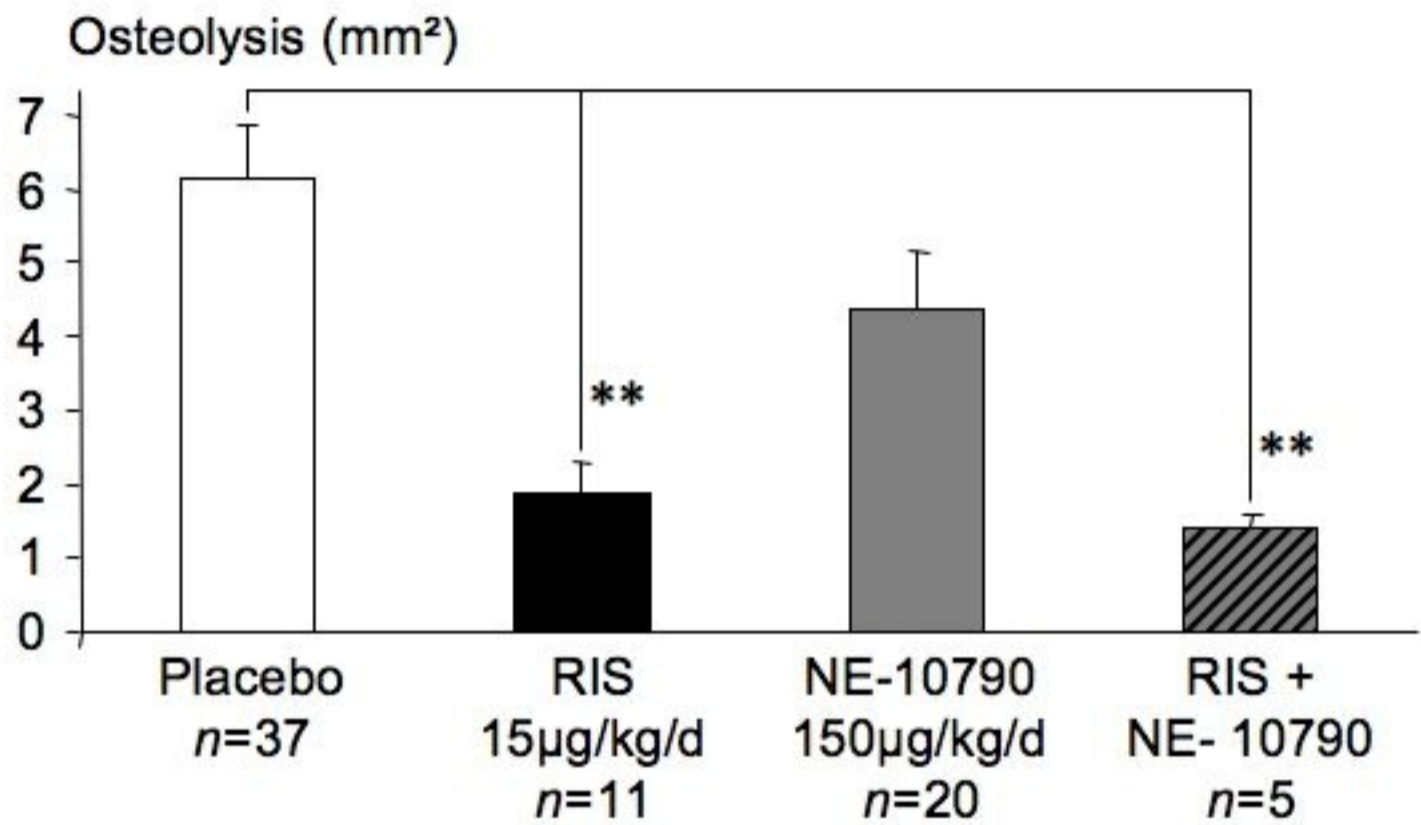
Figure S3: Effect of a combined treatment of RIS with NE-10790 on the extent of (**A**) bone destruction and (**B**) tumor burden in nude mice bearing B02-GFP breast cancer cells. B02-GFP cells were inoculated i.v. into animals. At the day of tumor cell inoculation, animals received a daily s.c. treatment for 35 days with a saline solution (placebo group) or with RIS (15µg/kg) or NE-10790 (150µg/kg), used as a single agent or in combination. Radiographic and fluorescent data were obtained on day 35 after tumor cell inoculation. Data are the mean ± SE of n animals. *, ** $P<0.05$ and $P<0.005$, respectively, using Mann-Whitney's U test.

A

B

Supplementary data; Figure *S1*: Fournier *et al*.
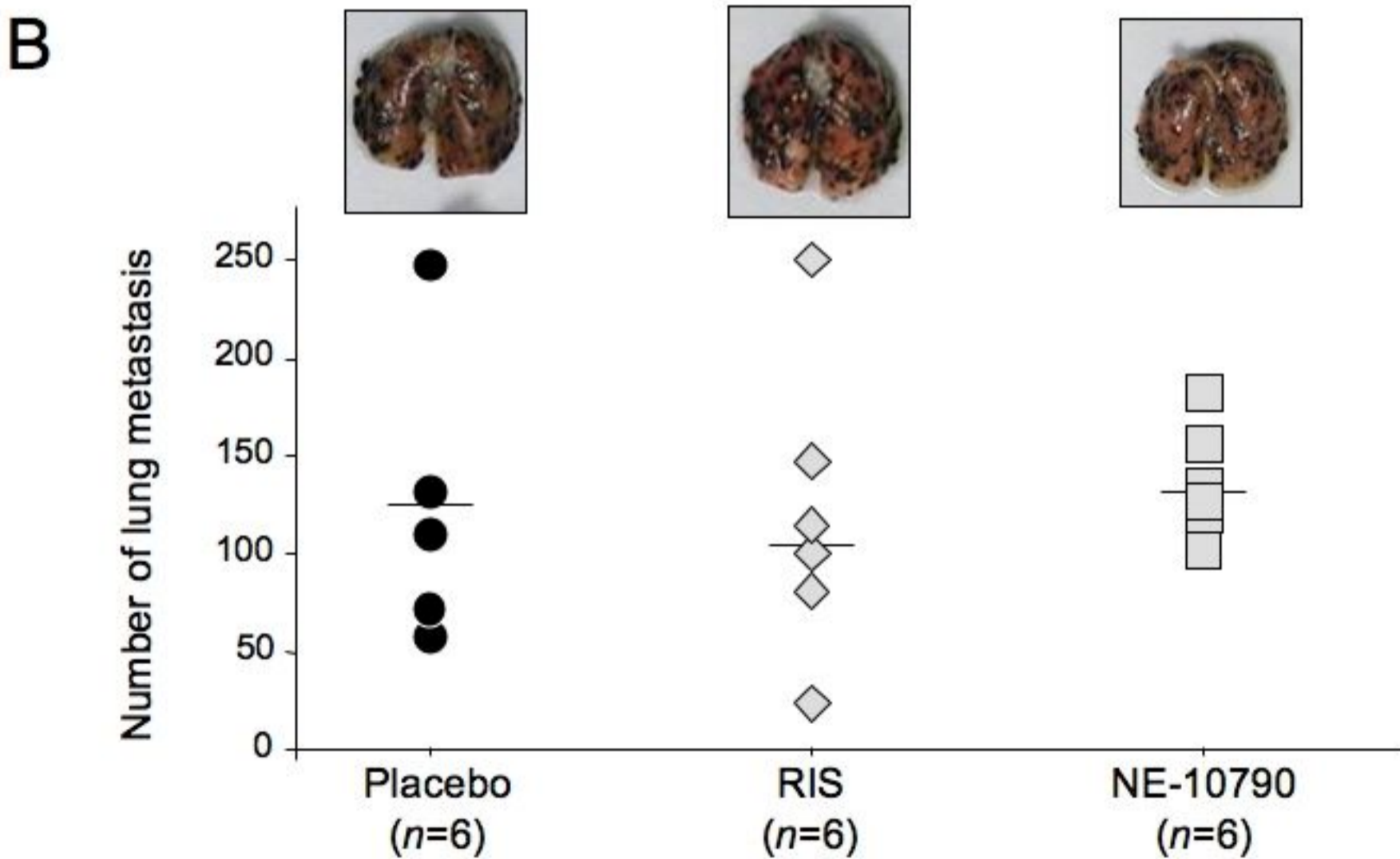
Supplementary data;
Figure S2: Fournier et al.

A

Osteolysis (mm²)

Placebo
n=37

RIS
15µg/kg/d
n=11

NE-10790
150µg/kg/d
n=20

RIS +
NE- 10790
n=5

B

Fluorescence (mm²)

Placebo
n=37

RIS
15µg/kg/d
n=11

NE-10790
150µg/kg/d
n=20

RIS +
NE- 10790
n=5

Supplementary data;
<u>Figure *S3*</u>: Fournier *et al*.
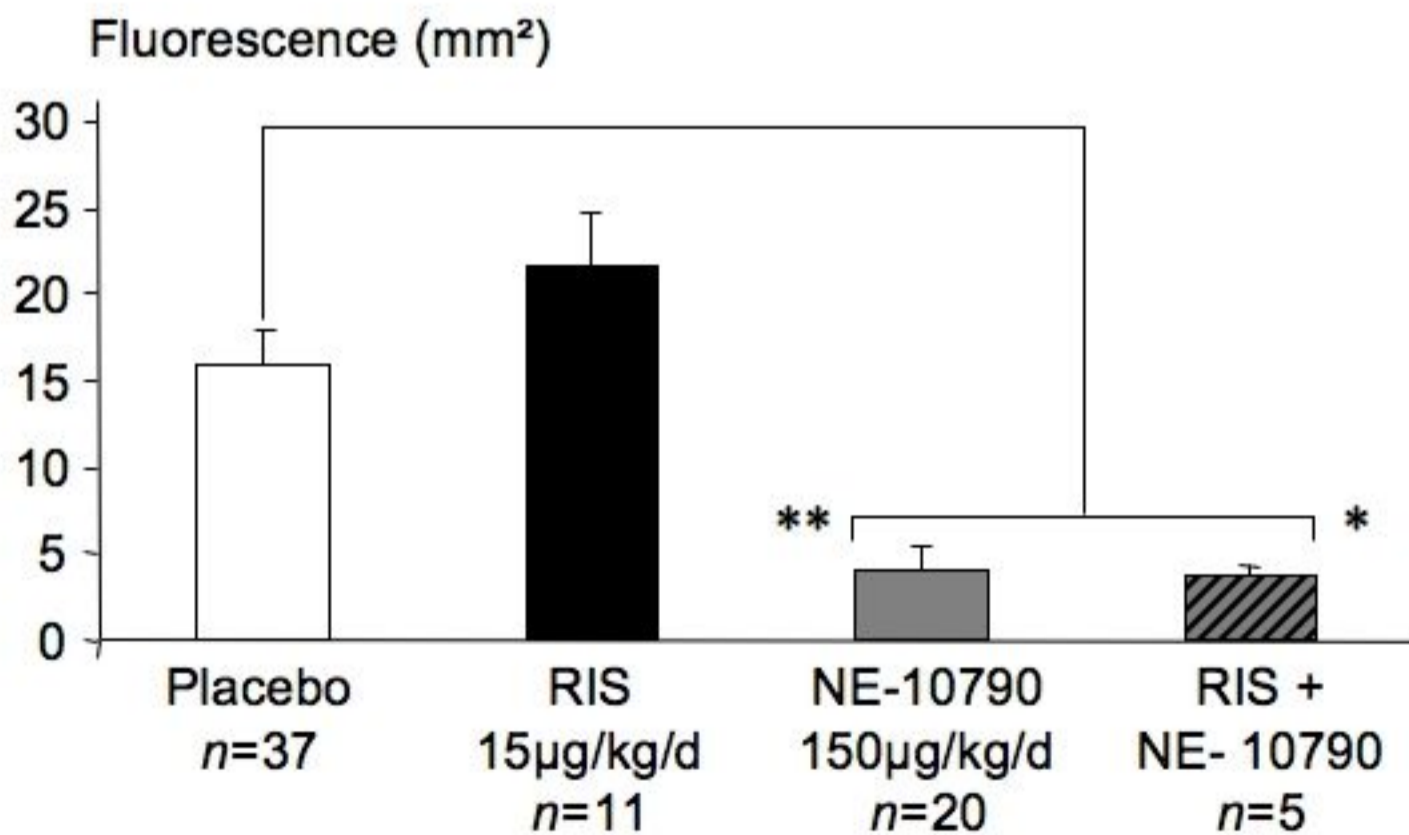
Table S1. Relative half-maximal inhibitory concentrations (IC_{50}) of risedronate and NE-10790 for growth inhibition of human breast cancer cell lines.

Cell line	IC_{50} (mM)*	
	Risedronate	NE-10790
B02-GFP	0.37 ± 0.04	2.74 ± 0.28
MDA-MB-231	0.24 ± 0.09	1.48 ± 0.28
MDA-MB-435s	0.01 ± 0.01	3.53 ± 0.47
MCF-7	0.07 ± 0.01	1.62 ± 0.10
Hs 578T	0.17 ± 0.04	3.21 ± 0.21
T-47D	0.25 ± 0.08	3.85 ± 0.10
ZR-75-1	0.25 ± 0.06	1.71 ± 0.34

* Results are expressed as the mean $\pm$ SD of 3 independent experiments

Hypoxia and TGF-β Drive Breast Cancer Bone Metastases through Parallel Signaling Pathways in Tumor Cells and the Bone Microenvironment

Lauren K. Dunn[1,2], Khalid S. Mohammad[1], Pierrick G.J. Fournier[1], C. Ryan McKenna[1], Holly W. Davis[1], Maria Niewolna[1], Xiang Hong Peng[1], John M. Chirgwin[1,2], Theresa A. Guise[1,*]

[1]Department of Medicine, Division of Endocrinology and

[2]Department of Biochemistry and Molecular Genetics, University of Virginia, Charlottesville, VA, 22903, USA

*Corresponding Author:

Theresa A. Guise

Department of Medicine, Division of Endocrinology,

University of Virginia, PO Box 801420

Charlottesville, VA 22908-1401

 434-243-0305

Fax: 434-982-3314

tguise@mac.com

Running title: Hypoxia and TGF-β in Bone Metastasis

Abstract

Background: Seventy percent of patients with advanced breast cancer develop bone metastases, which cause severe pain, hypercalcemia, pathologic fractures, nerve compression syndromes, and paralysis. Standard chemotherapy causes bone loss, and bone-specific treatments are only palliative. Breast cancers secrete numerous factors that act on the bone microenvironment to drive a feed-forward cycle of tumor growth in bone. Single agent therapy against many distinct targets is not a practical treatment option. Effective treatment of bone metastases thus requires inhibiting central regulators of groups of prometastatic factors. Two such regulators are hypoxia and transforming growth factor (TGF)-β. We asked whether the hypoxia (via HIF-1α) and TGF-β signaling pathways promote bone metastases independently or synergistically, and we tested molecular versus pharmacological combined inhibition strategies in an animal model.

Methods and Findings: We analyzed interactions between the HIF-1α and TGF-β signaling pathways in MDA-MB-231 breast cancer cells. Only vascular endothelial growth factor (VEGF) and the CXC chemokine receptor 4 (CXCR4), out of 16 candidate genes tested, were additively increased by both TGF-β and hypoxia through effects on the proximal promoters. We inhibited HIF-1α and TGF-β pathways alone or together in a mouse model of bone metastasis by tumor cell-autonomous molecular blockade. Inhibition of either pathway alone decreased bone metastasis, with no further effect of double blockade. We then compared single and combined treatment with pharmacologic inhibitors of the two pathways which targets both the tumor and the bone microenvironment. Unlike the molecular blockade experiment, combined treatment with

small molecule inhibitors decreased bone metastases more than either alone via effects of the drugs on bone in addition to actions on tumor cells. Specifically, small molecule inhibitors of HIF-1α and TGF-β significantly reduced osteoclastic bone resorption and increased osteoblast activity.

Conclusions: Hypoxia and TGF-β signaling independently drive tumor bone metastases and regulate a common set of tumor genes. In contrast, combined treatment with small molecule inhibitors to target HIF-1α and TGF-β signaling in both tumor cells and the bone microenvironment provides additive benefits to decrease tumor burden, while increasing skeletal health. Our studies suggest that therapeutic strategies to inhibit HIF-1α and TGF-β signaling may improve bone metastases treatment and patient survival by actions on both tumor and host.

Introduction

Breast cancers frequently metastasize to bone, where they disrupt normal bone remodeling to cause bone destruction, pain, pathologic fracture, hypercalcemia, and nerve compression [1]. Besides conventional radiation and chemotherapy, bisphosphonates are the only treatment available for patients with bone metastases. These drugs decrease skeletal morbidity and provide palliative relief but no cure [1]. Bone is a unique microenvironment in which breast cancer thrives. Growth factors, such as transforming growth factor-β (TGF- β) are stored in the mineralized bone matrix. Breast cancers that metastasize to bone secrete factors, such as parathyroid hormone-related protein (PTHrP) and interleukin-11 (IL-11), that stimulate osteoclastic bone destruction and the release

and activation of growth factors immobilized in the bone matrix. These factors in turn act on tumor cells to promote a feed-forward cycle of tumor growth and bone destruction which contributes to the incurability of bone metastases [2]. Hypoxia and high concentrations of TGF-β in the bone microenvironment enhance tumor production of factors that drive the feed-forward cycle of bone metastasis. We asked whether the hypoxia and TGF-β signaling pathways have additive or synergistic effects to promote breast cancer bone metastasis to determine if combined treatment with inhibitors of these pathways could be used to treat bone metastases.

Bone is the largest storehouse of TGF-β in the body. TGF-β has complex effects in cancer and is a growth suppressor early in tumorigenesis; however, many advanced cancers escape from growth inhibition by TGF-β and express prometastatic genes in response [3]. TGF-β signaling pathway is activated when TGF-β binds to the TGF-β type II receptor (TβRII) and promotes dimerization with and activation of the TGF-β type I receptor (TβRI) [3]. TβRI contains a kinase domain which phosphorylates the receptor-associated Smads, Smad2 and Smad3. These factors bind to Smad4 forming a heteromeric Smad complex which translocates to the nucleus and mediates gene transcription by binding to Smad binding elements (SBEs) in the promoters of target genes [4].

TGF-β has an additional role in cancer to promote bone metastasis by regulating many of the tumor-secreted factors that stimulate tumor growth and bone destruction [5] (Table 1), such as PTHrP [6], IL-11, connective tissue growth factor (CTGF), the CXC chemokine receptor 4 (CXCR4), and others [7-10]. Previous studies using mouse models have shown that blockade of TGF-β signaling in MDA-MB-231 breast carcinoma cells

4

by stable expression of a dominant-negative TβRII reduced bone metastases and increased survival [6]. Expression of a constitutively active TβRI reversed this effect, resulting in increased bone metastases and decreased survival [6]. Inhibition of TGF-β signaling by knockdown of Smad4 [11,12], overexpression of the inhibitory Smad7 [13], or treatment with pharmacologic inhibitors, such as SD-208 [14], an ATP-competitive inhibitor of the TβRI kinase or other TGF-β inhibitors [15-19] decreased bone metastases in animal models.

Bone is a hypoxic microenvironment (pO_2 between 1-7%) [20], which increases growth of metastatic tumor cells adapted for surviving in conditions of low O_2. Breast cancers and other solid tumors are susceptible to hypoxia because they proliferate and outgrow vascular supplies of oxygen and nutrients [21]. Tumor hypoxia causes radio- and chemotherapeutic resistance, which may contribute to the incurability of bone metastases [22]. Hypoxia activates signaling through hypoxia-inducible factor (HIF)-1α, which is overexpressed in many cancers, including breast. HIF-1α expression correlates with increasing tumor grade, invasion, and metastasis [23]. In conditions of high oxygen, HIF-1α is hydroxylated and targeted for proteasomal degradation by the von Hippel Lindau tumor suppressor. When oxygen is limiting, HIF-1α heterodimerizes with HIF-1β in the nucleus and mediates the transcription of hypoxia-regulated target genes [21,24].

Many bone metastases genes that are regulated by TGF-β are also regulated by hypoxia (Table 1), including those identified by Kang *et al*. to comprise a bone-metastatic gene signature in breast cancer cells: CTGF, CXCR4, IL-11, and MMP-1 [8,13,25-27]. These genes code for proteins that regulate different steps of the metastatic cascade: invasion, homing, angiogenesis and osteolysis. Breast cancer cells express there

and many other prometastatic genes. Thus, therapeutic targeting of individual proteins is unlikely to cure breast cancer bone metastases. Inhibitors of HIF-1α or TGF-β, which act upstream of multiple target genes, may be more effective and several are under investigation in phase I and II clinical trials for various cancers [15,16,28-32].

We investigated interactions between the hypoxia and TGF-β signaling pathways *in vitro* by examining bone-metastatic MDA-MB-231 breast cancer cells for changes in TGF-β and hypoxia-stimulated gene expression of 16 candidate genes. Of these, only vascular endothelial growth factor (VEGF) and CXCR4, showed additive responses to TGF-β and hypoxia, suggesting limited crosstalk between TGF-β and hypoxia signaling pathways in breast cancer cells. *In vitro* analyses, however, may not accurately represent *in vivo* function. Therefore, we used a mouse model of bone metastasis to assess global crosstalk between the hypoxia and TGF-β signaling pathways *in vivo*. In this model, the MDA-MB-231 breast cancer cell line reliably forms osteolytic bone lesions in nude mice when inoculated into the left cardiac ventricle. We tested the effects TGF-β and hypoxia on bone metastases in this model by genetic and pharmacologic approaches. In the first approach, we used genetic methods of shRNA knockdown and dominant-negative expression to specifically target the tumor cells. Genetic inhibition of HIF-1α and TGF-β signaling pathways in MDA-MB-231 cells significantly decreased osteolysis and enhanced survival of mice with bone metastases. Combined inhibition of HIF-1α and TGF-β in the tumor cells had no additional effect, suggesting parallel roles for hypoxia and TGF-β signaling in tumor cells. This approach provided proof of principle for the tumor autonomous effects of HIF-1α and TGF-β signaling in bone metastases, but it is not readily translatable to the clinic. In a second pharmacologic approach, we inhibited

HIF-1α and TGF-β signaling systemically using small molecule inhibitors to target both the tumor cells and the bone microenvironment. Inhibition of HIF-1α or TGF-β with these inhibitors also decreased osteolysis, reduced tumor burden, and enhanced survival of mice with bone metastases. In contrast to the genetic models, combined pharmacologic inhibition produced an additional decrease in tumor burden compared to either alone. Systemic inhibition of HIF-1α and TGF-β signaling also had independent effects on bone to decrease osteoclast and increase osteoblast activity. Thus, combined systemic inhibition of HIF-1α and TGF-β signaling is more beneficial than either alone due to activity on the tumor cells and the bone microenvironment.

Methods

Materials. Recombinant human TGF-β1 was purchased from R&D Systems (Minneapolis, MN). 2-methoxyestradiol (2ME2) was a gift from Entremed (Rockville, MD) and was provided as an orally-active, nanocrystalline dispersion [33]. SD-208 was obtained from Scios, Inc. (Fremont, CA) and Epichem (Murdoch, Australia). SD-208 is a potent inhibitor of TβRI (EC_{50} = 48nM) whose selectivity profile for a variety of kinases has been previously described [32]. The drug was resuspended in 1% methylcellulose and stored at 4°C.

Cell lines. MDA-MB-231 breast cancer cells [6] were cultured in Dulbecco's modified Eagle's media (DMEM) (Hyclone Laboratories, Logan, UT) containing 10% heat-inactivated fetal bovine serum (FBS) (Hyclone). HepG2 hepatocarcinoma cells (HB-8065, ATCC, Manassas, VA) were cultured in modified Eagle's media (MEM)

supplemented with 10% FBS, sodium pyruvate and non-essential amino acids. PC-3 prostate cancer cells (CRL-1435, ATCC) were cultured in RPMI with 10% FBS. 1205Lu melanoma cells were from Dr. Alain Mauviel, Institut National de la Sante et de la Recherche Medicale, Paris, France [13]. The cells were grown in a composite medium (W489) consisting of three parts of MCDB153 and one part of L15 supplemented with 4% FBS. Cells were maintained at $37^{\circ}C$ with 5% CO_2 in a humidified chamber. Hypoxia treatments were performed by placing tissue culture flasks in a modular incubator chamber (model MC-101, Billups-Rothenberg Inc., Del Mar, CA), flushed with premixed 94% N_2, 5% CO_2, 1% O_2 and maintained in a conventional tissue culture incubator.

Preparation of stable clones. Parental MDA-MB-231 cells were transfected with a pLKO.1 plasmid coding an shRNA against HIF-1α (TRCNo. TRCN0000003810, MISSION® shRNA, Sigma, St. Louis, MO) using FuGENE HD (Roche, Nutley, NJ). Cells transfected with a non-target shRNA control vector (SHC002, MISSION® shRNA, Sigma) were used as a control. Single clones were selected by limiting dilution in the presence of puromycin (Invitrogen, San Diego, CA). Knockdown of HIF-1α mRNA and protein were confirmed by semi-quantitative RT-PCR and Western blot analysis. Clones were retested for stability (> 80% knockdown) after culture in the absence of puromycin for 60 days. Two non-target controls (shNT) and two HIF-1α knockdown (shHIF) clones were selected for further study.

The MDA-MB-231 clonal line, MDA/TβRIIΔcyt, which stably expresses a cytoplasmically truncated type II TGF-β receptor [6], here referred to as dominant-negative receptor II (DNRII), was transfected to express either non-target or HIF-1α

shRNA. Single cell clones were isolated, selected for resistance to G418 (Alexis Biochemicals, San Diego, CA) and puromycin, and tested for stable knockdown of HIF-1α as described previously. Stable DNRII expression and blockade of TGF-β signaling were confirmed by Western blot for phosphorylated Smad2. Two DNRII/ shNT and two DNRII/shHIF clones were selected for *in vivo* and *in vitro* experiments.

MTT assay. Cell proliferation was assayed by MTT assay. Cells were plated at a density of 1000 cells/well in 96-well plates. MTT reagent (20μl, 5mg/ml) (Calbiochem, San Diego, CA) was added to each well. After a 5h-incubation at 37°C, 100μL of 0.01M HCL containing 10% SDS were added to lyse the cells and the plate was incubated at 37°C for an additional 16h. Absorbance was measured at 570nm using a Synergy™ HT spectrophotometer (Bio-tek, Winooski, VT).

Semi-quantitative RT-PCR. MDA-MB-231 cells were seeded in 24-well plates (10^5 cells/well). Forty-eight hours later, cells were starved overnight in basal DMEM media, then treated ± TGF-β1 (5ng/mL) in DMEM-FBS (1%) and cultured in 20% or 1% O_2 for 24h. Cells were rinsed in PBS and then lysed in Trizol (Invitrogen) for RNA extraction. Briefly, chloroform was added to cell lysates. Samples were centrifuged (12,000g, 15 min, 4°C) and the upper aqueous phase was collected. One volume of 70% ethanol was added, then sample was loaded on an RNeasy mini spin column (Qiagen, Valencia, CA) and total RNA was isolated according to manufacturer's instructions. DNase I treatment was performed to remove genomic DNA contamination, and RNA integrity was assessed on agarose gels. RNA (500ng per sample) was reverse transcribed using Superscript II (Invitrogen) according to the manufacturer's instructions with anchored oligo(dT)

(Abgene, Rochester, NY) for priming. The resulting cDNAs were prepared for semi-quantitative real-time PCR using QuantiTect SYBR Green PCR Kit (Qiagen) and analyzed in a MyiQ™ Single-Color Real-Time PCR Detection System (BioRad, Hercules, CA) for 40 cycles (95°C for 1 min, 58°C or 60°C for 30s, 72°C for 30s) after an initial 15-min incubation at 95°C. Primers were optimized for real-time PCR (amplification efficiency $100 \pm 5\%$). Primer sequences are listed in Table S1. Target gene expression was normalized against the housekeeping gene for the ribosomal protein L32, and data were analyzed using the $\Delta\Delta$Ct method.

Western blot analysis. MDA-MB-231 cells were plated in 12-well plates ($2X10^5$ cells/well). Forty-eight hours later, cells were serum starved overnight in basal DMEM, then cultured in DMEM-FBS (1%) for duration of treatment. Hypoxia treatments were performed by culturing in $1\%O_2$ for 6h. TGF-β1 (5ng/mL) treatment was for 2h. Cells were washed once with PBS, lysed in 200μl SDS-loading buffer, and heated to 95^oC for 5min. Samples were loaded onto a 10% polyacrylamide gel and electrophoresis was performed using a Mini Trans-Blot® cell (BioRad, Hercules, CA). Proteins were transferred onto a Hybond™-P membrane (GE Healthcare, Waukesha, WI) using a Mini-PROTEAN® Cell transfer system (BioRad). Membranes were blocked in TBS-T-5% milk for 1h, incubated overnight with the primary antibody and for 1h with the secondary antibody. Antibody detection was performed using Immobilon™ Western Chemiluminescent HRP Substrate (Millipore, Billerica, MA) according to the manufacturer's directions and signal was visualized on radiographic film. Antibodies used include HIF-1α (BD Biosciences, San Jose, CA), phospho-Smad2 (Ser465/467) and

Smad2 (Cell Signaling, Danvers, MA); α-tubulin (Sigma) was used as a control. Anti-mouse IgG (Fab specific) and anti-rabbit IgG secondary antibodies conjugated to peroxidase were purchased from Sigma.

Dual-luciferase assays. Cells were transfected with pGL3-luciferase constructs containing either the (CAGA)$_9$ [34], VEGF or CXCR4 promoter using FuGENE HD. (CAGA)$_9$ contains nine tandemly-repeated Smad binding elements. The 2.6 kb human CXCR4 promoter was from Dr. Robert Strieter, University of Virginia [35,36], and the 3.3kb human VEGF promoter was from Dr. Lee Ellis, University of Texas, MD Anderson Cancer Center [37]. Cells were also transfected with a phRL-renilla plasmid (Promega, Madison, WI) for normalization. Twenty-four hours later, cells were cultured serum-starved in basal DMEM medium for 4h, then treated in the presence or absence of TGF-β1 (5ng/mL) and 1% O_2 for 24h. Cells were washed once with PBS, lysed using Passive Lysis Buffer (Promega), and analyzed for luciferase activity using the Dual-Luciferase Reporter Assay System (Promega), according to the manufacturer's instructions on a FB12 Sirius luminometer (Berthold Detection Systems, Oak Ridge, TN).

Plasmids. pCEP4-HIF-1α (MBA-2) was purchased from the ATCC; pCMV-Smad2 and -Smad3 were from Dr. David Wotton (University of Virginia); pCMV-Smad4 was from Dr. Rik Derynk (University of California San Francisco). VEGF and CXCR4 promoter deletion mutants were generated using forward primers containing a 5' KpnI restriction site and 3' end complementary to the promoter (Table S2). Reverse primer (5'-

GTTCCATCTTCCAGCGGATA-3') binds a region of the luciferase coding sequence. Promoter fragments were amplified by PCR using PfuUltra™ Hotstart DNA polymerase (Stratagene, La Jolla, CA). Products were digested overnight with KpnI and XhoI, purified on agarose gel (QIAquick Gel Extraction kit, Qiagen), and ligated into the pGL3-luciferase vector using T4 DNA ligase (Roche) according to the manufacturer's instructions. QuikChange® II Site-Directed Mutagenesis kit (Stratagene) was used to mutate putative Smad-binding (SBE) and hypoxia response (HRE) elements in the VEGF and CXCR4 promoters. Primers were designed using the QuikChange® Primer Design Program (Stratagene) and mutagenesis performed according to the manufacturer's protocol.

VEGF enzyme-linked immunosorbant assays. MDA-MB-231 parental cells and clones were plated in 12-well plates ($2X10^5$ cells/well) and grown for 48h. After 4h serum starvation, cells were treated ± TGF-β1 (5ng/mL) in DMEM-FBS (1%) and ± 1% O_2 for 24h. Conditioned media was collected and analyzed by ELISA assay for VEGF-A (Bender MedSystems, Inc., Burlingame, CA), according to the manufacturer's instructions. Cell number per well was used for normalization.

Flow cytometry. MDA-MB-231 parental cells and clones were plated in triplicate in 6-well plates ($5X10^5$ cells/well). Forty-eight hours later, cells were trypsinized, counted, and $5x10^5$ cells per sample were transferred to 5mL tubes. Cells were centrifuged (1,000rpm, 5min, 4°C), washed twice with flow cytometry buffer (FCB) (2% bovine serum albumin and 0.2% sodium azide in PBS 1X) and incubated with phycoerythrin-conjugated CXCR4 antibody (eBiosciences, San Diego, CA) for 30min. Cells were

washed twice, fixed in paraformaldehyde (2% in PBS 1X, 15min, RT) and resuspended in FCB. A FACSCalibur flow cytometer (Becton Dickinson, Franklin Lakes, NJ) was used for flow cytometry, followed by analysis with FloJo software (TreeStar, Ashland OR).

In vivo protocols:

Animals. Animal protocols were approved by the Institution Animal Care and Use Committee at the University of Virginia and were in accordance with the National Institutes of Health Guide for the Care and Use of Laboratory Animals. Female athymic nude mice, 4 weeks of age, were housed in laminar flow isolated hoods. Autoclaved water and mouse chow were provided ad libitum. Mice were euthanized when they became moribund.

Bone metastasis model. Intracardiac inoculation of tumor cells was performed as previously described [38]. Tumor cells were trypsinized, washed twice and resuspended in PBS to a final concentration of 10^5 cells in 100μl. Animals were anesthetized with ketamine/xylazine and positioned ventral side up. MDA-MB-231 parental or clonally-derived cells (n=12-15) were inoculated into the left ventricle by percutaneous injection using a 26-gauge needle.

Mammary fat pad tumor model. Four week old female nude mice were anaesthetized with ketamine/xylazine and placed in supine position. MDA-MB-231 parental or clonally-derived cells (10^6 cells in 100μL PBS; n=10 mice per cell line) were inoculated into the

upper mammary fat pad using a 27-gauge needle. Tumor size was followed by measuring tumor diameters with calipers three times per week and tumor volume was calculated by the formula of an ovoid: tumor volume = $4/3\pi$ x $L/2$ $(w/2)^2$, where L and w equal mid-axis length and width, respectively.

Drug treatments. 2ME2 (150mg/kg) or its vehicle PBS was administered daily by i.p. injection. In the first experiment, SD-208 was administered preventively via the drinking water (either 0.3 or 1mg/mL) beginning two days prior to tumor inoculation. Vehicle control animals were given water without compound. In all subsequent experiments, SD-208 (60mg/kg) or its vehicle 1% methylcellulose was administered daily by oral gavage. In the preventive protocols, drug treatment was initiated two days prior to tumor cell inoculation and continued daily for the duration of the study. In the therapeutic protocol, drug treatment was initiated when osteolysis was observed on x-ray and then continued during the duration of the study.

Radiography. Osteolytic lesions were analyzed by radiography using a Faxitron MX-20 with digital camera (Faxitron X-ray Corporation, Wheeling, IL). Mice were imaged in a prone position at 1X magnification and 4X when osteolytic lesions were suspected. Osteolytic lesion area was quantified using MetaMorph software (Universal Imaging Corporation, Dowingtown, PA).

Bone mineral density (BMD) measurement. BMD was performed on live mice using a GE Lunar PIXImus II (GE Healthcare) mouse densitometer (Faxitron X-ray

Corporation). Measurements were performed one time/week throughout the experiment. The densitometer was calibrated with a plastic embedded murine phantom before use. Mice were anesthetized, placed on an adhesive tray in a prone position with limbs spread. Total body measurement was performed excluding the calvarium, mandible and teeth. A region of interest was defined at the distal femur, proximal tibia just beneath the growth plate (12x12 pixels) and the lower lumber spine (20x50 pixels). Values were expressed as percentage change in BMD over base line in mg/cm^2.

Bone histology & histomorphometry. Forelimbs, hindlimbs, and spine of the mice were collected upon euthanasia and fixed in 10% neutral buffered formalin for 48h and decalcified in 10% EDTA for 2 weeks. After decalcification tissues were processed in a Shandon Excelsior automated tissue processor (Thermo Fisher Scientific, Waltham, MA) and embedded in paraffin wax for sectioning. Longitudinal, mid-sagittal sections 3.5µm in thickness from the tibia, femur and lumbar spines were cut using an automated Microm HM 355 S microtome (Thermo Fisher Scientific). Tissue sections were stained with hematoxylin and eosin (H&E) and prepared for histomorphometric analysis. All sections were viewed on a Leica DM LB compound microscope (Leica Microsystems, Bannockburn, IL) with a Q-Imaging Micropublisher Cooled CCD color digital camera (Vashaw Scientific Inc., Washington, DC). Images were captured and analyzed using MetaMorph software (Universal Imaging Corporation). Tumor burden per bone, defined as area of bone occupied by the cancer cells, was calculated at the tibia, femur and humerus at 50X magnification on H&E stained sections, as previously described [39]. Osteoclast number at the tumor-bone interface (OC/mm bone surface) in the femur, tibia

and humerus was measured on TRAP stained slides at 200X magnification. For normal bone, osteoblast (OB) number and osteoclast (OCL) number at the bone surface were measured in the distal femur and proximal tibia at 200X magnification on H&E and TRAP stained slides, respectively.

Hypoxyprobe ^{TM}-1 staining for tumor hypoxia. For assessment of tumor hypoxia, mice were injected 2h prior to euthanasia with pimonidazole (60mg/kg i.p.) and sections stained with Hypoxyprobe^{TM}-1 kit (Natural Pharmacia International, Inc., Burlington, MA) according to the manufacturer's instructions. Tumor hypoxia in bone metastases tumor sections was scored semi-quantitatively on a 1-4 + scale, based on the percentage of positively stained tumor within a 400X field: grade 1: 25% staining, 2: 50%, 3: 75%, and 4: 100%.

Immunohistochemistry. Immunohistochemical analysis was performed on decalcified paraffin-embedded tissue sections. Antibodies against HIF-1α and CD31 were purchased from BD Biosciences. All staining was performed using VECTASTAIN® Elite ABC kit (Vector Laboratories, Burlingame, CA). Slides were stained using a 3,3, diaminobenzidine substrate kit (Vector Laboratories) and counterstained with hematoxylin. HIF-1α and CD31 staining were quantified by the percentage of positively staining nuclei per 400X field and number of vessels per 200X field, respectively. Three or more fields per animal were analyzed and averaged. Averages for 3 or more animals per group were compared.

TUNEL assay. Tumor cell apoptosis was analyzed in bone metastases tissue sections using the DeadEnd™ Colorimetric TUNEL system (Promega), according to the manufacturer's instructions.

Statistical Analyses.

In Vivo: All data were analyzed with the use of Graphpad Prism v4.0 software (GraphPad Software, Inc., La Jolla, CA). Differences in osteolytic lesion area between clones and treatment groups were analyzed by two-way ANOVA. Histomorphometry for tumor burden and osteoclast number was analyzed by one-way ANOVA and Tukey's or Newman-Keuls multiple comparison test. Kaplan-Meier survival curve data was analyzed by a Logrank test. All the results were expressed as mean ± SEM, and $p < 0.05$ was considered significant.

In Vitro: All data were analyzed with the use of Graphpad Prism v4.0 software (GraphPad Software, Inc., La Jolla, CA). Samples were analyzed in triplicate for RT-PCR, dual-luciferase assays, ELISA, and flow cytometry and statistics analyzed by unpaired t-test. Results are expressed as mean ± standard deviation, and $p < 0.05$ was considered significant. Immunostaining was analyzed by one-way ANOVA or unpaired t-test.

Results

Hypoxia induces HIF-1α expression in bone metastatic cancer cell lines in vitro and in vivo at sites of MDA-MB-231 breast cancer bone metastases. Three bone metastatic cancer cell lines: MDA-MB-231 breast cancer, PC-3 prostate cancer, and 1205Lu

melanoma cells, were tested for hypoxic responsiveness by culture in 20% or 1% O_2 for 6h. Western blot analysis showed induction of HIF-1α expression under hypoxic conditions, which was blocked by treatment with the HIF-1α inhibitor 2-methoxyestradiol (2ME2) [40-42] (Figure 1A). We next determined whether MDA-MB-231 breast cancer bone metastases are hypoxic *in vivo* by Hypoxyprobe™-1 staining [43-46]. Mice with MDA-MB-231 bone metastases were injected 2h prior to euthanasia with pimonidazole, which forms insoluble protein adducts in hypoxic cells. Staining was detected in bone metastases sections from pimonidazole-labeled mice but not in control animals (Figure 1B). Staining for HIF-1α protein was detected in serial bone metastases sections, at sites adjacent to pimonidazole-positive hypoxic regions. The results suggest a role for hypoxia-induced HIF-1α in bone metastases.

Hypoxia and TGF-β additively increase prometastatic factors VEGF and CXCR4. A literature search for bone metastatic genes combined with the keywords hypoxia or TGF-β, found that many were regulated by the two pathways (Table 1)**.** MDA-MB-231 cells treated ± TGF-β1 (5ng/mL) and ± 1% O_2 for 24h were then surveyed by semi-quantitative RT-PCR for changes in mRNA expression of candidate TGF-β and hypoxia-regulated genes selected from Table 1: VEGF; CXCR4; PTHrP; IL-6, 8, 11; and CTGF. We also measured the expression of components of the two signaling pathways: HIF-1α, prolyl hydroxylase 2 (PHD2), TGF-β1, Smads2, 3, 4 and 7, Ski and SnoN. Many genes were increased by TGF-β or hypoxia alone (data not shown) while only 2 of the 16 surveyed genes, VEGF and CXCR4, were increased by both TGF-β and 1% O_2 alone (Figure 2A). VEGF mRNA expression was additively increased by TGF-β and 1% O_2;

however, there was no additional increase in CXCR4 mRNA expression with combined treatment. Transcriptional activation of the VEGF and CXCR4 promoters by TGF-β and hypoxia was analyzed by dual-luciferase assay in HepG2 cells transfected with a pGL3-luciferase reporter vector containing either a 3.3kb human VEGF promoter fragment [37] or a 2.6kb human CXCR4 promoter fragment [35,36]. A (CAGA)$_9$ promoter-luciferase construct containing nine tandemly-repeated Smad-binding elements (SBEs) was used as positive control for TGF-β activation. Dual-luciferase activity was assayed after a 24h-treatment ± TGF-β1 and ± 1% O_2. VEGF and CXCR4 promoter activities were increased by treatment with TGF-β or hypoxia alone (Figure 2B). Combined treatment additively increased VEGF and CXCR4 promoter activation. (CAGA)$_9$ promoter activity was increased only by treatment with TGF-β, demonstrating that hypoxia does not directly regulate TGF-β/Smad signaling. These results suggest that crosstalk between the hypoxia and TGF-β signaling pathways regulates VEGF and CXCR4 mRNA expression and promoter activation.

Overexpression of HIF-1α and Smads increases VEGF and CXCR4 expression. Next we tested whether HIF-1α and Smads mediate promoter activation in response to hypoxia and TGF-β. HIF-1α or Smads2, 3, and 4 were overexpressed in MDA-MB-231 cells cotransfected with either the VEGF or CXCR4 promoter-luciferase plasmids. Dual-luciferase activity was assayed after a 24h-treatment with TGF-β1 and 1% O_2. Overexpression of either HIF-1α or Smads increased VEGF and CXCR4 promoter activity in response to TGF-β and hypoxia (Figure 2C). Coexpression of HIF-1α and Smads together resulted in a 10-fold increase in VEGF and CXCR4 promoter activities in

19

the presence of TGF-β and hypoxia, suggesting that VEGF and CXCR4 transcriptional responses to hypoxia and TGF-β are mediated through HIF-1α and Smads, respectively.

TGF-β and hypoxia interact to regulate VEGF and CXCR4 transcription. To identify promoter regions targeted by TGF-β and hypoxia signaling, constructs with 5'-deletion of the promoter, ranging in size from 3.3kb to 1.8kb for VEGF and 2.6kb to 1.0kb for CXCR4, were tested for TGF-β and hypoxia responsiveness by dual-luciferase assay. VEGF promoter response to TGF-β and hypoxia was blocked by deletion of bases -1181 to -843, while deletion of bases -2216 to -953 blocked CXCR4 responsiveness (Figure 3A). These results suggest that transcriptional activation by TGF-β and hypoxia is localized within 300 base pairs in the VEGF promoter and in a 1.2kb region for CXCR4.

Promoter sequences were scanned for putative hypoxia response elements (HREs) and SBEs using the consensus sequences 5'-RCGTG-3' and 5'-CAGAC-3', respectively. HREs and SBEs found in close proximity within the promoter regions identified above were mutated by site-directed mutagenesis (Figure 3B). TGF-β and hypoxia responsiveness were assayed using dual-luciferase. In the VEGF promoter, mutation of HRE (-975/-970) and SBEs (-992/-988) and (-797/-793) decreased the response to TGF-β and 1% O_2 (Figure 3C). The combined mutation of the HRE and one of the SBE nearly abolished promoter activity. Mutation of HRE (-1316/-1310) in the CXCR4 promoter blocked additive responses to TGF-β and hypoxia, while mutation of putative SBEs had little or no effect (Figure 3C). These data suggest that both TGF-β and hypoxia regulate VEGF promoter activity, while only hypoxia regulates CXCR4 promoter activity. The promoter may contain additional non-identified SBEs that mediate its response to TGF-β.

HIF-1α knockdown in MDA-MB-231 breast cancer cells decreases osteolytic bone metastases and improves survival in a mouse model. We further examined hypoxic responses of MDA-MB-231 cells *in vitro* by stable knockdown of HIF-1α. The cells were transfected with a plasmid expressing an shRNA targeting HIF-1α. Single cell clones were isolated and stability of the knockdown was tested after cultivating the cells for 60 days in absence of antibiotic. Two clones (shHIF#3 and #11) with >90% decrease of HIF-1α mRNA and undetectable levels of HIF-1α protein were further analyzed (Figure 4A). Two control shRNA clones (shNT#3 and #7) had HIF-1α mRNA expression similar to parental cells and were used as controls. The clones were also analyzed by semi-quantitative RT-PCR for changes in mRNA expression following TGF-β1 and 1% O_2 treatment for 24h. TGF-β- and hypoxia-induced VEGF and CXCR4 mRNA expression was significantly decreased in the shHIF clones compared to parental and shNT cells (Figure 4B). Secreted VEGF-A protein, measured by ELISA (Figure 4C), and CXCR4 protein, measured by flow cytometry (Figure 4D), were also decreased. The results demonstrate that knockdown of HIF-1α blocks expression of prometastatic factors VEGF and CXCR4 in MDA-MB-231 cells. An MTT assay showed no difference in proliferation for any of the shHIF or shNT clones compared to parental MDA-MB-231 cells in normoxic conditions. Proliferation of each clone was decreased by culture in hypoxic compared to normoxic conditions; however, there was no difference among the clones (data not shown).

We tested the effect of HIF-1α knockdown *in vivo* using a mouse model of bone metastases. Female nude mice (4 weeks old) were inoculated in the left cardiac ventricle

with parental MDA-MB-231 cells or one of the four different clones: shNT#3 and #7 controls, or shHIF#3 and #11 HIF-1α knockdown clones (n=12 per group). Osteolytic lesion area on x-ray was decreased in mice with shHIF knockdown bone metastases compared to those with controls of parental or shNT bone metastases ($P < 0.001$ for shHIF#3 and $P < 0.01$ for shHIF#11 compared to parental or shNT clones) (Figure 5A-B). HIF-1α knockdown in bone metastatic cells also significantly improved survival of mice compared to control animals (Figure 5C). Quantitative histomorphometry showed no difference in tumor burden in the mice with shHIF bone metastases compared to those with parental or shNT bone metastases (Figure 5D-E). This was not unexpected in this survival experiment in which the mice with shHIF bone metastases lived longer than the parental or shNT controls.

Staining for HIF-1α in bone metastases tumor sections was decreased in shHIF bone metastases compared to parental and shNT controls, confirming the stability of HIF-1α knockdown throughout the *in vivo* experiment (Figures 6A-B). Since HIF-1α knockdown *in vitro* resulted in decreased mRNA expression of the angiogenic factor VEGF, we analyzed tumor angiogenesis *in vivo* by staining for the endothelial cell marker CD31. The number of vessels/tumor area was significantly decreased in shHIF bone metastases compared to parental and shNT bone metastases (Figure 7A-B). These data suggest that knockdown of HIF-1α in tumor cells decreases bone metastases by suppressing tumor secretion of proangiogenic factors and blocking vessel formation.

HIF-1α knockdown or TGF-β blockade in tumor cells reduces bone metastases and improves survival in vivo. To evaluate the effect of single and combined inhibition of

HIF-1α and TGF-β specifically in tumor cells *in vivo*, we generated a series of MDA-MB-231 cell lines which stably expressed either HIF-1α shRNA alone or in combination with a dominant-negative TGF-β type II receptor (DNRII). Knockdown of HIF-1α mRNA and protein was confirmed by semi-quantitative RT-PCR and Western blot (Figure 8A-B). Blockade of TGF-β signaling in the DNRII expressing clones was confirmed by decreased phosho-Smad2 on Western blot (Figure 8C) and decreased (CAGA)$_9$ promoter activation in response to TGF-β (Figure 8D). TGF-β and 1% O_2-stimulated VEGF and CXCR4 mRNAs were decreased in the DNRII and DNRII/shHIF clones compared to parental control (Figure 8E)**.** *In vivo*, mice inoculated with the DNRII/shHIF-1α clones had decreased osteolytic lesion area and improved survival compared to mice with bone metastases caused by parental or DNRII cell lines (data not shown). DNRII/shHIF#22 and DNRII/shNT#2 control clones were selected for a subsequent experiment in which we directly compared the effect of HIF-1α knockdown alone or combined with TGF-β blockade *in vivo*. Female nude mice (n=12 per group) were inoculated in the left cardiac ventricle with one of the six MDA-MB-231 cell lines: parental, shNT#3, shHIF#3, DNRII, and DNRII/shNT#2 or DNRII/shHIF#22. Mice were followed by radiography for the development of osteolytic lesions. Lesion area on x-ray was decreased by knockdown of HIF-1α (shHIF#3) or blockade of TGF-β (DNRII or DNRII/shNT#2) (*P*< 0.001 shHIF#3 and DNRII compared to parental and *P*< 0.05 shHIF#3 compared to shNT#3) (Figure 9A-B). Combined inhibition of TGF-β and HIF-1α (DNRII/shHIF#22) had no additional effect on osteolysis. Survival of mice with MDA-MB-231 bone metastases was improved with HIF-1α knockdown or TGF-β blockade (Figure 9C). Combined inhibition of these pathways yielded no further

improvement in survival. There was no difference in tumor burden by quantitative histomorphometry in the mice with shHIF, DNRII, or shHIF/DNRII bone metastases compared to the control groups (Figure 9D), which was not unexpected because the survival of these mice was increased.

To determine if the observed effects were bone specific, we analyzed tumor growth following inoculation of these clones into the mammary fat pad. Tumor take and rate of growth were similar for the parental, DNRII, and DNRII/shNT#2 clones, but decreased in the shHIF#3 and DNRII/shHIF#22 clones (data not shown). The data suggest that HIF-1α knockdown may decrease bone metastases by inhibiting tumor cell proliferation rather than increasing apoptosis, as TUNEL staining of bone metastases tumor sections demonstrated no difference in tumor cell apoptosis in shHIF compared to parental or shNT bone metastases (data not shown).

Pharmacologic inhibition of HIF-1α with 2ME2 decreases osteolytic lesion area and tumor burden in a preventive model of bone metastasis. The preceding studies provide proof of principle that the HIF-1α and TGF-β signaling pathways in breast cancer cells promote skeletal metastases. Molecular blockade of either pathway prevents tumor growth in bone although the effects were not additive. To determine whether systemic inhibition of these pathways in tumor and host cells provided similar benefit, we used a pharmacologic approach with the HIF-1α inhibitor, 2-methoxyestradiol (2ME2) [40-42]. We showed that 2ME2 decreases HIF-1α protein expression in MDA-MB-231 breast cancer cells *in vitro* (Figure 1A). 2ME2 was also previously shown to decrease osteolysis in a 4T1 breast cancer metastasis model [47]. Here, we tested a nanocrystalline dispersion

formulation with improved bioavailability [33] in a prevention model for breast cancer bone metastases. Drug treatment (150mg/kg i.p.) was initiated two days prior to the inoculation of tumor cells and continued daily during the experiment. Female nude mice (n=15 per group) were inoculated into the left cardiac ventricle with MDA-MB-231 cells and the development of osteolytic lesions was followed by radiography.

Preventive treatment with 2ME2 significantly reduced osteolysis area ($P< 0.01$) (Figure 10A) with a consistent decrease in tumor burden by histomorphometric analyses ($P< 0.005$) (Figure 10B). Staining for nuclear HIF-1α in the tumor cells was significantly decreased in mice treated with 2ME2 compared to vehicle-treated mice, confirming that the 2ME2 treatment was effective *in vivo* (Figure 10C). Tumor hypoxia was also decreased in 2ME2-treated mice as demonstrated by Hypoxyprobe[TM]-1 staining (Figure 10D). The data indicate that 2ME2 effectively inhibits HIF-1α expression within the tumor microenvironment.

2ME2 increases bone mass by increasing osteoblasts and inhibiting osteoclasts in bone unaffected by tumor. To determine the effects of 2ME2 in normal bone, mice were treated with 2ME2 (150 mg/kg i.p) daily for 4 weeks. Bone mineral density (BMD) was measured weekly by DXA throughout the experiment. Mice treated with 2ME2 had significantly increased BMD at the tibia ($P< 0.001$) and femur ($P< 0.05$), but not at the spine (Figure 11A). Trabecular bone was increased at the distal femur and proximal tibia by 2ME2 treatment, as demonstrated by histology of bones from the mice (Figure 11B). To determine if alterations in bone resorption or bone formation were responsible for the increase bone mass, we counted osteoclast and osteoblast on histologic sections of bone

using histomorphometric analysis. Osteoclast number per bone surface was decreased (*P*= 0.0077, Figure 11C-D), while osteoblast number was increased (*P*= 0.0002, Figure 11E-F) in the 2ME2-treated mice compared to vehicle-treated controls. The data suggest that 2ME2 may inhibit bone metastases through direct effects on bone by inhibiting osteoclast and increasing osteoblast activity, in addition to its effects on tumor cells.

Pharmacologic inhibition of TβRI reduces the development and progression of breast cancer metastases to bone and improves survival. To compare single systemic inhibition of HIF-1α with inhibition of TGF-β signaling, we tested the efficacy of SD-208, a small molecule inhibitor of TβRI kinase, in a prevention model of bone metastasis. Mice were treated with either 0.3 or 1.0mg/mL SD-208 in the drinking water, beginning two days prior to tumor inoculation and continuing for the duration of the study. Both doses of SD-208 significantly reduced the osteolytic lesions detectable on radiography (Figure 12A-B). Histomorphometric analysis of total tumor area showed a similar reduction in tumor burden (Figure 12C-D). Furthermore, SD-208 treatment resulted in a dose-dependent increase in median survival compared to control animals (25, 35 and 37 days for vehicle, 0.3 and 1.0 mg/mL SD-208, respectively, p=0.008) (Figure 12E).

Combined inhibition of HIF-1α and TGF-β with small molecule inhibitors additively decreases bone metastases in mice. Next, we tested whether combined systemic inhibition of HIF-1α with 2ME2 and TGF-β with a TβRI kinase inhibitor SD-208 [14,32] provided additional therapeutic benefit in a therapuetic model of breast cancer bone metastasis. Mice were inoculated with MDA-MB-231 cells and were followed by x-ray

for the development of bone metastases. Treatment was initiated when osteolytic lesions were observed on x-ray at 12 days post tumor inoculation and continued daily during the experiment. Mice (n=15/group) were randomized to one of four treatment groups: vehicle, 2ME2 alone (150mg/kg i.p.), SD-208 alone (60mg/kg by oral gavage), or 2ME2 and SD-208 combined. To control for the effects of the different methods of drug administration, all mice received daily i.p. injection with either 2ME2 or PBS vehicle and oral gavage with either SD-208 or 1% methylcellulose vehicle. Treatment with either 2ME2 or SD-208 alone significantly decreased x-ray lesion area ($P<0.01$ SD-208 and $P<0.001$ 2ME2 compared to vehicle) (Figure 13A), which was further decreased with combined treatment ($P<0.01$ and $P<0.05$ SD-208 + 2ME2 compared to SD-208 and 2ME2, respectively). Histomorphometric analysis showed a corresponding decrease in tumor burden in the femora, tibiae and humeri of 2ME2 and SD-208-treated animals compared to vehicle-treated mice (Figure 13B-C). Tumor burden was further decreased by treatment with SD-208 and 2ME2 combined, compared to SD-208 alone ($P<0.05$) (Figure 13B-C). A trend towards an additional decrease with combined treatment compared to 2ME2 treatment alone did not reach significance.

We observed similar effects in a preventive model for breast cancer bone metastasis (data not shown). In this model, treatment with 2ME2 and SD-208 was initiated two days prior to tumor inoculation. Tumor burden was significantly decreased by combined treatment compared to SD-208 alone, with a trend towards an additional decrease compared to 2ME2. Together, these studies suggest that combined pharmacologic targeting of HIF-1α and TGF-β effectively reduces the development and progression of osteolytic bone metastases greater than either alone.

Combined treatment with 2ME2 and SD-208 decreases osteoclast number at sites of bone metastases. We hypothesized that combined 2ME2 and SD-208 additionally decrease bone metastases by targeting other cells in the bone metastatic microenvironment in addition to tumor cells. Because breast cancer cells secrete factors which stimulate osteoclast formation and bone resorption in osteolytic metastases, we analyzed osteoclast number at sites of bone metastases from 2ME2- and SD-208-treated mice. Significantly fewer osteoclasts per millimeter of tumor-bone interface were present in bone metastases from 2ME2- or SD-208-treated mice compared to control mice ($P< 0.01$). This number was further reduced with combined 2ME2/SD-208 treatment ($P< 0.01$) (Figure 13D). These results suggest that 2ME2 and SD-208 decrease bone metastases through combined effects to reduce osteoclasts at sites of bone metastases, in addition to their actions on tumor cells.

Discussion

Bone metastases occur in eighty percent of patients with advanced breast cancer. They are incurable and cause significant morbidity, including pain, pathologic fractures, hypercalcemia, and nerve compression syndromes due to tumor-induced osteoclastic bone resorption [1]. Standard bisphosphonate therapies improve skeletal morbidity by reducing this osteolysis [48,49], but do not cause regression of established bone metastases. The bone microenvironment by its unique composition of growth factors housed in the mineralized bone matrix, bone resorbing and bone forming cells, promotes a feed-forward cycle of site-specific metastasis through high concentrations of growth

factors, such as TGF-β [2], and local hypoxia [50]. Active TGF-β in bone [2] promotes bone metastases by increasing tumor production of factors that stimulate osteoclastic bone resorption and tumor growth [6,7]. TGF-β-regulated factors, such as CTGF, IL-11, CXCR4 [13,27], and MMP-1 [25,26] are involved in multiple steps of the metastatic cascade, including invasion, homing, angiogenesis, and osteolysis [5] and constitute a gene signature for tumors that metastasize preferentially to bone [8] (Table 1). The bone microenvironment is also hypoxic [20]. Hypoxia activates signaling through HIF-1α which, like TGF-β, increases many of the factors that promote the feed-forward metastatic cycle. Although previous studies have shown that both HIF-1α and TGF-β signaling pathways are important in bone metastases, interactions between these factors have not been reported. The aim of these studies was to determine whether TGFβ and hypoxia act synergistically or work redundantly to promote bone metastases.

We first investigated interactions between the pathways *in vitro* by analyzing changes in gene expression in MDA-MB-231 breast cancer cells treated with TGF-β and 1% O_2. Of 16 candidate genes, only two were increased by TGF-β and hypoxia: VEGF and CXCR4. VEGF, but not CXCR4, mRNA was additively increased by combined treatment with TGF-β and 1% O_2, and promoter activation of the two factors was also additively increased by combined treatment. Previous studies of VEGF in mouse macrophages showed increased promoter activity in response to TGF-β and hypoxia and to overexpression of HIF-1α/β and Smads3/4 *in vitro* [51]. Elements responsible for TGF-β and hypoxia response were localized in the proximal region of the mouse VEGF promoter and homolog sites were identified in the human VEGF promoter [52]. The study demonstrated that TGF-β and hypoxia signaling directly crosstalk to regulate the

expression of VEGF in macrophages [51]. The data here suggest that VEGF is regulated similarly by TGF-β and hypoxia in human MDA-MB-231 cells. An HRE located 1.3kb from the transcription start site in the human CXCR4 promoter was found to mediate its response to hypoxia. Mutation of either of two putative SBEs did not significantly inhibit TGF-β-stimulated CXCR4 promoter activation. The results suggest that TGF-β regulates CXCR4 through other SBEs in the promoter that were not tested here.

MDA-MB-231 cells did not show significant additive responses to TGF-β and hypoxia for the other 14 genes examined, but other targets could be responsive. Therefore we used a comprehensive approach to genetically approach to inhibit the pathways in the tumor cells by expression of HIF-1α shRNA and a dominant-negative TβRII, which then were analyzed an *in vivo* bone metastasis model. This approach permits assessment of the tumor autonomous effects of hypoxia and TGF-β, separate from their roles in the metastatic microenvironment. Knockdown of HIF-1α mRNA in MDA-MB-231 breast cancer cells decreased osteolytic lesion area and improved survival of mice *in vivo*. Our results are consistent with previous studies in which inhibition of hypoxic signaling by a dominant-negative HIF-1α decreased bone metastases, while a constitutively active HIF increased osteolytic lesions [50]. Knockdown of HIF-1α had no effect on cell proliferation *in vitro*, but it decreased primary tumor take and growth in the mammary fat pad in our experiments. Consistent with our results, Liao *et al.* reported that conditional deletion of HIF-1α from the mammary epithelium in transgenic mice delayed onset of spontaneous breast tumors and retarded their growth [53].

Together, our *in vitro* and *in vivo* results suggest that HIF-1α promotes bone metastases by regulating factors such as CXCR4, which promotes tumor cell homing to

bone [54] and VEGF, which promotes angiogenesis. HIF-1α knockdown in MDA-MB-231 cells decreased CXCR4 expression *in vitro* and inhibited bone metastasis *in vivo*, with no difference in metastasis to other organs, such as the lungs or adrenal glands. The results suggest that HIF-1α knockdown may specifically inhibit skeletal metastases by blocking CXCR4-mediated homing to bone [55]. CXCR4 is more highly expressed in human breast cancer metastases to bone than to the lungs or brain [56]. Previous studies showed that treatment with CXCR4 antagonists inhibited breast cancer metastasis to bone and lung [57,58] and decreased bone destruction due to myeloma bone metastases [59] in mice, which supports our results.

In addition, our results suggest a role for HIF-1α to regulate interactions between tumor cells and other cells in the bone microenvironment, such as endothelial cells. Knockdown of HIF-1α in MDA-MB-231 cells decreased VEGF expression *in vitro*, and inhibited tumor angiogenesis at sites of bone metastasis *in vivo*, as demonstrated by CD31 staining for endothelial cells. There was no difference in the number of vessels in shHIF mammary fat pad tumors compared to parental and shNT control tumors (data not shown). The results suggest that knockdown of HIF-1α specifically inhibits vessel formation within the hypoxic bone microenvironment, which may contribute to decreased bone metastasis in the mice. Consistent with this, treatment with a VEGF neutralizing antibody decreased tumor angiogenesis and osteolytic bone metastases in rats [60,61].

Inhibition of either HIF-1α or TGF-β signaling in the tumor cells by shRNA knockdown or expression of a dominant-negative TβRII [6] decreased osteolytic lesion area and increased survival of mice with bone metastases compared to those bearing control cells. However, there was no additional survival benefit or reduction in lesion

area with combined inhibition of these pathways. The results suggest that the two signaling pathways function in parallel and independently of one another in tumor cells. This conclusion is supported by the results *in vitro* where HIF-1α and TGF-β regulated many of the same prometastatic factors independently, with few additive responses.

Genetic inhibition tests the role of tumor cell HIF-1α and TGF-β signaling in bone metastasis but fails to address contributions from the microenvironment. In addition, shRNA knockdowns and dominant-negative receptors are not readily translatable to the clinic. Therefore we used small molecule inhibitors to inhibit these pathways systemically. 2ME2 is a naturally occurring, poorly-estrogenic metabolite of estradiol with anti-HIF, anti-angiogenic, and anti-microtubule properties [40,62,63]. The drug decreased osteolytic lesion area in a 4T1 mouse model of bone metastasis [47]. In our studies a soluble formulation of 2ME2 effectively inhibited HIF-1α protein expression *in vitro* for three bone metastatic cell lines: MDA-MB-231 breast, PC-3 prostate and 1205Lu melanoma cells, as demonstrated previously [40]. Systemic inhibition of HIF-1α by 2ME2 significantly decreased osteolytic lesion area and reduced tumor burden in a prevention model of MDA-MB-231 breast cancer bone metastasis, consistent with the previous studies using 4T1 cells [47]. Staining for HIF-1α and tumor hypoxia were decreased in bone metastases sections from 2ME2-treated animals, demonstrating on-target effects of 2ME2 in tumor cells *in vivo*.

Similarly, we showed that a TβRI kinase inhibitor, SD-208, significantly reduced osteolytic lesion area and decreased tumor burden in mice, while increasing survival in a dose dependent manner. SD-208 was previously shown to increase survival following

orthotopic implantation of glioma cells [32]. Inhibition of TGF-β by another TβRI kinase inhibitor decreased breast cancer metastases to lungs and skeleton in mice [16].

Combined treatment with 2ME2 and SD-208 significantly decreased osteolytic lesion area on x-ray and reduced tumor burden by quantitative histomorphometry compared to vehicle or either drug alone in a clinically relevant therapeutic, as well as a prevention model of bone metastasis. Unlike the previous genetic studies where inhibition of HIF-1α and TGF-β in tumor cells had no additional effect, combined pharmacologic inhibition of these pathways with 2ME2 and SD-208 provided added therapeutic benefit, which may be due actions of the drugs on tumor cells and other cells in the bone microenvironment, such as osteoclasts. In the bone metastasis model, treatment with 2ME2 or SD-208 alone decreased the number of osteoclasts at the tumor-bone interface, which was further reduced with combined treatment. These data, together with the additive effect of 2ME2 and SD-208 on radiographic bone destruction induced by MDA-MB-231 cells, suggest that these drugs may prevent tumor-induced bone destruction by inhibiting osteoclast formation.

Systemic TGF-β blockade with SD-208 was previously shown to have profound effects on normal bone remodeling to increase bone mass in part by inhibiting osteoclast formation and bone resorption, as well as to stimulate osteoblast activity and new bone formation [64]. Here we show that 2ME2 also has direct effects on bone to increase bone mass by decreasing osteoclasts and increasing osteoblasts. 2ME2 is an inhibitor of HIF-1α, but the effects of HIF-1α in bone have been shown to be complex. Mice with a conditional deletion of HIF-1α in osteoblasts had smaller, less vascularized bones with decreased bone density [65]. In contrast, partial HIF-1α deficiency in mice heterozygous

for HIF-1α prevented osteoblast apoptosis and enhanced bone mineralization and fracture repair [66]. Our results are consistent with the latter study in that 2ME2 inhibits HIF-1α but increases bone mass. In addition, HIF-1α also regulates osteoclast formation and bone resorption [67,68] by increasing VEGF expression which substitutes for M-CSF to promote osteoclastogenesis together with RANKL [69,70]. 2ME2 may therefore inhibit osteoclast formation and activity indirectly by blocking HIF-1α activity and VEGF secretion by osteoblasts. 2ME2 has also been shown to induce apoptosis in mature osteoclasts [47], and may have other effects in bone [71]. Importantly, we observed no deleterious effects of these drug treatments on the bones of animals. Unlike most current cancer therapies, including aromatase inhibitors, which cause bone loss [72], 2ME2 and SD-208 have bone-sparing effects that may contribute the beneficial effect on bone metastases [64,73].

Our data establish that hypoxia and TGF-β signaling pathways regulate tumor-secreted factors such as CXCR4 which promotes tumor cell homing to the bone [54], and VEGF which stimulates tumor angiogenesis and increases both osteoclast [69,74] and osteoblast activity [65]. Genetic inhibition of either HIF-1α or TGF-β in tumor cells provides proof of principle that these signaling pathways promote bone metastasis through tumor-autonomous effects. Systemic inhibition with 2ME2 or SD-208 also decreased bone metastases, while combined treatment provided additional benefit through effects on the tumor cells, as well as the bone microenvironment. Thus, combination therapy with inhibitors of hypoxia and TGF-β may significantly improve treatment and impact survival of patients with bone metastases, and provide a welcome addition to current armamentarium for bone metastases.

References

1. Roodman GD (2004) Mechanisms of bone metastasis. N Engl J Med 350: 1655-1664.
2. Mundy GR (2002) Metastasis to bone: causes, consequences and therapeutic opportunities. Nat Rev Cancer 2: 584-593.
3. Massague J (2008) TGFbeta in Cancer. Cell 134: 215-230.
4. Massague J, Seoane J, Wotton D (2005) Smad transcription factors. Genes Dev 19: 2783-2810.
5. Chiang AC, Massague J (2008) Molecular basis of metastasis. N Engl J Med 359: 2814-2823.
6. Yin JJ, Selander K, Chirgwin JM, Dallas M, Grubbs BG, et al. (1999) TGF-beta signaling blockade inhibits PTHrP secretion by breast cancer cells and bone metastases development. J Clin Invest 103: 197-206.
7. Kakonen SM, Selander KS, Chirgwin JM, Yin JJ, Burns S, et al. (2002) Transforming growth factor-beta stimulates parathyroid hormone-related protein and osteolytic metastases via Smad and mitogen-activated protein kinase signaling pathways. J Biol Chem 277: 24571-24578.
8. Kang Y, Siegel PM, Shu W, Drobnjak M, Kakonen SM, et al. (2003) A multigenic program mediating breast cancer metastasis to bone. Cancer Cell 3: 537-549.
9. Bendre MS, Margulies AG, Walser B, Akel NS, Bhattacharrya S, et al. (2005) Tumor-derived interleukin-8 stimulates osteolysis independent of the receptor activator of nuclear factor-kappaB ligand pathway. Cancer Res 65: 11001-11009.
10. Bendre MS, Gaddy-Kurten D, Mon-Foote T, Akel NS, Skinner RA, et al. (2002) Expression of interleukin 8 and not parathyroid hormone-related protein by human breast cancer cells correlates with bone metastasis in vivo. Cancer Res 62: 5571-5579.
11. Deckers M, van Dinther M, Buijs J, Que I, Lowik C, et al. (2006) The tumor suppressor Smad4 is required for transforming growth factor beta-induced epithelial to mesenchymal transition and bone metastasis of breast cancer cells. Cancer Res 66: 2202-2209.
12. Kang Y, He W, Tulley S, Gupta GP, Serganova I, et al. (2005) Breast cancer bone metastasis mediated by the Smad tumor suppressor pathway. Proc Natl Acad Sci U S A 102: 13909-13914.
13. Javelaud D, Mohammad KS, McKenna CR, Fournier P, Luciani F, et al. (2007) Stable Overexpression of Smad7 in Human Melanoma Cells Impairs Bone Metastasis. Cancer Res 67: 2317-2324.
14. Mohammad KS, Stebbins E, Kingsley LA, Fournier PGJ, Niewolna M, et al. (2008) Combined transforming growth factor-β receptor I kinase inhibitor and bisphosphonates are additive to reduce breast cancer bone metastases. American Society for Bone and Mineral Research 30th Annual Meeting. Montreal, Canada.
15. Ge R, Rajeev V, Ray P, Lattime E, Rittling S, et al. (2006) Inhibition of growth and metastasis of mouse mammary carcinoma by selective inhibitor of transforming growth factor-beta type I receptor kinase in vivo. Clin Cancer Res 12: 4315-4330.

16. Bandyopadhyay A, Agyin JK, Wang L, Tang Y, Lei X, et al. (2006) Inhibition of pulmonary and skeletal metastasis by a transforming growth factor-beta type I receptor kinase inhibitor. Cancer Res 66: 6714-6721.

17. Yang YA, Dukhanina O, Tang B, Mamura M, Letterio JJ, et al. (2002) Lifetime exposure to a soluble TGF-beta antagonist protects mice against metastasis without adverse side effects. J Clin Invest 109: 1607-1615.

18. Muraoka RS, Dumont N, Ritter CA, Dugger TC, Brantley DM, et al. (2002) Blockade of TGF-beta inhibits mammary tumor cell viability, migration, and metastases. J Clin Invest 109: 1551-1559.

19. Hayashi T, Hideshima T, Nguyen AN, Munoz O, Podar K, et al. (2004) Transforming growth factor beta receptor I kinase inhibitor down-regulates cytokine secretion and multiple myeloma cell growth in the bone marrow microenvironment. Clin Cancer Res 10: 7540-7546.

20. Hirao M, Hashimoto J, Yamasaki N, Ando W, Tsuboi H, et al. (2007) Oxygen tension is an important mediator of the transformation of osteoblasts to osteocytes. J Bone Miner Metab 25: 266-276.

21. Harris AL (2002) Hypoxia--a key regulatory factor in tumour growth. Nat Rev Cancer 2: 38-47.

22. Brown JM, and Wilson, W. R. (2004) Exploiting tumour hypoxia in cancer treatment. Nat Rev Cancer 4: 437-447.

23. Zhong H, De Marzo AM, Laughner E, Lim M, Hilton DA, et al. (1999) Overexpression of hypoxia-inducible factor 1alpha in common human cancers and their metastases. Cancer Res 59: 5830-5835.

24. Semenza GL (2003) Targeting HIF-1 for cancer therapy. Nat Rev Cancer 3: 721-732.

25. Duivenvoorden WC, Hirte HW, Singh G (1999) Transforming growth factor beta1 acts as an inducer of matrix metalloproteinase expression and activity in human bone-metastasizing cancer cells. Clin Exp Metastasis 17: 27-34.

26. Iida J, McCarthy JB (2007) Expression of collagenase-1 (MMP-1) promotes melanoma growth through the generation of active transforming growth factor-beta. Melanoma Res 17: 205-213.

27. Ao M, Franco OE, Park D, Raman D, Williams K, et al. (2007) Cross-talk between paracrine-acting cytokine and chemokine pathways promotes malignancy in benign human prostatic epithelium. Cancer Res 67: 4244-4253.

28. LaVallee TM, Burke PA, Swartz GM, Hamel E, Agoston GE, et al. (2008) Significant antitumor activity in vivo following treatment with the microtubule agent ENMD-1198. Mol Cancer Ther 7: 1472-1482.

29. Albertella MR, Loadman PM, Jones PH, Phillips RM, Rampling R, et al. (2008) Hypoxia-selective targeting by the bioreductive prodrug AQ4N in patients with solid tumors: results of a phase I study. Clin Cancer Res 14: 1096-1104.

30. Eccles SA, Massey A, Raynaud FI, Sharp SY, Box G, et al. (2008) NVP-AUY922: a novel heat shock protein 90 inhibitor active against xenograft tumor growth, angiogenesis, and metastasis. Cancer Res 68: 2850-2860.

31. Ehata S, Hanyu A, Fujime M, Katsuno Y, Fukunaga E, et al. (2007) Ki26894, a novel transforming growth factor-β; type I receptor kinase inhibitor, inhibits in vitro invasion and in vivo bone metastasis of a human breast cancer cell line. Cancer Science 98: 127-133.

32. Uhl M, Aulwurm S, Wischhusen J, Weiler M, Ma JY, et al. (2004) SD-208, a novel transforming growth factor beta receptor I kinase inhibitor, inhibits growth and invasiveness and enhances immunogenicity of murine and human glioma cells in vitro and in vivo. Cancer Res 64: 7954-7961.

33. Tevaarwerk AJ, Holen KD, Alberti DB, Sidor C, Arnott J, et al. (2009) Phase I trial of 2-methoxyestradiol NanoCrystal dispersion in advanced solid malignancies. Clin Cancer Res 15: 1460-1465.

34. Bartholin L, Wessner LL, Chirgwin JM, Guise TA (2007) The human Cyr61 gene is a transcriptional target of transforming growth factor beta in cancer cells. Cancer Lett 246: 230-236.

35. Caruz A, Samsom M, Alonso JM, Alcami J, Baleux F, et al. (1998) Genomic organization and promoter characterization of human CXCR4 gene. FEBS Lett 426: 271-278.

36. Phillips RJ, Mestas J, Gharaee-Kermani M, Burdick MD, Sica A, et al. (2005) Epidermal growth factor and hypoxia-induced expression of CXC chemokine receptor 4 on non-small cell lung cancer cells is regulated by the phosphatidylinositol 3-kinase/PTEN/AKT/mammalian target of rapamycin signaling pathway and activation of hypoxia inducible factor-1alpha. J Biol Chem 280: 22473-22481.

37. Akagi Y, Liu W, Zebrowski B, Xie K, Ellis LM (1998) Regulation of vascular endothelial growth factor expression in human colon cancer by insulin-like growth factor-I. Cancer Res 58: 4008-4014.

38. Guise TA, Yin JJ, Taylor SD, Kumagai Y, Dallas M, et al. (1996) Evidence for a Causal Role of Parathyroid Hormone-related Protein in the Pathogenesis of Human Breast Cancer-mediated Osteolysis. J Clin Invest 98: 1544-1549.

39. Yin JJ, Mohammad KS, Kakonen SM, Harris S, Wu-Wong JR, et al. (2003) A causal role for endothelin-1 in the pathogenesis of osteoblastic bone metastases. Proc Natl Acad Sci U S A 100: 10954-10959.

40. Mabjeesh NJ, Escuin D, LaVallee TM, Pribluda VS, Swartz GM, et al. (2003) 2ME2 inhibits tumor growth and angiogenesis by disrupting microtubules and dysregulating HIF. Cancer Cell 3: 363-375.

41. Ricker JL, Chen Z, Yang XP, Pribluda VS, Swartz GM, et al. (2004) 2-methoxyestradiol inhibits hypoxia-inducible factor 1alpha, tumor growth, and angiogenesis and augments paclitaxel efficacy in head and neck squamous cell carcinoma. Clin Cancer Res 10: 8665-8673.

42. Zhou D, Matchett GA, Jadhav V, Dach N, Zhang JH (2008) The effect of 2-methoxyestradiol, a HIF-1 alpha inhibitor, in global cerebral ischemia in rats. Neurol Res 30: 268-271.

43. Raleigh JA, Calkins-Adams DP, Rinker LH, Ballenger CA, Weissler MC, et al. (1998) Hypoxia and vascular endothelial growth factor expression in human squamous cell carcinomas using pimonidazole as a hypoxia marker. Cancer Res 58: 3765-3768.

44. Varia MA, Calkins-Adams DP, Rinker LH, Kennedy AS, Novotny DB, et al. (1998) Pimonidazole: a novel hypoxia marker for complementary study of tumor hypoxia and cell proliferation in cervical carcinoma. Gynecol Oncol 71: 270-277.

45. Janssen HL, Haustermans KM, Sprong D, Blommestijn G, Hofland I, et al. (2002) HIF-1A, pimonidazole, and iododeoxyuridine to estimate hypoxia and perfusion in human head-and-neck tumors. Int J Radiat Oncol Biol Phys 54: 1537-1549.
46. Carmeliet P, Dor Y, Herbert JM, Fukumura D, Brusselmans K, et al. (1998) Role of HIF-1alpha in hypoxia-mediated apoptosis, cell proliferation and tumour angiogenesis. Nature 394: 485-490.
47. Cicek M, Iwaniec UT, Goblirsch MJ, Vrabel A, Ruan M, et al. (2007) 2-Methoxyestradiol suppresses osteolytic breast cancer tumor progression in vivo. Cancer Res 67: 10106-10111.
48. Coleman RE (2008) Risks and benefits of bisphosphonates. Br J Cancer 98: 1736-1740.
49. Lipton A (2008) Emerging role of bisphosphonates in the clinic--antitumor activity and prevention of metastasis to bone. Cancer Treat Rev 34 Suppl 1: S25-30.
50. Hiraga T, Kizaka-Kondoh S, Hirota K, Hiraoka M, Yoneda T (2007) Hypoxia and hypoxia-inducible factor-1 expression enhance osteolytic bone metastases of breast cancer. Cancer Res 67: 4157-4163.
51. Jeon SH, Chae BC, Kim HA, Seo GY, Seo DW, et al. (2007) Mechanisms underlying TGF-beta1-induced expression of VEGF and Flk-1 in mouse macrophages and their implications for angiogenesis. J Leukoc Biol 81: 557-566.
52. Sanchez-Elsner T, Botella LM, Velasco B, Corbi A, Attisano L, et al. (2001) Synergistic cooperation between hypoxia and transforming growth factor-beta pathways on human vascular endothelial growth factor gene expression. J Biol Chem 276: 38527-38535.
53. Liao D, Corle C, Seagroves TN, Johnson RS (2007) Hypoxia-inducible factor-1alpha is a key regulator of metastasis in a transgenic model of cancer initiation and progression. Cancer Res 67: 563-572.
54. Wang J, Loberg R, Taichman RS (2006) The pivotal role of CXCL12 (SDF-1)/CXCR4 axis in bone metastasis. Cancer Metastasis Rev 25: 573-587.
55. Pulaski BA, Ostrand-Rosenberg S (2001) Mouse 4T1 breast tumor model. Curr Protoc Immunol Chapter 20: Unit 20 22.
56. Cabioglu N, Sahin AA, Morandi P, Meric-Bernstam F, Islam R, et al. (2009) Chemokine receptors in advanced breast cancer: differential expression in metastatic disease sites with diagnostic and therapeutic implications. Ann Oncol.
57. Richert MM, Vaidya KS, Mills CN, Wong D, Korz W, et al. (2009) Inhibition of CXCR4 by CTCE-9908 inhibits breast cancer metastasis to lung and bone. Oncol Rep 21: 761-767.
58. Tamamura H, Hori A, Kanzaki N, Hiramatsu K, Mizumoto M, et al. (2003) T140 analogs as CXCR4 antagonists identified as anti-metastatic agents in the treatment of breast cancer. FEBS Lett 550: 79-83.
59. Diamond P, Labrinidis A, Martin SK, Farrugia AN, Gronthos S, et al. (2009) Targeted Disruption of the CXCL12/CXCR4 Axis Inhibits Osteolysis in a Murine Model of Myeloma-Associated Bone Loss. J Bone Miner Res.
60. Bauerle T, Bartling S, Berger M, Schmitt-Graff A, Hilbig H, et al. (2008) Imaging anti-angiogenic treatment response with DCE-VCT, DCE-MRI and DWI in an animal model of breast cancer bone metastasis. Eur J Radiol.

61. Bauerle T, Hilbig H, Bartling S, Kiessling F, Kersten A, et al. (2008) Bevacizumab inhibits breast cancer-induced osteolysis, surrounding soft tissue metastasis, and angiogenesis in rats as visualized by VCT and MRI. Neoplasia 10: 511-520.

62. Mooberry SL (2003) Mechanism of action of 2-methoxyestradiol: new developments. Drug Resist Updat 6: 355-361.

63. Mooberry SL (2003) New insights into 2-methoxyestradiol, a promising antiangiogenic and antitumor agent. Curr Opin Oncol 15: 425-430.

64. Mohammad KS, Chen CG, Balooch G, Stebbins E, McKenna CR, et al. (2009) Pharmacologic inhibition of the tgf-Beta type I receptor kinase has anabolic and anti-catabolic effects on bone. PLoS ONE 4: e5275.

65. Wang Y, Wan C, Deng L, Liu X, Cao X, et al. (2007) The hypoxia-inducible factor alpha pathway couples angiogenesis to osteogenesis during skeletal development. J Clin Invest 117: 1616-1626.

66. Komatsu DE, Bosch-Marce M, Semenza GL, Hadjiargyrou M (2007) Enhanced bone regeneration associated with decreased apoptosis in mice with partial HIF-1alpha deficiency. J Bone Miner Res 22: 366-374.

67. Arnett TR, Gibbons DC, Utting JC, Orriss IR, Hoebertz A, et al. (2003) Hypoxia is a major stimulator of osteoclast formation and bone resorption. J Cell Physiol 196: 2-8.

68. Bozec A, Bakiri L, Hoebertz A, Eferl R, Schilling AF, et al. (2008) Osteoclast size is controlled by Fra-2 through LIF/LIF-receptor signalling and hypoxia. Nature 454: 221-225.

69. Knowles HJ, Athanasou NA (2008) Hypoxia-inducible factor is expressed in giant cell tumour of bone and mediates paracrine effects of hypoxia on monocyte-osteoclast differentiation via induction of VEGF. J Pathol 215: 56-66.

70. Knowles HJ, Athanasou NA (2009) Acute hypoxia and osteoclast activity: a balance between enhanced resorption and increased apoptosis. J Pathol.

71. Mohammad KS, Duong V, Kingsley L, McKenna CR, Walton H, et al. (2008) Skeletal effects of 2-methoxyestradiol in combination with other prostate cancer therapies. American Society for Bone and Mineral Research 30th Annual Meeting. Montreal, Canada.

72. Guise TA (2006) Bone loss and fracture risk associated with cancer therapy. Oncologist 11: 1121-1131.

73. Sibonga JD, Lotinun S, Evans GL, Pribluda VS, Green SJ, et al. (2003) Dose-response effects of 2-methoxyestradiol on estrogen target tissues in the ovariectomized rat. Endocrinology 144: 785-792.

74. Zhang Q, Guo R, Lu Y, Zhao L, Zhou Q, et al. (2008) VEGF-C, a lymphatic growth factor, is a RANKL target gene in osteoclasts that enhances osteoclastic bone resorption through an autocrine mechanism. J Biol Chem 283: 13491-13499.

Competing Interests

The authors declare that no competing interests exist.

Non-standard abbreviations: 2-methoxyestradiol (2ME2), 3,3′,5,5′-tetramethylbenzidine (TMB), bone mineral density (BMD), connective tissue growth factor (CTGF), CXC chemokine receptor 4 (CXCR4), dominant-negative TβRII (DNRII), hematoxylin and eosin (H&E), hypoxia inducible factor-1α (HIF-1α), hypoxia response element (HRE), parathyroid hormone-related protein (PTHrP), Smad binding element (SBE), HIF-1α shRNA (shHIF), non-target shRNA (shNT), TGF-β type I receptor (TβRI), TGF-β type II receptor (TβRII), transforming growth factor-β (TGF-β), tartrate resistant acid phosphatase (TRAP)

Figure 1. Hypoxia induces HIF-1α in bone-metastatic cancer cells *in vitro* and in bone metastases *in vivo*. (**A**) MDA-MB-231, PC-3 and 1205Lu cells were treated with 2ME2 and cultured ± 1% O_2 during 6h. Protein lysates from the treated cells were analyzed for HIF-1α protein expression by Western blotting. α-tubulin was used as loading control. (**B**) Representative demineralized bone sections from mice with MDA-MB-231 bone metastases stained for tumor hypoxia with Hypoxyprobe™-1 (HP), with an antibody against HIF-1α, or with hematoxylin and eosin (H&E). Arrows indicate HIF-1α positive nuclei. Images are at 200X magnification with scale bar equal to 100μm, inset is at 630X magnification with scale bar equal to 50μm. Staining without primary antibody was used as negative control.

Figure 2. Hypoxia and TGF-β increase VEGF and CXCR4 mRNA expression and promoter activity. (**A**) MDA-MB-231 cells were cultured ± 1% O_2 during 6h and total RNA was extracted. VEGF and CXCR4 mRNA expression (mean ± SEM) was measured by semi-quantitative RT-PCR (n=3). * $P < 0.05$, *** $P < 0.005$, **** $P < 0.001$, using an unpaired Student's t test. (**B**) HepG2 hepatocarcinoma cells co-transfected with a renilla luciferase plasmid (phRL-CMV) and a pGL3 plasmid containing a fragment of the human VEGF (3.3kb) or CXCR4 (2.6kb) promoter, or the TGF-β-sensitive $(CAGA)_9$ promoter were treated ± TGF-β (5ng/mL) and ± 1% O_2 during 24h before measuring dual-luciferase activity. (**C**) MDA-MB-231 breast cancer cells were transfected with a pGL3 plasmid containing the human VEGF or CXCR4 promoter and the phRL-CMV plasmid, as well as plasmids to overexpress HIF-1α and/or Smad2, 3 and 4. Cells were treated ± TGF-β (5ng/mL) ± 1% O_2 during 24h before measuring dual-luciferase activity. Results are expressed as the mean ± SEM (n=3) of the relative luciferase activity. * $P < 0.05$, ** $P < 0.01$, *** $P < 0.005$, **** $P < 0.001$, using an unpaired Student's t test.

Figure 3. Hypoxia and TGF-β increase VEGF and CXCR4 transcription through proximal promoter response elements. (**A**) HepG2 cells were transfected with pGL3 plasmids containing full-length for 5'-deleted fragments of the human VEGF or CXCR4 promoter and the phRL-CMV plasmid. Cells were treated ± TGF-β (5ng/mL) ± 1% O_2 during 24h before measuring dual-luciferase activity. Results are expressed as the mean ± SEM (n=3) of the relative luciferase activity, analyzed using an unpaired Student's t test. (**B**) Schematic representation of wild-type (WT), HRE-mutant (mH1) and SBE-mutant (mS1 or mS2) VEGF and CXCR4 promoters. One to three nucleotides (underlined, bold letters) within HRE and SBEs were substituted as indicated. (**C**) HepG2 cells were transfected with pGL3 plasmids containing a wild-type VEGF or CXCR4 promoter or promoters with mutations to the HRE or SBE and the phRL-CMV plasmid. Cells were treated ± TGF-β (5ng/mL) ± 1% O_2 during 24h before measuring dual-luciferase activity. Results are expressed as the mean ± SEM (n=3) of the relative luciferase activity, analyzed using an unpaired Student's t test. * $P < 0.05$, ** $P < 0.01$, *** $P < 0.005$, **** $P < 0.001$.

Figure 4. Knockdown of HIF-1α inhibits VEGF and CXCR4 mRNA and protein expression *in vitro*. (**A**) MDA-MB-231 parental cells (P) or cells transfected with a

pLKO.1 vector expressing a non-target shRNA (shNT#3 and #7) or an shRNA against HIF-1α (shHIF#3 and #11) were cultured ± 1% O_2 during 6h. Total RNA was extracted and mean ± SEM expression of HIF-1α was measured using semi-quantitative RT-PCR (n=3). Proteins were extracted from treated cells and HIF-1α level was assayed by Western-blotting, α-tubulin was used as loading control. * $P<0.05$, using an unpaired Student's t test. **(B)** Parental (P) cells and shNT and shHIF clones were treated ± TGF-β (5ng/mL) ± 1% O_2 for 24h. Total RNA was extracted and mean ± SEM VEGF and CXCR4 expression was measured using semi-quantitative RT-PCR (n=3). * $P< 0.05$, ** $P< 0.01$, **** $P< 0.001$, using an unpaired Student's t test. **(C)** MDA-MB-231 parental (P) cells and clones were treated ± TGF-β (5ng/mL) ± 1% O_2 and conditioned media were collected 24h later. VEGF-A levels were measured by ELISA assay. Results are expressed as mean ± SEM nanograms VEGF-A per 10^6 cells. **** $P< 0.001$, using an unpaired Student's t test. **(D)** MDA-MB-231 parental (P) cells and clones were treated ± 1% O_2 for 24h and then analyzed by flow cytometry for CXCR4 protein expression. Results are reported as the percentage of maximal CXCR4 expression.

Figure 5. Knockdown of HIF-1α decreases osteolytic lesions and improves survival of mice *in vivo*. **(A)** Representative x-ray images from hindlimbs of mice 4 weeks post inoculation with MDA-MB-231 parental, shNT and shHIF cells. Arrows indicate osteolytic lesions. **(B)** Osteolytic lesion area measured on radiographs of hindlimbs and forelimbs of mice with bone metastases. Results are expressed as the mean area ± SEM per mouse (n=5-10 per group). † $P< 0.01$ and * $P< 0.001$ compared to parental or shNT clones using a two-way ANOVA with a Bonferroni post-test at 4 weeks. **(C)** Kaplan-Meyer analysis of mouse survival. * $P< 0.05$ shHIF#3 compared to Parental or shNT clones, † $P< 0.005$ and ‡ $P= 0.089$ shHIF#11 respectively compared to Parental and shNT#7 using a Logrank test. **(D)** Representative histology of femurs with tumor indicated by arrows. Scale bar equal to 500μm. **(E)** Tumor burden in hindlimbs was measured by quantitative histomorphometry. Results are expressed as the mean ± SEM area per bone. A one-way ANOVA with a Newman-Keuls multiple comparison test showed no significant differences (*N.S.*) between groups.

Figure 6. Knockdown of HIF-1α in MDA-MB-231 cells is stable *in vivo*. **(A)** Representative HIF-1α staining in demineralized bone sections from mice inoculated with MDA-MB-231 parental, shNT or shHIF cells. Arrows indicate HIF-1α positive nuclei. Scale bar equals 50μm. Staining without primary antibody was used as negative control (Neg. Control). **(B)** The percentage of nuclei positive for HIF-1α was calculated in three non-overlapping fields at 400X magnification for each mouse (n=3 per group). Results are the mean ± SEM number of HIF-1α positive nuclei per field.

Figure 7. HIF-1α knockdown decreases tumor angiogenesis at sites of bone metastases in mice. **(A)** Representative sections from mice with bone metastases stained for the endothelial cell marker CD31. Arrows indicate CD31+ vessels. Scale bar equals 50μm **(B)** The number of vessels in bone metastases was counted in three non-overlapping fields at 200X magnification per mouse (n=3 per group). Results are expressed as the mean ± SEM number of vessel per tumor area. * $P< 0.05$, ** $P< 0.01$,

**** *P*< 0.001, using a one-way ANOVA with a Newman-Keuls multiple comparison test.

Figure 8. HIF-1α knockdown and TGF-β blockade decreases VEGF and CXCR4 mRNA expression *in vitro*. (A) MDA-MB-231 dominant-negative TβRII expressing cells (DNRII) were transfected with a pLKO.1 vector expressing a non-target shRNA (DNRII/shNT#2 and #4) or an shRNA against HIF-1α (DNRII/shHIF#22 and #26) were cultured ± 1% O_2 during 6h. Total RNA was extracted and mean ± SEM expression of HIF-1α was measured using semi-quantitative RT-PCR (n=3). * *P*<0.05 compared to parental (P), using an unpaired Student's t test. **(B)** Proteins were extracted from treated cells and HIF-1α level was assayed by Western-blotting. α-tubulin was used as loading control. **(C)** MDA-MB-231 parental cells (P) and DNRII clones were treated ± TGF-β (5ng/mL) for 2h. Proteins were extracted and analyzed for phosphorylated Smad2 (pSmad2) and total Smad2 by Western-blotting. **(D)** MDA-MB-231 parental cells (P) and DNRII clones transfected with pGL3-(CAGA)$_9$ and phRL-CMV plasmids were treated ± TGF-β (5ng/mL) during 24h before measuring dual-luciferase activity. Results are expressed as the mean ± SEM of the relative luciferase activity (n=3). **** *P*< 0.001, using an unpaired Student's t test. **(E)** Total RNA was extracted from MDA-MB-231 parental (P) and DNRII clones treated ± TGF-β (5ng/mL) and ± 1% O_2 during 24h. Mean ± SEM VEGF and CXCR4 expression was measured using semi-quantitative RT-PCR (n=3). * *P*< 0.05, ** *P*< 0.01, *** *P*< 0.005, using an unpaired Student's t test.

Figure 9. Combined HIF-1α knockdown and TGF-β blockade provides no further benefit in mice with bone metastases. (A) Representative x-ray images from hindlimbs of mice 4 weeks post inoculation with MDA-MB-231 parental, shNT#3, shHIF#3, DNRII, DNRII/shNT#2 and DNRII/shHIF#22 cells. Arrows indicate osteolytic lesions. **(B)** Osteolytic lesion area measured on radiographs of hindlimbs and forelimbs of mice with bone metastases. Results are expressed as the mean area ± SEM per mouse (n=6-11 per group). * *P*< 0.001 compared to parental and † *P*< 0.05 compared to shNT#3 using a two-way ANOVA with a Bonferroni post-test at 3 weeks. **(C)** Kaplan-Meyer analysis of mouse survival. * *P*< 0.001 shHIF#3 and DNRII compared to Parental and † *P*< 0.005 shHIF#3 compared to shNT#3 using a Logrank test. **(D)** Tumor burden in hindlimbs was measured by quantitative histomorphometry. Results are expressed as the mean ± SEM area per bone. A one-way ANOVA with a Newman-Keuls multiple comparison test showed no significant differences (*N.S.*) between groups.

Figure 10. Preventive treatment with the HIF-1α inhibitor 2ME2 inhibits bone metastases in mice. (A) Representative 4-week x-rays from mice inoculated with MDA-MB-231 cells and treated ± 2ME2 (150mg/kg), arrows indicate osteolytic lesions. Osteolytic lesion area was measured on radiographs of hindlimbs and forelimbs of mice with bone metastases. Results are expressed as the mean ± SEM area per mouse (n=10-12 per group). * *P*< 0.01 using a two-way ANOVA with a Bonferroni post-test at 4 weeks. **(B)** Representative histology of tibias with tumor indicated by arrows. Scale bar equal to

500μm. Tumor burden in hindlimbs and humeri was measured by quantitative histomorphometry. Results are expressed as the mean ± SEM area per bone, analysis by unpaired Student's t test. (**C**) Representative HIF-1α staining in demineralized bone metastases sections from mice treated ± 2ME2. Arrows indicate HIF-1α positive nuclei. Scale bar equals 25μm. The percentage of nuclei positive for HIF-1α was calculated in three non-overlapping fields at 400X magnification for each mouse (n=6 per group). Results are the mean ± SEM number of HIF-1α positive nuclei per field using an unpaired Student's t test. (**D**) Hypoxyprobe™-1 staining for tumor hypoxia in bone metastases sections. Hypoxic regions indicated by asterisks. Staining was graded on a 1-4+ scale in three non-overlapping fields at 400X magnification per mouse (n=3 per group). Results are the mean ± SEM staining per field using an unpaired Student's t test.

Figure 11. 2ME2 increases bone density, inhibits osteoclasts and increases osteoblasts in normal bone unaffected by tumor. (**A**) Bone mineral density of the femur, tibia, and spine measured by DXA in mice treated ± 2ME2 (150 mg/mL). Results are expressed as the mean ± SEM % change in BMD (n=10 per group). Statistical analysis by two-way ANOVA with a Bonferroni post-test at week 4. (**B**) Representative histology of tibias from mice ± 2ME2 (150 mg/mL) for 4 weeks. Trabecular bone is indicated by arrows. Scale bar equal to 500μm. (**C**) Representative TRAP staining of bone histology of the proximal tibias from the mice. TRAP+ osteoclasts (OC) are indicated by arrows. Scale bar is equal to 50μm. (**D**) Osteoclast number was measured in the distal femur and proximal tibia at 200X magnification on TRAP stained slides. Results are expressed as the number of osteoclasts (OC) per mm^2 bone surface (BS). (**E**) Representative H&E stained bone histology of the proximal tibias from mice treated ± 2ME2 (150 mg/mL). Osteoblasts (OB) indicated by arrows. Scale bar is equal to 50μm. (**F**) Osteoblast number was measured below the primary spongiosa in the distal femur and proximal tibia at 200X magnification on H&E stained slides. Results are expressed as the number of osteoblasts (OB) per mm^2 bone surface (BS).

Figure 12. Preventive treatment with SD-208 reduces osteolytic bone lesions and increases survival. (**A**) Representative x-ray images from hindlimbs of mice inoculated with MDA-MB-231 cells and treated ± SD-208 (0.3 mg/mL or 1.0 mg/mL), arrows indicate osteolytic bone lesions. (**B**) Osteolytic lesion area measured on radiographs of hindlimbs and forelimbs from mice with bone metastases. Results are expressed as the mean area ± SEM per mouse (n=XXX per group). **** $P< 0.0001$ 0.3mg/mL and 1.0mg/mL SD-208 compared to vehicle, using a two-way ANOVA with a Bonferroni post-test at 4 weeks. (**C**) Representative histology of femurs with tumor indicated by arrows. Scale bar equal to 500μm. (**D**) Tumor burden in hindlimbs and humeri was measured by quantitative histomorphometry. Results are expressed as the mean ± SEM area per bone. Statistical analysis by one-way ANOVA with a Newman-Keuls multiple comparison test. (**E**) Kaplan-Meyer analysis of mouse survival analyzed using a Logrank test.

Figure 13. Combined treatment with 2ME2 and SD-208 additively decreases bone metastases in a mouse model. (**A**) Representative x-ray images from hindlimbs of mice

inoculated with MDA-MB-231 cells and treated ± 2ME2 (150mg/kg) and ± SD-208 (60mg/kg), arrows indicate osteolytic lesions and osteolytic lesion area measured on radiographs of hindlimbs and forelimbs from mice with bone metastases. Results are expressed as the mean area ± SEM per mouse (n=12-14 per group). * $P< 0.01$ SD-208 and ** $P< 0.001$ 2ME2 compared to vehicle, † $P< 0.01$ SD-208 and ‡ $P< 0.05$ 2ME2 compared to SD-208 + 2ME2, using a two-way ANOVA with a Bonferroni post-test at 3 weeks. **(B)** Representative histology of femurs with tumor indicated by arrows. Scale bar equal to 500µm. **(C)** Tumor burden in hindlimbs and humeri was measured by quantitative histomorphometry. Results are expressed as the mean ± SEM area per bone. * $P< 0.05$, **** $P< 0.001$, using a one-way ANOVA with a Newman-Keuls multiple comparison test. **(D)** Osteoclast number per mm bone surface (BS) was counted in TRAP stained bone metastases sections. Results are expressed as mean ± SEM OC number per millimeter BS per bone. ** $P< 0.01$, **** $P< 0.001$, using a one-way ANOVA with a Newman-Keuls multiple comparison test.

Table 1. Regulation of bone metastases genes by hypoxia and TGF-β.

Gene Type	Gene	Hypoxia	Both	TGF-β
Bone Metastatic Genes (Kang *et al.* 2003)	CTGF	34*	6	632*
	CXCR4	87*	1	55*
	OPN	61*	4	314*
	IL-11	5	0	171*
	MMP-1	24*	7	216*
Tumor-Secreted Factors	PTHrP	9	1	193*
	IL-6	384*	20*	2974*
	IL-8	200*	6	816*
	Endothelin-1	590*	17*	313*
	Adrenomedullin	140*	3	38*
	VEGF	3152*	108*	1182*
	PDGF	128*	23	1823*
	Stanniocalcin	12*	0	3
	Thrombospondin	59*	9	314*
	Cyr61	17*	1	28*

Number of hits returned from a Pubmed literature search conducted in February 2009 for the name of each gene with the keywords TGF-β and/or hypoxia. Asterisk (*) indicates genes for which regulation by these pathways has been published.

Supporting Information

Table S1. Sequences of primers for human genes analyzed by semi-quantitative RT-PCR.

Table S2. PCR primer sequences for 5'→3' deletion of VEGF and CXCR4 promoters.

A

Normoxia (20% O$_2$)   Hypoxia (1% O$_2$)

2ME2 (µM)   0   50   100   200   0   50   100   200

MDA-MB-231   HIF-1α

α-tubulin

PC-3   HIF-1α

α-tubulin

Normoxia   1%O$_2$

2ME2 (µM)   0   100   0   100

1205Lu   HIF-1α

α-tubulin

B

HP   HIF-1α   H&E

− Primary Ab

+ Primary Ab

B

VEGF (WT), mS1, mH1, mS2 promoter constructs with SBE1 (CAGAC), HRE1 (TACGTG), SBE2 (GTCTG) sites from −2352 to +957 driving Luc. Mutations: mS1 (**AT**G**C**C), mH1 (TGC**CGC**), mS2 (GTCT**C**).

CXCR4 (WT), mS1, mH1, mS2 promoter constructs with SBE1 (CAGACA), HRE1 (TCCGTG), SBE2 (GTCTG) sites from −2620 to +2 driving Luc. Mutations: mS1 (**AT**GGCA), mH1 (**C**C**ATG**G), mS2 (GTCT**A**).

C

VEGF   **CXCR4**

A Parental shNT#3 shNT#7 shHIF#3 shHIF#11

B

Osteolytic lesion area (mm²)

- ✕ Parental
- ● shNT#3
- ▼ shNT#7
- ○ shHIF#3
- ▽ shHIF#11

*

†

Weeks post tumor inoculation

C

% survival

- ✕ Parental
- ● shNT#3
- ▼ shNT#7
- ○ shHIF#3
- ▽ shHIF#11

* † ‡

Days post tumor inoculation

D Parental shNT#3 shNT#7 shHIF#3 shHIF#11

E

Tumor area (mm²)

P = N.S.

P   shNT#3   shNT#7   shHIF#3   shHIF#11

A HIF-1α immunostaining

Neg. Control

Parental

shNT#3

shNT#7

shHIF#3

shHIF#11

B

A

CD31 immunostaining

Neg. Control

Parental

shNT#3

shNT#7

shHIF#3

shHIF#11

B

Vessels/tumor area (mm^{-2})

100

75

50

25

0

P | #3 | #7 | #3 | #11

shNT

shHIF

*

**

A

Relative HIF-1α mRNA

2.5, 2.0, 1.5, 1.0, 0.5, 0.0

P, DNRII, #2, #4 (DN/NT), #22, #26 (DN/HIF)

↓95% ↓98%

* *

B

P DN DN/NT #2 #4 DN/HIF #22 #26

20% O₂ — HIF-1α

α-tubulin

1% O₂ — HIF-1α

α-tubulin

C

P DNRII NT#2 NT#4 HIF#22 HIF#26

TGFβ − + − + − + − + − + − +

pSmad2

Smad2

D

(CAGA)₉

Rel. luciferase activity

250, 200, 150, 100, 50, 0

P, DNRII, #2, #4 (DN/NT), #22, #26 (DN/HIF)

****

□ Vehicle
■ TGF-β

E

VEGF

Relative mRNA

2.4, 2.0, 1.6, 1.2, 0.8, 0.4, 0.0

P, DNRII, NT#2, HIF#22, HIF#26 (DNRII)

* *** * **

CXCR4

Relative mRNA

14, 12, 10, 8, 6, 4, 2, 0

P, DNRII, NT#2, HIF#22, HIF#26 (DNRII)

*** *** * * *

□ Vehicle
▨ TGF-β
■ 1% O₂
▤ TGF-β/1% O₂

A

Parental

shNT#3

shHIF#3

DNRII

DNRII/
shNT#2

DNRII/
shHIF#22

B

Parental
shNT#3
shHIF#3
DNRII
DNRII/shNT#2
DNRII/shHIF#22

Osteolytic lesion area (mm^2)

Weeks post tumor inoculation

C

Parental
shNT#3
shHIF#3
DNRII
DNRII/shNT#2
DNRII/shHIF#22

% survival

Days post tumor inoculation

D

P= N.S.

Tumor area (mm^2)

P   NT#3   HIF#3   DNRII   NT#2   HIF#22

DNRII

A

Osteolytic lesion area (mm²)

Weeks post tumor inoculation

Vehicle   2ME2

— Vehicle
--- 2ME2

*

B

Tumor area (mm²)

Vehicle   2ME2

$P < 0.005$

Vehicle   2ME2

C

HIF-1α positive nuclei (%)

Vehicle   2ME2

$P < 0.05$

Vehicle

2ME2

D

Hypoxyprobe™-1 staining

Vehicle   2ME2

$P < 0.01$

Vehicle

2ME2

A

Tibia

Femur

Spine

P < 0.001

P < 0.05

P = N.S.

Vehicle
2ME2 (150 mg/kg)

B

Vehicle

2ME2

A Osteoblasts

Vehicle

2ME2

B

P = 0.0002

OB/BS (mm^{-2})

Vehicle 2ME2

C Osteoclasts

Vehicle

2ME2

D

P = 0.0077

OC/BS (mm^{-2})

Vehicle 2ME2

A

Vehicle   0.3 mg/mL SD-208   1.0 mg/mL SD-208

B

p<0.0001

C

Vehicle   0.3 mg/mL SD-208   1.0 mg/mL SD-208

D

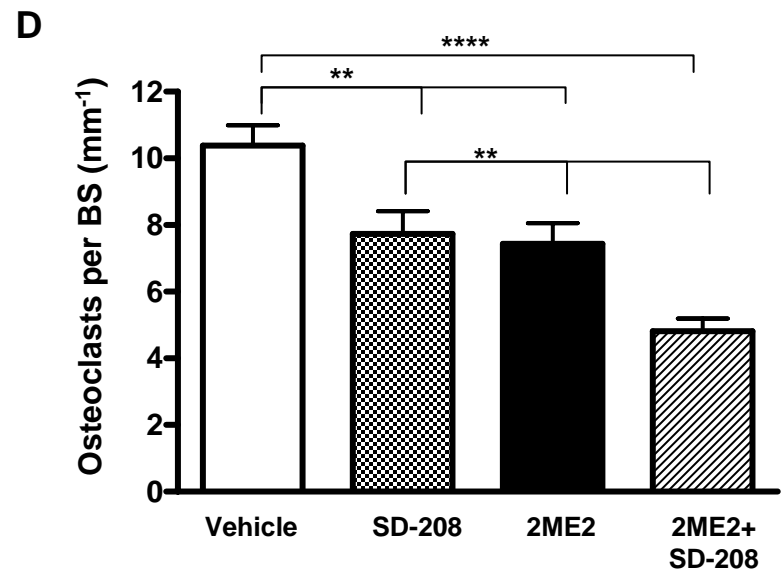p=0.017   p=0.037

E

p=0.008
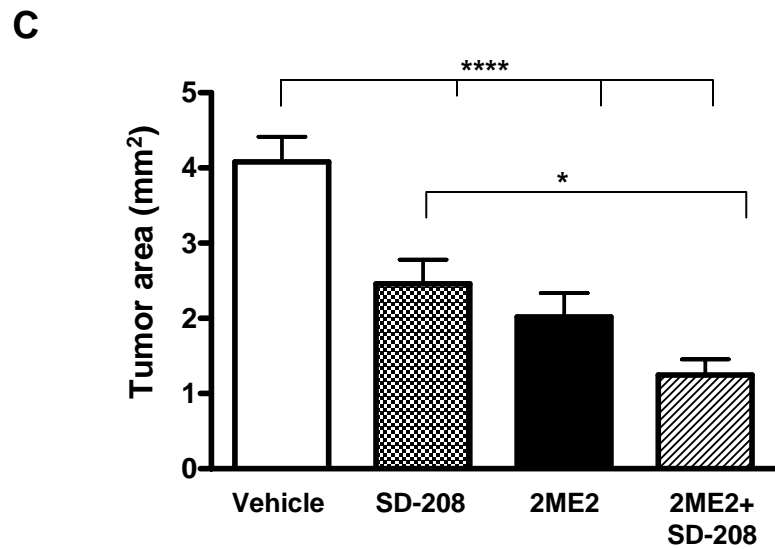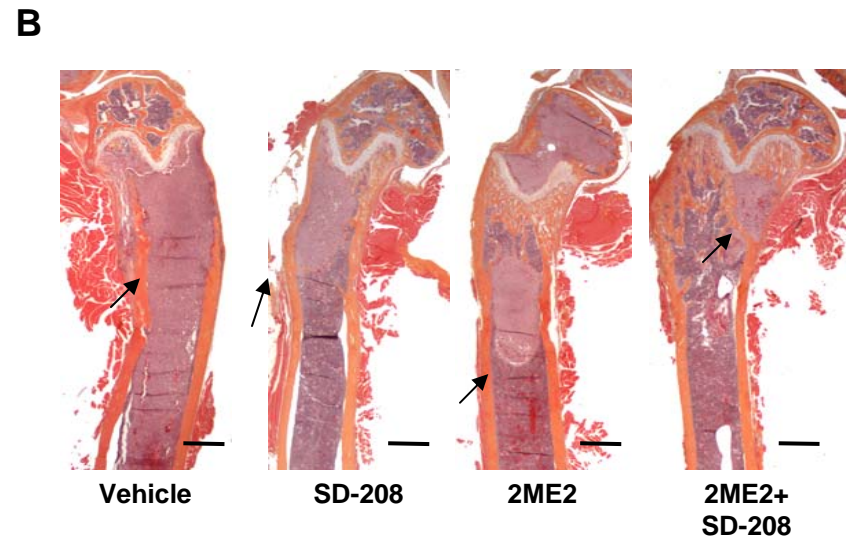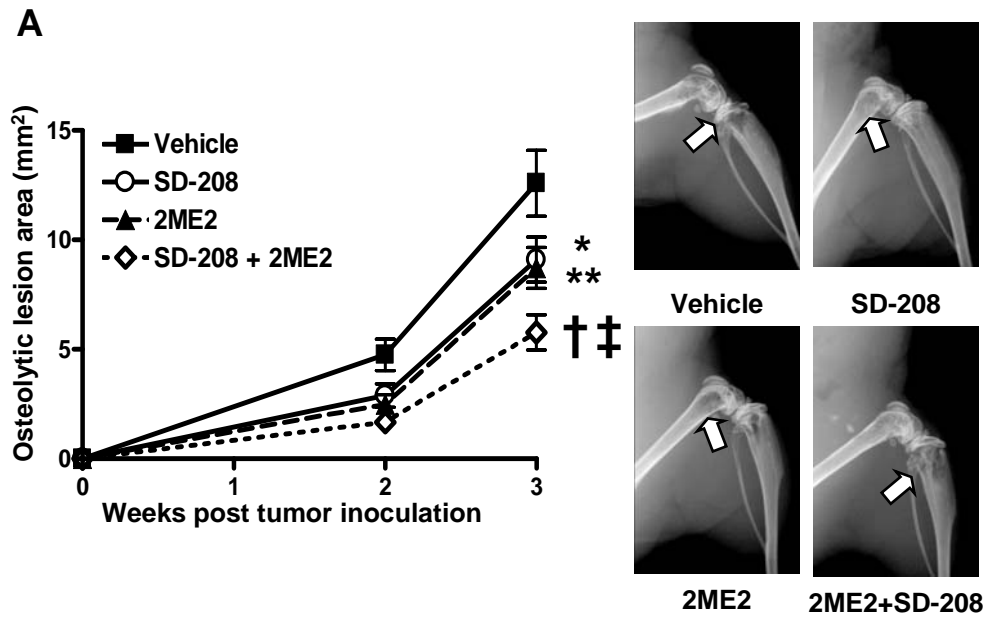
A

B

C

D

Table S1. Sequences of primers for human genes analyzed by semi-quantitative RT-PCR.

RT-PCR Primer	GeneID	Sense (5'→3')	Antisense (5'→3')
CTGF	1490	GCTACCACATTTCCTACCTAGAAATCA	GACAGTCCGTCAAAACAGATTGTT
CXCR4	7852	CCGTGGCAAACTGGTACTTT	GACGCCAACATAGACCACCT
HIF-1α	3091	CACAGAAATGGCCTTGTGAA	CCAAGCAGGTCATAGGTGGT
IL-6	3569	GAAAGCAGCAAAGAGGCACT	TTTCACCAGGCAAGTCTCCT
IL-8	3576	ACTGAGAGTGATTGAGAGTGGAC	AACCCTCTGCACCCAGTTTTC
IL-11	3589	TGAAGACTCGGCTGTGACC	CCTCACGGAAGGACTGTCTC
PHD2	54583	AATCTGGGAGCCTGATTCCT	GTGGCTATTGCGATCCTCAT
PTHrP	5744	ACTCGCTCTGCCTGGTTAGA	GGAGGTGTCAGACAGGTGGT
RPL32	6161	TCAGGTGATCTTCCCACCTC	ACCACATCCCATATCCCTCA
Ski	6497	CAGGAGCTGGAGTTCCTACG	GTGACTCGTTGGCCTCTTTC
Smad2	4087	GGAATTTGCTGCTCTTCTGG	TCTGCCTTCGGTATTCTGCT
Smad3	4088	CATAGGTGCTTTGGGCGTAT	CTGCTATCCAGTCACCAGCA
Smad4	4089	TTGGGGCCCTTAACCTTATC	AGCCATGCCTGACAAGTTCT
Smad7	4092	CCAACTGCAGACTGTCCAGA	CAGGCTCCAGAAGAAGTTGG
SnoN	6498	TGCCCCAAATGTGTCACTTA	TCCATTTTCTCCTGTTCCTCA
TGF-β1	7040	AGGACTGCGGATCTCTGTGT	GGGCAAAGGAATAGTGCAGA
VEGF	7422	AAGGAGGAGGGCAGAATCAT	CACACAGGATGGCTTGAAGA

Table S2. PCR primer sequences for 5'→3' deletion of VEGF and CXCR4 promoters.

Promoter	Length	Bases	Primer (5'→3')
CXCR4	2.2kb	-2216 to +2	**CGGGGTACCCCG**CTTCCTTTTAGTAGAGATCCC
CXCR4	1.0kb	-953 to +2	**CGGGGTACCCCG**CTCCGGGCTTATTTGCTGG
VEGF	2.1kb	-1187 to +957	**CGGGGTACCCCG**GCTCTGGGCAGCTGGCC
VEGF	1.8kb	-843 to +957	**CGGGGTACCCCG**GGACCCCAGTCACTCCAG

Bold indicates KpnI restriction site.